UNIVERSITY OF KWAZULU-NATAL

Measurements of Phase Equilibrium for Systems Containing Oxygenated Compounds

By

Mqondisi Edmund Nala

BSc. Eng
University of KwaZulu Natal

JULY 2012

PREFACE

The work presented in this dissertation entitled “Measurements of Phase Equilibrium for Selected Systems Containing Oxygenated Compounds” was performed in the School of Engineering, University of KwaZulu-Natal, Howard College Campus, South Africa and Ecole de mines, Fontainebleau, CEP/TEP Laboratory, France from January 2010 to December 2011. The work supervised by Professor D. Ramjugernath, Dr. P. Naidoo and Dr. C. Coquelet has been submitted in fulfilment of the academic requirements for the degree of Master of Science in Engineering at the School of Engineering, University of KwaZulu-Natal, Durban.

Declaration

I, Mqondisi Nala, declare that:

(i) The research reported in this research proposal, except where otherwise indicated, is my original work.

(ii) This research proposal has not been submitted for any degree or examination at any other university.

(iii) This research proposal does not contain other persons‘data, pictures, graphs or other information, unless specifically acknowledged as being sourced from other persons.

(iv) This research proposal does not contain other persons‘writing, unless specifically acknowledged as being sourced from other researchers. Where other written sources have been quoted, then:

a. Their words have been re-written but the general information attributed to them has been referenced;

b. Where their exact words have been used, their writing has been placed inside quotation marks, and referenced.

(v) This thesis does not contain text, graphics or tables copied and pasted from the internet, unless specifically acknowledged, and the source being detailed in the thesis and in the References sections.

Signed:

_____ _____

Mqondisi Nala Date

As the candidate’s supervisor, I agree/do not agree to the submission of this thesis.

_____ _____

Professor D. Ramjugernath Doctor C. Coquelet

_____

Doctor P. Naidoo

ACKNOWLEDGEMENTS

I would like to take this opportunity to acknowledge and thank the people and organizations who have made a significant contribution to this project and my study career:

- My supervisors, Prof. D. Ramjugernath, Dr. P. Naidoo and Dr. C. Coquelet for their support and guidance during this study.
- Dr. P. Stringari for his work done in the CEP/TEP Laboratories, Ecole des Mines de Paris
- The workshop and laboratory staff at UKZN.
- The workshop and laboratory staff at the Ecole des Mines de Paris in France.
- Sasol Limited for financial assistance during my degree.

Finaly, to my family, for continuous love, support and motivation during my study career.

ABSTRACT

Accurate and reliable vapour-liquid equilibrium (VLE) and liquid-liquid equilibrium (LLE) data are the key to a successful design and simulation of most important industrial separation processes (traditional distillation, extractive and azeotropic distillation). This work focuses on measurement of new phase equilibrium data for systems comprising of propan-1-ol, water and diisopropyl ether which are of important use in the petrochemical industry. In addition, an investigation of phase equilibrium behavior for systems of interest constituted by solvents and high added-value oxygenated compounds deriving from lignocelluloses biomasses (bio-fuels) was conducted at the Ecole des Mines de Paris CEP/TEP laboratories (France).Various data bases such as Science Direct, ACS publications and Dortmund Data Bank (DDB, 2009) were used to confirm that no literature data is available for these systems.

The VLE data measurements for the system of propan-1ol + water and propan-1ol + diisopropyl ether (DIPE) (333.15, 353.15 and 373.15 K) were carried out using a dynamic still of Lilwanth (2011), with a test system (ethanol + cyclohexane at 40 kPa) undertaken prior measurements to confirm the accuracy of the method and apparatus.The phase equilibrium (VLE and LLE) behaviours for furan + n-hexane and furan + Methylbenzene, furfural + n-hexane and furan + water were determined at 101.3 kPa. The atmospheric dynamic ebulliometry was used to measure VLE systems at 101.3 kPa. A set of LLE data for furfural + n-hexane and furan + water systems were obtained using a static analytical method, with a newly commissioned LLE apparatus. Furfural + n-hexane system was compared used as test system, to verify the reliability of the new equipment. The NRTL model was used to correlate the LLE data, with Cox-Herington model used to predict the entire LLE curve for furfural+ n-hexane system. The experimental VLE data were correlated using the combined $\gamma - \varphi$ method. The vapour phase non idealities were described using the methods from Nothnagel *et al.* (1973), Hayden and O'Connell (1975) and the Peng-Robinson (1976) model. The activity coefficients were correlated using the NRTL model of Renon and Prausnitz (1968) and the modified UNIQUAC model of Abrams and Prausnitz (1976).

A propan-1-ol dehydration process was simulated using Aspen to illustrate the use and importance of thermodynamic models in industrial process design and simulation. The model used in the simulation was validated with measured VLE and literature LLE data.

Table of Contents

PREFACE…….. ii

ACKNOWLEDGMENTS ……... iv

ABSTRACT …….. v

TABLE OF CONTENTS ……..... vi

LIST OF FIGURES……..... xiii

LIST OF TABLES.……... xxix

NOMENCLATURE ……..... xxxii

CHAPTER 1

INTRODUCTION…….....**1**

1.1 Review of Ethers, Alcohols and Biofuel Constituents…….…....**3**

1.1.1 Alcohols…….…….3

1.1.1.1 Uses of Alcohols…….……...……..4

1.1.1.2 Hydrogen Bonding in Alcohols……...……4

1.1.1.3 Solubility of Alcohols in Water…….……..……5

1.1.2 Ethers …….……5

1.1.2.1 Uses of Ethers……...……...……6

1.1.2.2 Solubility of Ethers in Water……..…….……6

1.1.3 Biofuels and its Constituents……...……...……...…..7

1.1.3.1 Uses of Furfural……...…8

1.1.3.2 Uses of Furan ……..…….…..8

1.2 Background of Azeotropic Distillation and Propan-1-ol Dehydration Process…….....**9**

1.2.1 The Azeotropic Distillation.....9

1.2.2 The Propan-1-ol Dehydration Process……...…….……...……...……..11

CHAPTER 2

THERMODYNAMIC PRINCIPLES FOR VAPOUR-LIQUID EQUILIBRIUM…..…...12

2.1 Phase equilibrium behavior……. 12

2.1.1 Vapour liquid equilibrium Diagrams…….……..……..….12

2.1.2 Liquid-liquid equilibrium Diagrams…….……..…..…..….13

2.2 Criterion for Phase Equilibrium……...…..……..…….. 15

2.3 Fugacity and fugacity coefficient……..……16

2.4 Activity and activity coefficients……..…….18

2.5 VLE Treatment Methods…….…….20

2.5.1 The Combined Method (gamma-phi approach)…….…….20

2.5.2 The Direct Method (phi-phi approach)…….……..22

2.5.3 Regression Algorithm (Gamma-phi and phi-phi)……...….……22

2.6 Thermodynamic Models……... 28

2.6.1 The Peng Robinson Equation of State……...……28

2.6.2 Equations of State for Associating Systems ……...……...……30

2.6.2.1 The Virial EOS and The Hayden –O'Conell correlation (HOC)…….…….. 30

2.6.2.2 The Pertubation-Chain Statistical Association Fluid Theory (PC-SAFT)…..…..32

2.6.2.3 The Cubic Plus Association Equation of State (CPA) ……...…33

2.6.3 Excess Gibbs Energy Activity Coefficient Models…….…….…....…34

2.6.3.1 The Wilson Model……..……...….34

2.6.3.2 The NRTL (Non Random Two Liquid) Model…….……..35

2.6.3.3 The UNIQUAC (Universal Quasi-Chemical) Model…….38

2.7 Liquid-Liquid Equilibrium Methods…….…….41

2.7.1 Activity Coefficient Approach……...……41

2.7.2 The Cox Herington Plot for Coexistence……...……44

2.8 Choice of Models for Data Correlation.……..……..……..…….45

2.9 Thermodynamic Consistency…….…..…….39

2.9.1 Point Test……46

2.9.2 Direct Test……..…47

CHAPTER 3

REVIEW OF EQUIPMENT AND EXPERIMENTAL METHODS…….…….. 49

3.1 Static Equilibrium Apparati……...…… 50

3.1.1 Static Equilibrium Apparatus of Kolbe and Gmehling …….50

3.1.1 Static Equilibrium Apparatus of Kolbe and Gmehling …….52

3.2 Dynamic (Recirculating) Equilibrium Stills……53

3.3 Liquid –Liquid Equilibrium (LLE) for Binary Systems……55

3.3.1 Synthetic Method (Cloud point and Titration)……56

3.3.2 Volumetric method……..……56

3.3.3 Direct Analytic Method……...……57

CHAPTER 4

EQUIPMENT DESCRIPTION AND OPERATING PROCEDURES..... 58

4.1 Description of VLE Equipment used in this Project……..58

4.1.1 Equilibrium Still of Lilwanth (2011)……...…58

4.1.1.1 Temperature Measurement and Control……...……61

4.1.1.2 Pressure Measurement and Control……..……61

4.1.1.3 Sampling and Composition Analysis……..……..61

4.1.2 The atmospheric VLE still (2011)……...…61

4.2 Description of LLE equipment used in this project…….. 62

4.2.1 Previous LLE Apparatus …….63

4.2.2 New VLLE Apparatus ……...…….64

4.2.2.1 Apparatus Design and Auxiliary equipment…….64

CHAPTER 5

EXPERIMENT PROCEDURE……...…..… 69

5.1 Preparation of experimental Apparatus……..…..…. 69

5.1.1 Leak Detection Procedure……69

5.1.2 Cleaning of the VLE Still……... 70

5.2 Calibration of Sensors……..……70

5.2.1 Pressure Calibration……...……..70

5.2.2 Temperature Calibration ……...……..71

5.2.3 Composition anaysis……...…….71

5.2.3.1 Gas Chromatograph Detector Calibration……...…….71

5.2.3.2 Density meter calibration…….74

5**.3 Operating Procedure of the Automated VLE Still…….74**

5.3.1 Isobaric Mode (vacuum)…….74

5.3.2 Isobaric Mode (above atmospheric pressure)…….76

5.3.3 Isothermal Mode ……....76

5.3.4 Shutdown Procedure……..…….77

5.4 LLE Measurements……..……77

5.4.1 Cleaning of LLE Cell…….77

5.4.2 Temperature Calibration, Measurement and Control……77

5.4.3 Gas Chromatograph Detector Calibration Composition Analysis…….78

5.4.4 Procedure……...……78

5.5 Chemicals and Equipment Calibration Results……..……79

5.5.1 Chemical Used in this Study…….79

5.5.1 Calibrations Results of the Equipment Used in this Project….…….80

5.5.2.1 Pressure and Temperature Sensor Calibrations……80

5.5.2.2 GC Calibrations and Operating Conditions…….……86

CHAPTER 6

EXPERIMENTAL RESULTS…….…….88

6.1 Uncertainty in Measurements.....88

6.1.1 Uncertainty in pressure, temperature and composition.....89

6.1.2 Basic equations used for statistical analysis of results 90

6.2 Pure component Data……...……...……..90

6.2.1 Vapour Pressure.....90

6.3. Binary Vapour-Liquid Equilibrium Results……..……..…….94

6.3.1 Results for the test system: Cyclohexane (1) + ethanol (2)……..……...…….94

6.3.2 Diisopropyl ether (1) + propan-1-ol (2) system.....97

6.3.3 Water (1) + propan-1-ol (2) system.....103

6.3.4 Furan (1) + n-hexane (2) system.....108

6.3.4.1 Density of mixtures: furan (1) + n-hexane (2) system ……..……...…108

6.3.4.2 Vapour-liquid equilibrium data for furan (1) + n-hexane (2) system.....110

6.3.5 Furan (1) + methylbenzene (2) system.....112

6.3.5.1 Density of mixtures: furan (1) + methylbenzene (2) system….……112

6.3.5.2 Vapour-liquid equilibrium data for furan (1) + methylbenzene (2) system...114

6.4 Binary LLE Experimental Data.....116

CHAPTER 7

DATA REDUCTION AND DISCUSSIONS……..…….120

7.1 Vapour pressure Data Regression……..……120

7.2 Binary VLE Data Regression 122

7.2.1 Modeling results for: Diisopropyl ether (1) + propan-1-ol (2) system 123

7.2.2 Modeling results for: Water (1) + propan-1-ol (2) system 132

7.2.3 Modeling results for: Furan (1) + n-hexane (2) system 138

7.2.3 Modeling results for: Furan (1) + methylbenzene (2) system 140

7.3 Thermodynamic Consistency Testing.....142

7.3.1 Diisopropyl ether (1) + propan-1-ol (2) system 142

7.3.2 Water (1) + propan-1-ol (2) system 143

7.3.3 Furan (1) + n-hexane (2) system 145

7.3.4 Furan (1) + methylbenzene (2) system 146

7.3.5 Root mean square deviation (direct test).....147

7.4 Relative Volatility.....147

7.3.1 Diisopropyl ether (1) + propan-1-ol (2) system 148

7.3.2 Water (1) + propan-1-ol (2) system 150

7.3.3 Furan (1) + n-hexane (2) system 151

7.4.4 Furan (1) + methylbenzene (2) system 151

7.5 Reduction of Binary LLE Data.....152

7.6 Simulation of the Propan-1-ol Dehydration Process via Azeotropic Distillation in Aspen Plus.....156

7.6.1 Thermodynamic Model Validation.....157

7.6.2 Aspen input Data.....159

7.6.3 Process Flowsheet and Simulation Sequence.....160

7.6.4 Sensitivity Analysis.....166

7.6.5 Diisopropyl Ether as an Entrainer Benchmarked Against n-Pentanol…….168

CHAPTER 8

CONCLUSIONS……..……..170

8.1 Experimental Measurements……..170

8.2 Theoretical Analysis…….... 171

8.3 Aspen Plus Simulation of the Propan-1-ol Dehydration Process……. 172

CHAPTER 9

RECOMMENDATIONS……..…173

REFERENCES…….174

Appendix A (Experimental Activity Coefficients And Relative Volatility).....…186

Appendix B (Point Test Results) …….....190

Appendix C (Experimental Data Comparison with PSRK) …….....202

Appendix D (Propan-1-ol Dehydration Process Stream Results) …….....205

LIST OF FIGURES

CHAPTER 1

Figure 1-1: An example of different classes of alcohols…….…..…....3

Figure 1-2: Hydrogen bonding between alcohol molecules…….…….5

Figure 1-3: Comparison of boiling point between alcohols and alkanes……....5

Figure 1-4: An example of two types of ethers……..……6

Figure 1-5: Chemical structure of furfural……..……8

Figure 1-6: Chemical structure of furan…….……8

Figure 1-7: A Ternary diagram for the system of ethanol + water + benzene at 101.325 kPa.10

Figure 1-8: A typical sequence of columns for heterogeneous azeotropic distillation (Doherty, 2008)…….…….10

Figure 1-9: Process flow scheme of propan-1-ol dehydration using cyclohexane (Lee and Shen, 2003)……..……..11

CHAPTER 2

Figure 2-1: The three common types of binary phase diagrams for T-x-y, P-x-y and x-y plots..... 13

Figure 2-2: The phase diagram of a ternary system exhibiting a wide miscibility gap..... 14

Figure 2-3: Flow diagram for bubble-point pressure iteration using combined method (Smith *et al.* , 2001).....24

Figure 2-4: Flow diagram for bubble-point temperature iteration using combined method (Smith *et al.* , 2001).....25

Figure 2-5: Flow diagram for bubble-point pressure iteration using direct method (Smith *et al* , 2001).....26

Figure 2-6: Flow diagram for bubble-point temperature iteration using direct method (Smith *et al* , 2001).....27

Figure 2-7: Solution algorithm developed for determination of binary interaction parameters (NRTL Model) for LLE system…….43

Figure 2-8: Frequency of best fit models for mixtures with alcohols for Dechema VLE Data Collection.....46

CHAPTER 3

Figure 3-1: Classification of experimental high pressure vapour-liquid equilibrium equipment (Raal and Mühlbauer, 1994)……...……...50

Figure 3-2: The static apparatus used for the P-x measurements (Kolbe and Gmehling, 1985)…….…….……51

Figure 3-3a: Overview of the static apparatus of Baba-Ahmed *et al*, (1999)…….……..52

Figure 3-3b: Schematic view of the cell of Baba-Ahmed *et al*, (1999)……..……...53

Figure 3-4: The original apparatus of Gillespie (1946).....54

Figure 3-5: Schematic diagram of Vapour liquid equilibrium still (Raal and Mühlbauer, 1998)…….….55

CHAPTER 4

Figure 4-1: Schematic diagrams of VLE apparatus of Lilwanth (2011)……..……60

Figure 4-2: Photograph of the dynamic VLE still used for atmospheric pressure measurements (CEP/TEP Laboratorie, Fontainebleau, France)…….……..…..62

Figure 4-3: Previously used LLE cell with auxiliary equipment……..……63

Figure 4-4: Mechanical design of new VLLE cell…….……..……65

Figure 4-5: Schematic diagram of the new VLLE apparatus used for measurements.....66

Figure 4-6 (a): Photograph of the new VLLE cell with auxiliary equipment…….……..67

Figure 4-6 (b): Photograph of a fully constructed VLLE cell.....67

Figure 4-6 (c): Photograph of a fully constructed VLLE submerged in the water bath during data measurements.....68

CHAPTER 5

Figure 5-1: Chromatograms of furan, toluene and furfural mixture, to illustrate good separation of chemical species in gas chromatograph.....73

Figure 5-2: Chromatograms of furan, toluene and furfural mixture, to illustrate poor separation of chemical species in gas chromatograph.....73

Figure 5-3: Calibration of the Pt-100 surface element for the low pressure VLE dynamic-analytic apparatus, linear relation between the actual and probe temperature…..80

Figure 5-4: Deviations from the actual temperature, resulting from the use of linear relation for the low pressure dynamic analytic VLE apparatus…….…….……80

Figure 5-5: Calibration of the pressure transducer for the low pressure VLE dynamic-analytic apparatus, linear relation between the actual and display pressure……...81

Figure 5-6: Deviations from the actual pressure, resulting from the use of a linear relation for the low pressure dynamic analytic VLE apparatus….…….……..81

Figure 5-7: Calibration of the Pt-100 surface element for the medium pressure VLE dynamic-analytic apparatus, linear relation between the actual and probe temperatures……..…….82

Figure 5-8 Deviations from the actual temperature, resulting from the use of a linear relation for the medium pressure dynamic analytic VLE apparatus……...……82

Figure 5-9: Calibration of the pressure transducer for the medium pressure VLE dynamic-analytic apparatus, second-order relation between the actual and display pressure……...…….……..83

Figure 5-10: Deviations from the actual pressure, resulting from the use of a second-order equation for the low pressure dynamic analytic VLE apparatus…….……..83

Figure 5-11: Calibration of the Pt-100 surface element for the dynamic atmospheric VLE apparatus, linear relation between the actual and probe temperatures……..…84

Figure 5-12: Deviations from the true temperature, resulting from the use of a linear relation for the dynamic atmospheric VLE apparatus……...…….…….84

Figure 5-13: Calibration of the Pt-100 surface element for the static analytic LLE apparatus, linear relation between the actual and probe temperatures….……..…….85

Figure 5-14: Deviations from the true temperature, resulting from the use of a linear relation for the static analytic LLE apparatus……...…..85

CHAPTER 6

Figure 6-1: Vapour pressure data……...…….....……....…….93

Figure 6-2: Literature vapour pressure correlation by Wagner equation from triple point to critical point for furan, n-hexane and methylbenzene…….…….....……94

Figure 6-3: TCD Calibration for the ethanol (1) + cyclohexane (2) system using the area ratio method of Raal and Muhlbauer, (1998).(Cyclohexane dilute region)…….95

Figure 6-4: TCD Calibration for the ethanol (1) + cyclohexane (2) system using the area ratio method of Raal and Muhlbauer, (1998).(Ethanol dilute region)……...95

Figure 6-5: Experimental T-x-y data for the ethanol (1) + cyclohexane (2) system at 40 kPa……..……..……..96

Figure 6-6: Experimental x-y data for the ethanol (1) + cyclohexane (2) system at 40 kPa……..……..……97

Figure 6-7: TCD Calibration for the diisopropyl ether (1) + propan-1-ol (2) system using the area ratio method of Raal and Muhlbauer,(1998). (Diisopropyl ether dilute region)…….....……..……98

Figure 6-8: TCD Calibration for the diisopropyl ether (1) + propan-1-ol (2) system using the area ratio method of Raal and Muhlbauer, (1998). (1-propanol dilute region)…..……..…98

Figure 6-9: Experimental P-x-y data for the diisopropyl ether (1) + propan-1-ol (2) system at 333.15 K……..……..……..……..……..……..…..…..……99

Figure 6-10: Experimental x-y data for the diisopropyl ether (1) + propan-1-ol (2) system at 333.15 K……..……...…….……..…100

Figure 6-11: Experimental P-x-y data for the diisopropyl ether (1) + propan-1-ol (2) system at 353.15 K……..……...…….101

Figure 6-12: Experimental x-y data for the diisopropyl ether (1) + propan-1-ol (2) system at 353.15 K……..…..……...…101

Figure 6-13: Experimental P-x-y data for the diisopropyl ether (1) + propan-1-ol (2) system at 373.15 K……...……102

Figure 6-14: Experimental x-y data for the diisopropyl ether (1) + propan-1-ol (2) system at 373.15 K……..……..…..…..103

Figure 6-15: TCD Calibration for the water (1) + propan-1-ol (2) system using the area ratio method of Raal and Muhlbauer, (1998). (Water dilute region)…….…….….104

Figure 6-16: TCD Calibration for the water (1) + propan-1-ol (2) system using the area ratio method of Raal and Muhlbauer,(1998). (1-propanol dilute region)…...…….....104

Figure 6-17: Experimental P-x-y data for the water (1) + propan-1-ol (2) system at 358.15 K……..……..…105

Figure 6-18: Experimental x-y data for the water (1) + propan-1-ol (2) system at 358.15 K……..……...……..……106

Figure 6-19: Experimental P-x-y data for the water (1) + propan-1-ol (2) system at 368.15 K…….……...……..…….107

Figure 6-20: Experimental x-y data for the water (1) + propan-1-ol (2) system at 368.15 K…….……..……..…….107

Figure 6-21: Liquid density against temperature for system furan (1) + n-hexane (2) at different molar composition of furan…….…….109

Figure 6-22: Absolute deviation of composition-density model equation, from the measured values for the system furan (1) + n-hexane (2) at 298.15 K……...…....109

Figure 6-23: Excess Volume against molar composition for the furan (1) + n-hexane (2) system at different isothermal temperatures in comparison with Redilich-Kister correlation……...…….110

Figure 6-24: Experimental T-x-y data for the system of furan (1) + n-hexane (2) at 101.3 kPa.....111

Figure 6-25: Experimental x-y data for the system of furan (1) + n-hexane (2) at 101.3 kPa.....111

Figure 6-26: Liquid density against temperature for system furan (1) + methylbenzene (2) at different molar composition of furan…….…….….113

Figure 6-27: Absolute deviation of composition-density model equation, from the measured values for the system furan (1) + methylbenzene(2) at 298.15 K……..…..….113

Figure 6-28: Excess Volume against molar composition for the furan (1) + methylbenzene (2) system at different temperatures in comparison with Redilich-Kister correlation……...…….……114

Figure 6-29: Experimental T-x-y data for the system of furan (1) + methylbenzene (2) at 101.3 kPa.....115

Figure 6-30: Experimental x-y data for the system of furan (1) + methylbenzene (2) at 101.3 kPa.....115

Figure 6-31: Absolute Deviation % of correlated furfural mole fraction from measured values……...…….……...116

Figure 6-32: Absolute Deviation % of correlated n-hexane mole fraction from measured values……...……...…….116

Figure 6-33: Absolute Deviation % of correlated water mole fraction from measured values…….…….…….117

Figure 6-34: Absolute Deviation % of correlated furan mole fraction from measured values……..…..117

Figure 6-35: Experimental and literature T-x data for furfural (1) + n-hexane (2) system at atmospheric pressure.....118

Figure 6-36: Experimental T-x data for water (1) + furan (2) system at atmospheric pressure.....119

CHAPTER 7

Figure 7-1: Experimental VLE and modeling results, comparison between PR, HOC and NTH model fits to P-x-y data for the diisopropyl ether (1) + propan-1-ol (2) system at 333.15 K…….……..…….125

Figure 7-2: Experimental VLE and modeling results, comparison between PR, HOC and NTH model fits to x-y data for the diisopropyl ether (1) + propan-1-ol (2) system at 333.15 K……..…….125

Figure 7-3: Experimental VLE and modeling results, comparison between NRTL, WILSON and UNIQUAC model fits to P-x-y data for the diisopropyl ether (1) + propan-1-ol (2) system at 333.15 K……..…….…..……....126

Figure 7-4: Experimental VLE and modeling results, comparison between NRTL, WILSON and UNIQUAC model fits to x-y data for the diisopropyl ether (1) + propan-1-ol (2) system at 333.15 K……..……..126

Figure 7-5: Experimental VLE and modeling results, comparison between HOC, NTH and PR model fits to P-x-y data for the diisopropyl ether (1) + propan-1-ol (2) system at 353.15 K…….…….……..127

Figure 7-6: Experimental VLE and modeling results, comparison between HOC, NTH and PR model fits to x-y data for the diisopropyl ether (1) + propan-1-ol (2) system at 353.15 K……..127

Figure 7-7: Experimental VLE and modeling results, comparison between Wilson, UNIQUAC and NRTL model fits to P-x-y data for the diisopropyl ether (1) + propan-1-ol (2) system at 353.15 K……..…….…….……128

Figure 7-8: Experimental VLE and modeling results, comparison between Wilson, UNIQUAC and NRTL model fits to x-y data for the diisopropyl ether (1) + propan-1-ol (2) system at 353.15 K…….…….……...……...128

Figure 7-9: Experimental VLE and modeling results, comparison between PR, HOC and NTH model fits to P-x-y data for the diisopropyl ether (1) + propan-1-ol (2) system at 373.15 K…….……...…….…….….129

Figure 7-10: Experimental VLE and modeling results, comparison between PR, HOC and NTH model fits to x-y data for the diisopropyl ether (1) + propan-1-ol (2) system at 373.15 K…….……..…….…..129

Figure 7-11: Experimental VLE and modeling results, comparison between NRTL, WILSON and UNIQUAC model fits to P-x-y data for the diisopropyl ether (1) + propan-1-ol (2) system at 373.15 K…….…….…..……..……..130

Figure 7-12: Experimental VLE and modeling results, comparison between NRTL, WILSON and UNIQUAC model fits to x-y data for the diisopropyl ether (1) + 1-propanol (2) system at 373.15 K……..……..……...…..…130

Figure 7-13: Comparison between the experimentally determined liquid-phase activity coefficients and those calculated from the NRTL, Wilson and UNIQUAC model with Peng-Robinson the di-isopropyl ether (1) + propan-1-ol (2) system at 333.15 K…….……..……..…….131

Figure 7-14: Comparison between the experimentally determined liquid-phase activity coefficients and those calculated from the NRTL, Wilson and UNIQUAC model with Peng-Robinson equation, for the diisopropyl ether (1) + propan-1-ol (2) system at 353.15 K……...…..….131

Figure 7-15: Comparison between the experimentally determined liquid-phase activity coefficients and those calculated from the NRTL, Wilson and UNIQUAC model

with Peng-Robinson equation, for the diisopropyl ether (1) + propan-1-ol (2) system at 373.15 K……..……...…….…..…131

Figure 7-16: Experimental VLE and modeling results, comparison between PR, HOC and NTH model fits to P-x-y data for the water (1) + propan-1-ol (2) system at 358.15 K……..……..……...……..133

Figure 7-17: Experimental VLE and modeling results, comparison between PR, HOC and NTH model fits to x-y data for the water (1) + propan-1-ol (2) system at 358.15 K……...……..…..133

Figure 7-18: Experimental VLE and modeling results, comparison between NRTL, WILSON and UNIQUAC model fits to P-x-y data for the water (1) + propan-1-ol (2) system at 358.15 K……...…...…….134

Figure 7-19: Experimental VLE and modeling results, comparison between NRTL, WILSON and UNIQUAC model fits to x-y data for the water (1) + propan-1-ol (2) system at 358.15 K…….…...……134

Figure 7-20: Experimental VLE and modeling results, comparison between PR, HOC and NTH model fits to P-x-y data for the water (1) + propan-1-ol (2) system at 368.15 K……..…….……...……..135

Figure 7-21: Experimental VLE and modeling results, comparison between PR, HOC and NTH model fits to x-y data for the water (1) + propan-1-ol (2) system at 368.15 K……..……...…….135

Figure 7-22: Experimental VLE and modeling results, comparison between NRTL, WILSON and UNIQUAC model fits to P-x-y data for the water (1) + propan-1-ol (2) system at 368.15 K…….…...……136

Figure 7-23: Experimental VLE and modeling results, comparison between NRTL, WILSON and UNIQUAC model fits to x-y data for the water (1) + propan-1-ol (2) system at 368.15 K……...……136

Figure 7-24: Comparison between the experimentally determined liquid-phase activity coefficients and those calculated from the NRTL, Wilson and UNIQUAC model with Hayden and O'Connell correlation, for the water (1) + propan-1-ol (2) system at 358.15 K……..……..…137

Figure 7-25: Comparison between the experimentally determined liquid-phase activity coefficients and those calculated from the NRTL, Wilson and UNIQUAC model with Hayden and O'Connell correlation, for the water (1) + propan-1-ol (2) system at 368.15 K…….……..137

Figure7-26: Experimental VLE and modeling results, comparison between NRTL, WILSON and UNIQUAC model fits to T-x-y data for the furan (1) + n-hexane (2) system at 101.3 kPa.....138

Figure 7-27: Experimental VLE and modeling results, comparison between NRTL, WILSON and UNIQUAC model fits to x-y data for the furan (1) + n-hexane (2) system at 101.3 kPa.....139

Figure 7-28: Comparison between the experimentally determined liquid-phase activity coefficients and those calculated from the NRTL, Wilson and UNIQUAC model with Peng-Robinson the furan (1) + n-hexane (2) system at 101.3 kPa….....139

Figure 7-29: Comparison between NRTL and UNIQUAC model fits to T-x-y data for the furan (1) +methylbenzene (2) system at 101.3 kPa.....140

Figure 7-30: Comparison between NRTLand UNIQUAC model fits to x-y data for the furan (1) + toluene (2) system at 101.3 kPa.....141

Figure 7-31: Comparison between the experimentally determined liquid-phase activity coefficients and those calculated from the NRTL, Wilson and UNIQUAC model with Peng-Robinson the furan (1) + methylbenzene (2) system at 101.3 kPa….141

Figure 7-32: Deviation of the PR-NRTL model activity coefficients from the experimental values for the diisopropyl ether (1) + propan-1-ol (2) system.....143

Figure 7-33: Deviation of the HOC-NRTL model activity coefficients from the experimental values for the water (1) + propan-1ol (2) system.....144

Figure 7-34: Deviation of the PR-NRTL model activity coefficients from the experimental values for the furan (1) + n-hexane (2) system at 101.3 kPa.....145

Figure 7-35: Deviation of the PR-NRTL model activity coefficients from the experimental values for the furan (1) + methylbenzene (2) system at 101.3 kPa.....146

Figure 7-36: Comparison between the experimentally determined relative volatility and values calculated from the NRTL, Wilson and UNIQUAC model with Peng-Robinson the diisopropyl ether (1) + propan-1-ol (2) system at 333.15 K…….....148

Figure 7-37: Comparison between the experimentally determined relative volatility and values calculated from the NRTL, Wilson and UNIQUAC model with Peng-Robinson the diisopropyl ether (1) + propan-1-ol (2) system at 353.15 K……..……149

Figure 7-38: Comparison between the experimentally determined relative volatility and values calculated from the NRTL, Wilson and UNIQUAC model with Peng-Robinson the diisopropyl ether (1) + propan-1-ol (2) system at 373.15 K……..…....149

Figure 7-39: Comparison between the experimentally determined relative volatility and values calculated from the NRTL, Wilson and UNIQUAC model with Hayden and O'Connell technique the water (1) + propan-1-ol (2) system at 358.15 K……..150

Figure 7-40: Comparison between the experimentally determined relative volatility and values calculated from the NRTL, Wilson and UNIQUAC model with Hayden and O'Connell technique the water (1) + propan-1-ol (2) system at 368.15 K……..150

Figure 7-41: Comparison between the experimentally determined relative volatility and values calculated from the NRTL, Wilson and UNIQUAC model with Peng-Robinson for the system of furan (1) + n-hexane (2) at 101.3 kPa.....151

Figure 7-42: Comparison between the experimentally determined relative volatility and values calculated from the NRTL, Wilson and UNIQUAC model with Peng-Robinson for the system of furan (1) + methylbenzene (2) at 101.3 kPa.....151

Figure 7-43: Experimental LLE and modeling results, comparison between NRTL and Cox-Herington model fits to T-x data for furfural (1) + n-hexane (2) system at 101.3 kPa……..…….154

Figure 7-44: Selectivity for furfural (1) + n-hexane (2) system in comparison with NRTL model calculation……..…….…….……155

Figure 7-45: Experimental LLE and NRTL modeling fit to T-x data for water (1) + furan (2) system at 101.3 kPa…….……..……...…155

Figure 7-46: Selectivity data for water (1) + furan (2) system at atmospheric pressure…….156

Figure 7-47: Model validation with experimental data for water (1) + propan-1-ol (2) binary system at 358.15 K…….…….158

Figure 7-48: Model validation with experimental data for diisopropyl ether (1) + propan-1-ol (2) binary system at 353.15 K……...…….…..158

Figure 7-49: Comparison of HOC-NRTL and UNIFAC models with measured data for (water + propan-1-ol + diisopropyl ether) system at 308.2 K……...…...…….159

Figure 7-50: The propan-1-ol dehydration process via azeotropic distillation of water (1) + propan-1-ol (2) using diisopropyl ether as an entrainer….……....…162

Figure 7-51: Aspen Plus flowsheet of the propan-1-ol dehydration process via azeotropic distillation of water (1) + propan-1-ol (2) using diisopropyl ether as an entrainer …….163

Figure 7-52: Composition profile in the azeotropic column……..…..…….……165

Figure 7-53: Composition profile in the first recovery column……..……..165

Figure 7-54: Composition profile in the second recovery column…….....…..166

Figure 7-55: Sensitivity analysis of propan-1-ol purity against solvent (DIPE) molar flow..167

Figure 7-56: Sensitivity analysis of propan-1-ol purity against feed stage of the solvent.….167

Figure 7-57: Model prediction for propan-1-ol (1) + n-pentanol (2) binary system at 353.15 K…….……..169

Appendix B

Figure B-1: Point test (varying EoS) pressure-residual for the diisopropyl ether (1) + propan-1-ol (2) system at 333.15 K……..……...190

Figure B-2: Point test (varying EoS) Δy_1 for the diisopropyl ether (1) + propan-1-ol (2) system at 333.15 K…….…..…190

Figure B-3: Point test (varying activity coefficient model): pressure-residual for the diisopropyl ether (1) + propan-1-ol (2) system at 333.15 K……..……..191

Figure B-4: Point test (varying activity coefficient model): Δy_1 for the diisopropyl ether (1) + propan-1-ol (2) system at 333.15 K……..……...191

Figure B-5: Point test (varying EoS) pressure-residual for the diisopropyl ether (1) + propan-1-ol (2) system at 353.15 K….……..……..192

Figure B-6: Point test (varying EoS) Δy_1 for the diisopropyl ether (1) + propan-1-ol (2) system at 353.15 K……..……192

Figure B-7: Point test (varying activity coefficient model) pressure-residual for the diisopropyl ether (1) + propan-1-ol (2) system at 353.15 K……..……..193

Figure B-8: Point test (varying activity coefficient model) Δy_1 for the diisopropyl ether (1) + propan-1-ol (2) system at 353.15 K……..……...193

Figure B-9: Point test (varying EoS) pressure-residual for the diisopropyl ether (1) + propan-1-ol (2) system at 373.15 K……...……...194

Figure B-10: Point test (varying EoS) Δy_1 for the diisopropyl ether (1) + propan-1-ol (2) system at 373.15 K……...……194

Figure B-11: Point test (varying activity coefficient model) pressure-residual for the diisopropyl ether (1) + propan-1-ol (2) system at 373.15 K……..……..195

Figure B-12: Point test (varying activity coefficient model) Δy_1 for the diisopropyl ether (1) + propan-1-ol (2) system at 373.15 K……..……...195

Figure B-13: Point test (varying EoS) pressure-residual for the water (1) + propan-1-ol (2) system at 358.15 K……...……196

Figure B-14: Point test (varying EoS) Δy_1 for the water (1) + propan-1-ol (2) system at 358.15 K……..……196

Figure B-15: Point test (varying activity coefficient model) pressure-residual for the water (1) + propan-1-ol (2) system at 358.15 K……..……...197

Figure B-16: Point test (varying activity coefficient model) Δy_1 for the water (1) + propan-1-ol (2) system at 358.15 K……..…..197

Figure B-17: Point test (varying EoS) pressure-residual for the water (1) + propan-1-ol (2) system at 368.15 K……..……198

Figure B-18: Point test (varying EoS) Δy_1 for the water (1) + propan-1-ol (2) system at 368.15 K……198

Figure B-19: Point test (varying activity coefficient model): pressure-residual for the water (1) + propan-1-ol (2) system at 368.15 K……199

Figure B-20: Point test (varying activity coefficient model): Δy_1 for the water (1) + propan-1-ol (2) system at 368.15 K……..199

Figure B-21: Point test (varying activity coefficient model): temperature-residual for the furan (1) + n-hexane (2) system at 101.3 kPa…….....200

Figure B-22: Point test (varying activity coefficient model): Δy_1 for the furan (1) + n-hexane (2) system at 101.3 kPa…….200

Figure B-23: Point test (varying activity coefficient model), temperature-residual for the furan (1) + methylbenzene (2) system at 101.3 kPa…….201

Figure B-22: Point test (varying activity coefficient model), Δy_1 for the furan (1) + methylbenzene (2) system at 101.3 kPa……201

Appendix C

Figure C-1: Comparison of the experimental and predicted data for diisopropyl ether (1) + propan-1-ol (2) at 333.15 K……202

Figure C-2: Comparison of the experimental and predicted data for diisopropyl ether (1) + propan-1-ol (2) at 353.15 K……...……...……202

Figure C-3: Comparison of the experimental and predicted data for diisopropyl ether (1) + propan-1-ol (2) at 373.15 K……...203

Figure C-4: Comparison of the experimental and predicted data for water (1) + propan-1-ol (2) at 358.15 K……...203

Figure C-5: Comparison of the experimental and predicted data for water (1) + propan-1-ol (2) at 358.15 K……...204

LIST OF TABLES

CHAPTER 2

Table 2-1: The mathematical relation of the Peng and Robinson equation of state ……..28

Table 2-2: The mathematical relation of the Wong and Sandler mixing rule ……...……..29

Table 2-3: Consistency Table for the direct test……..……..48

CHAPTER 5

Table 5-1: Purity of chemicals used in this project……..…….79

Table 5-2: Operating conditions for the Shimadzu 2010 gas chromatograph……...….86

Table 5-3: Operating conditions for the Shimadzu 2014 gas chromatograph……..……...86

Table 5-4: Specifications for columns used for GC analyses……..…87

CHAPTER 6

Table 6-1: Experimental uncertainties for temperature, pressure, and mole fraction of the VLE binary systems ……...…90

Table 6-2: Measured vapour pressure data ……...……..……...91

Table 6-3: Comparison between literature vapour pressure data and values calculated with the Wagner equation for furan……...…….... 93

Table 6-4: Comparison between literature vapour pressure data and values calculated with the Wagner equation for methylbenzene and n-hexane…….……93

Table 6-5: Vapour-liquid equilibrium data for the cyclohexane (1) + ethanol (2) system at 40 kPa…….…….96

Table 6-6: P-x-y data for diisopropyl ether (1) + propan-1-ol (2) at 333.15 K……....…..…99

Table 6-7: P-x-y data for diisopropyl ether (1) + propan-1-ol (2) at 353.15 K…..…….…100

Table 6-8: P-x-y data for diisopropyl ether (1) + propan-1-ol (2) at 373.15 K…..……102

Table 6-9: P-x-y data for water (1) + propan-1-ol (2) system at 358.15 K…….…..105

Table 6-10: P-x-y data for water (1) + propan-1-ol (2) system at 368.15 K……..……106

Table 6-11: Density data for furan (1) + n-hexane (2) at selected temperatures……..…108

Table 6-12: T-x-y data for furan (1) + n-hexane (2) at 101.3 kPa……..……110

Table 6-13: Density data for furan (1) + methylbenzene (2) at selected temperatures…...…112

Table 6-14: T-x-y data for furan (1) + methylbenzene (2) at 101.3 kPa…….…...…….114

Table 6-15: Binary LLE data for furfural (1) + n-hexane 2) system……...…118

Table 6.16: Binary LLE data for water (1) + furan (2) system…….……...…119

CHAPTER 7

Table 7-1: Parameter values regressed from the vapour data with the Wagner equation.…121

Table 7-2: Parameter values regressed from the vapour data with Antoine equation……...112

Table 7-3: Modeling Result for diisopropyl ether (1) + propan-1-ol (2) system……...…..124

Table 7-4: Modeling result for water (1) + propan-1-ol (2) system…….....….132

Table 7-5: Modeling results for: furan (1) + n-hexane (2) system at 101.3 kPa……...138

Table 7-6: Modeling results for: furan (1) + methylbenzene (2) system at 101.3 kPa…….140

Table 7-7: Results of the thermodynamic consistency testing for the diisopropyl ether (1) + propan-1-ol (2) systems at 333.15, 353.15 and 373.15 K.....142

Table 7-8: Results of the thermodynamic consistency testing for the water (1) + propan-1-ol (2) systems at 358.15 , 368.15 K.....144

Table 7-9: Furan (1) + n-hexane (2) system at 101.3 kPa.....145

Table 7-10: Furan (1) + methylbenzene (2) system at 101.3 kPa.....146

Table 7-11: Root Mean Square deviation between model and experimental activity coefficient – Van Ness (1995) direct test.....147

Table 7-12: NRTL binary interaction parameters for LLE system…….153

Table 7-13: Cox-Herington regression parameters for LLE system……..…..154

Table 7-14: Azeotropic column initial input data used in the simulation…….…….160

Table 7-15: Column specifications for the propan-1-ol dehydration process……..…..…….164

Table 7-16: Comparison between DIPE and n-pentanol as potential extraction solvent…....168

Appendix A

Table A-1: Experimental activity coefficient and relative volatility data for diisopropyl ether (1) + propan-1-ol (2) system at 333.15, 353.15 and 373.15 K…….....…..….186

Table A-2: Experimental activity coefficient and relative volatility data for water (1) + propan-1-ol (2) system at 358.15 , 368.15 K……..…….187

Table A-3: Experimental activity coefficient and relative volatility data for furan (1) + n-hexane (2) system at 101.3 kPa……..……..……188

Table A-4: Experimental activity coefficient and relative volatility data for furan (1) + methylbenzene (2) system at 101.3 kPa……...189

Appendix D

Table D-1: Stream results for the propan-1-ol dehydration process……205

NOMENCLATURE

English Letters

a_i	Activity of liquid
A_i	Constant in the Antoine equation
a_{ij}	Constants for temperature dependency of model parameters
B_i	Constant in the Antoine equation
B_{ii}	Second virial coefficient of pure component *i* [cm3/mol]
b_{ij}	Constants for temperature dependency of model parameters
B_{ij}	Second virial coefficient for species $_i$ – species $_j$ interaction [cm^3/mol]
C_i	Constant in the Antoine equation
c_{ij}	Constants for temperature dependency of model parameters
d_{ij}	Constants for temperature dependency of model parameters
f	Fugacity [kPa]
$\hat{f}$	Fugacity in solution [kPa]
f_i	Fugacity of the pure component *i* [kPa]
G_i	Molar or specific Gibbs energy [J/mol]
$\bar{G}_i$	Partial molar Gibbs free energy
g_{ij}-g_{ii}	Parameter in NRTL (1968) model representing interactions between species
H	Enthalpy [J/mol]
$\bar{H}_i$	Partial molar Helmholtz energy
l	Parameter in the UNIQUAC (1975) model
n_i	Number of moles of component *i*
N	Number of chemical species or components present in a system
P	System pressure [kPa]
P_i^{sat}	Pure component vapour pressure [kPa]

q_i	Pure component area parameter in the UNIQUAC (1975) model
r_i	Pure component volume parameter in the UNIQUAC (1975) model
R	Universal gas constant [J/mol.K]
S	Molar or specific entropy
T	System temperature [^{0}C or K]
U	Molar or specific internal energy
V	Molar or specific volume [cm^3/mol]
$\bar{V}_i$	Partial molar volume
x	Liquid phase mole fraction (or composition)
y	Vapour phase mole fraction (or composition)

Greek Letters

α_{ij}	Non-randomness parameter in NRTL (1968) model
γ_i	Activity coefficient of component *i*
δ	Denotes a residual (e.g. δP)
Δ	Denotes the residual for the point test
θ_i	Area fractions in UNIQUAC (1975) equation
Φ_{ij}	Segment fractions in UNIQUAC (1975) equation
$\lambda_{ij} - \lambda_{ii}$	Parameter representing interactions between species in the Wilson (1964) model
Λ_{ij}	Parameter in Wilson (1964) model
μ	Chemical potential of component i
π	Number of phases present in a system (Gibbs phase rule)
τ_{ij}	Parameter in the NRTL (1968) model and UNIQUAC (1975) model

φ	Fugacity coefficient
$\widehat{\varphi}_i$	Fugacity coefficient of component *i* in solution
Φ	Ratio of fugacity coefficients, with the Poynting correction factor

Subscript

1	Denotes component 1
2	Denotes component 2
c	Denotes a critical property
i	Denotes component *i*

Superscript

E	Denotes an excess property
id	Denotes an ideal solution
l	Denotes the liquid phase
lit	Refers to literature data
sat	Denotes a saturated value
v	Denotes the vapour phase

Abbreviations

AAD	Average absolute deviation
EoS	Equation of state
LLE	Liquid liquid equilibrium
RMS	Root mean square
VLE	Vapour liquid equilibrium
VLLE	Vapour liquid-liquid equilibrium

CHAPTER 1

INTRODUCTION

Most industrial companies use distillation for critical separation of various reaction mixtures into useful final products. The technique can be traced back to middle ages where it was used in the manufacture of brandy from wine (The distillation group Inc, 2010). The technique grew to be famous and has been applied for years by various industries which include petrochemical refining, chemical processes, natural gas processing, etc. Various distillation methods have been developed over the years with respect to different applicability of each. These include conversional distillation, azeotropic and extractive distillation. The common basis of these techniques is phase equilibria, and they involve either vapour-liquid equilibrium (VLE) or vapour-liquid-liquid equilibrium (VLLE).

The design and simulation of such distillation processes rely on accurate phase equilibrium data (VLE, LLE, solubility). The major problem often faced by process designers is the scarcity of experimental data in literature for various systems, thus imposing difficulties in designing separation process for specific systems. To resolve this issue, industries have employed estimation methods (use of thermodynamic models) to predict phase behavior for particular systems of interest. Most importantly, the models used for phase behavior predictions require a set of experimental data points to adjust model parameters in order to proper correlate the system of interest (Ashour and Aly, 1996). It is also important to note that most industrial systems are often comprised of chemicals that are dissimilar in nature, thus prediction methods can lead to unreliable design which can prove to be costly for the entire chemical plant. Such losses can be observed when small errors between experimental and predicted data are neglected in the final design and proved to turn into significant errors during the distillation column operation. Based on these facts, it is unquestionable that a set of experimental data is necessary for both process design and improvement of predicted data by introducing model parameters obtained from measured data.

This project was conceived in response to the need for VLE and VLLE data for the separation of mixtures containing oxygenated compounds (alcohols, furanics, ketones etc). These compounds originate in chemical reactions such as thermal decomposition of biomass, cellulose lignin etc. Alternatively, they are formed as by-products of various petrochemical processes and their recovery is of high importance in the petrochemical industry. This work closely looks at phase behavior of light alcohols in the present of water. The occurrence of azeotrope in the light alcohol-water systems limits the use of tradition distillation for such systems, as it is economically unfeasible for recovery of highly pure products. The measured VLE data will be used in the design and simulation of separation processes (e.g. heterogeneous azeotropic distillation) to recover the light alcohols from water. The systems involving ethers and alcohols have also been associated with gasoline blending to improve knocking efficiency in motor engines and minimize contamination of automobile catalyst (Alonso-Trist´an *et al*, 2006). As a result, proper characterization of these systems provides a good insight with regards to possibilities in gasoline blending with such mixtures. The phase equilibrium data obtained will also contribute towards availability of data in open literature. The aim of this project is to measure and model phase equilibrium data for the systems consisting of:

- Propan-1-ol + water
- Propan-1-ol + diisopropyl ether (DIPE)

These systems were chosen based on the need for recovering 1-propanol from water (propan-1-ol dehydration) using advanced distillation techniques (azeotropic and extractive distillation). A further discussion of propan-1-ol dehydration is presented in section 1.2.

The project also involves measurements of phase equilibrium data for biofuels, undertaken at the CEP/TEP laboratory in France. The biofuels are good alternative energy sources, and further understanding of their phase equilibrium behavior is critical for their integration to process level. The thermodynamic behavior of the furanic compounds with hydrocarbons is closely addressed to generate phase diagrams. In addition the presence of water is critical in the study as it create liquid-liquid split which has detrimental effects on fuel. The measured data are correlated using

appropriate thermodynamic models, to acquire model parameters that can be used for design and analysis of distillation and allied separation processes.

1.1 Review of Ethers, Alcohols and Biofuel Constituents

This section provides a brief description of some of the properties of the chemical compounds used in this work.

1.1.1 Alcohols

The existence of alcohol compounds is owed to development of processes such as fermentation of molasses, oil pyrolisis and normal oxidation of hydrocarbons. They are characterized by OH group referred to as hydroxy group. The -OH group gives rise high polarity of the alcohols thus their boiling point is found to be higher than that of hydrocarbons with same number of carbon atoms. Alcohols can be classified into three groups: i) primary alcohol; where the hydroxyl group is bonded to one R group (e.g. CH3CH2-), ii) secondary alcohol; where the hydroxyl group is bonded to a carbon atom with two R groups attached to the carbon atom, and iii) tertiary alcohol for which the hydroxyl group is bonded to a carbon atom with three R groups attached (Petrucci *et al*, 2006). Another notable factor in classifying the alcohols is observed when they are subjected to air/oxygen. The primary alcohols are oxidized to aldehydes and further to carboxylic acids with excess oxygen, while secondary alcohols can only be oxidized to ketones. The structure of tertiary alcohol suggests no oxidation of such to a different compound.

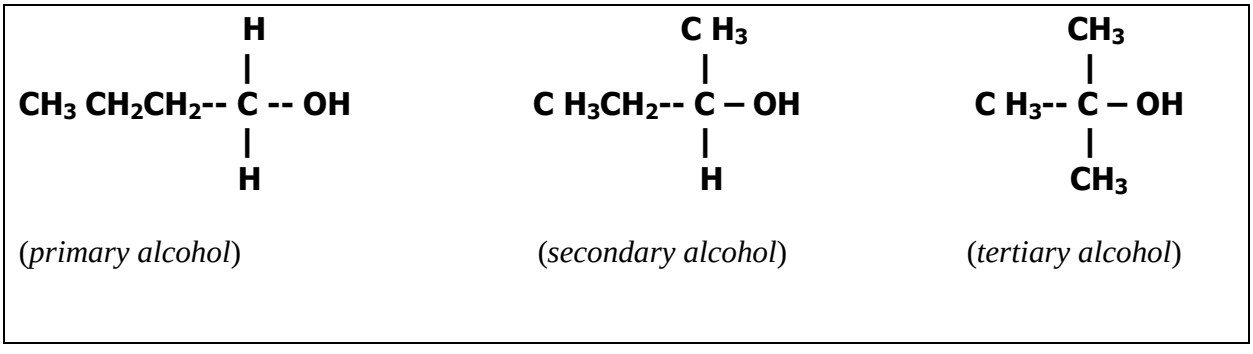

Figure 1-1: An example of different classes of alcohols (Petrucci *et al*. 2006)

1.1.1.1 Uses of Alcohols

Various uses of alcohols have been found in the both industry and general public. The difference of one carbon atom in alcohols can be found to completely change the chemical nature of one alcohol from another; in particular methanol is considered extremely poisonous when swallowed, attacks the nervous system and optic nerve (causing blindness/death), while ethanol on the other hand is used in the manufacture of alcoholic beverages (Introducing Alcohols, 2010).In some cases, ethanol has been used as a biofuels (bio-ethanol for running certain engines. For instance, ethanol is blended with gasoline forming alcohol–gasoline blends. The blending improves fuel's octane rating and reduces carbon monoxide emissions in spark ignition engines (Alonso-Trist´an *et al.* 2006). The most common industrial use of alcohols: is used as a solvent in the recovery of certain non polar compounds.

1.1.1.2 Hydrogen Bonding in Alcohols

Hydrogen bonding can be described as the bonding formed when a hydrogen (H+) atom bonded to one highly electronegative atom is simultaneously attracted to another highly electronegative atom(oxygen in case of alcohols) in the neighboring molecule. The electronegative atom which is covalently bonded to the hydrogen atom attracts and pulls away electron density from the H nucleus, leaving a proton which is attracted to a lone pair of electrons on a electronegative atom of a neighboring molecule (Petrucci *et al*. 2006). Figures 1-2 and 1-3 show the hydrogen bonding in alcohols and boiling point comparison of alcohols with alkanes respectively. The latter figure illustrate the effect of hydrogen bonding on the physical properties of alcohols due to formation of double molecules: for example during boiling, extra heat is required to break the bonds. It is important to note that alcohol molecules with two or more -OH groups have the highest probability of forming hydrogen bonds, thus these will have higher boiling temperatures and greater viscosities compared to simple alcohols.

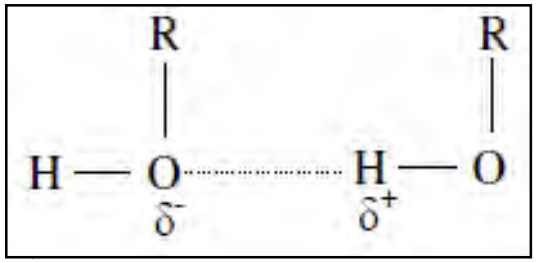

Figure 1-2: Hydrogen bonding between alcohol molecules (Introducing alcohols, 2010)

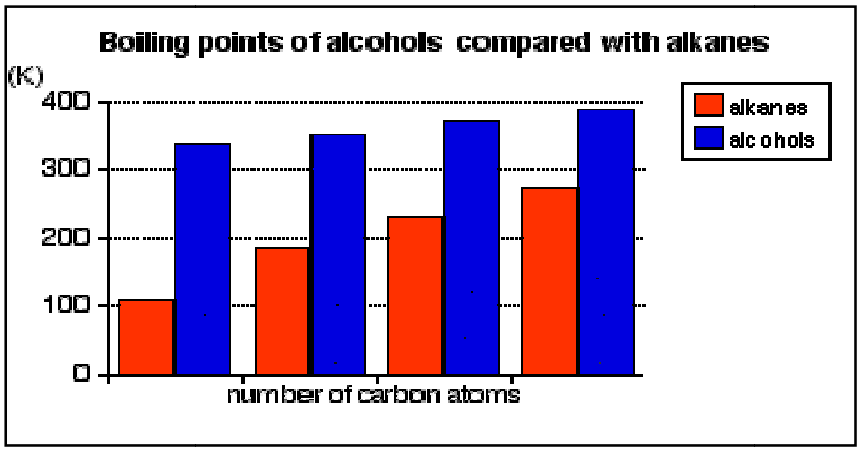

Figure 1-3: Comparison of boiling point between alcohols and alkanes (Introducing alcohols, 2010).

1.1.1.3 Solubility of Alcohols in Water

Light alcohols are completely soluble in water. A mixture of any proportion of light alcohol and water results in a single solution. However a decrease in solubility of alcohols is observed from four carbons onwards, resulting in two liquid phases when mixed with water. This is because alcohols display two solubility trends where the non polar R group (carbon chain) tends to inhibit solubility, while the hydroxyl group (OH^-) promotes solubility.

1.1.2 Ethers

Ethers are compounds with a general formula R–O–R. They are normally formed by the elimination of water from two alcohol molecules using strong dehydrating agent (e.g. concentrated sulphuric acid), Petrucci *et al*. 2006). The structure of the ethers makes them comparably non-reactive; this is shown by the stability of the linkage to most oxidizing and

reducing agents. Below are the structures of two types of ethers: acyclic (straight chain) and cyclic. Although comparably non-reactive with most organic compounds, they are highly flammable and can form violently explosive peroxides, thus they should be handled with high precaution.

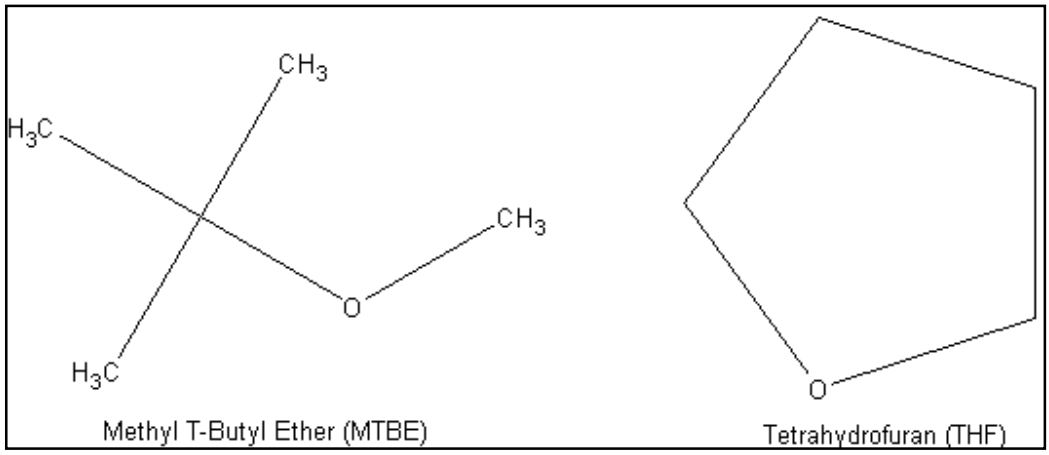

Figure 1-4: An example of two types of ethers (Wikibooks, 2010)

1.1.2.1 Uses of Ethers

Ethers have been found to have great a contribution in gasoline blending. MTBE in particular has been extensively used in replacing lead to improve anti-knocking in motor engines. The only limitation with MTBE is the relative high solubility in water. It has also been found to contaminate ground water. Various ethers are continuously investigated for gasoline blending to improve on the limitations of using MTBE (Alonso-Trist´an *et al*. 2006). Other ethers such as diethyl ether and methyl propyl ether have been extensively used as anesthetics (Wikibooks, 2010). Other important use of ethers is as a solvent in recovery of non-polar compounds.

1.1.2.2 Solubility of Ethers in Water

Ethers are not highly soluble in water, and are often considered immiscible with water. The oxygen atom in ethers is responsible for their slight solubility in water; this is observed in small molecular weight ethers such as dimethyl ether, while solubility in large molecular weight ethers can be considered negligible.

1.1.3 Biofuels and its Constituents

Biomass energy can be traced back to prehistoric times, where thermal conversion of wood in the form of fire was used to provide heating and cooking. To date the biomass energy in form of liquid extracted from plants forms part of petroleum blends in biofuels. According to the International Energy Outlook (2008), biomass energy forms around 50 % of the worlds renewable energy sources. This is owed to the variety of raw materials such as forestry residues, common crops and algae, which all can be used as biomass source. Depending on the raw material used, a spectrum of products obtained from biomass includes biogas, biochar, bio-alcohol (bio-ethanol) and biodiesel (Tan and Culaba, 2004). The fruitful benefits for use biomass derived fuel is the carbon neutrality which is based on carbon recycle (i.e. the carbon emission from biomass is reabsorbed by plants for growth via photosynthesis. The plants are then processes as biomass energy source).

The ever increasing industrialization and motorization of the world has promoted a steep rise for the demand of petroleum-based fuels, thus a major focus on development of alternative fuel sources (Renewable Energy Policy Network for the 21st Century, 2009). Avantium, which spun-off from Shell in 2000, is one of the successful organizations that focus on the development of second generation biofuels and catalytic processes for the efficient production of novel biofuels and bio-based chemicals. They derive their furan-based biofuels from a chemical intermediate HMF (hydroxyl methyl furfural, $C_6H_6O_3$), which is synthesized from furfural. Furfural, a biofuels basis is obtained as a by-product in the production of sugar. It is an oily, colorless liquid compound which turns yellow to dark brown when exposed to air. Another basic compound important in biofuels is furan, which is one of a class of heterocyclic aromatic compounds. It is characterized by five-membered ring structure consisting of four CH_2 groups and one oxygen atom. It is a clear, volatile and mildly toxic liquid with a significantly solubility in water.

The study of phase equilibrium for furfural and furanic compounds is of high importance in the in the production of biofuels. As a result, liquid-liquid equilibrium (LLE) data measurements and development of theoretical models for systems consisting of these compounds is of high importance in the design of extraction process (Kumar and Mohan, 2011). LLE studies have been conducted in the past for systems consisting of furfural alcohol with most the recent studies

conducted by Letcher *et al.* (2003); with furfural + aromatics (benzene, toluene, xylenes) + alkanes (hexane, dodecane, hexadecane) and Skrollahzadeh *et al* (2008), with the removal of benzene and toluene from AW-406 (petroleum solvent) tetrahydrofurfuryl alcohol and water solvents. Figures 1-5 and 1-6 below shows the chemical structures of furfural and furan respectively.

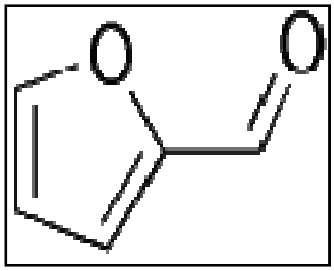

Figure 1-5. Chemical structure of furfural (Wikibooks. 2011).

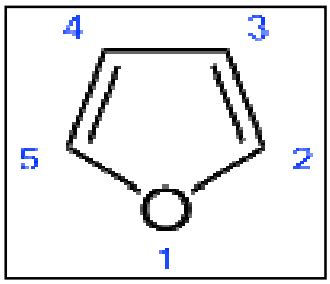

Figure 1-6. Chemical structure of furan (Wikibooks, 2011).

1.1.3.1 Uses of furfural (Furan-2-carbaldehyde)

There are various industrial uses of furfural, one of them being as an intermediate in the production of nylon and resins used for moulding powders and another as a selective solvent for the refining of lubricating oils. It is also important in the production of tetrahydrofuran, an important industrial solvent. Furthermore, furfural along with its sister molecule hydroxymethyl furfural, serves as a building block for other potential furanic based transportation fuels including dimethylfuran and ethyl levulinate (Singh and Singh , 2011).

1.1.3.2 Uses of Furan

Furan is the simplest structure of furanic compounds, which are used as potential biofuels in automobiles. Various blends of furanics with regular diesel are tested and used in engines. Other industrial use of furan is as a solvent as well as in the synthesis of furfural.

1.2 Background of the Azeotropic Distillation and Propan-1-ol Dehydration Processes

1.2.1 The azeotropic Distillation Process

Azeotropic distillation falls in a category of enhanced separation methods. The technique exploits azeotrope formation of binary system, through the use of a third component known as the entrainer. The entrainer alters the boiling characteristics and separability of the given mixture, and can results in a high purity of distillate or bottom product from either a binary or from a ternary azeotropic mixture (Udeye *et al.* 2009). According to Udeye *et al.* (2009), the azeotropic distillation technique can successfully dehydrate a 95.0% azeotropic ethanol-water mixture to produce 99.5% ethanol. The azeotropic distillation system can be designed in two ways: the homogenous and heterogeneous azeotropic distillation. The former involves the use of an entrainer to alter the relative volatility of the binary azeotropic mixture without formation of liquid-liquid phase. The detailed description and understanding of homogenous azeotropic distillation, unusual behaviours and entrainer selection is described in the great work by Laroche (1991). Heterogeneous azeotropic distillation is industrially preferred over homogenous due to the decantation involved in the column condenser (no extra heat requirements), thus results in a more economically attractive process scheme. A notable drawback of the heterogeneous scheme is tricky operation due to the possibility of phase separation forming within the column thus loss of separation efficiency (Kovack and Seider, 1987). In addition to the tricky operation, an accurate thermodynamic model is required to proper characterize the system. (i.e. Accurate calculation of azeotropic compositions).

The water + propan-1-ol + diisopropyl ether system investigated in this work give rise to heterogeneous azeotrope, thus it is necessary to look at some of the operational processes designed based on heterogeneous azeotropic distillation. This provides a good building block for a feasible flowsheet simulation.A typical heterogeneous azeotropic distillation process is dehydration of ethanol with benzene as an entrainer. Figure 1-7 below shows the ternary diagram of water + ethanol + benzene. The stable nodes shown on the figure, illustrate the azeotropic compositions and temperature at 101.325 kPa. Indicated on the figure is the ethanol + water distillation boundary, for which a tradition distillation system cannot achieve separation beyond. The addition of an adequate amount of benzene allows for formation of the heterogonous azeotrope and by LLE formation, the distillation boundary is crossed. Figure 1-8, the organic

phase is recycled back to the column and alters the water-alcohol azeotropic composition. Pure ethanol is recovered at the bottom and the water rich stream is distilled in the recovery column to recycle solvent and traces of ethanol.

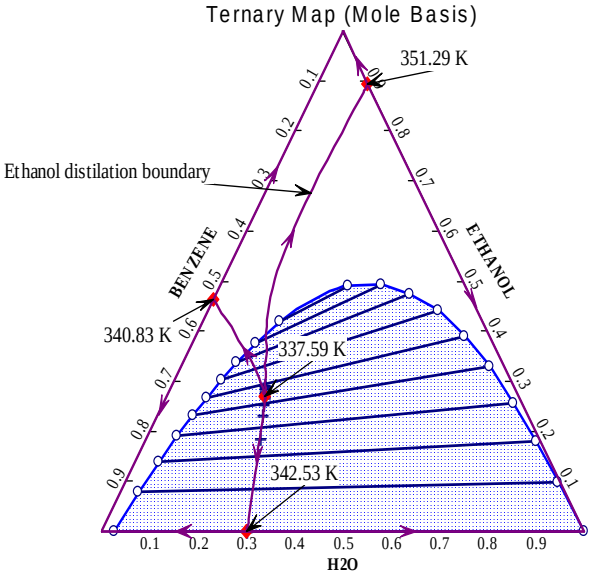

Figure 1-7: A Ternary diagram for the system of ethanol + water + benzene at 101.325 kPa predicted by UNIFAC-DMD.

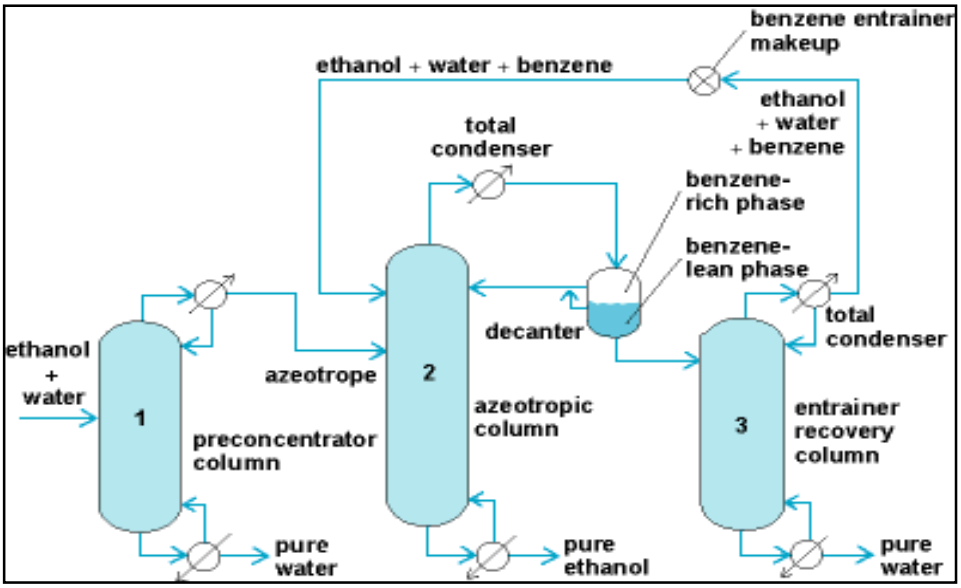

Figure 1-8: A typical sequence of columns for heterogeneous azeotropic distillation (Doherty, 2008).

1.2.2 The Propan-1-ol Dehydration Process

Propan-1-ol is widely used in various industrial processes as a raw material in the synthesis of propionic acid, propionic aldehyde, propyl acetate, propylamine as well as an intermediate in pharmaceuticals where highly pure product is required. It is also important in the manufacture of pesticide and surface-active substances (CHEMINDUSTRY.RU, 2011). The azeotropic dehydration of light alcohols is not a new subject. Various solvents such as benzene, cyclohexane and pentane have been used in such dehydration processes (Black *et al.* 1980). The important subject is to find cost effective operations with high recovery, and thus some of these known processes have become less common due to high costs (Gil *et al*. 2005). As a result, various studies are implemented to find the most effective solvents to drive process cost to minimal, with high recoveries. For instance, Ghanadzadeh *et al.* (2009) undertook an investigation of the LLE ternary mixture of water + propan-1-ol + diisopropyl ether (DIPE) at three different temperatures (298.2 to 313.2 K). They reported separation factors varying between 2.82 and 258.03 which is significantly greater than one, thus DIPE is deemed a potential solvent for this separation. Figure 1-9 shows a typical process flow scheme proposed by Lee and Shen, (2003) for propan-1-ol dehydration using cyclohexane as solvent.

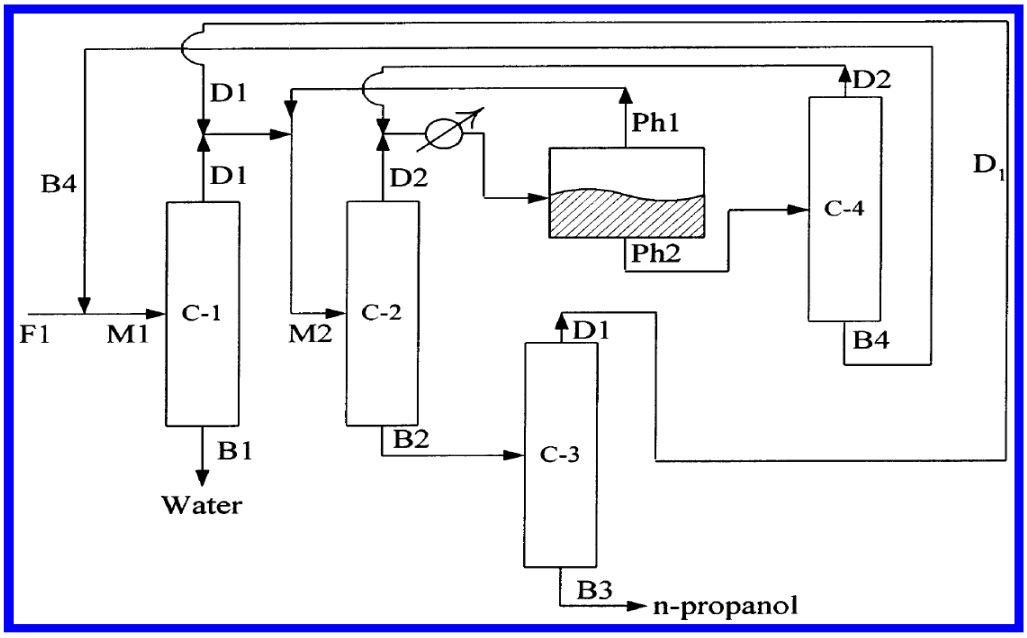

Figure 1-9: Process flow scheme of propan-1-ol dehydration using cyclohexane (Lee and Shen, 2003).

CHAPTER 2

THERMODYNAMIC PRINCIPLES FOR VAPOUR-LIQUID EQUILIBRIUM

Phase equilibrium thermodynamics is applied to understand molecular interactions between different species and different phases. The most common processes for which phase equilibrium is encountered are extraction, distillation, absorption, and leaching. In particular, distillation is known to be the most effective separation technique for mixtures with compounds of different boiling temperatures. Therefore it is important to have accurate and reliable experimental and correlation data for the design and simulation of these separation processes. This chapter presents the fundamental theory for treatment of experimentally measured binary VLE and LLE data.

2.1 Phase Equilibrium Behavior

The fundamental objective of experimental measurements and modeling in solution thermodynamics is to present phase equilibrium behavior in a form of phase diagrams. Chemical systems exhibits different equilibrium behaviors can be easily observed from phase equilibrium plots. These diagrams aid in the design and configuration of separation units (Decanters, distillation columns, azeotropic distillation columns, extractors etc). A typical example of direct application of VLE phase diagrams (particularly x-y curve) can be observed in preliminary sizing of a distillation column to separate two binary components using the McCabe-Thiele graphical method. The numerous types of phase diagrams expanded to various system behaviors can be found in solution thermodynamics literature. A short overview of types of binary VLE and ternary LLE diagrams are presented below.

2.1.1 Vapour Liquid Equilibrium Diagrams

Raal and Mühlbauer, (1998) present the five types of phase diagram to categorize VLE behaviour of binary systems. The first three types commonly encountered are shown in Figure 2-1 below. Type *I* classifies systems (also known as intermediate-boiling systems) that exhibits boiling points which are in between those of pure components for all mixture compositions. The second two types; *II* and *III* are used to classify systems exhibiting homogenous azeotropes.

These are known as minimum boiling homogenous azeotrope (type *II*) and maximum boiling homogenous azeotrope (type *III*). The azeotrope concept can be easily explained by direct observation from the Figure 2-1(a & b), where both the liquid and vapour compositions are exactly the same. A conventional distillation system will never separate the binary system past azeotropic composition, thus other means (e.g. pressure swing) can be employed to either eliminate or move the azeotrope. Types *IV* and *V* not shown below classify mixtures of; (i) partial miscible liquid phase split, with a single heterogeneous azeotrope and (ii) partial liquid miscibility with both a homogenous and heterogeneous azeotrope respectively.

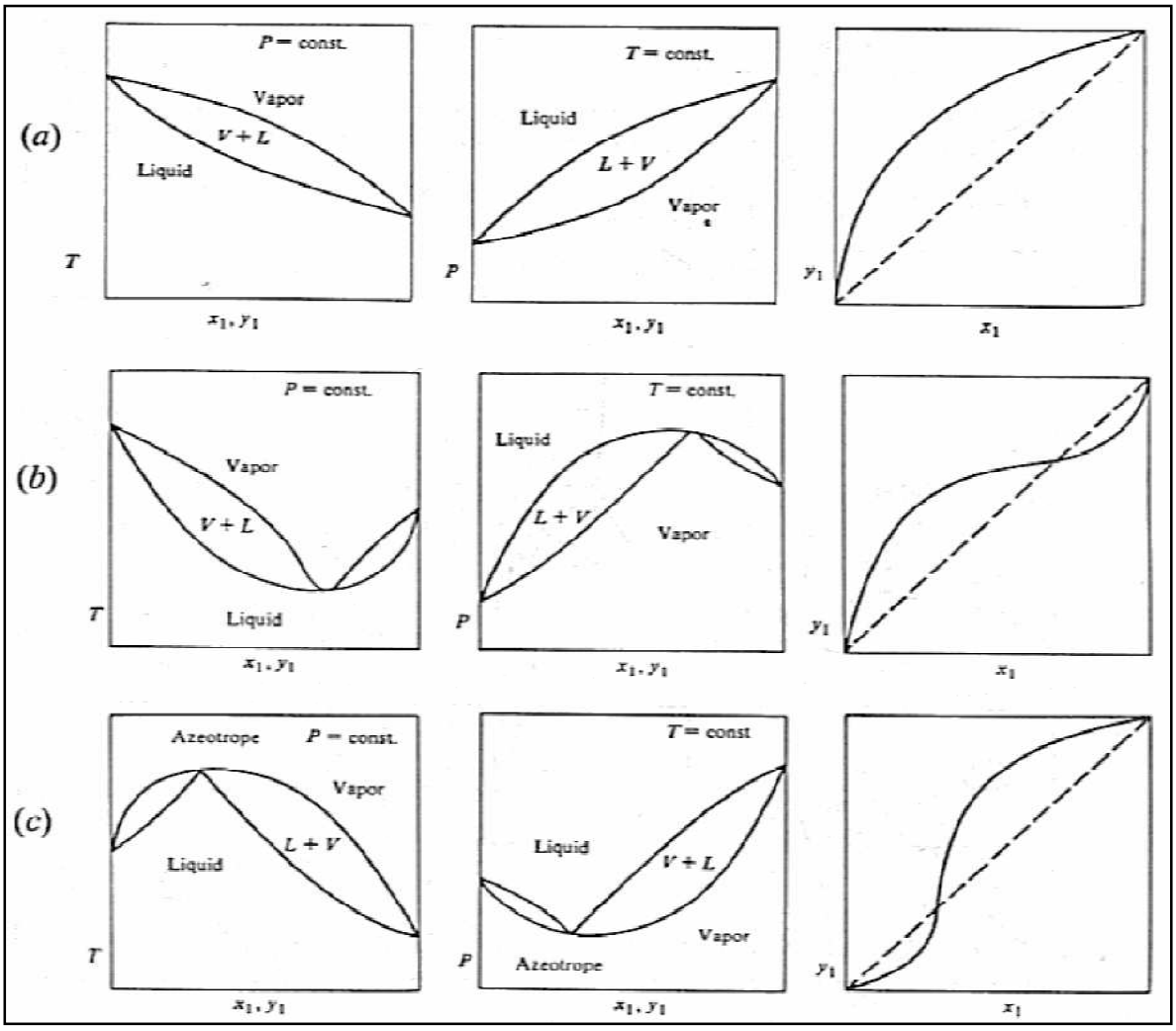

Figure 2-1: The three common types of binary phase diagrams for T-x-y, P-x-y and x-y plots: (a) intermediate-boiling; (b) minimum boiling azeotrope; (c) maximum boiling azeotrope (Raal and Mühlbauer, 1998).

2.1.2 Liquid-liquid Equilibrium Diagrams

The phase description of heterogeneous azeotrope systems is of high importance in azeotropic distillation. A qualitative representation of phase diagram for a heterogeneous system is shown in Figure 2-2 below. This system represents a classical example of two binary components A and B exhibiting wide miscibility gab and upper critical solution temperature (UCST) as shown in the binodal curve of AB. For a given overall mixture composition, two types of phase equilibrium are observed, the LLE phase split and single liquid region. An extension to ternary system at constant temperature T_0 is shown by binodal curve of ABC. Other types of LLE phase behavior not shown in the figure include; lower critical solution temperature (LCST) which is an inverse of the bionodal curve of AB and island curve which consists of both (UCST) and (LCST) forming an elliptic shape. The latter is very rare and seldom encountered in thermodynamic systems.

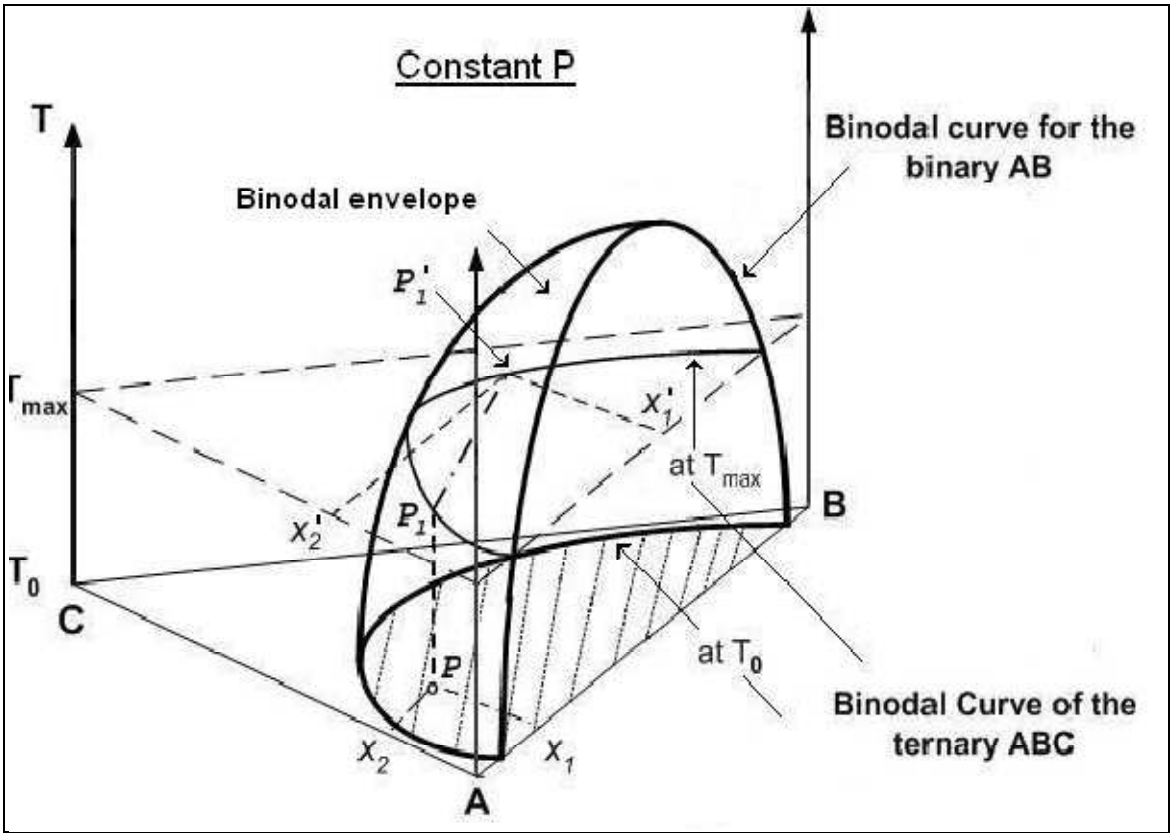

Figure 2-2: The phase diagram of a ternary system exhibiting a wide miscibility gap (Schmitz and Mendez, 2005).

2.2 Criterion for Phase Equilibrium

Although the main objective is set at obtaining model representation of phase diagrams, it is crucial to understand the core development of phase equilibrium principles. Therefore, one can start from the definition of thermodynamic equilibrium and build up to methods developed for reduction of VLE and LLE experimental data.

By defined, thermodynamic equilibrium is a state of no change on a microscopic level. In vapour liquid equilibrium measurements of multiphase system, the system is said to be in equilibrium when the temperature, pressure and chemical potential is the same in all phases. The chemical potential (μ) is an intensive variable (it does not depend on material present in a system) that drives the transfer of mass of individual component present in the system. It has been the basis for the derivation and linkage of equations describing different phases in the treatment of VLE experimental data. By definition, the chemical potential may be written as:

$$\mu_i = \left(\frac{\partial(nG)}{\partial n_i}\right)_{P,T,n_j} = \bar{G}_i \tag{2.1}$$

The above expression is a partial molar quantity as the pressure, temperature and mole fraction n_j are held constant. Equation (2.1) is important in the development of activity coefficient discussed in section 2.4.

Smith *et al*. (2001) described equilibrium for multiple phases at the same T and P as the condition when the chemical potential of each constituent species is the same in all phases. This is described by the following equation for π phases and *N* components:

$$\mu_i^{\alpha} = \mu_i^{\beta} = \cdots = \mu_i^{\pi} \ (i = 1, 2 \ldots .N) \tag{2.2}$$

At equilibrium both temperature and pressure can be easily measured, whereas the chemical potential can neither be measured experimentally nor easily related to measurable quantities. According to Gess *et al*. (1991), the thermodynamic relationship for a system is useful if it can be expressed in terms of quantities that can be measured experimentally. To solve this problem, another thermodynamic property called *fugacity* related to both chemical potential and experimentally accessible properties is introduced. The derivation of the criterion for phase

equilibrium is available for further reading in standard thermodynamic textbooks such as smith *et al*. (2001).

2.3 Fugacity and Fugacity Coefficient

According to Gess *et al*. (1991), G.N. Lewis defined fugacity, a more meaningful physical quantity than chemical potential. For pure species *i* the fugacity can be defined as:

$$dG_i = RTdln(f_i), \ \ (T = const) \tag{2.3}$$

$$\lim_{P \to 0} \frac{f}{P} = 1$$

Furthermore we can define a dimensionless quantity called fugacity coefficient:

$$\varphi = \frac{f}{P} \tag{2.4}$$

Considering a chemical species *i* in solution, equation (2.3) can be written as:

$$d\bar{G}_i = RTdln\left(\hat{f}_i\right), \ \ (T = const) \tag{2.5}$$

$$\lim_{P \to 0} \frac{\hat{f}_i}{x_i P} = 1$$

$\bar{G}_i$ is the partial molar Gibbs free energy and $\hat{f}_i$ is the fugacity of species *i* in solution.

Furthermore for species *i* in the vapour and liquid phases:

$$\hat{\varphi}_i^V = \frac{\hat{f}_i^{\mathrm{V}}}{y_i P} \tag{2.6}$$

$$\hat{\varphi}_i^L = \frac{\hat{f}_i^{\mathrm{L}}}{x_i P} \tag{2.7}$$

From equation (2.1) $\mu_i = \bar{G}_i$, integrating equation (2.5) at constant T gives:

$$\mu_i = \Gamma_i(T) + RTln\left(\hat{f}_i\right) \tag{2.8}$$

Substituting equation (2.8) to equation (2.2) with Γ_i function of temperature only, it can be shown that for system at equilibrium:

$$f_i^{\alpha} = f_i^{\beta} = \cdots = f_i^{\pi} \ (i= 1, 2\ldots..N), (\alpha, \beta, \ldots\ldots \pi) \tag{2.9}$$

For a system with two phases vapour (v) and liquid (L) in equilibrium, it follows that:

$$\hat{f}_i^{\mathrm{V}} = \hat{f}_i^{\mathrm{L}} \tag{2.10}$$

Fugacity is still an abstract quantity, but unlike the chemical potential it is easily related to measurable properties such as temperature (T), pressure (P) and molar volume (V). With a use of a suitable equation of state (EoS), the fugacity or fugacity coefficient can be evaluated. Using the definition of thermodynamic properties such as enthalpy, entropy, Helmholtz energy and Gibbs energy, it can be shown that for component i in a mixture (Smith *et al*. 2001):

$$ln\widehat{\varphi}_\iota = \int_0^P \left(\frac{\partial(nZ-n)}{\partial n_i}\right)_{P,T,n_j} \frac{dP}{P} \tag{2.11}$$

$$ln\varphi_i^{sat} = \int_0^{P_i^{sat}} (Z-1)\frac{dP}{P} \tag{2.12}$$

Here Z is the compressibility factor defined as:

$$Z = \frac{PV}{RT} \tag{2.13}$$

The fugacity coefficient for a species in solution $\widehat{\varphi}_\iota$ and the fugacity coefficient for a pure species φ_i^{sat} can be calculated from an appropriate expression for the compressibility factor. Z is obtained from the equations of state (EoS) discussed in section 2.6.1.

2.4 Activity and Activity Coefficients

Activity and activity coefficients are usually suitable to describe the non-idealities in the liquid phase of mixtures. According to Lewis and Randall (1923) the activity is defined as the ratio between the fugacity of the substance in solution at (T, P, x_i) and the fugacity of pure component at the same (T, P).

Therefore:

$$a_i = \frac{\widehat{f}_i(T,P,x_i)}{f_i(T,P)} \tag{2.14}$$

Where a_i is the activity of the pure liquid and $f_i(T,P)$ is the fugacity of the pure component *i* at the mixture temperature and pressure. The activity coefficient is simply defined as:

$$\gamma_i = \frac{a_i}{x_i} = \frac{\hat{f}_i(T,P,x_i)}{x_i\, f_i(T,P)} \tag{2.15}$$

The liquid phase behaviour is best described using the concept of activity coefficients to account for non-ideality of a solution. To obtain some sense of the activity coefficient; the concept of excess properties (the value of the mixture at specified conditions minus the value of the property for an ideal mixture at the same conditions) needs to be introduced. Writing equation (2.8) for an ideal solution:

$$\mu_i^{id} = \Gamma_i(T) + RTln\hat{f}_i^{id} \tag{2.16}$$

The fugacity of a species in an ideal solution is given by:

$$\hat{f}_i^{id} = x_i\, f_i \tag{2.17}$$

Subtracting equation (2.16) from equation (2.8), an expression for the partial molar excess Gibbs energy is obtained:

$$\mu_i - \mu_i^{id} = \bar{G}_i - \bar{G}_i^{id} = RTln\,\frac{\hat{f}_i}{x_i f_i} = \bar{G}_i^E \tag{2.18}$$

Combining equation 2.15 and equation 2.18 it follows that:

$$\bar{G}_i^E = RTln\,\gamma_i \tag{2.19}$$

2.5 VLE Reduction Methods

2.5.1. The Combined Method ($\gamma - \varphi$ approach)

The $\gamma - \varphi$ approach involves the use of fugacity coefficient and activity coefficient to describe the non idealities in liquid and vapour and phases respectively. The method is commonly used in the reduction of low pressure data, and merely relies upon liquid phase activity coefficient models such as; the Wilson (Wilson, 1964), NRTL (Renon and Prausnitz, 1968) and the UNIQUAC of Abrams and Prausnitz, (1975) discussed in section 2.6.2. The use of different models is due to the fact that specific models will give a better representation of the phase equilibrium data for a particular system.

Recalling the definition of fugacity equation (2.6) and activity coefficient equation (2.15), combining the two equations with Criteria for phase equilibrium results in the equation for the combined method is given as:

$$y_i \widehat{\varphi}_i P = x_i \gamma_i f_i \tag{2.20}$$

P is the total pressure, y_i is the mole fraction of component *i* in the vapour and $\widehat{\varphi}_i$ denotes the fugacity coefficient used for describing non-idealities in the vapour phase, x_i denotes the mole fraction of component *i* in the liquid and γ_i is the activity coefficient describing non-idealities in the liquid phase. The fugacity of pure component at mixture *T* and *P* is given by (see Appendix A. for derivation):

$$f_i = \varphi_i^{sat} P_i^{sat} exp\left[\frac{V_i^L (P - P_i^{sat})}{RT}\right] \tag{2.21}$$

The exponential term in equation (2.21) is referred to as the Poynting factor and it allows for the correction of liquid phase fugacity from vapour pressure to the system pressure.

$$y_i \Phi_i P = x_i \gamma_i P_i^{sat} \tag{2.22}$$

Where:

$$\Phi_i = \frac{\widehat{\varphi_i}}{\varphi_i^{sat}} \exp\left[\frac{V_i^L(P - P_i^{sat})}{RT}\right] \tag{2.23}$$

The Poynting factor approaches unity, differing by only a few parts per thousand for low to moderate pressures, introducing an error of about 0.01% on $ln\,\gamma$. Thus, omission of the Poynting factor introduces negligible error (Sebastiani and Lacquaniti, 1967). According to Prausnitz *et al*. (1980), the assumption is claimed to within reason for non-polar molecules at low pressures. The exception is for mixtures containing polar or associating molecules, for which the error cannot be neglected.

Equation (2.20) is known as the $\gamma - \varphi$ equation, and is used in the reduction of VLE data. The equation can be simplified to Raoult's Law for an ideal system, where the vapour phase is modeled as an ideal gas and the liquid phase as an ideal solution, thus both γ_i and Φ_i in equation (2.21) become equal to a unity (Smith *et al*. 2001). The $\gamma - \varphi$ approach involves use of equations of state and excess Gibbs energy models for the calculation of Φ_i and γ_i respectively. The molar volume of the saturated liquid V_i^L in equations (2.22) and (2.23) need to be determined. To solve this, the Rackett (1970) equation is employed:

$$V_i^L = V_C Z_c^{(1-T_r)^{2/7}} \tag{2.24}$$

Where Z is the compressibility factor, $T_r = T/T_c$ is the reduced temperature and the subscript c indicates the critical point.

2.5.2. The Direct Method ($\varphi - \varphi$ approach)

An alternative equation for describing liquid and vapour idealities can also be derived based on the phase equilibrium criterion. When equation (2.2) is written for both liquid and vapour phases, with behavior of both phases described by an equation of state (EoS), it follows that:

$$\hat{f}_i^{\mathrm{V}} = y_i \hat{\varphi}_i^{V} = \hat{f}_i^{\mathrm{L}} = x_i \hat{\varphi}_i^{L} \tag{2.25}$$

The fugacity coefficients for liquid and vapour phases are determined from a suitable EoS. Equation (2.25) is known as direct $\varphi - \varphi$ method. Both the combined and direct equations are employed in modeling of VLE data. The latter is said to have an advantage of being applicable in both low and high pressure systems, while the combined method has been traditionally used for moderate pressure systems.

2.5.3 Regression Algorithm ($\gamma - \varphi$ and $\varphi - \varphi$)

A suitable algorithm must be selected in order to obtain model parameters. Various techniques are used for regression such as the least squares, by Marquardt (1963) and Gess *et al*. (1991).The regression method is normally conducted by minimising the deviation between the experimental and model values for a particular quantity (also known as the residual). For VLE data, we define primary residuals as:

$$\delta y_i = y_i^{exp} - y_i^{calc} \tag{2.26}$$

$$\delta P_i = P_i^{exp} - P_i^{calc} \tag{2.27}$$

The symbol δ denotes the residual, δy_i and δP_i are referred to as primary residuals since all other residual quantities (temperature, liquid composition, excess Gibbs energy and activity coefficients) may be written in terms of these quantities (Van Ness and Abbott, 1982). The

residuals are used to obtain the objective function, which is minimised till a certain tolerance ε is reached. A simply objective function used by Barker (1953) is expressed as:

$$Objective\ Function = \sum (\delta P_i)^2 \tag{2.28}$$

Various forms of objective functions have been proposed in literature, these will give better optimisation for certain data types such as isobaric or isothermal data sets. One of the most effective technique used in this work, is that of combining both δy_i and δP_i into one objective function as follows:

$$Objective\ Function = \sum (\delta P_i)^2 + (\delta y_i)^2 \tag{2.29}$$

Figures 2-3 to 2-6 below show the regression algorithm for isobaric and isothermal data (bubble point pressure and bubble point temperature iteration).

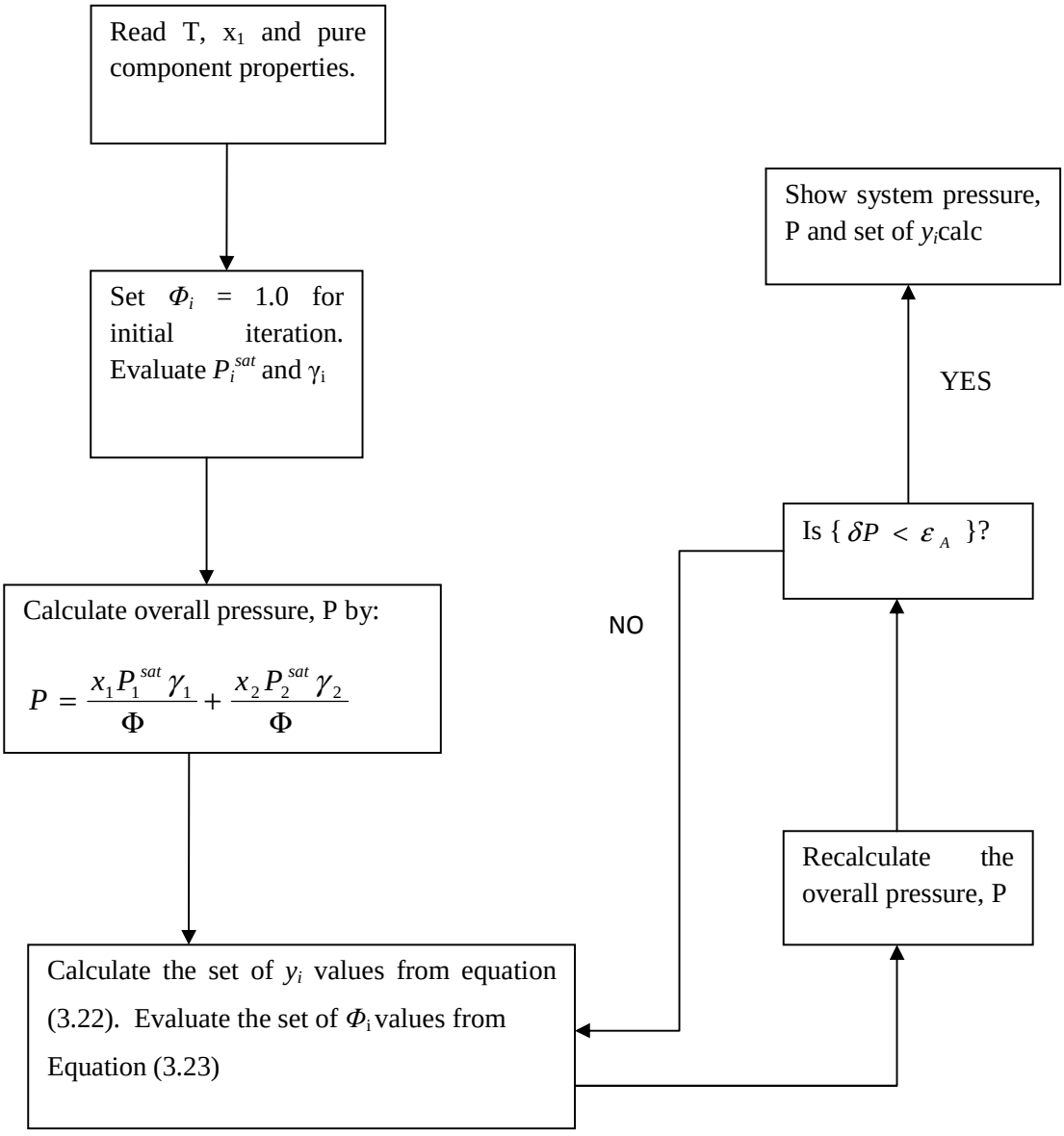

Figure 2-3: Flow diagram for bubble-point pressure iteration using combined method (Smith *et al.*, 2001).

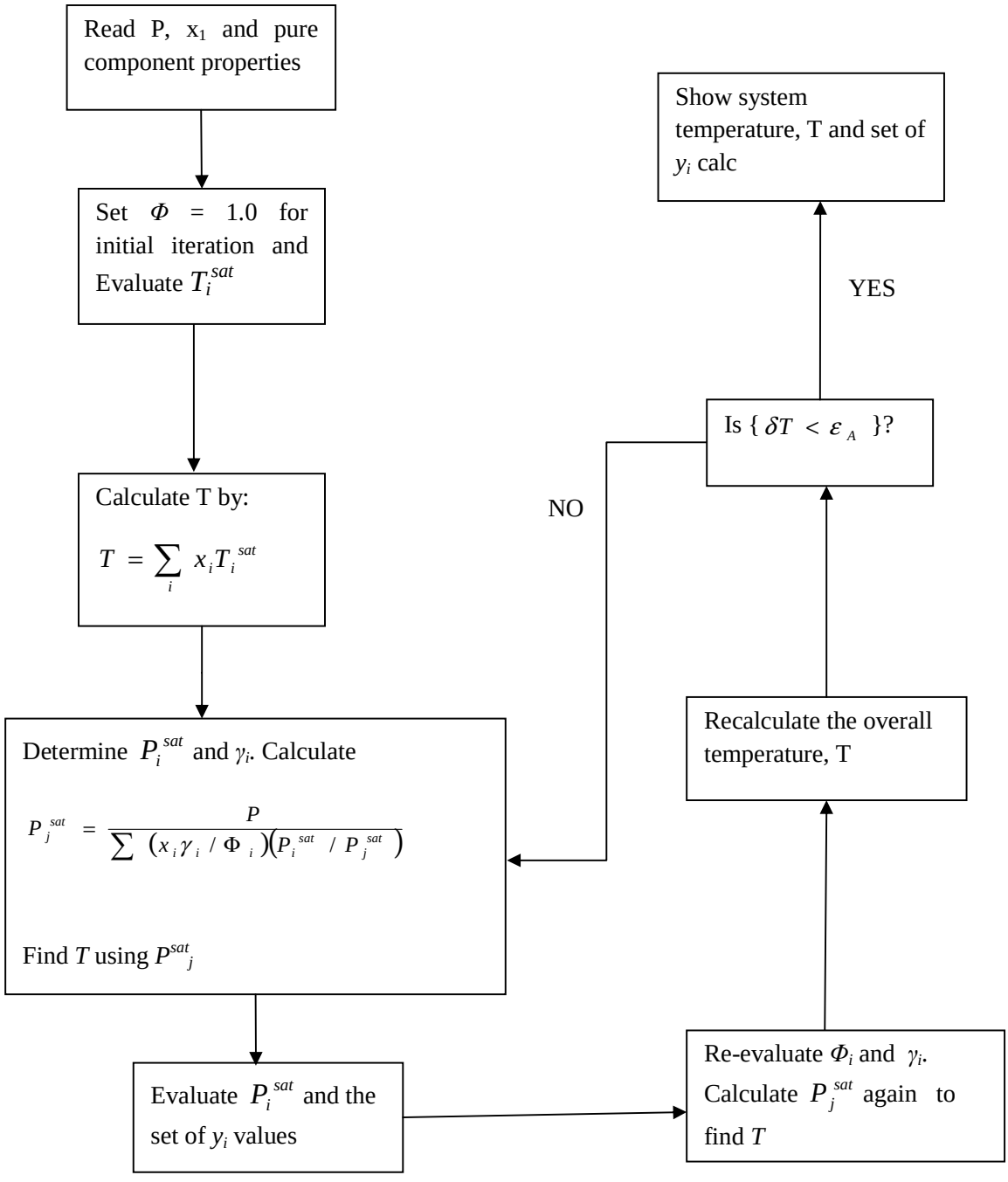

Figure 2-4: Flow diagram for bubble-point temperature iteration using combined method (Smith *et al.*, 2001).

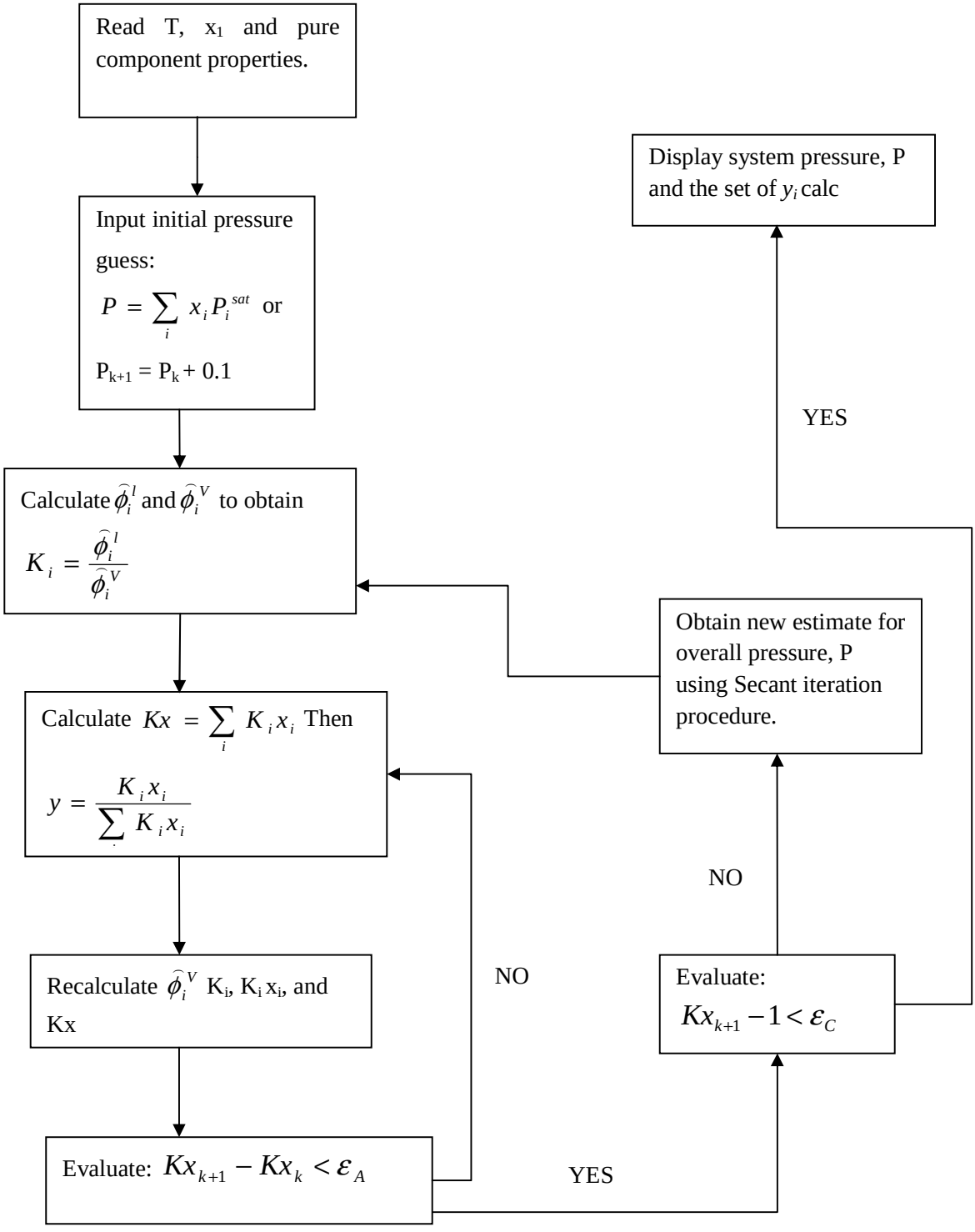

Figure 2-5: Flow diagram for bubble-point pressure iteration using direct method (Smith *et al.*, 2001).

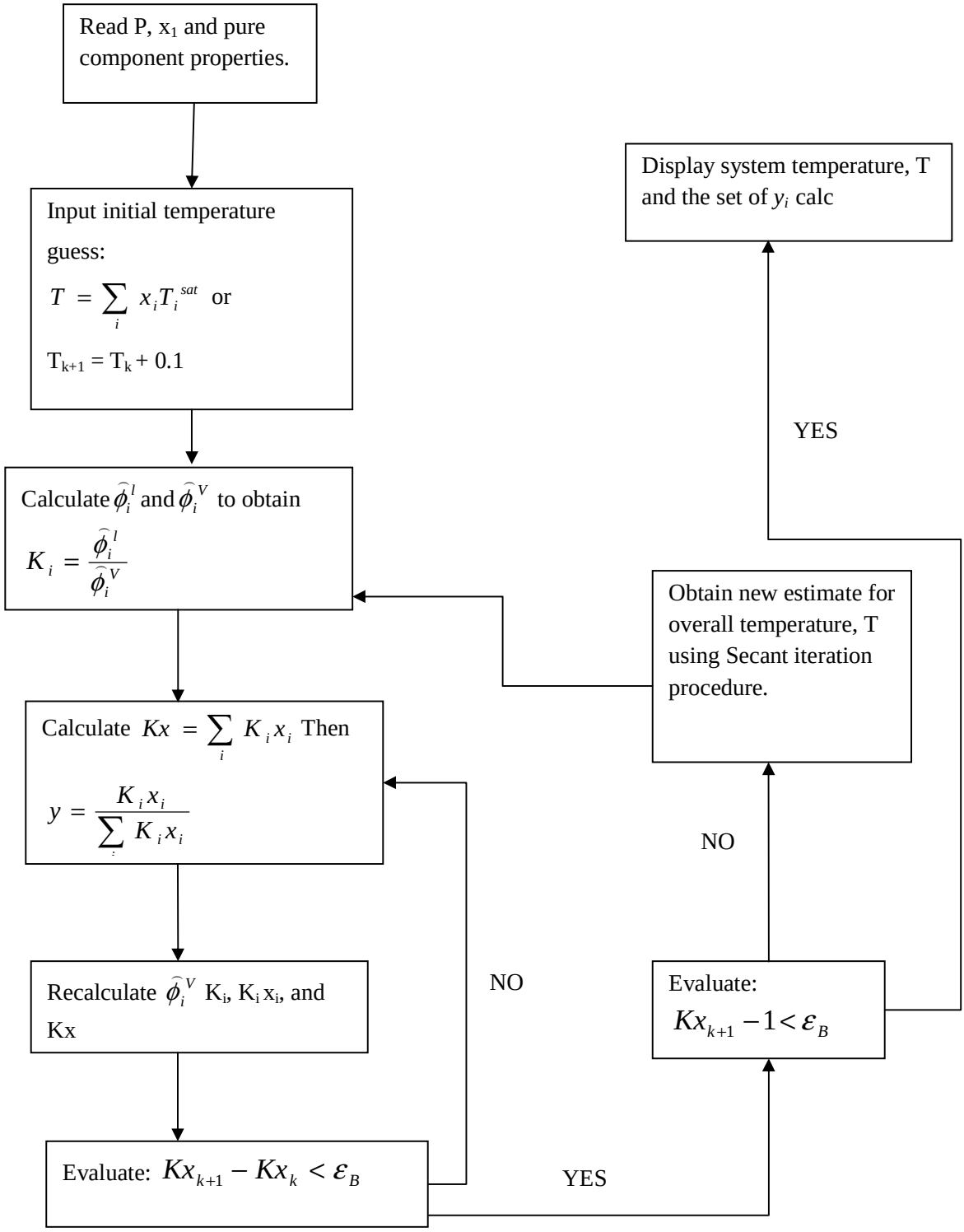

Figure 2-6: Flow diagram for bubble-point temperature iteration using direct method (Smith *et al.*, 2001).

2.6. Thermodynamic Models

Thermodynamic models can be referred to as an ultimate tool in the prediction of phase equilibrium behaviour, physical properties; etc. The scarcity of experimental phase equilibrium data in literature due to the extensive number of components and vast combination of possible systems has led to the use of thermodynamic models to predict phase behaviour for several systems. An additional factor contributing to use of models is the fact that the measured data often do not cover the entire temperature and pressure ranges of the systems of interest. In this work, activity coefficient models and equations of state were utilized to model the measured experimental data. These models are briefly presented below.

2.6.1 The Peng Robinson Equation of State

The Peng Robinson equation of state is to date a successful tool in the calculation of vapour-liquid equilibrium for fluid mixtures. The Peng Robinson equation presented in Table 2-1 has earned its merits in comparison to the hundreds of variations of the original van der Waals equation of state of 1873. Peng and Robinson, (1976) provided an optimum balance of attractive and repulsive terms to give a remarkably close representation of the thermodynamic properties for vast number of pure fluids and their mixtures. It has been successfully used in the mixtures encountered in the petroleum and natural gas industries.

Despite the remarkable qualities of the Peng-Robinson model equation, it is also important to point out some of its limitations. The model is known to provide poor representation of fluids in the critical region, inaccurate in calculation of liquid densities, unreliability for fluids with very large molecules and in applicability to highly polar fluids (Wu and Prausnitz, 1998). Often other limitation not well accounted in process industry is consideration of Peng-Robinson model with one parameter for mixtures (classical mixing rules). The drawback is for particular species such as oxygenated compounds, where the mixing rule parameter value is > 0.1 varying to 0.3, thus failing to provide a good representation of all interactions.

Consequently, it is good practice to consider Peng Robinson accompanied by complex mixing rules with excess Gibbs energy models. Table 2-2 provides the Wong-Sandler mixing, (1992) which can be used due its applicability in wide range of mixtures containing hydrocarbons and inorganic gases, also mixtures containing aromatic, polar systems. The only drawback with such application is large number of data requirement to avoid poor extrapolation. The model also does not take into account, the most important molecular association, polarity and induced polarity often exhibited by water-alcohol systems and carboxylic acids. As a result, it is important to also consider models developed for better representation of associating systems.

Table 2-1: The mathematical relation of the Peng and Robinson (1976) equation of state used for evaluation of fugacity coefficients for deviation to ideal vapour phase.

The Peng-Robinson equation of state	
$P = \frac{RT}{V-b} - \frac{a(T,\omega)}{V(V+b)+b(V-b)}$	$a_i(T,\omega) = a_{ci}\alpha_i(T,\omega)$
$a_{ci} = 0.45724\left(\frac{R^2 T_{c_i}^2}{P_{c_i}}\right)$	$a_i\{(T_c)_i;\omega_i\} = \left[1+\kappa_i\left(1-(T_r)_i^{1/2}\right)\right]^2$
$\kappa_i = 0.37464 + 1.54226\,\omega_i - 0.26992\,\omega_i^2$	$b_i(T) = b_i(T_c)_i$
$b_i = 0.07780\left(\frac{RT_{c_i}}{P_{c_i}}\right)$	$a_{ci} = 0.45724\left(\frac{R^2 T_{c_i}^2}{P_{c_i}}\right)$

Table 2-2: The mathematical relation of the Wong and Sandler mixing rule (1992).

The Wong-Sandler mixing rule	
$\frac{a_m}{RT} = \frac{QD}{(1-D)}$	$b_m = \frac{Q}{(1-D)}$
$Q = \sum_i \sum_j x_i x_j \left(b - \frac{a}{RT}\right)_{ij}$	$D = \sum_i x \frac{a_i}{b_i RT} + \frac{A_\infty{}^E}{cRT}$

2.6.2 Equations of State for Associating Systems

2.6.2.1. The Virial EoS, Hayden-O'Connell (HOC) and Nothnagel (NTH) correlation

Various methods exist for determining the fugacity coefficients of species in gaseous mixtures. For low to moderate pressures, the pressure explicit form of the Virial equation of state (truncated at second term) can be used to evaluate the fugacity coefficients:

$$Z = 1 + \frac{BP}{RT} \tag{2.30}$$

The second Virial coefficient, B, is function of temperature and composition in a mixture and is obtained from a rigorous mixing rule based on statistical mechanics:

$$B_{mixture} = \sum_i \sum_j y_i y_j B_{ij}(T) \tag{2.31}$$

Where B_{ij} represents the pure component and mixture second Virial coefficients. It accounts for bimolecular interaction between the molecules *i* and *j*. Thus, $B_{ij} = B_{ji}$. According to Tsonopoulos

(1974), the effect of vapour-phase non-ideality can be calculated using only the second virial coefficient *B* of the pure components and cross coefficients for each binary. Equation (2.23) is modified as a consequence of the assumption that the truncated Virial equation of state describes the vapour phase in the VLE system:

$$\Phi_i = \exp\left[\frac{(B_{ii} - V_i^L)(P - P_i^{sat}) + Py_j^2\delta_{ij}}{RT}\right] \tag{2.32}$$

Where: $$\delta_{ij} = 2B_{ij} + B_{ii} - B_{jj}$$

The second Virial coefficients for mixtures, B_{ij}, and for pure species, B_{ii}, may be evaluated using various experimental methods and are available in various compilations such as those by Dymond and Smith (1980) and Cholinski *et al*. (1986). However, it is often difficult to obtain experimental values for the species of interest. Thus, a satisfactory correlation is essential to determine the second virial coefficients. The most used correlations are those of Black (1958), O'Connell and Prausnitz (1967), Nothnagel *et al*. (1973), Tsonopoulos (1974) and Hayden and O'Connell (1975).

The Hayden and O'Connell (1975) method is selected for determining second Virial coefficients due to its applicability to a large range of compounds, including both polar and non-polar chemicals. The method incorporates the chemical theory of dimerization and accounts for strong association and solvation effects of higher densities. The calculation procedure is complex and thus only the most relevant discussion is presented here. The procedure is given in detail in Appendix A of Prausnitz *et al*. (1980). The Virial coefficient can be considered the sum of several individual contributions:

$$B_{ij}(T) = \left(B_{free\ polar}\right)_{ij} + \left(B_{free-nonpolar}\right)_{ij} + (B_{metastable})_{ij} + (B_{bound})_{ij} + (B_{chem})_{ij} \tag{2.33}$$

Where $\left(B_{free\ polar}\right)_{ij}$ and $\left(B_{free-nonpolar}\right)_{ij}$ are contributions by free pairs of non-polar and non-association molecules and $(B_{metastable})_{ij}, (B_{bound})_{ij}, (B_{chem})_{ij}$ are contributions by chemically bonding species. The input parameters involved in the calculation are the components critical

properties and molecular parameters (mean radius of gyration, dipole moment, solvation and association parameters). These are obtained from literature sources such as Fredenslund *et al.* (1977), Reid *et al.* (1988), Prausnitz et *al.* (1980) and Dortmund Data Bank (DDB, 2011). The dipole moments are acquired from either the extensive compilation of McClellan (1974) or through a calculation procedure using the method proposed by Smyth (1955). Values for the mean radius of gyration are obtained from the group contribution method suggested by Poling *et al.* (2001). The mean radius of gyration is evaluated using a property known as the *parachor*, P', which is obtained using the group contribution method mentioned above. According to Harlacher and Braun (1970), the radius of gyration and the parachor factor are related by the following equation:

$$P' = 50 + 7.6R_D + 13.75R_D^2 \tag{2.34}$$

After obtaining the parachor factor for each species, the mean radius of gyration is obtained by solving the quadratic equation (2.34) for R_D. The positive real root is the mean radius of gyration. The salvation and association parameters are found from the tables given by Prausnitz *et al.* (1980). If the system of interest is not available in the tables given, it is suggested by Prausnitz *et al.* (1980) that the values of similar chemical system should be taken.

2.6.2.2 The Perturbation-Chain Statistical Associating Fluid Theory (PC-SAFT)

The PC-SAFT equation was not utilized in the thermodynamic modelling of chemical systems in this work, but rather provides an alternative model to describe non-idealities in associating systems. The work of Soo, (2011) and Passerello *et al.* (2011) shows the merits of both PC-SAFT and group contribution SAFT (GC-SAFT) models in describing the association in systems containing oxygenated compounds (alcohols, ethers, aldehydes etc). The complexity involved in the development and application of these models could not suit the time frame of this project. However it is worth mentioning these models and their capabilities, and may be in future used to model the given systems for comparison.

Looking at the historical development of SAFT and PC-SAFT models, Wertheim, (1984, 1986) first order perturbation theory was utilized by Chapman *et al.* (1988, 1990) to develop the

statistical associating fluid theory (SAFT) equation of state for chain mixtures. In the SAFT model molecules are treated as chains of equal-sized spherical segments (i.e. the chain structure was not accounted for in their dispersion term). Association in the SAFT equation is described by assigning molecules bonding sites, with the interactions between these sites modelled using the square well potential (Wolbach and Sandler, 1997). The square well potential forms part of intermolecular potential functions SAFT equation developments. It was proposed as an attempt to simplify the Lennard-Jones potential. However, its use in the SAFT equation do not account for connectivity of the chain segments.

Gross and Sadowski (2001) published a new equation of state that uses the same chain term and association term from the earlier SAFT equations. This equation of state uses fluid chain as reference for perturbation theory, as opposed to the spherical molecules in SAFT modifications. The model is known as the perturbed chain SAFT (PC-SAFT). The application of this model includes real chain of any length, from spheres to polymers (Mahapatra, 2009). The publication of Gross and Sadowski (2001, 2002) presents the equations used in the model development. Capabilities, limitations and challenges of a simplified PC-SAFT equation of state are given in the publication of Kontogeorgis *et al*. (2006). Some of notable advantages of PC-SAFT include direct calculation of thermodynamic properties such heat of mixing and density data.

2.6.2.3 The Cubic Plus Association Equation of State (CPA)

Similarly, the CPA equation was not used in this project, but remained one of the known models to describe association in chemically associating systems. Kontogeorgis *et al*. (1996) developed an interesting equation of state that combines the simplicity of physical term in the cubic SRK EOS (Soave, 1972) with the chemical (association) term taken from SAFT. The association strength in both SAFT and CPA is expressed through a function of the reduced density and association volume. The main difference between the two chemical equations of state is the equilibrium constant K (independent of density). The mathematical equations and relations are in Kontogeorgis *et al.* (1996).

According to Kontogeorgis *et al*. (1996), the CPA EOS has resulted in superior correlations of vapour pressures and saturated liquid volumes for primary-alcohols, phenol, tert-butyl alcohol,

triethylene glycol, and water. Kontogeorgis *et al.* (2007) extended the CPA EoS in the thermodynamic modelling of multi-component mixtures containing carboxylic acids (methanol + propanoic acid, and the 2-butanol + propanoic acid system), for which satisfactory results were obtained. The major limitation of the CPA EoS has been underestimation of solvation in cross-associating and self associating systems (observed by high values of the binary interaction parameters for such systems). Mixtures such as alcohol-alcohol systems or alcohol-water have shown great difficulty when models such as CPA and SAFT are used (Kontogeorgis *et al.* 2006).

2.6.3 Excess Gibbs Energy Activity Coefficient Models

Activity coefficient models are essentially used for the description of liquid phase deviations from ideality. In attempting to characterize the varying systems behaviors, different models can be utilized and compared in order to obtain a model that best describes the system of interest. The difference in the chemical nature of species in a chemical system as well as molecular size, have been found to pose difficulties during data correlation and generally require more complex models. The most common liquid activity coefficient models used in describing the liquid phase imperfections includes; Van Laar, Wilson and TK Wilson, NRTL (Non-Random Two Liquid) and UNIQUAC (Universal Quasi Chemical). Below is a brief discussion of the models selected in this work.

2.6.3.1 The Wilson Model

Wilson (1964) proposed a regular model to describe non-idealities in the liquid mixtures. He derived his equations for excess Gibbs energy $G^E(T, P, x_i)$ by considering local compositions, which account for the short-range order and non-random molecular orientation that results from inter molecular forces and differences in molecular size (Van Ness and Abbott, 1997). The excess Gibbs energy for the system consisting of c components is given by Wilson model as:

$$\frac{\mathrm{G}^E}{RT} = -\sum_{i=1}^{c} x_i \, ln\left(\sum_{j=1}^{c} x_i \Lambda_{ji}\right) \tag{2.35}$$

The corresponding equation that allows calculation of the activity coefficient for any component k is given by:

$$\ln \gamma_k = -ln\left(\sum_{j=1}^{c} x_i \Lambda_{ki}\right) + 1 - \sum_{i=1}^{c} \frac{x_i \Lambda_{ik}}{\sum_{j=1}^{c} x_j \Lambda_{ij}} \tag{2.36}$$

Λ_{ji} and Λ_{ij} are the adjustable Wilson parameters, which are related to the pure component liquid volumes by:

$$\Lambda_{ij} = \frac{V_j}{V_i} exp\left[-\frac{\lambda_{ij} - \lambda_{ii}}{RT}\right] \tag{2.37a}$$

Where V_j and V_i are the molar volumes of pure liquids at temperature T, $\lambda_{ij} - \lambda_{ii}$ represent the molecular interactions between the species in a system. The Aspen version of equation (2.37a) is given as

$$\Lambda_{ij} = exp\left(a_{ij} + \frac{b_{ij}}{T} + c_{ij} \ln(T) + d_{ij} T\right) \tag{2.37b}$$

Some of the notable advantages of the Wilson model include: accurate representation of phase equilibrium data with only a few parameters and the accurate predictions of multi-component properties from binary data. The distinct limitations of the Wilson model are inability to predict the excess molar heat capacities, it cannot be applied to systems exhibiting activity coefficients extrema (the Wilson model predicts that the activity coefficient always increases monotonically as x_i approaches infinite dilution) and inability to predict limited solubility.

2.6.3.2 The NRTL (Non Random Two Liquid) Model

The NRTL model, like the Wilson model is considered as regular model as it also does not incorporate excess entropy. Its basis is only based on molecular interactions unlike the UNIQUAC model, which account for entropic effects. The three parameter NRTL activity

coefficient model of Renon and Prausnitz, (1968), shows great capabilities in correlation and prediction of vapor-liquid and liquid-liquid phase equilibria for wide variety of mixtures. The basis of the model is the local composition theory which is expressed as follows:

$$x_{ji} = \frac{x_j exp\left(-\alpha_{ij}\tau_{ij}\right)}{\sum_{k=1}^{c} x_k exp\left(\alpha_{ki}\tau_{ij}\right)} \tag{2.38}$$

Where x_{ji} is the local mole fraction of a central molecule *i* surrounded by molecules *j*, τ_{ij} and τ_{ji} are adjustable parameters, and ($\alpha_{ij} = \alpha_{ji}$) is third parameter (non-randomness parameter) that can be fixed or adjusted depending on the availability of data. When considering only binary molecular interactions, the excess Gibbs free energy for the liquid system is described by the following equation:

$$\frac{\mathrm{G}^E}{RT} = \sum_{i=1}^{c} x_i \left[\sum_{j=1}^{c} x_{ji}\tau_{ji}\right] \tag{2.39}$$

$$\left(\frac{\partial(n\mathrm{G}^E)}{\partial n_i}\right)_{T,P,n_{j\neq i}} = RT ln\, \gamma_i \tag{2.40}$$

The activity coefficient for component *i* in the multi-component mixture is given as:

$$ln\, \gamma_i = \frac{\sum_{i=1}^{c}\left(x_j\tau_{ji}\, G_{ji}\right)}{\sum_{k=1}^{c}\left(G_{kj}x_k\right)} + \sum_{j=1}^{c}\left[\frac{\left(x_j G_{ij}\right)}{\sum_{k=1}^{c}\left(G_{kj}x_k\right)}\left(\tau_{ij} - \frac{\sum_{k=1}^{c}\left(x_k\tau_{kj}G_{kj}\right)}{\sum_{k=1}^{c}\left(G_{kj}x_k\right)}\right)\right] \tag{2.41}$$

Where G_{ji}=$exp\left(-\alpha_{ji}\tau_{ji}\right)$; $\tau_{ij} = \frac{\mathrm{g}_{ij} - \mathrm{g}_{jj}}{RT}$ and $\tau_{ji} = \frac{\mathrm{g}_{ji} - \mathrm{g}_{ii}}{RT}$

g_{ij}, g_{ji}, g_{ii} and g_{jj} are energies of interaction between the molecular pairs. It is important to note that $G_{ji} \neq G_{ij}$; $G_{ii} = G_{jj} = 1$;$\tau_{ij} \neq \tau_{ji}$;$\tau_{ii} = \tau_{jj} = 0$

Writing equation (2.41) for binary system, the activity coefficients for each component are given as:

$$ln\,\gamma_1 = x_2^2\left[\left(\frac{\tau_{21}G_{21}}{x_1+x_2G_{21}}\right)^2 + \frac{\tau_{12}G_{12}}{(x_2+x_1G_{12})^2}\right] \tag{2.42}$$

$$ln\gamma_2 = x_1^2\left[\left(\frac{\tau_{21}G_{12}}{x_2+x_1G_{12}}\right)^2 + \frac{\tau_{21}G_{21}}{(x_1+x_2G_{21})^2}\right] \tag{2.43}$$

$$G_{12} = exp(-\alpha_{12}\tau_{12}) \text{ and } G_{21} = exp(-\alpha_{21}\tau_{21}) \tag{2.44}$$

$$\tau_{12} = \frac{g_{12}-g_{22}}{RT} \quad \text{and} \quad \tau_{21} = \frac{g_{21}-g_{11}}{RT} \tag{2.45a}$$

The Aspen version of equation (2.45a) is given as

$$\tau_{12} = a_{12} + \frac{b_{12}}{T} + e_{12}\ln(T) + f_{12}T \tag{2.45b}$$

$$\tau_{21} = a_{21} + \frac{b_{21}}{T} + e_{21}\ln(T) + f_{21}T \tag{2.45c}$$

The adjustable parameters in Aspen are given by a 4 term expression (equation2.45b&c) for which during regression only the first two terms are essential. According to Aspen plus conventions, the a_{12} and a_{21} can be set to zero for isothermal data, thus equations (2.45b&c) resolve into the equation (2.45a) in DECHEMA tables. The non-randomness parameter in equation (2.44), α_{12} is given as c_{12} in Aspen and with a default value of 0.3. Aspen propose a value of 0.2 to be used when dealing with saturated hydrocarbons with polar non-associated liquids and mixtures with immiscible liquids, and a value of 0.47 for strongly self-associated substances with non-polar components. According to Walas (1985) the non-randomness parameter values for should be roughly set to 0.3 for non-aqueous mixtures and 0.4 for aqueous organic systems. Raal and Mühlbauer (1998), strongly suggest that this non-randomness parameter should be regressed from experimental data when sufficient data is available.

Some of the distinct advantages of the NRTL model include: its superiority in representing aqueous systems relative to other models; relative to Wilson model it is able to effectively represent partially miscible and completely miscible liquid systems, a simpler algebraic form compared to the UNIQUAC model. Some of the drawbacks of the model are: an increased interdependence of the three parameters, the arbitrary assignment non-randomness parameter can present many problems, thus in some cases affect the accuracy of the correlation (Reddy, 2006).

2.6.3.3 The UNIQUAC (Universal Quasi-Chemical) Model

Abrams and Prausnitz (1975) developed the UNIQUAC model with only two adjustable parameters per binary system. The major applicability of the model is liquid mixtures exhibiting different structural shape and size. Parameters incorporating the effect of size and shape are obtained from pure component data of each chemical species in the mixture.According to Abrams and Prausnitz (1975), the UNIQUAC model offers a good representation of vapour-liquid and liquid-liquid equilibria for both binary and multi-component systems. These include: polar and non-polar fluids such as hydrocarbons, ketones, esters, amines, alcohols, nitriles and water.The only exception which was lately suggested by Prausnitz *et al*. (1986) was region of highly precise and plentiful data for systems consisting of a variety of non-electrolytes.

The UNIQUAC model equation is composed of two parts, the combinatorial and residual part. The combinatorial part is attributed to dominance in entropic contribution, and is easily obtained from the knowledge of molecules composition, their size and shape only (Prausnitz *et al*. 1986). On the other hand the residual part mainly accounts for intermolecular forces that are responsible for the enthalpy of mixing. The residual part depends only on intermolecular interactions, thus the two adjustable interaction parameters appear only in this part of the equation. The UNIQUAC equation for excess Gibbs energy can be written as follows:

$$\frac{\mathrm{G}^E}{RT} = \left(\frac{\mathrm{G}^E}{RT}\right)_{Combitorial} + \left(\frac{\mathrm{G}^E}{RT}\right)_{Residual} \tag{2.46}$$

Where for binary system

$$\left(\frac{\mathrm{G}^E}{RT}\right)_{Combitorial} = x_i ln\frac{\Phi_i}{x_i} + x_j ln\frac{\Phi_j}{x_j} + \frac{z}{2}\left(q_i x_i ln\frac{\theta_i}{\Phi_i} + q_j x_j ln\frac{\theta_j}{\Phi_j}\right) \quad (2.47)$$

and

$$\left(\frac{\mathrm{G}^E}{RT}\right)_{Residual} = -q_i x_i ln\left[\theta_i + \theta_j \tau_{ji}\right] - q_j x_j ln\left[\theta_j + \theta_i \tau_{ij}\right] \quad (2.48)$$

The segment fraction, Φ_{ij} and area fraction, θ_{ij} are given as:

$$\Phi_{ij} = \frac{x_i r_i}{x_i r_i + x_j r_j} \quad (2.49)$$

$$\theta_{ij} = \frac{x_i q_i}{x_i q_i + x_j q_j} \quad (2.50)$$

The parameters *r* and *q* are the pure component volume and area parameters respectively and they are available in literature for various components. *z* is the coordination number and is often set to 10. The adjustable binary interaction parameters are given by:

$$\tau_{12} = \frac{\mathrm{u}_{12} - \mathrm{u}_{11}}{RT} \text{ and } \tau_{21} = \frac{\mathrm{u}_{21} - \mathrm{u}_{22}}{RT} \quad (2.51a)$$

Where $\mathrm{u}_{12} - \mathrm{u}_{11}$ and $\mathrm{u}_{21} - \mathrm{u}_{22}$ are the characteristic energies and are said to be often weakly dependent on temperature (Prausnitz *et al*. 1986). Similarly to NRTL, an Aspen version of UNIQUAC adjustable parameters is available for equation (2.51a) and is given as:

$$\tau_{12} = exp\left(a_{12} + \frac{b_{12}}{T} + c_{12}\ln(T) + d_{12}T + \frac{e_{12}}{T^2}\right) \quad (2.51b)$$

$$\tau_{21} = exp\left(a_{21} + \frac{b_{21}}{T} + c_{21}\ln(T) + d_{21}T + \frac{e_{21}}{T^2}\right) \quad (2.51c)$$

The activity coefficient expression for UNIQUAC model takes similar form to the equation (2.46), as shown below.

$$ln\,\gamma_i = (ln\,\gamma_i)_{combitorial} + (ln\,\gamma_i)_{Residual} \quad (2.52)$$

Where

$$(ln\,\gamma_i)_{combitorial} = ln\frac{\Phi_i}{x_i} + \frac{z}{2}q_i ln\frac{\theta_j}{\Phi_i} + \Phi_1\left(l_i + q_2 l_j \frac{r_i}{r_j}\right) \quad (2.53)$$

and

$$(ln\,\gamma_i)_{Residual} = -q_i ln\left(\theta_i + \theta_j\tau_{ji}\right) + \theta_j q_i\left(\frac{\tau_{ji}}{\theta_i + \theta_j\tau_{ji}} - \frac{\tau_{ij}}{\theta_j + \theta_i\tau_{ij}}\right) \quad (2.54)$$

and

$$l_i = \frac{z}{2}(r_i - q_i) - (r_i - 1) \quad (2.55)$$

Some of the advantages of the UNIQUAC model suggested by Reid *et al*. (1988) include: a more readily applicability to mixtures with macromolecules such as polymers since the surface areas available for interaction (i.e. it uses surface fractions for concentration variable as opposed to use mole fractions). A simple drawback of the model is the complexity of the model equation.

2.7. Liquid-Liquid Equilibrium Methods

2.7.1 Activity coefficient Method

In order to correlate binary LLE data it is necessary to recall the criterion for phase equilibrium equation (2.9) and by definition for liquid phase α and β:

$$f_i^{\alpha}(T,P,x_i) = x_i^{\alpha}\gamma_i^{\alpha} f_i^{\alpha,o}(T,P) \tag{2.56}$$

$$f_i^{\beta}(T,P,x_i) = x_i^{\beta}\gamma_i^{\beta} f_i^{\beta,o}(T,P) \tag{2.57}$$

Where $f_i^{\beta,o}(T,P)$ is the fugacity of pure component i at the temperature and pressure of the mixture. Combining equation (2.9) with equations (2.56) and (2.57), the equilibrium relation for LLE is expressed as:

$$x_i^{\alpha}\gamma_i^{\alpha} = x_i^{\beta}\gamma_i^{\beta} \tag{2.58}$$

To explicitly represent the composition of each component in each phase as function of activity coefficients only, it is necessary to consider a simple mathematical manipulation of equation (2.57) for binary mixture. It is important to note that the summation of the fractional compositions of all components in each phase must be equal to one, thus using that criterion together with equation (2.58) the equilibrium compositions for species 1 and 2 in a binary mixture can be calculated as follows:

$$x_1^{\beta} = \gamma_1^{\alpha}\left(\frac{\gamma_2^{\alpha}-\gamma_2^{\beta}}{\gamma_1^{\beta}\gamma_2^{\alpha}-\gamma_1^{\alpha}\gamma_2^{\beta}}\right) \tag{2.59}$$

$$x_1^{\alpha} = \gamma_1^{\beta}\left(\frac{\gamma_2^{\alpha} - \gamma_2^{\beta}}{\gamma_1^{\beta}\gamma_2^{\alpha} - \gamma_1^{\alpha}\gamma_2^{\beta}}\right) \tag{2.60}$$

$$x_2^{\beta} = \gamma_2^{\alpha}\left(\frac{\gamma_1^{\alpha} - \gamma_1^{\beta}}{\gamma_2^{\beta}\gamma_1^{\alpha} - \gamma_2^{\alpha}\gamma_1^{\beta}}\right) \tag{2.61}$$

$$x_2^{\alpha} = \gamma_2^{\beta}\left(\frac{\gamma_1^{\alpha} - \gamma_1^{\beta}}{\gamma_2^{\beta}\gamma_1^{\alpha} - \gamma_2^{\alpha}\gamma_1^{\beta}}\right) \tag{2.62}$$

The general objective function for obtaining the binary interaction parameters can be expressed as follows:

$$F = \sum_{j}^{n}\sum_{k}^{\pi}\sum_{i}^{c}\left|x_{i,j}^{k\,exp} - x_{i,j}^{k\,cal}\right| \tag{2.63}$$

Where n, π and c represent the number of data points, the number phases and the number of components respectively. The objective function F is minimized by developing a solution algorithm that allows for determination of the adjustable binary interaction parameters for the activity coefficient models. The algorithm is presented below and is programmable to computational software such a Matlab™.

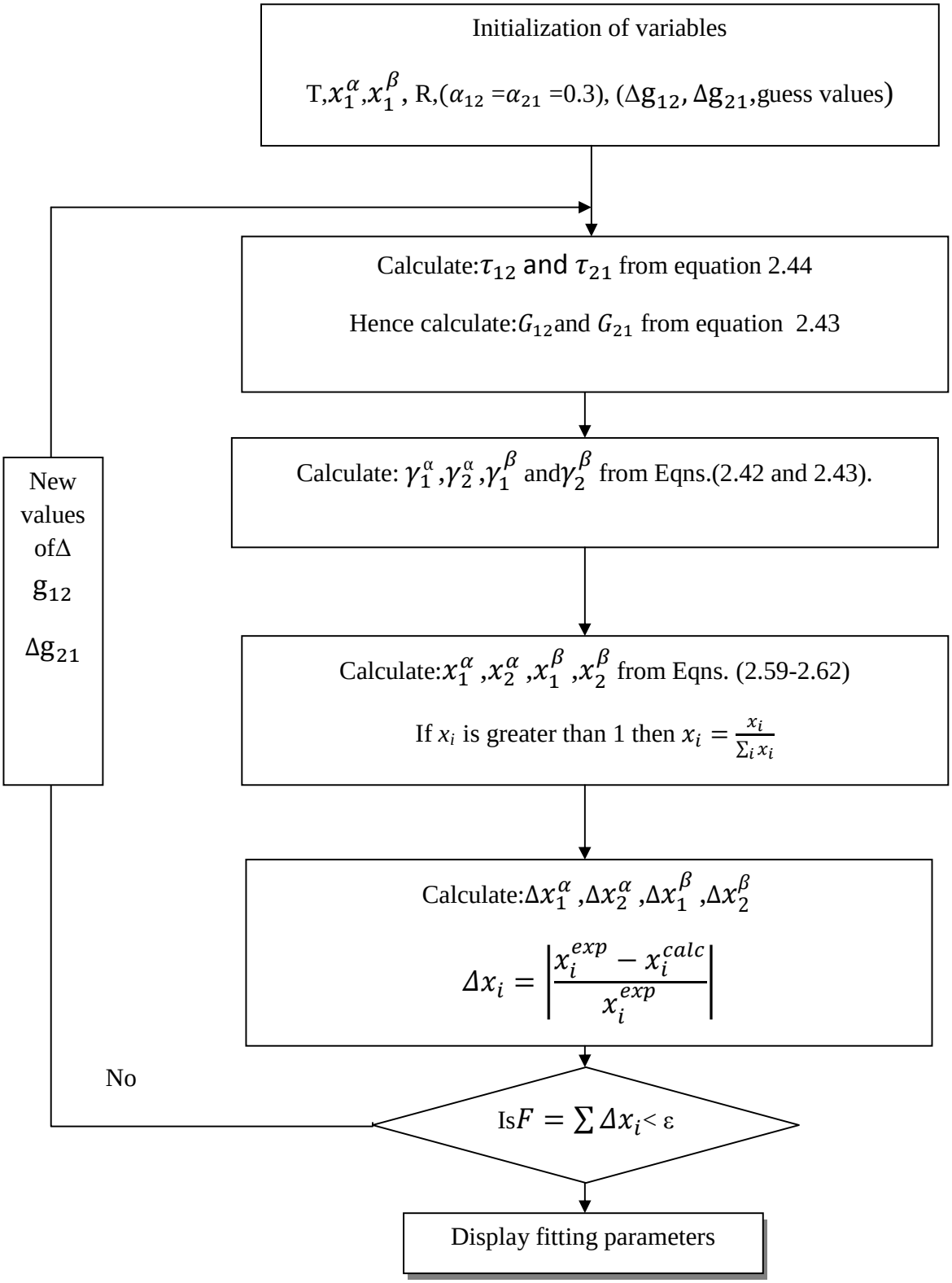

Figure 2-7: Solution algorithm developed for determination of binary interaction parameters (NRTL Model) for LLE system.

2.7.2 The Cox Herington Plot for Coexistence Data

The equilibrium behavior of LLE systems in the critical region has been widely investigated in literature. The understanding of the phase behavior of chemical systems near critical points is attributed to several researchers such as Guggenheim (1945). The understanding of LLE behavior near the critical region for the furfural + n-hexane was made possible by application of the Cox and Herington (1956) equation. The Cox Herington (1956) equation had been developed based on the Guggenheim (1945) equation based on density of the two liquid phases and is given by:

$$\rho^{\alpha} - \rho^{\beta} = K(T_c - T)^{1/3} \tag{2.64}$$

Where *K* is the correlating parameter. Cox and Herington (1956) represented the temperature and composition relation in each phase for coexistence data with two correlating parameters:

$$(T_c - T)^{1/3} = A^{\alpha} log \frac{x_1^{\alpha}}{1-x_1^{\alpha}} + B^{\alpha} x_1^{\alpha} < x_{1c} \tag{2.65}$$

$$(T_c - T)^{1/3} = A^{\beta} log \frac{x_1^{\beta}}{1-x_1^{\beta}} + B^{\beta} x_1^{\alpha} > x_{1c} \tag{2.66}$$

α and β represent the upper and lower liquid phases, respectively. *x* is molar composition and the two constants A and B are two correlating parameters related by the following expression:

$$B = A\ log \frac{1-x_c}{x_c} \tag{2.67}$$

They showed that an expansion of logarithm near critical composition x_c yields the following model equation for representation of equilibrium composition as function of temperature:

$$x^{\alpha} - x_c = K^{\alpha}(T_c - T)^{1/3} \tag{2.68}$$

$$x^{\beta} - x_c = K^{\beta}(T_c - T)^{1/3} \tag{2.69}$$

The form of the equation is similar to that given by Guggenheim (1945) but rather uses molar composition of the two immiscibly compounds instead of phase densities and is used to better correlate the coexistence curve in the critical region. The 1/3 factor in equations (2.68 and 2.69) justifies the linearity of the Cox-Herington plot and can be varied to obtain the best fit of data. A universal parameter σ = 0.325 is normally used instead of 1/3. The critical composition x_c is also obtained by regression.

2.8 Choice of Models for Data Correlation

The objective of data correlation is to find a best model, to accurately describe phase behaviour of systems of interest. This is essential for reliable design and simulation of separation units. However, various limiting factors need to be considered prior selection of a particular model; importantly choosing a good model which is less sophisticated. This helps engineers avoid expending more time on tedious model calculations during their design preparations. Other contributing factors in model choices include: successful past applications of the model to systems of similar nature under similar conditions (i.e. low or high pressure measurements) and the availability of model in the well used process design simulators such as Aspen Plus.

The models chosen in this work are known to have provided very satisfactory results in describing VLE and LLE behaviour for various systems. The systems measured exhibits solvation, high polarity and induced polarity; thus the use of less sophisticated and well defined methods of Hayden and O'Connell (1974) and Nothnagel *et al*. (1973) in describing the vapour non-idealites is justified. The Peng-Robinson (1976) on the other hand has earned its merits for its successful application to various process industries, thus was chosen to establish comparison to the other two models. The three activity coefficient models chosen: Wilson, NRTL and UNIQUAC described in section 2.6.3 are well known and used models. The models are widely used and available in Aspen Plus process simulator which was used for regression of model parameters. In addition, the capabilities and limitations of these models are also well understood. Figure 2-6 below shows the frequency of best fit results using various activity coefficient models for mixtures with alcohols Walas, (1985). Clearly the Wilson and NRTL models stand out as best models earning their consideration for VLE data correlation for systems investigated in this

project. Although the UNIQUAC model shows low best fit frequency its capabilities prompted its consideration in the data correlation for the measured system.

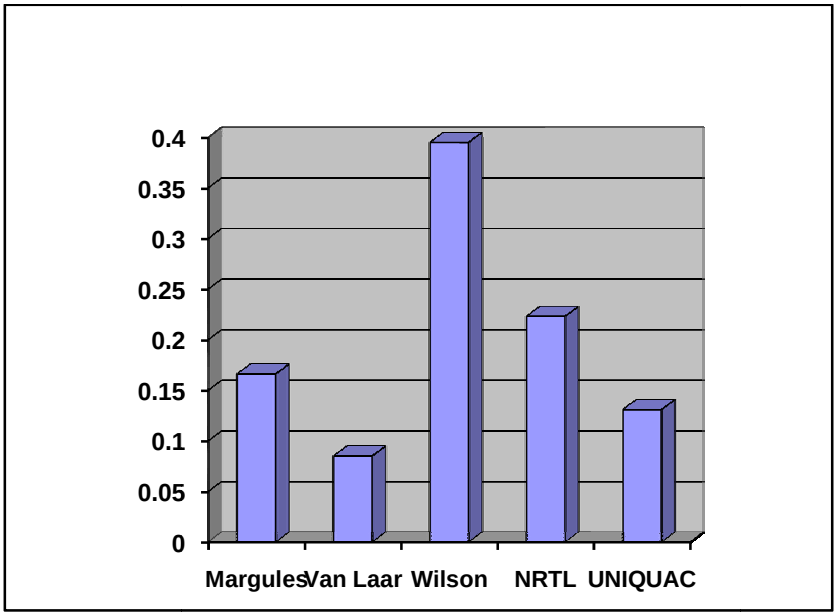

Figure 2-8: Frequency of best fit models for mixtures with alcohols for Dechema VLE Data Collection (Walas, 1985)

2.9 Thermodynamic Consistency

In order to establish the quality of the measured experimental data, it is important to test the measured data for thermodynamic consistency. According to Smith *et al*. (2001), the Gibbs-Duhem equation is the ultimate basis for all thermodynamic consistency tests and is given by:

$$\sum_i x_i d\ln\gamma_i = \frac{\bar{V}^E}{RT} dP - \frac{\bar{H}^E}{RT^2} dT \qquad (2.70)$$

When the VLE data set agrees with the above equation, then the experimental data set is said to be thermodynamically consistent. Two thermodynamic consistency tests were used in this work to determine the consistency of the experimental data; these include the point test and direct test.

2.9.1 Point Test

Van Ness *et al.* (1973) proposed the point test for assessment of VLE data consistency. The test is based on the set of measurable VLE data (P, T, x, y). During measurements it is essential to measure all four variables in order to employ the point test. It is found that in most cases the vapour phase compositions introduces most of the error (Smith *et al*. 2001), thus predicted vapour molar composition data are used for data consistency testing. The procedure for data testing involves regression of the experimental data using either combined method or direct method, for which vapour molar compositions are calculated from the three other variables. The calculated vapour molar composition values are then compared to experimentally measured values. Average absolute deviation in the vapour mole fractions is calculated and compared to the general value of 0.01 (Gess *et al*. 1991). The deviation should be less than or equal to this value for the data to pass the consistency test.

2.9.2 Direct Test

Van Ness (1995) formulated the direct test. He developed a test for which each VLE data point is tested with respect to the Gibbs-Duhem equation. The formulation of direct test is outlined in his work; only the final results are shown below. Two necessary definitions need to be outline first, and are given below.

$$\varepsilon_p = \frac{V^E}{RT}\frac{dP}{dx_1} \tag{2.71}$$

$$\varepsilon_T = \frac{H^E}{RT^2}\frac{dT}{dx_1} \tag{2.72}$$

To test the data for consistency one of two equations is used. Equation (2.72) is used when testing for isobaric data consistency, where the quantity ε_P naturally goes to zero. Similarly for isothermal data ε_T in equation (2.71) equals to zero. The direct test equation for binary VLE data is given as:

$$\delta ln\frac{\gamma_1}{\gamma_2} = x_1\frac{dln\gamma_1^{ex}}{dx_1} + x_2\frac{dln\gamma_2^{ex}}{dx_1} - \varepsilon \tag{2.73}$$

The value of ε rely on whether the data are isothermal or isobaric. The superscript *ex* on the γ indicates that experimental gamma values are used. The VLE data (either isothermal or isobaric) is reduced by minimizing the Gibbs energy residual$\sum(\delta g)^2$, where:

$$g = \frac{G}{RT} = x_1 ln\,\gamma_1 + x_2 ln\,\gamma_2 \tag{2.74}$$

According to the Gibbs-Duhem equation, for the experimental data to be consistent, the right hand side of equation (2.73) must be zero. The residual on the left hand side measures the deviations of the experimental data from the Gibbs-Duhem equation, and the extent to which the residual fails to scatter about the zero axis provides a measure of the departure of the data set from consistency (Van Ness, 1995). Table 2-3 below shows indices which quantify the degree of departure of the experimental data from consistency. The data are classified as of high quality if RMS falls under index 1, while index 10 indicates the data is of low quality.

Table 2-3: Consistency table for the direct test (Van Ness, 1995).

Index	RMS $\delta \ln(\gamma_1/\gamma_2)$	
1	> 0	≤ 0.025
2	> 0.025	≤ 0.050
3	> 0.050	≤ 0.075
4	> 0.075	≤ 0.100
5	> 0.100	≤ 0.125
6	> 0.125	≤ 0.150
7	> 0.150	≤ 0.175
8	> 0.175	≤ 0.200
9	> 0.200	≤ 0.225
10	> 0.225	

CHAPTER 3

REVIEW OF EQUIPMENT AND EXPERIMENTAL METHODS

The ever increasing synthesis and use of organic compounds in the chemical industry (in particular separations industry) has presented the greatest challenge to research and design engineers. The number of possible mixtures has exponentially increased to effectively infinite, adding large number systems to be investigated for phase equilibrium behavior. Design engineers have addressed this issue by turning to predictive methods, which to an extent have proven to predict data with reasonable accuracy for preliminary designs. However, for final design purposes they are often faced with neglecting the errors in prediction results, which can lead to poor design of the separation process. Thus, the measurement of accurate and reliable phase equilibrium data remains a considerable priority in the foreseeable future (Weir *et al*. 2005). Experimental measurements of phase equilibria involve temperature, pressure and equilibrium phase compositions. The reliability if these measurements lie within proper development of equipment and experimental methods.

The reviews of experimental methods and equipment for both low pressure and high pressure Phase equilibrium are well presented by Hala *et al*. (1967), Malanowski (1982), Abbott (1986), Raal and Mühlbauer (1998). Dohrn *et al.* (2002, 2011), also provides great reviews on high pressure experimental methods and various systems measured. In this work, a brief review of some of the available methods is presented and the reader is advised to consults afore mentioned reviews for a well detailed description of phase equilibria methods and available equipment. Raal and Mühlbauer (1994) classified the equilibrium cells as static or dynamic depending upon whether either the liquid or vapour, or both, are circulated through the equilibrium chamber. If circulation takes place, the cell is regarded as a dynamic cell otherwise static cell. Figure 3-1 below shows the classification of cells.

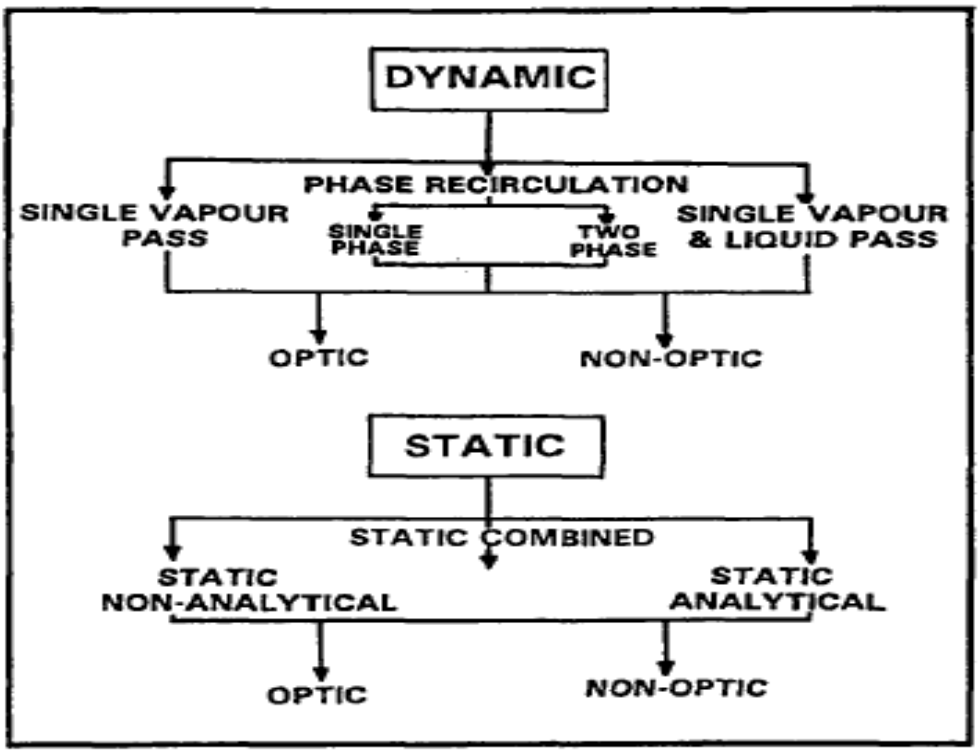

Figure 3-1: Classification of experimental high pressure vapour-liquid equilibrium equipment (Raal and Mühlbauer, 1994).

3.1 Static Equilibrium Apparati

3.1.1 Static Equilibrium Apparatus of Kolbe and Gmehling

Static equilibrium cells were mostly designed to allow for measurement of VLE data at high pressures. The static equilibrium cell is filled with thoroughly degassed liquid mixture, which is agitated by mechanical means for it to reach equilibrium with its vapour at constant temperature. The normal design of a static cell is to operate under isothermal conditions as opposed to recirculating cells which in their normal mode operate to produce isobaric data (Raal and Mühlbauer, 1998). In most static equilibrium cells, only the liquid composition is sampled. The vapour phase compositions are thus calculated from the measured (P-x) data. This procedure represents a considerable economical effort (i.e. No online Gas sampling and analysis), but comes short when data need to be tested for thermodynamic consistency (only P, *x* and T data is available).

Degassing of components in a static cell is considered one of the most important and difficult procedures. The cell tends to be highly affected by the presence of air in the closed space at low pressures, and can result in variation of equilibrium composition if the air is not removed. Figure 3-2 below shows one of the static cells used by Fisher and Gmehling (1994) and De Haan (1995). The cell is based on the development by Kolbe and Gmehling (1985).

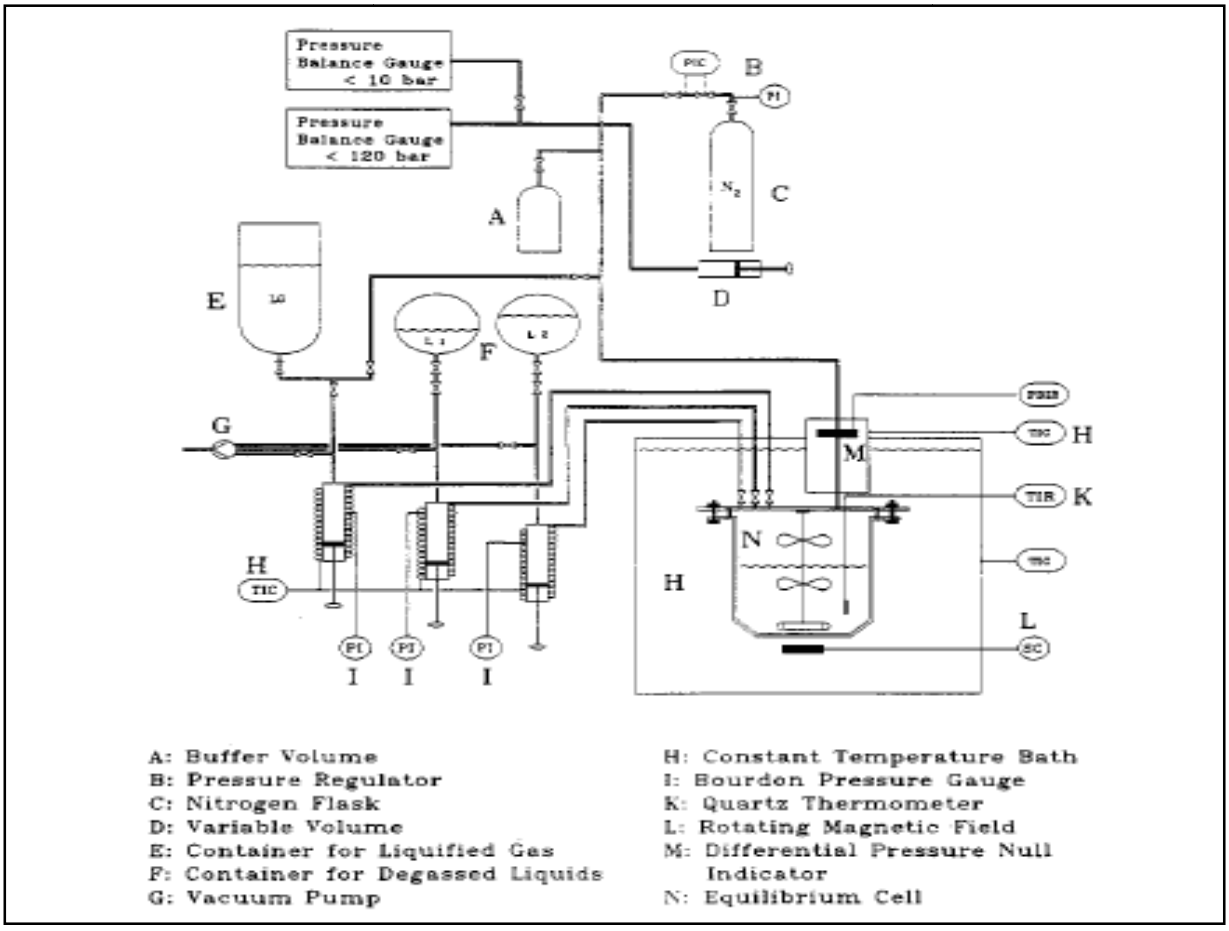

Figure 3-2: The static apparatus used for the P-x measurements (Kolbe and Gmehling, 1985).

The static cell of Kolbe and Gmehling (1985) had been built with a glass equilibrium cell that allows for measurements of up to a pressure of 1 MPa, making it more useful for high pressure measurements. The uncertainties in the measurements carried out by the Kolbe and Gmelhling, (1985) apparatus were ± 0.0001 for molar composition, ± 0.1 kPa and 0.02 K for the temperature. The reader is referred to Kolbe and Gmehling (1985), and Fischer and Gmehling (1994) for the operating procedure and description of the equipment.

3.1.2 Static Equilibrium Apparatus of Laugier and Richon (with online sampling)

The static analytic apparatus of Laugier and Richon (1986) forms the basis of the most successful developments of high pressure equipment with accurate online sampling. The apparatus was designed to work up to 10 MPa and 423 K. A modern example of well developed static analytic apparatus (based on the evolution of Laugier and Richon (1986) apparatus) for VLE measurements is given by Baba-Ahmed *et al*. (1999). The apparatus represents one of the great developments on static analytic methods due to its ability to carry measurements under cryogenic conditions. Figures 3-3a and 3-3b gives the apparatus of Baba-Ahmed *et al*. (1999). Some of the key features of this apparatus are a Hastelloy C276 cell with capacity: 43 cm^3, a well fitted PID thermal regulator to maintain ± 0.05 K temperature stability down to 77 K. A 0 – 4 MPa operational pressure range with an estimated uncertainty of ± 0.005 MPa. An analytic procedure is used for composition analysis with an automated Rapid On-Line Sampler-Injector (Rolsi^{TM}). A fruitful description of the apparatus is given in Baba-Ahmed *et al*. (1999).

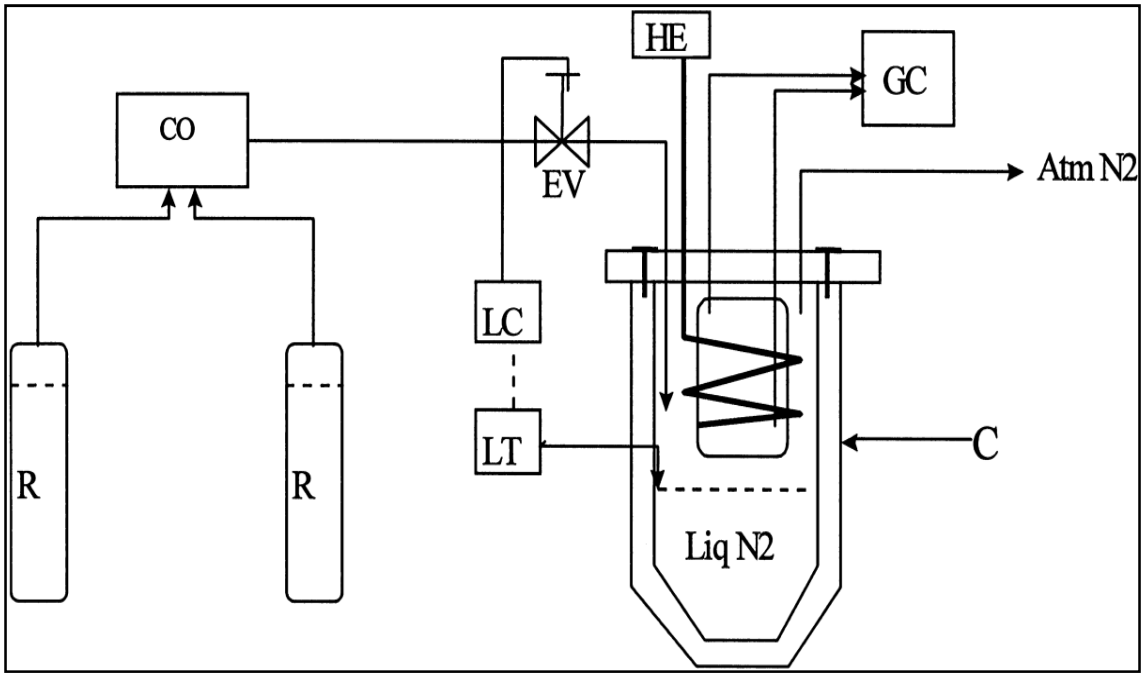

Figure 3-3a: Overview of the static apparatus of Baba-Ahmed *et al*, (1999): *HE: heat exchanger; LT: level transducer; LC: level control; EV: electrovalve; GC: gas chromatograph; C: cryostat; R: liquid nitrogen vessels. CO: commutator.*

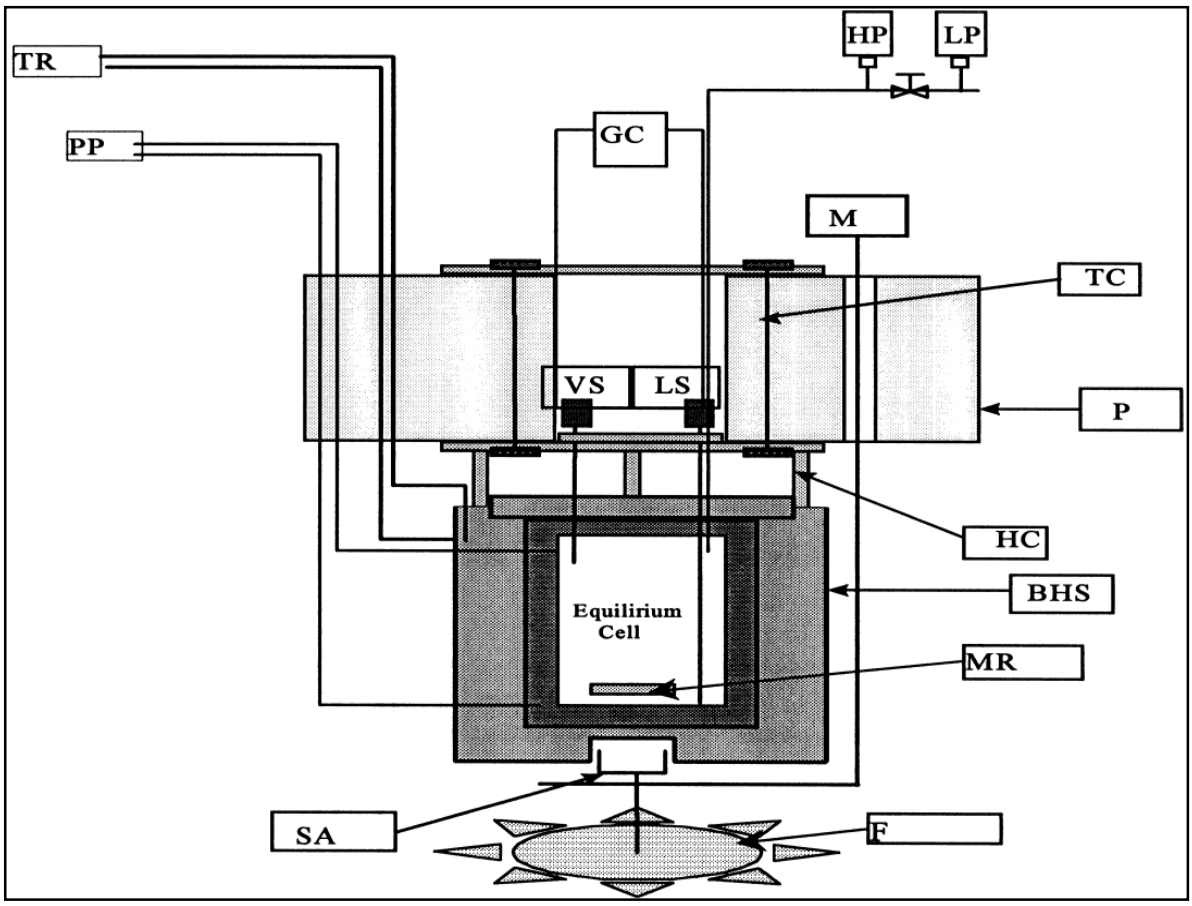

Figure 3-3b: Schematic view of the static cell of Baba-Ahmed *et al,* (1999): *F: fan; M: variable speed motor; PP: platinum probe; MR: magnetic rod; P: plug of the cryostat; BHS: brass heating sleeve with rounded heating resistance; GC: gas chromatograph; HC: holding columns; HP, LP: high and low pressure transducers; VS, LS: vapour and liquid samplers; TR: PID temperature regulator; TC: Teflon thermal shield columns; SA: stirring assembly.*

3.2 Dynamic (Recirculation) Equilibrium Stills

The dynamic (circulating) method has been found to be more effective for measurement of low pressure VLE, as it allows for the use of simpler techniques of acquiring VLE data of high accuracy. The design of a dynamic cell can be classified based on two types of circulating categories, the circulation of only the vapour phase and circulation of both vapour and liquid phases (Hala *et al*. 1967). The cell to be used in this work is based on the circulation of both liquid and vapour phases. Figures 3-4 and 3-5 below shows the dynamic equilibrium cell of Gillespie (1946) and a modern dynamic still of Raal and Mühlbauer (1998) respectively. The

VLE Still of Gillispie (1946) showed better qualities than earlier designs of Scatchard *et al.* (1938) and Othmer (1943) of which had numerous limitations briefly discussed in Coulson *et al* (1948). However the still of Gillispie (1946) also had some drawbacks and better designs have been proposed over the years to give better VLE measurement results. One of the modern VLE stills used for low pressure measurements is that of Raal and Mühlbauer (1998) with various notable key features which are mentioned for example by Clifford, (2003).

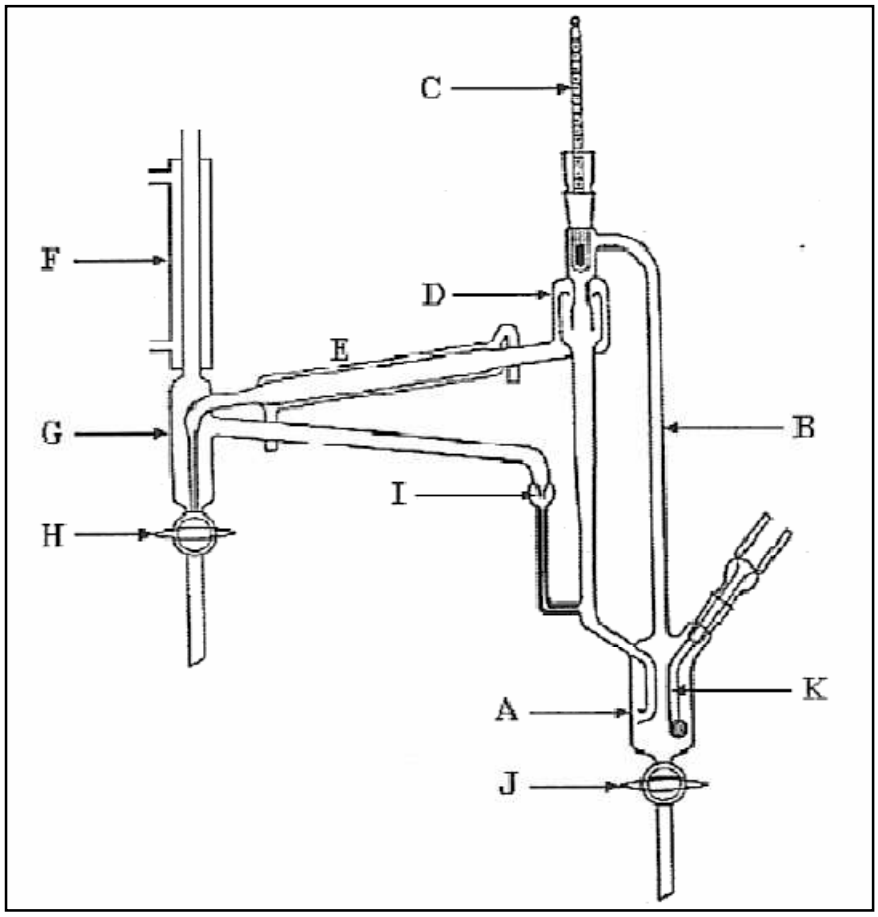

Figure 3-4: The original apparatus of Gillespie (1946).

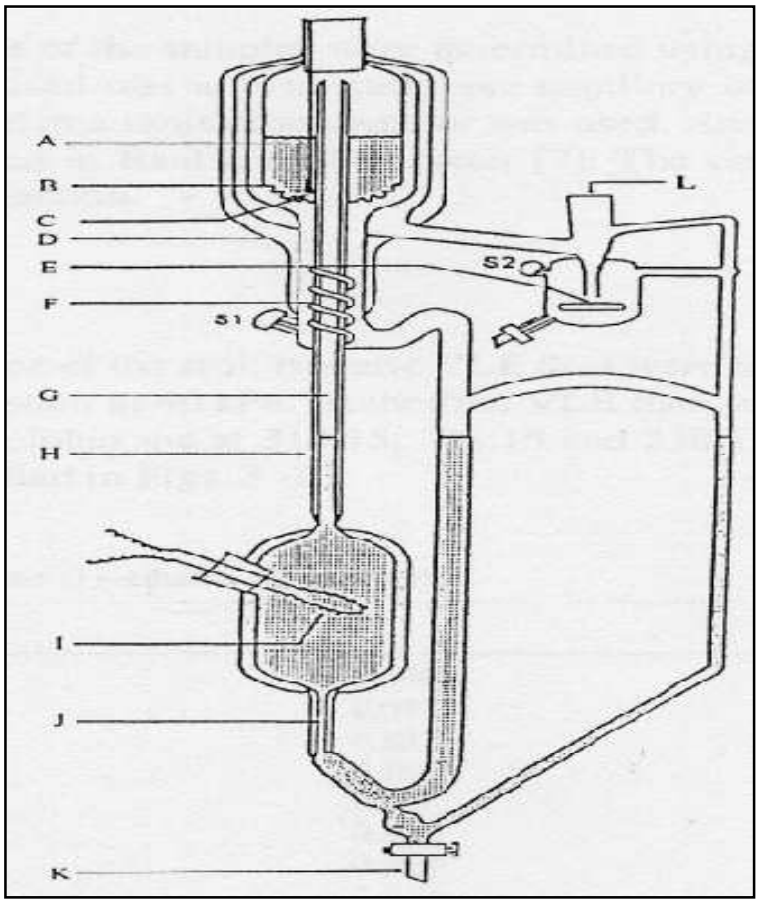

Figure 3-5: Schematic diagram of VLE equilibrium still (Raal and Mühlbauer, 1998)*: A, stainless steel wire mesh packing; B, drain holes; C, Pt-100 sensor; D, vacuum jacket; E, magnetic stirrer; F, stainless steel mixing spiral; G, insulated Cottrell pump; H, vacuum jacket; I, internal heater; J, capillary tube; K, drain valve; L, condenser attachment position; S1, liquid sampling point; S2, vapour sampling point.*

3.3 Liquid-Liquid Equilibrium (LLE) for Binary Systems

Liquid-liquid equilibrium (LLE) phenomenon occurs when a mixture of two or more chemical species do not form a single homogeneous phase, but rather splits into two liquid phases. This normally occurs at a certain range of compositions. There are three techniques that can be used in the experimental determination of LLE in multi-componet mixtures; that is, synthetic or turbidimetric, volumetric and the direct analytic method (Novák *et al*. 1987).

3.3.1 Synthetic Method (Cloud point and Titration)

The basic principle used in this method is visual observation of the appearance and disappearance of turbidity, due to the presence of a second phase. This is achieved by either a change in the system temperature at constant composition or by adding the second component holding the system temperature constant. The shortcoming of visual observation is the fact that formation or disappearance of turbidity is to a certain degree and often quite tedious (Schneider, 1976). Šobr, and Hynek, (1976) eliminated this by constructing an apparatus that employs optical method based on measuring the intensity of the transmitted light. Hefter *et al*. (1991) used a semi automated optical method through measurements of intensity of scattered light.

The titration method on the other hand, uses continuously addition of one component at constant temperature until turbidity is observed to a thermostatted vessel filled with a known quantity of the other component. A micro-burette is used to add the first component to the vessel while stirring intensively until a second phase appears. The two phase mixture is left to stand, forming a sharp boundary. The second phase is poured into a capillary and its volume measured. A more detailed discussion on the titration method is presented in the work of Briggs and Comings (1943), Rifai and Durandet (1962) and Letcher *et al*. (1989).

3.3.2 Volumetric Method

The principle used in volumetric methods for determining mutual solubility involves measuring of equilibrium phases at two or more various ratios of components, while keeping the temperature constant (Hill, 1923). The two components divided between the two phases and the equilibrium compositions in the individual phases at constant temperature do not change. The reader is advised to consult the work of Řehák *et al.* (2005) for a detailed description and mathematical analysis of this method.

3.3.3 Direct Analytic Method

The direct analytical method involves placing a heterogeneous mixture in an isothermal equilibrium cell, with an intense mixing for an adequate time period. The conjugate phases are then allowed to separate by standing. Samples of individual phases are taken using an injection syringe and analyzed. Various physical properties of substances (density, refractive index etc) can be used for composition analysis; however gas and liquid chromatography are generally used for analysis of binary mixtures. Novák *et al.* (1987), Lohmann *et al.* (1998) and Řehák (1999) present different types of equipment used in the direct methods and detailed description sampling procedures.

A newly designed equilibrium cell was used in this work to measure LLE data based on the direct analytic approach coupled with gas chromatography for composition analysis. The equipment is presented in Chapter 4 and procedure presented in section 5.4.4.

CHAPTER 4

EQUIPMENT DESCRIPTION AND OPERATING PROCEDURES

4.1 Description of VLE Equipment Used in this Project

4.1.1 Equilibrium Still of Lilwanth (2011)

The still, used for the measurement of VLE data presented in this work, is a modification of Josephs et al (2001) low pressure glass still which was developed by Lilwanth (2011) in order to handle measurements conducted in the low to moderate pressure ranges (0-5 bar). The features of the Automated still of Lilwanth (2011) include the following equipment in the apparatus in order to handle measurements over a specified range of pressures:

1. AC power supplier
2. 2x National instruments Modules N19263 and N19216 (for temperature measurements)
3. 2x DC motor brushes and 2 magnetic stirrers
4. 2x Pt-100 temperature sensors
5. 2x 50 ohms precision resistors
6. 3x solenoid valves and 6 manual valves
7. A Wika TXM 0-5 bars pressure transducer
8. ACS Shinko pressure controller
9. An Edwards Speedivac Vacuum pump
10. 113L Ballast tank
11. Nitrogen gas cylinder with a regulator
12. Water bath with ethylene glycol solution as the cooling medium and a pump

The equipment is easily operated and uses a similar method described by Joseph *et al*. (2001). The schematic diagram of the VLE apparatus of Lilwanth (2011) is shown with its auxiliary

equipments in Figure 4-1 below. The key features of this still are similar with that of Joseph *et al*. (2001) thus closely similar operating procedure.

With reference to Figure 4-1 below, the boiling chamber (reboiler) is charged with a sample of liquid mixture. The mixture is boiled by use of internal and external heaters. The internal heater provides the principal boiling with a heating cartridge, while the external heater is mainly nichrome wire coiled around the boiling chamber to compensate for heat losses to the surroundings. During boiling, a vapour-liquid mixture is carried upward by the Cottrell tube to the equilibrium chamber that is packed with 3 mm rolled stainless steel wire mesh cylinders. The packing is essential for a larger interfacial area, allowing significant vapour-liquid contact. This allows rapid achievement of equilibrium within the still for all types of species including those with high relative volatility. At the tip of the equilibrium chamber is a temperature sensor, the PT 100. It is placed within the packing of the equilibrium chamber. The vapour liquid equilibrium mixture is allowed to flow downwards through the packing and exit at the bottom of the equilibrium chamber via small holes. The vapour and liquid disengage, with vapour flowing upward around the chamber until it is contacted with the condenser. The vapour condensate flows downwards to vapour condensate sample point, where samples are withdrawn. The overflow condensate returns to the boiling chamber via standpipe leg below the sample point. The liquid mixture from the equilibrium chamber flows to liquid sample point allowing for liquid phase sampling. Overflowing liquid is allowed to mix with vapour condensate at the return union line and returned to boiling chamber. Some of the notable features of the VLE glass still mentioned by Iwarere (2010) are:

- Vacuum insulated Cottrell tube, which is concerned with preventing heat transfer from the slightly superheated mixture within the Cottrell tube.
- The equilibrium chamber is angularly symmetric about the Cottrell tube; preventing temperature and concentration gradients formation, since there is no preferred radial direction for their development.
- A concentric design around the packed section of the equilibrium chamber is used to minimize liquid drop entrainment in the vapour phase and forces the vapour to surround the equilibrium chamber, serving as a thermal lagging.

- Mechanical agitation and magnetic stirrers are included in boiling chamber and sampling points respectively. The mechanical agitation in boiling chamber aims to provide a nucleation site for boiling, while stirring in the sample traps allows for uniform composition of sample and overflowing mixture that is returned to the boiling chamber to prevent flashing during evaporation.

- Pt-100 temperature sensor situated within the packing. This allows the returning liquid to flow around the sensor thus better precision of system temperature.

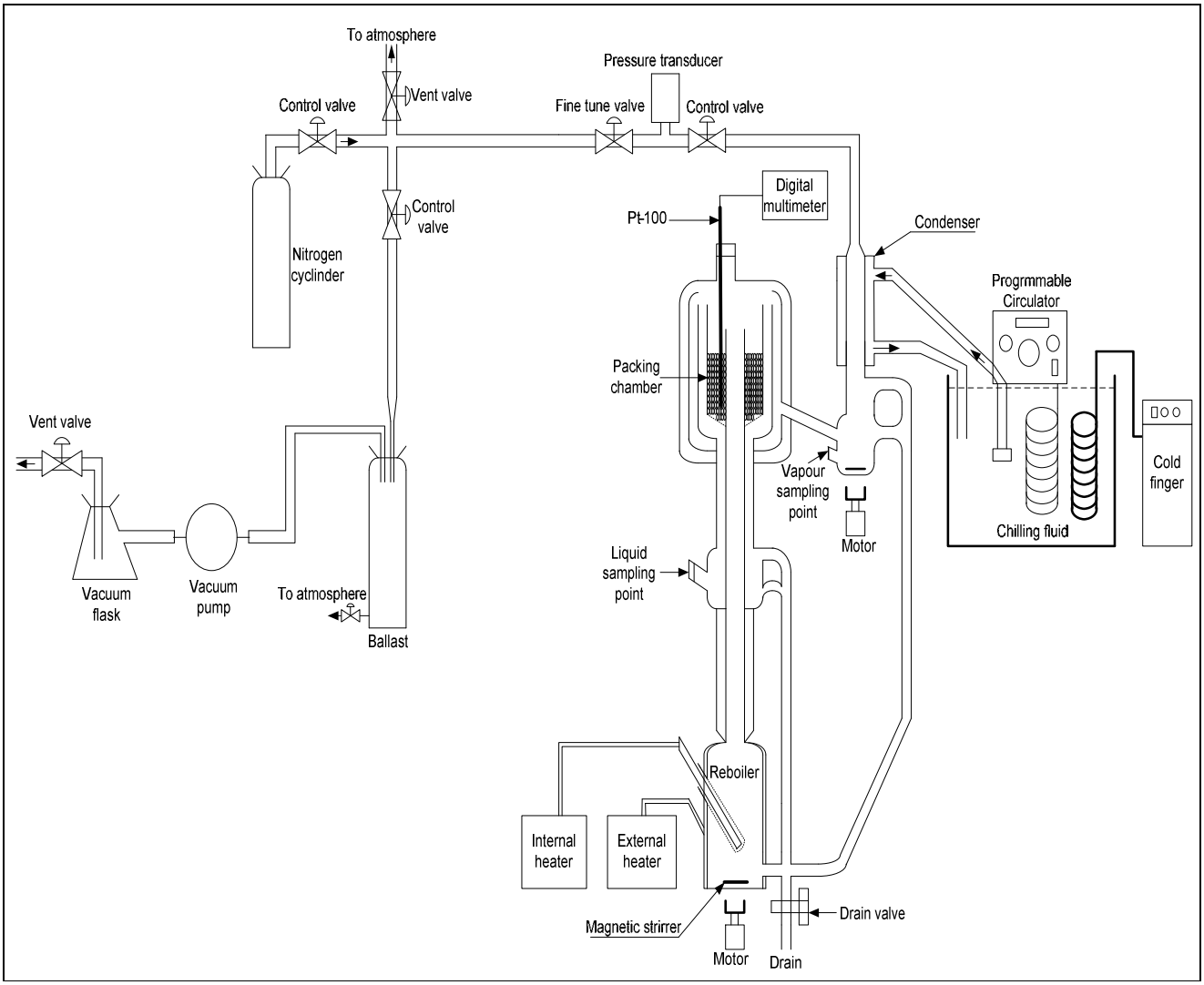

Figure 4-1: Schematic diagram of the VLE apparatus of Lilwanth (2011)

4.1.1.1 Temperature Measurement and Control

A 4-wire 1/10 DIN Pt100 sensor (supplied by WIKA Instruments) connected to the Labview® program is used for temperature measurement. Automated temperature control scheme is employed in the equipment by the use of Labview® temperature control VI (in-house program specifically designed for isothermal temperature control). The temperature VI program is cascaded to pressure control scheme which changes pressure by use of three solenoid valves. The temperature uncertainty is estimated to be ±0.02 K (A *Type B*, uncertainty, NIST).

4.1.1.2 Pressure Measurement and Control

The SENSOTEC Super TJE pressure transducer and the WIKA P-10 capable of transmitting pressure up to 1000 kPa are fitted on the apparatus Joseph (2001) and Lilwanth (2011) respectively. The pressure control was achieved with a use of the BUCHI model B721 that uses a two way solenoid valve, connected directly to a vacuum pump and a vent to the atmosphere. The pressure uncertainty is estimated to be ±0.23 kPa (A *Type B*, uncertainty, NIST) and the pressure control scheme allows for control to within 0.1 kPa during operation.

4.1.1.3 Sampling and Composition Analysis

2 ml samples are taken via the provided liquid and vapour condensate sample points into well sealed sample vials. A 5 µl sample is taken by gas tight liquid syringe and analysed using a Shimadzu GC 2014 or Shimadzu GC 2010. The two Shimadzu GC's are equipped with thermal conductivity detector (TCD). GC 2014 uses a poropack Q packed column and thus separating chemical species based on molecular size, while a HP-5 capillary column is used in GC 2010 and separates a given system based on volatility (i.e. the more volatile component is removed first in the column).

4.4.2 The Atmospheric VLE Still

Figure 4-2 shows the dynamic atmospheric vapour liquid equilibrium still. The equilibrium still allows circulating both liquid and vapour phases. Samples of the liquid and vapour phases can be taken through the sampling points indicated on figure 4-2. The design is simple; the heating

system of the liquid mixture is provided through the heat Cottrell with external heating source. The temperature of the system is measured using a calibrated aluminium probe inserted into the probe well. The equipment is used for atmospheric pressure measurements thus no pressure control scheme is put in place (i.e. the pressure controller line is open to atmosphere). The condenser at the top allows recirculation of vapour phase back to boiling chamber as condensate. One shortcoming of this cell is inability to obtain the overall vapour condensate composition for systems that form two liquid phases.

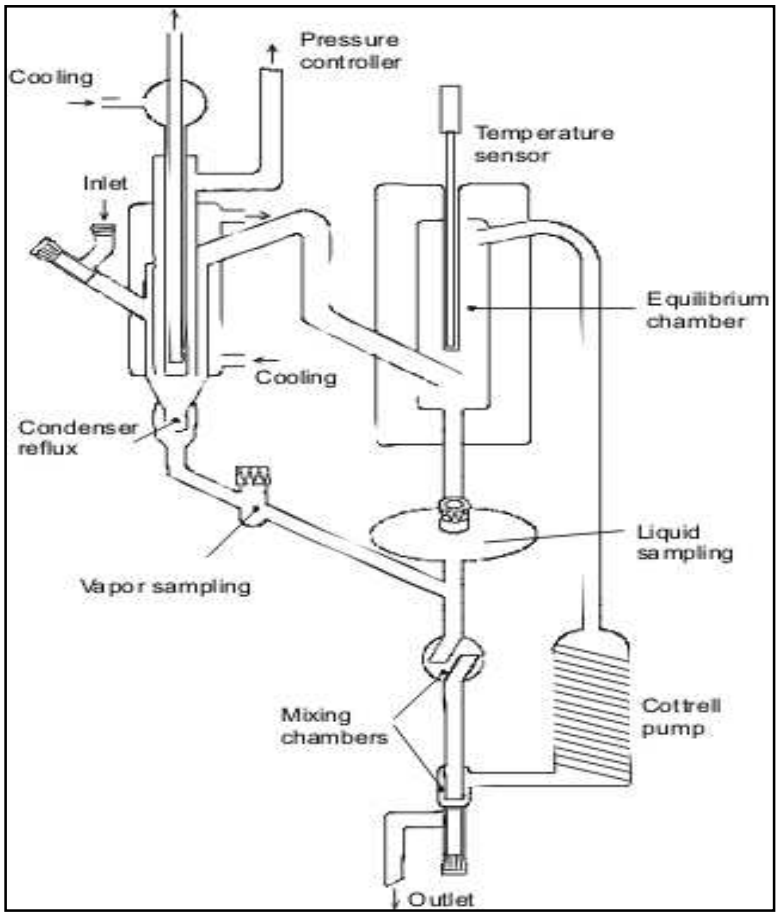

Figure 4-2: The dynamic VLE still used for atmospheric pressure measurements (Swietoslawski ebulliometer, as described by Rogalski and Malanowski,1980).

4.2 Description of the LLE Equipment Used in this Project

This section provides a description of the new VLLE apparatus which was commissioned for LLE measurements in the CEP/TEP laboratory in France. Figure 4-3 shows the old apparatus

previously available for LLE measurements in the CEP/TEP laboratory, which had been found to have several shortcomings for measurements of the given LLE systems. An improved apparatus capable of measuring VLLE data was designed as replacement of the old apparatus; and is presented in section 4.2.2.

4.2.1 Previous LLE Apparatus

The apparatus used for measurement of liquid-liquid equilibrium data was based on a modification of the cell previously available at CEP/TEP laboratory. The original design was based on a normal glass beaker with rubber cap to minimise rapid loss of highly volatile components. It consisted of two sampling points for the two liquid phases and a small hole for inserting a temperature sensor. A picture of this cell is shown in the Figure 4-3.

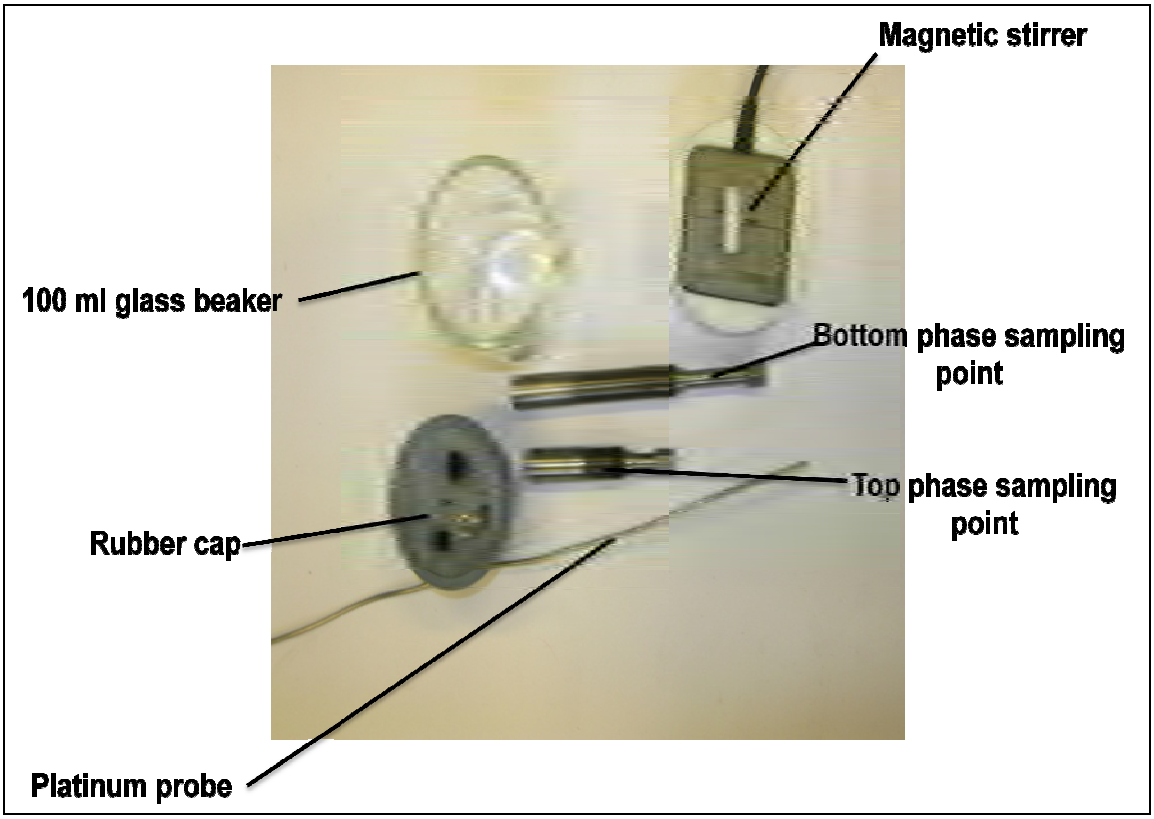

Figure 4-3: Previously used LLE cell with auxiliary equipment

During experimentation, the glass part of the cell is submerged in temperature regulated water bath. The observed shortcomings of this design during LLE measurements were:

- The compatibility of the rubber with chemicals used in this project (furfural-hexane system in particular). The chemicals were absorbed into the rubber, and thus increased the diameter of the rubber cap, thus no proper fitting to the glass beaker.

- The cell was opened to atmosphere which prevented attaining stable equilibrium in the lighter phase. This is due to continuous loss of most volatile component.

4.2.2 New VLLE Apparatus

Equipment list

1. Glass Equilibrium Cell
2. Stainless steel cap with 3 sampling points
3. Stainless steel support bracket
4. Teflon coated magnetic stirrer bar
5. O-ring
6. Bath with distilled water for cooling (Minimum temperature 253.15 K)
7. Vacuum pump
8. Nitrogen tank
9. Pt 100 platinum probe

4.2.2.1 Apparatus Design and Auxiliary Equipment

The newly designed VLLE cell is equipped with a stainless steel cap which closes the cell completely, preventing any loss of material. The new design consists of three sampling points allowing sampling of liquid phase I, liquid phase II and vapour phase. The sampling points are equipped with air-tight rubber septa to hold any loss of pressure within the cell. The temperature is measured using a Pt-100 platinum probe which is inserted through a port at the top of the stainless steel cap. The port is designed to fit the Pt-100 with an adjustable bolt fitting which also eliminates the loss of pressure within the cell. The pressure inside the cell is determined by the

chemicals used. The glass used for this cell is capable of withstanding pressures up to 400 kPa. The pressure testing was undertaken by introducing nitrogen gas in the cell at room temperature. The safe operation pressure recommended is 3 bar taking into account the effect of temperature in the glass. The cell caparcity is up to 60 ml, which is adequate for continuous measurements and sampling without disturbance of equilibrium. A vacuum pump line is installed at the top of the cap. This is suitable during loading of the cell by inducing a small vacuum and allowing materials to flow into the cell. Air which may be present after loading the cell is removed by inducing the vacuum. Figures 4-4 and 4-5 show a mechanical drawing of the new VLLE cell and schematic diagram of VLLE apparatus setup used for measurements respectively. In figure 4-4, a detailed scheme of the cell is shown with the necessary fitting lines shown. Figure 4-6(a) shows a picture of unconstructed VLLE cell with auxiliary equipment. The cell was constructed and ready for measurements as shown in figure 4-6 (b&c) below.

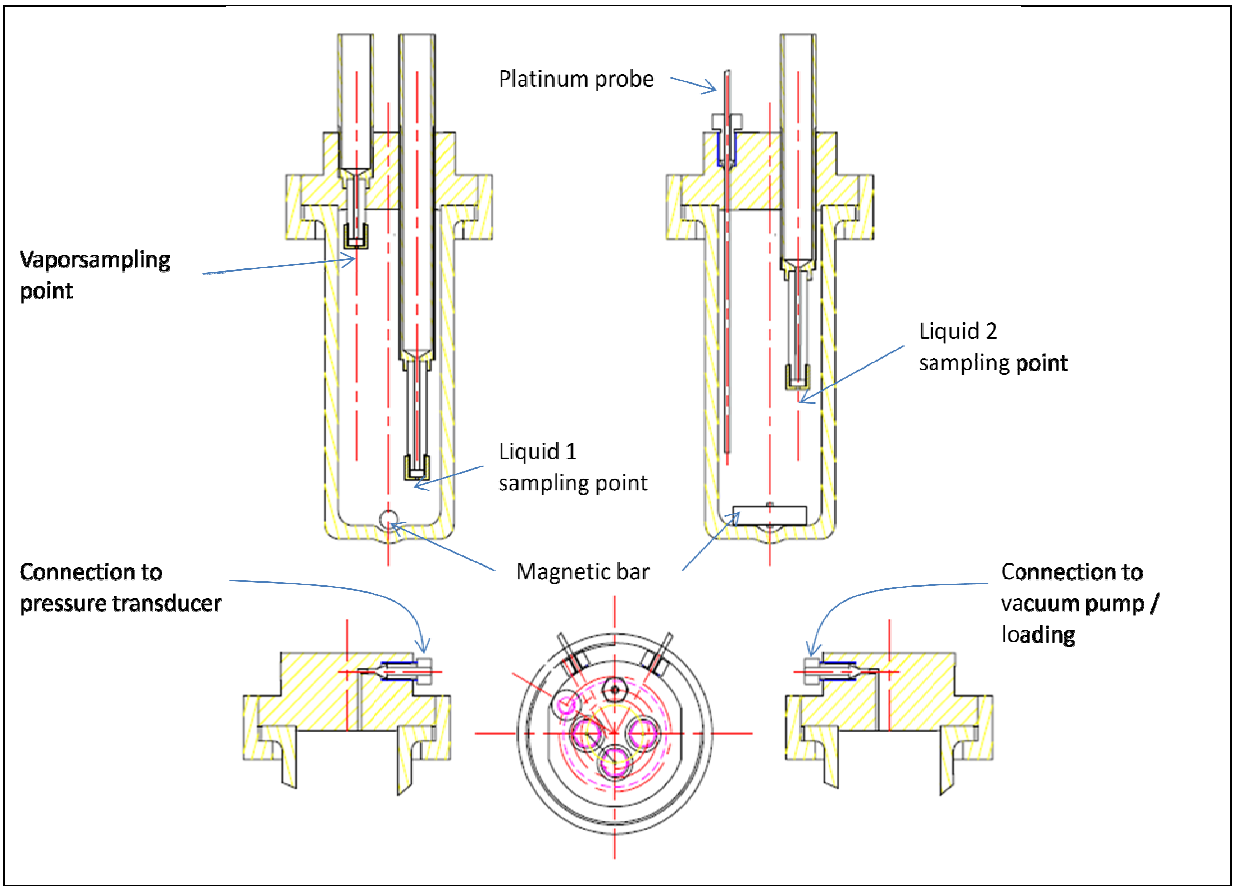

Figure.4-4: Mechanical design of new VLLE cell.

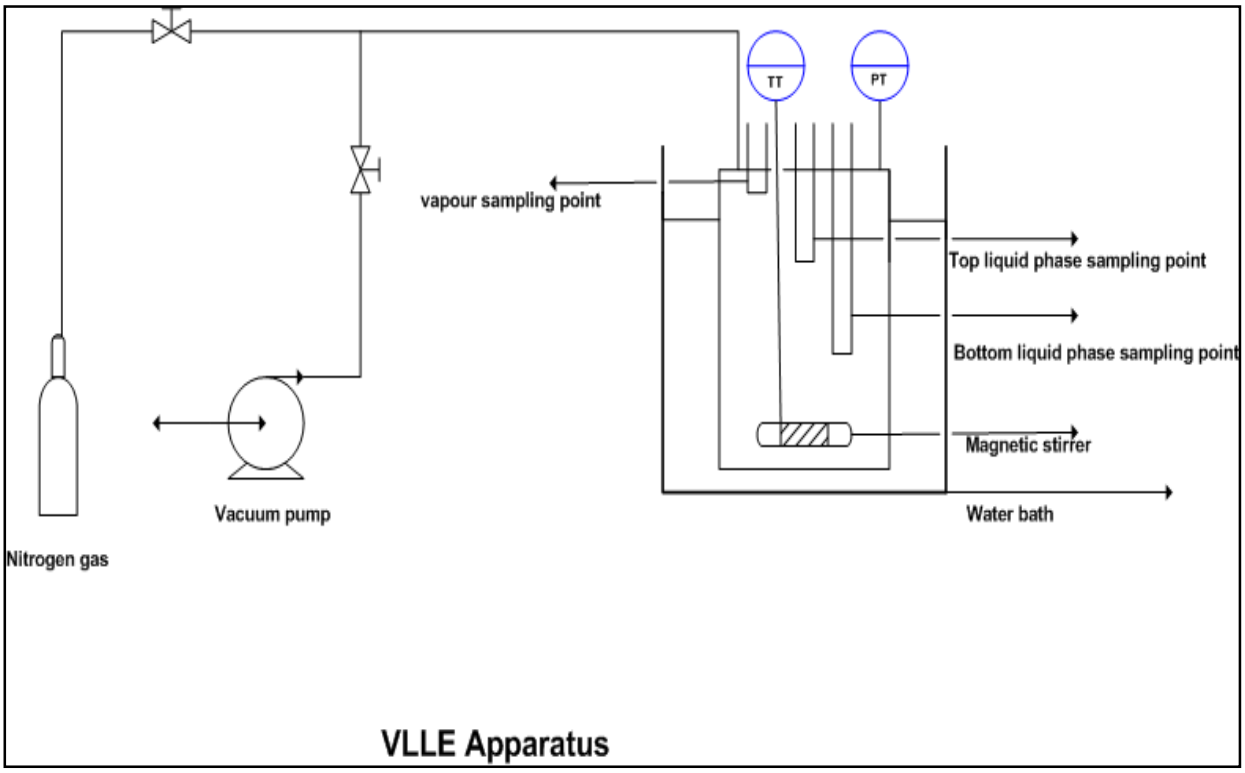

Figure 4-5: Schematic diagram of the new VLLE apparatus used for measurements.

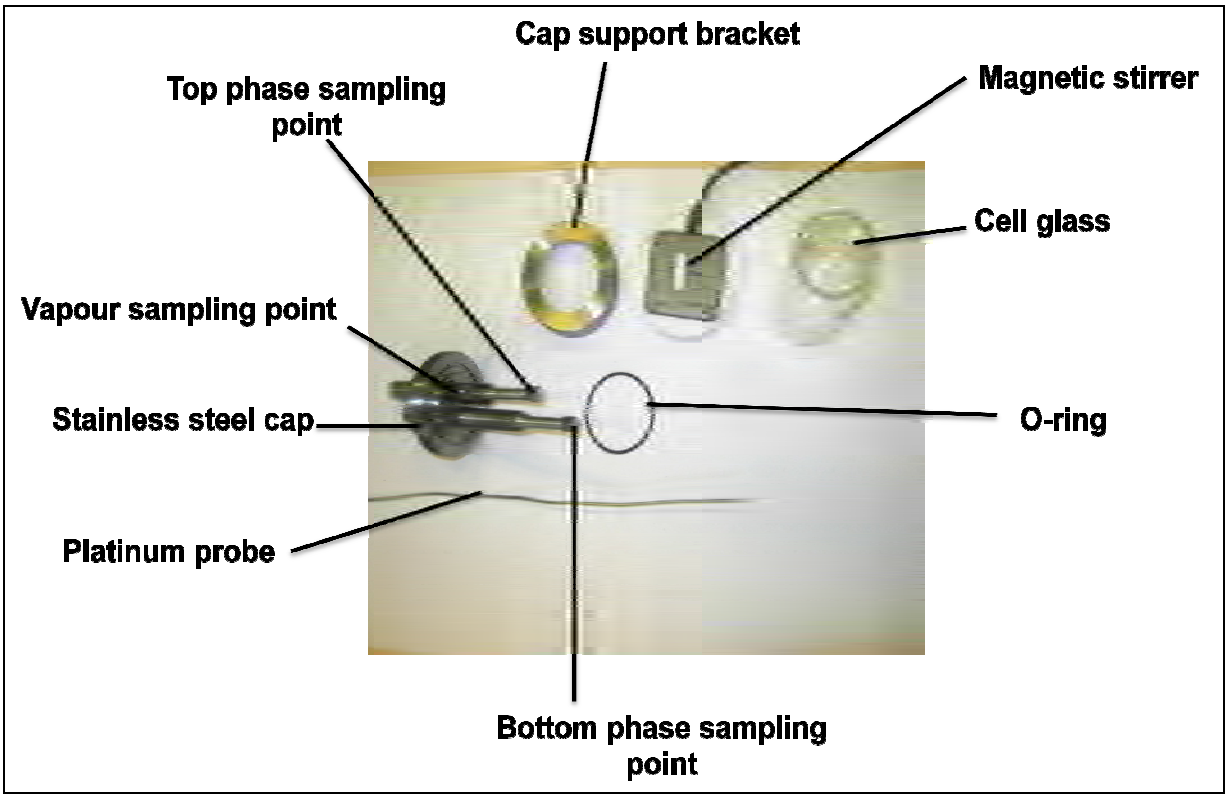

Figure 4-6 (a): Photograph of the new VLLE cell with auxiliary equipment.

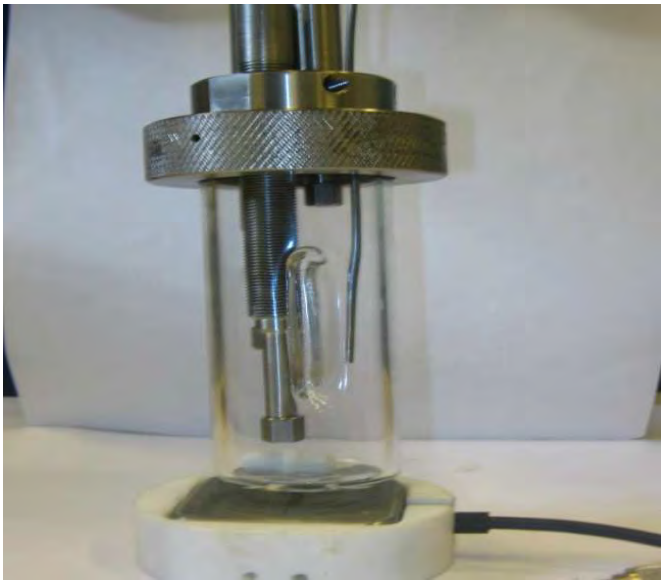

Figure 4-6 (b): photograph of a fully constructed VLLE cell.

Figure 4-6(c): Photograph of a fully constructed VLLE submerged in the water bath during data measurements.

CHAPTER 5

EXPERIMENTAL PROCEDURE AND SENSOR CALIBRATION RESULTS

This chapter outlines the general procedure employed in obtaining the VLE and LLE data using the Apparatuses discussed in Chapter 4. The efficiency of equipment operation and reliability of data measured rely on the systematic and careful approach during data measurement. The main focus of this chapter is to outline the preparation of the experimental apparatus, calibration of pressure sensors, temperature sensors and gas chromatograph detectors (TCD); and to present a step by step operation of the equipment during experimental measurements.

5.1 Preparation of Experimental VLE Apparatus

5.1.1 Leak Detection Procedure

Leaks are one of the major issues that need to be addressed before using the experimental apparatus. They continuously cause instability as they affect pressure measurements and control during operation. It is further observed that leaking equipment results in loss of material and thus adversely affect composition measurements in both liquid and vapour phases.

To detect leaks, the medium pressure VLE apparatus was pressurized to about 4 bars and systematically applying Snoop® (commercial leak detection soapy solution) in various fittings and seals. The forming of bubbles in a fitting or seal indicated a leak at that point. The identified leak was eliminated by proper sealing. The second leak test was undertaken under vacuum conditions, where the system was evacuated to about 1 kPa and isolated from the ballast. This was done to avoid the effect of the large ballast on the rapid detection of leaks. The pressure was then monitored with time (high rate of change of pressure indicated that the system was leaking). The second leak detection method was the only method employed in the still of Joseph (2001).

5.1.2 Cleaning of the VLE Still

Impurities in chemical systems and experimental apparatus can affect/comprise the accuracy of the measured data, thus, it is crucial to clean the equipment before commencing with calibration and data measurement. With leaks eliminated, the VLE stills of Joseph (2001) and Lilwanth (2011) were cleaned using low boiling acetone. The solvent was circulated by boiling it under atmospheric conditions for about 12 hours, followed by draining the effluent from the still. A vacuum was induced using a vacuum pump and taking the pressure down to about 1 kPa and slight heating of the still to about 50 ^{o}C to remove any residual solvent in the still.

The atmospheric VLE apparatus was cleaned using ethanol. The solvent was circulated by boiling it under atmospheric conditions for about 12 hours, followed by draining the effluent from the still. A slight heating of the still is induced to remove any residual solvent that may be present in the still.

5.2 Calibration of Sensors

Prior to undertaking any VLE measurements, the temperature and pressure sensors had to be calibrated. The necessity of calibration is to eliminate bias introduced by equipment used for measurements. Calibration of sensors is considered as a vital phase of VLE measurements and needed to be accomplished as accurate as possible based on the fact that the measured VLE data depends directly on the precision of sensor calibrations.

5.2.1 Pressure Calibration

The Sensotec pressure transducer used in the low pressure VLE still of Josephs et al (2001) was calibrated against a WIKA CPH 6000 digital calibrator multimeter, fitted with a standard reference transducer (WIKA) with a maximum pressure of 1 atm. A pneumatic hand pump (WIKA, model WICP M500) was connected to both the reference and the Sensotec transducer. The pressure to the reference and Sensotec transducers was increased by compressing the hand pump, and decreased via a precision needle valve and fine-tuned to a desired pressure.

The SENSOTEC Super TJE pressure transducer and the WIKA P-10 transmitter used in the medium pressure VLE still of Lilwanth (2011) was calibrated using a different approach. A WIKA standard pressure instrument was connected in series with the pressure transducer and readings were taken for both transducers. A value on theWIKA CTH 6500 display was taken as the true pressure value and recoded against the display value indicated on the Labview® software. A series of pressures covering the range of anticipated experimental pressures were measured and a plot of actual pressure against the display pressure was utilized to get the equation relating the two.

The atmospheric VLE still needed not to be calibrated for pressure, since no pressure control scheme was put in place.

5.2.2 Temperature Calibration

The Pt-100 temperature sensor fitted inside the equilibrium chamber in both Joseph e*t al*. (2001) and Lilwanth (2011) VLE still had to be calibrated. This was achieved using a standard Pt-100 reference probe connected to a WIKA CTH 6500 display and submerging both Pt-100 probes into the WIKA 9100 oil bath filled with silicon oil.To detect presence of hysteresis, the temperature of the oil bath was increased and decreased monotonically until the entire temperature range was covered. A plot of actual temperature versus display temperature was generated and a linear fit of data allowed for the determination of the slope and intercept of the line.

The temperature probe used in the atmospheric VLE still was calibrated using a Fluke hart scientific 5628 standard probe connected to an Agilent digital multi-meter in a Fluke 9144 Field Metrology calibration instrument capable of handling temperatures between 50 and 660 ^{o}C.

5.2.3 Composition Analysis

5.2.3.1 Gas Chromatograph Detector Calibration

For the VLE measurements undertaken on the stills of Joseph (2001) and Lilwanth (2011), the Shimadzu GC 2010 and GC 2014 were used to analyze the equilibrium compositions. The GC's were operated at conditions that allow appropriate generation of separate sharp peaks. Figure 5-1 and 5-2 below gives an example of good and poor separation of chemical species in gas

chromatograph respectively. To attain good chromatographic separation, GC parameters such as column oven temperature, split ratio and carrier gas flow were varied until best separation results are obtained. Should there be no separation after variation of these parameters; the separation column was changed using literature recommendations until separation is possible.

The columns used in the GC's were conditioned to remove any contaminants present which may adversely affect the analysis. The conditioning process involved heating the column at higher temperatures for example 20 ^{o}C below the maximum allowable temperature for period of 12 hours at constant flow of the helium gas. Afterwards the column is used for analysis at normal conditions predetermined for analysis of each system.

During the GC analysis process, peak areas for each component present are obtained rather than absolute compositions. To obtain absolute composition, the chromatograph area ratio method described by Raal and Mülhbauer (1998) was employed for analysis for VLE measurements in the UKZN laboratories. Defining a response factor F_i (proportional constant) between the number of moles passing the detector n_i and peak area A_i for each component, it can be deduced that:

$$n_i = A_i F_i \tag{5.1}$$

The absolute areas depend on the amount of substance injected, and usually not very reproducible. From equation (5.1) it can be shown that for binary mixture:

$$\frac{n_1}{n_2} = \left(\frac{A_1}{A_2}\right)\left(\frac{F_1}{F_2}\right) = \frac{x_1}{x_2} \tag{5.2}$$

A plot of the area ratios A_i/A_j against the mole fractions x_i/x_j for $0 \leq x_i \leq 0.5$ and $0.5 \leq x_i \leq 1$

is generated. The slopes of both plots give the response factor ratios, which ideally for constant response factors. The slope of the first plot should be equal to the inverse of the slope of the second plot. To generate the calibration curves for each system, synthetic mixtures were accurately prepared from pure components and analyzing them to obtain area ratios. The calculated maximum mole fractions uncertainty is estimated to ±0.01 observed for the system of diisipropyl ether (1) + propan-1-ol (2).

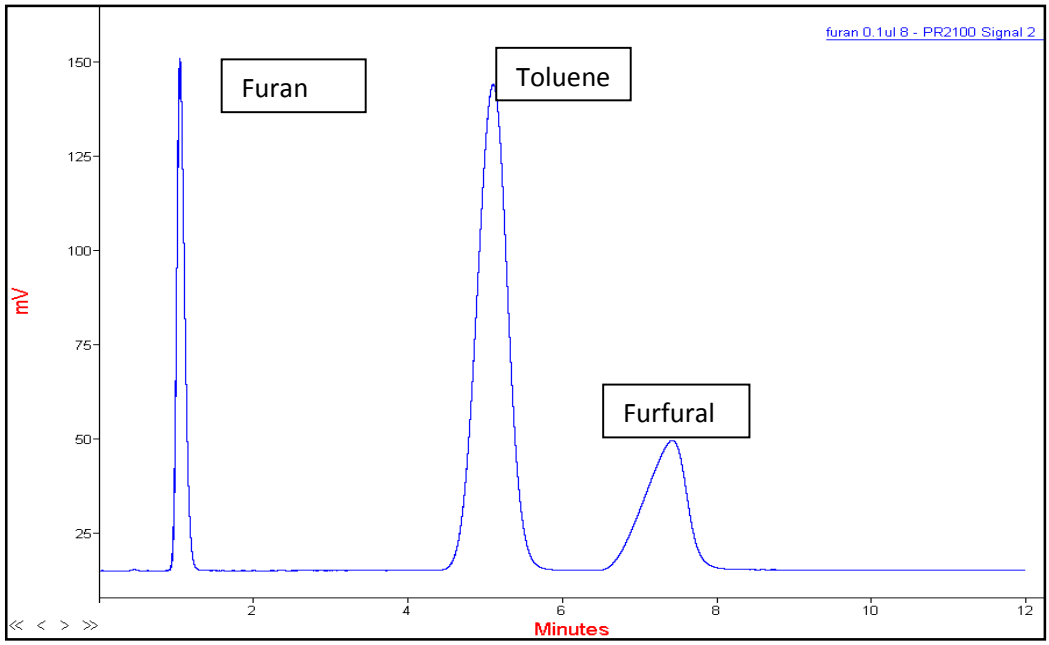

Figure 5-1: Chromatograms of furan, toluene and furfural mixture, to illustrate good separation of chemical species in gas chromatograph.

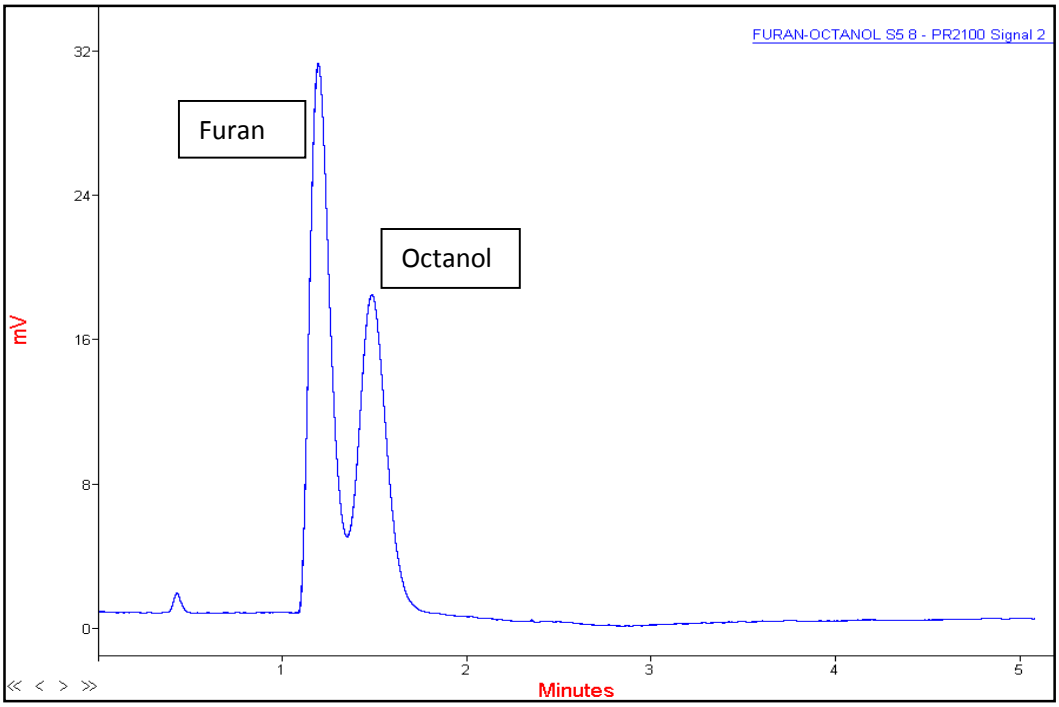

Figure 5-2: Chromatograms of furan, toluene and furfural mixture, to illustrate poor separation of chemical species in gas chromatograph.

5.2.3.2 Density Meter Calibration

A different approach to that of GC analysis was used for the systems measured with atmospheric VLE still. The composition of the sampled liquid and condensed vapour phase were determined using an Anton Paar^{TM} DM5000 density meter, with a reported uncertainty of ±0.01 K (*Type B*, uncertainty, NIST) in temperature and $\pm 10^{-5}$ g/cm^3 in density. Several mixtures of known composition were prepared for each system and density values were determined by the instrument at different temperatures. A plot of composition against density was utilized to obtain a model equation for the correlation of density and composition values. The densities obtained were also used to obtain excess molar volumes of each system at different temperatures. A plot of composition against density was utilized to obtain a model equation for correlation of density and composition. The densities obtained were also used to obtain excess molar volume of each system at different temperatures.

5.3 Operating Procedure of the Automated VLE Still

5.3.1 Isobaric Mode (vacuum)

Startup Procedure

During equipment operation, the electronic display units (computer, temperature and pressure display units), together with the cooling unit were switched on. The temperature in the cooling unit (water bath) is set to about - 5 ^{o}C and equipment is only operated when the circulating fluid reaches a temperature closer to 0 ^{o}C to avoid loss of material in the condenser during boiling. The VLE still and ballast tank are evacuated by opening the by-pass valve on the vacuum line. This is done to remove any vapours including air that might have been present within the apparatus. During this degassing procedure, the pressure control scheme is switched off, thus the solenoid valves on the pressure lines are in their “normal closed” positions. The evacuation is considered complete when the pressure on the display unit was at a minimum (no significant change in the pressure). The VLE still is filled with approximately 80 ml (about 3 cm higher than the top of the boiling chamber) of the liquid mixture, which is the specified capacity range of the boiling chamber (variable based on pressure and temperature of operation). With the liquid

mixture fed into the boiling chamber, the pressure is set to the desired set point in the Labview™ program created by Lilwanth (2011), (i.e. the isobaric operating pressure for measurements). The pressure control scheme is activated to keep the pressure at a set value by automatic activation of the solenoid valves. The electrical power supplies for the heaters (internal and external) and stirrers are switched on. The internal heater provides the principal heating to boil the liquid mixture, while the external heater of the boiling chamber compensated for heat losses to the surrounding environment. It is important to note that the value of external heat input should not be so high as to control the process of determining the equilibrium region, yet high enough to ensure no heat loss. Temperature in the equilibrium chamber is monitored and sufficient heat is supplied to ensure continuous and smooth boiling (observed inside the transparent Cottrell tube) and high circulation rate (judged by counting the condensate drop rate). The internal heater is incremented systematically in predetermined constant quantities and therefore the plateau region is located.

According to Kneisl *et al*. (1989), the boiling point temperature to be a function of power input. They established the plateau region as state where the boiling temperature does not change for a slight increase in the power input. It is critical that the measurements are taken inside the plateau region to prevent the recording of incorrect boiling point temperature values, which is the case for readings taken outside this region. Ideally, it is expected that the plateau region should be flat line. However, in most cases the plateau region is found to exhibit a slight slope and region of lowest slope is accepted as a plateau region.

When the plateau region has been established, the system is allowed to run at the internal and external heater setting for that region for approximately 50 minutes. The system is assumed to be in equilibrium when both the temperature and composition of system are constant. The equilibrium temperature is then noted, the liquid and vapour samples are then withdrawn through the sample septa using a gas-tight liquid syringe (about 2 ml). The samples are stored in gas chromatograph sample bottles, and later analyzed by gas chromatography. The sample is injected at least three times into the GC to ensure reproducibility and the average of the three compositions is utilized. After removal of the samples, a small volume of liquid is removed from the still and replaced by similar volume of the second component to adjust the system

composition. The system is again brought into equilibrium and samples taken for phase composition analysis. The procedure is repeated till the midpoint of the composition range is reached (half of VLE curve) and thereafter, the still is drained and cleaned before charged with the second component of the binary mixture. A similar procedure is employed to measure data for the other half of VLE curve. This technique is set to allow for many points in dilute regions and in addition provides confirmation of the accuracy of the results, since the two halves of the VLE curve must meet without any discontinuity.

5.3.2 Isobaric Mode (above atmospheric pressure)

For operating above atmospheric pressure, the nitrogen regulator is opened and the vacuum pump is switched off. Initially, when attempting to reach the desired set point pressure, the bypass loop may be opened to hasten the process, thus allowing the nitrogen to flow through faster and enable the new pressure to be reached quickly. When the set point pressure is reached, the programmed computer software will automatically control the solenoid valves connected to the nitrogen tank, and the atmosphere to maintain the conditions necessary for operation. The daunting problem encountered during this operation was the process of sampling at above atmospheric conditions. The GC syringe is at atmospheric pressure; therefore, the sample shoots out of the syringe once it is removed from the septum of the still. Therefore, slightly more sample than required for analysis must be withdrawn using a 10 ml liquid syringe. This allows compensate for sample lost during retraction of the syringe from the sampling septum. The samples are then stored in 2ml sample vials and placed in the freezer until analysis takes place.

5.3.2 Isothermal Mode

The isothermal procedure depends merely on the success of operating the still in isobaric mode. The procedures employed in isobaric mode are the same in isothermal (equilibrium determination, composition analysis, etc). The only difference between the two operations is that, pressure is varied to maintain constant system temperature. The set point temperature is inputted on the Labview^{TM} software interface. The program automatically controls the pressure within the still, to achieve the requested temperature, via the alternation of the solenoid valves. For the system below atmospheric pressure, the vacuum pump is switched on. The nitrogen tank is opened at all times during isothermal mode. This enables easier control of the system pressure,

as well as a simplistically maneuvered transition from low to high pressures. Once the required temperature is reached, and the plateau region is located, the samples are withdrawn, analyzed and the next composition set is reached by addition of the diluter component, to yield an equilibrium temperature closet to the operating temperature.

5.3.3 Shutdown Procedure

It is necessary to employ a safe shut down procedure after acquiring of data from the VLE apparatus. The heaters are switched off; while the cooling unit remains on to ensure that all vapours formed are condensed. The system is then allowed to cool to about 40 ^{o}C before the control program is turned off and pressure returned to atmosphere using one of the two bypass lines on the high and low pressure side of the ballast tank, depending on whether the system was operated at high pressure or under vacuum.

5.4 LLE Measurements

5.4.1 Cleaning of LLE Cell

The cell was dismantled and thoroughly cleaned with ethanol and allowed to dry in the fumehood for at least 1 hour. The cleaning procedure was employed prior to introducing a new system into the cell.

5.4.2 Temperature Calibration, Measurement and Control

The LLE cell used in this work was operated under atmospheric pressure thus only temperature was monitored. A standard probe Fluke-hart scientific 5628 was used for calibrating the platinum probe temperature sensor used in the LLE cell. The two probes were placed in an Ultra Krymat® Lauda temperature controlled water bath, for which it is allowed to reach stable thermal equilibrium. After the thermal equilibrium was reached in the water, temperature readings were taken for each probe. This was done for different bath temperatures starting from low to high temperature. To check for any hysteresis the procedure was repeated starting from high

temperature to low temperature. The two recorded temperatures from each probe were use to plot the actual temperature vs. the measured temperature curve.

5.4.3 Gas chromatograph Detector Calibration and Composition Analysis

Gas chromatography was used for composition analysis for liquid-liquid equilibrium measurements. The main advantage in this case is the micro sample size required during analysis, thus allowing for continuous sampling without disturbance of equilibrium. The procedure of GC analysis involves finding a suitable column with good separation of the two components in each binary system and TCD calibration. Appendix B shows separation results of the proposed systems with a chosen column. Prior to system measurements, the TCD of the Perichrom PR2100 GC was calibrated. The method employed for calibration involved injecting a known volume of each pure component and recording surface peak area detected by the TCD. With a use of density correlation (from the commercial software Component Plus) at the temperature and pressure of calibration, the injected volumes are converted into number of moles of the component, and a plot of moles against detected surfaces is utilised to obtain the calibration curve. It is essential to undertake several injections of constant volume so as to check repeatability of the results, thus increase confidence in resulting calibration results. The graphical results of percentage deviations of the calibration curve with respect to the actual number of moles injected during the calibration are also found in appendix B. Alternatively, the method of area ratios suggested by Raal and Mülhbauer (1998) can be used. Even if this last method is usually found to provide very accurate results for GC calibration, it is important to note that the method fails for systems forming liquid-liquid equilibrium, thus was discarded for this application.

5.4.4 Experimental Procedure

The LLE cell used in this work was operated under atmospheric pressure thus only temperature was monitored. A standard probe Fluke-hart scientific 5628 were used for calibrating the platinum probe temperature sensor used in the LLE cell. The two probes were placed in an Ultra Krymat® Lauda temperature controlled water bath, for which it is allowed to reach stable thermal equilibrium. The cell is dismantled and thoroughly cleansed with ethanol and allowed to dry in the fumehood for at least 1 hour. The cleaning procedure is employed prior to introducing a new system into the cell. The chemicals are introduced into the cell in adequate amounts such that a

two phase mixture is formed, and also to ensure that the interface is above the dense phase sampling point (i.e. the interface must be between the sampling points for the liquid phases). The cell is then immersed in the water bath set to a desired temperature and the magnetic stirrer switched on. The speed of stirring motor is well controlled during stirring to prevent emulsion of the liquid mixture. The two phase mixture is then stirred for at least 2 hours there after the motor is switched off and the mixture is allowed to reach equilibrium. In 30 minute interval, the liquid samples for each phase are withdrawn using a 5 µl gas tight liquid syringe and injected into Perichrom GC. Equilibrium is achieved when the composition in each phase remains constant and the mixture temperature is recorded. For each system, the new temperature set is employed and above procedure employed to get the next equilibrium point.

5.5 Chemicals and Equipment Calibration Results

5.5.1 Chemical Used in this Study

Purities of the chemicals used in this project were checked and verified by measuring the refractive indices using the ATAGO® 7000 α refractometer with an indicated accuracy of ±0.00001. The measured values were compared to literature values. A Shimadzu GC 2010 (TCD) with HP-5 capillary column was used to verify the purity of the chemicals and that the stated values were similar to those values specified by the supplier.

Table 5-1: Purity of chemicals used in this project.

Reagent (IUPAC name)	CAS NO	supplier	Refractive indices(298.15K)		min.purity[a]	GC analysis
			This work	Literature[b]		Peak area(%)
Furan	110-00-9	Sigma-Aldrich	1.4234	1.4187	99.00	99.99
Furan-2-carbaldehyde	98-01-1	Sigma-Aldrich	1.5236	1.5234	99.00	99.99
Cyclohexane	110-82-7	Merck	1.4234	1.4235	99.85	100.00
diisopropyl ether	108-20-3	Sigma-Aldrich	1.3653	1.3655	99.50	100.00
Ethanol	64-17-5	Merck	1.3591	1.3594	99.50	100.00
n-hexane	110-54-3	Merck	1.3724	1.3723	99.00	99.99
Methylbenzene	108-88-3	Sigma-Aldrich	1.4942	1.4941	99.85	100.00
Propan-1-ol	71-23-8	Sigma-Aldrich	1.3834	1.3837	99.50	100.00
Phenol	108-95-2	Sigma-Aldrich	---------	1.5418	99.50	------
Water	7732-18-5	Laboratory	1.3325	1.3325	100.00	100.00

[a] supplier

[b]Yaws Handbook of Thermodynamic and Physical Properties of Chemical Compounds ,Kovel, (2003).

5.5.2 Calibrations Results of the Equipment Used in this Project

5.5.2.1 Pressure and Temperature Sensor Calibrations

The calibration of pressure and temperature was undertaken using methods described in section 5.2 for all apparatuses used in this project. The pressure and temperature transducers calibration curves for all equipment used in this project are presented below. The deviations resulting from calibration curves are also given.

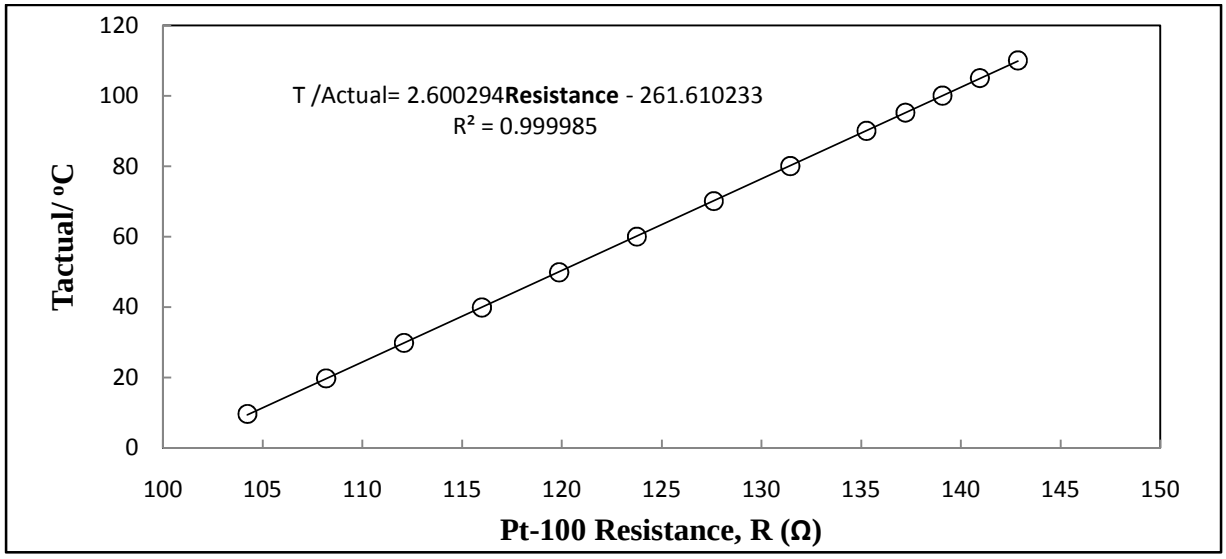

Figure 5-3: Calibration of the Pt-100 surface element for the low pressure VLE dynamic-analytic apparatus, linear relation between the actual and probe temperatures.

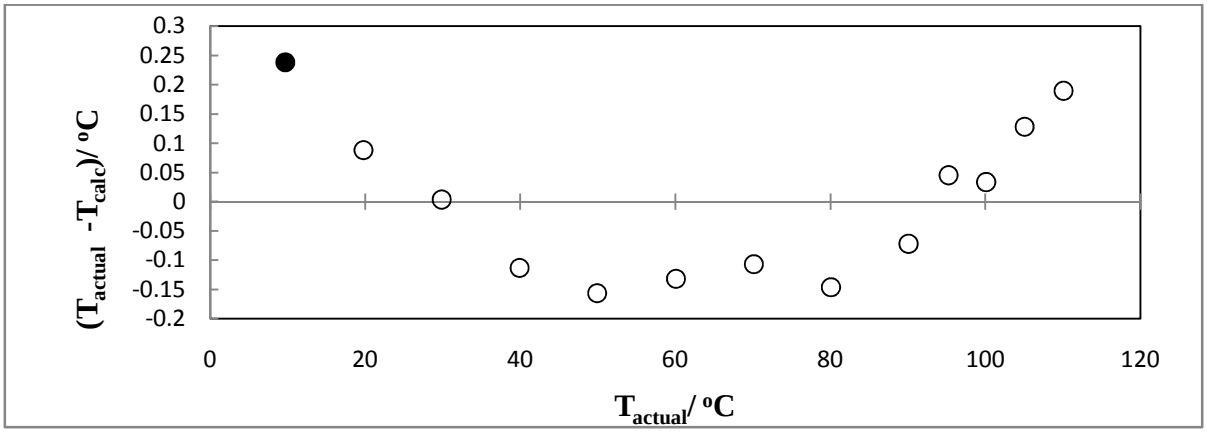

Figure 5-4: Deviations from the actual temperature, resulting from the use of a linear relation for the low pressure dynamic analytic VLE apparatus, ●maximum deviation.

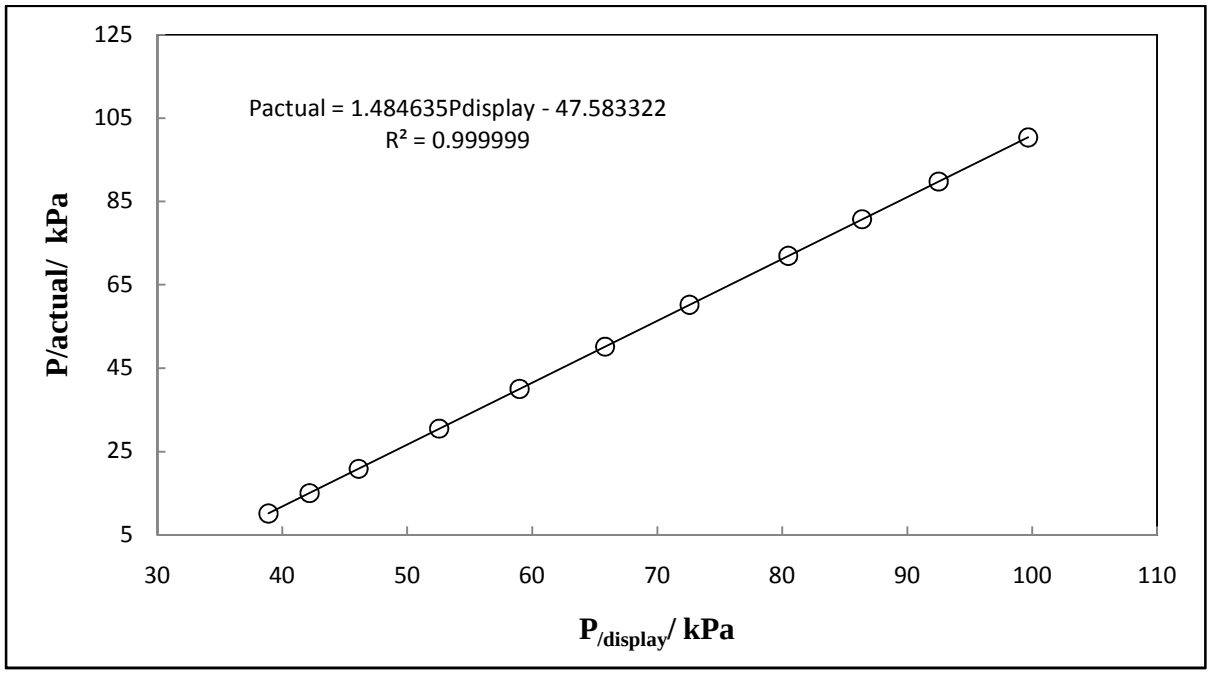

Figure 5-5: Calibration of the pressure transducer for the low pressure VLE dynamic-analytic apparatus, linear relation between the actual and display pressure.

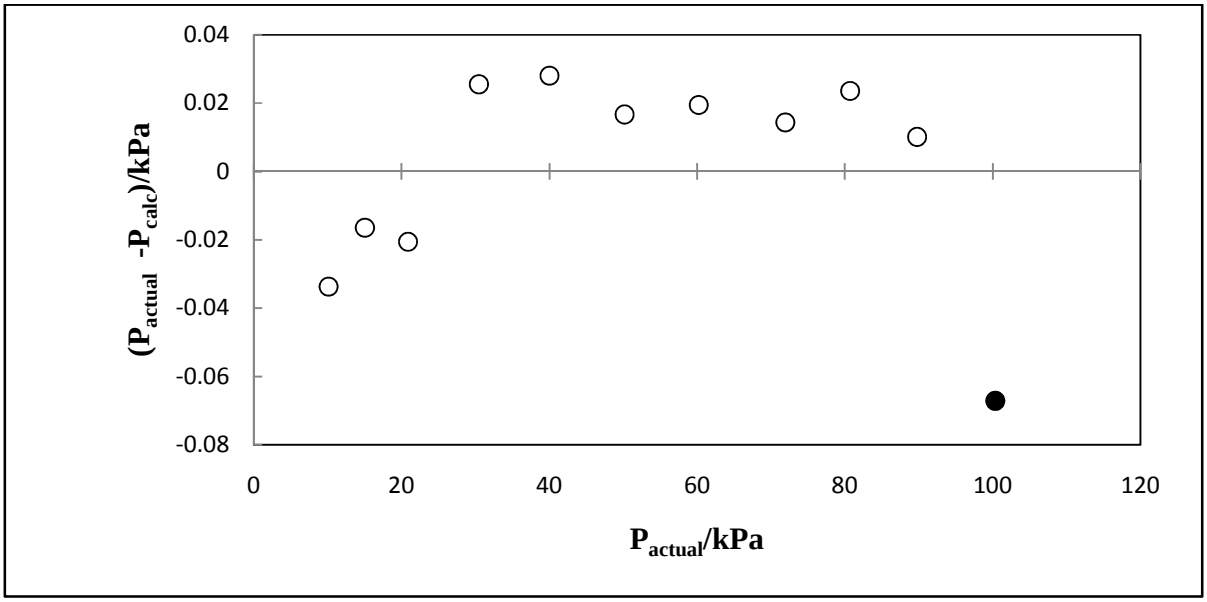

Figure 5-6: Deviations from the actual pressure, resulting from the use of a linear relation for the low pressure dynamic analytic VLE apparatus, ●maximum deviation.

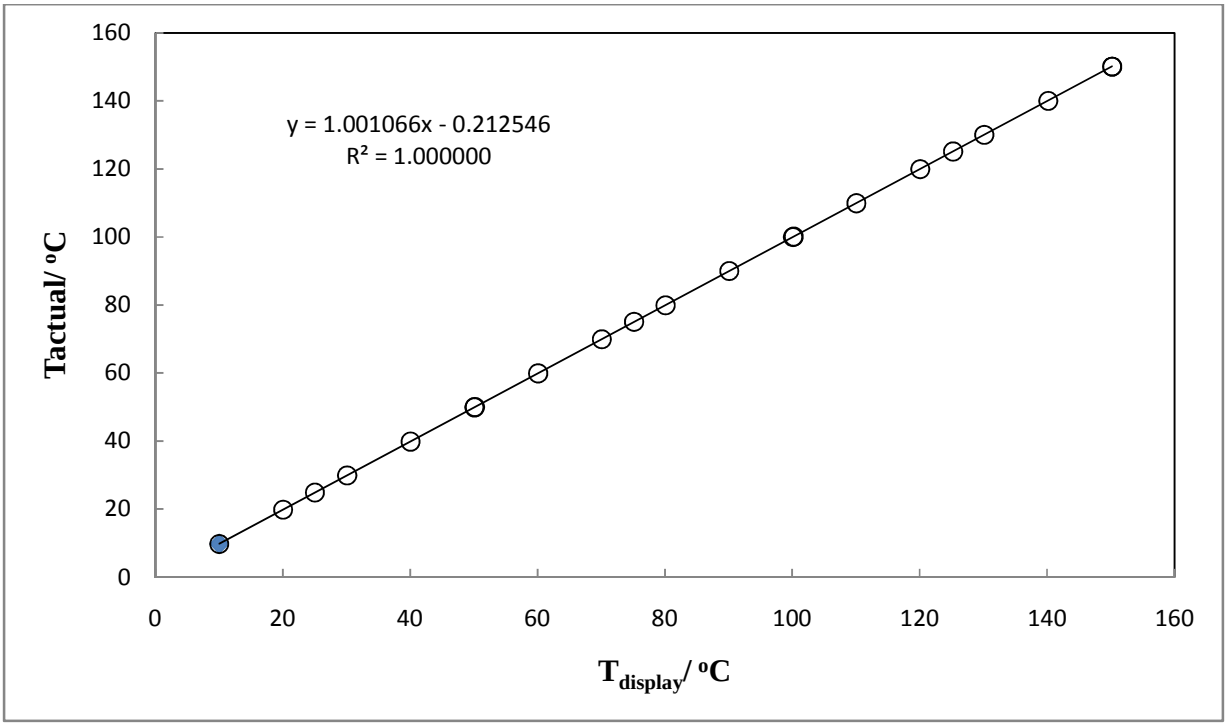

Figure 5-7: Calibration of the Pt-100 surface element for the medium pressure VLE dynamic-analytic apparatus, linear relation between the actual and probe temperatures.

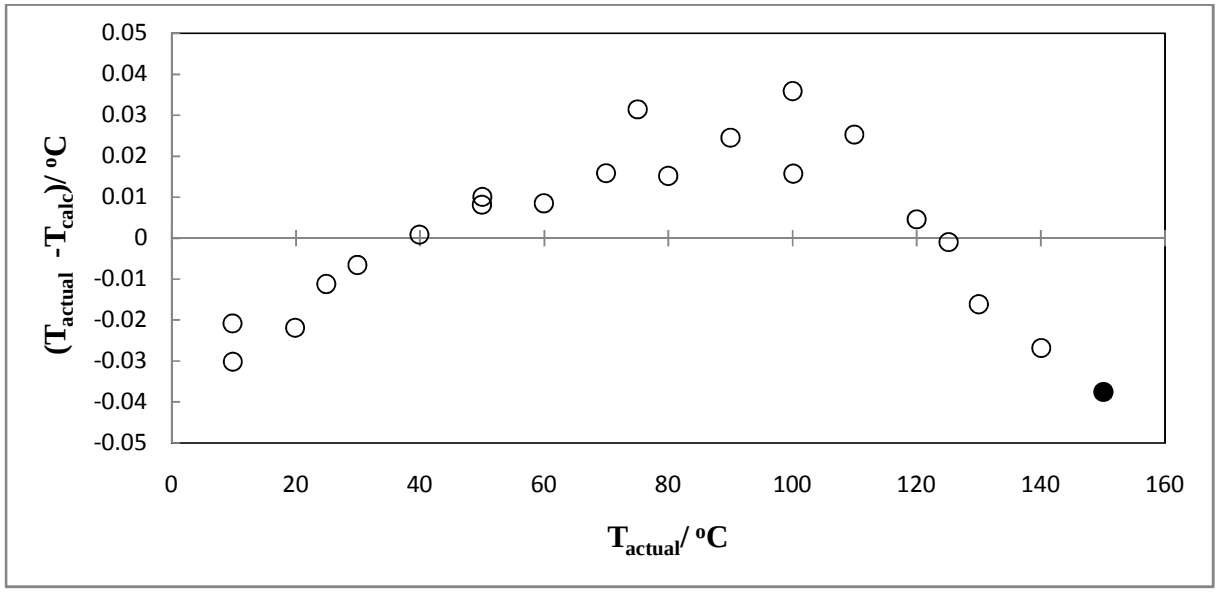

Figure 5-8: Deviations from the actual temperature, resulting from the use of a linear relation for the medium pressure dynamic analytic VLE apparatus, ●maximum deviation.

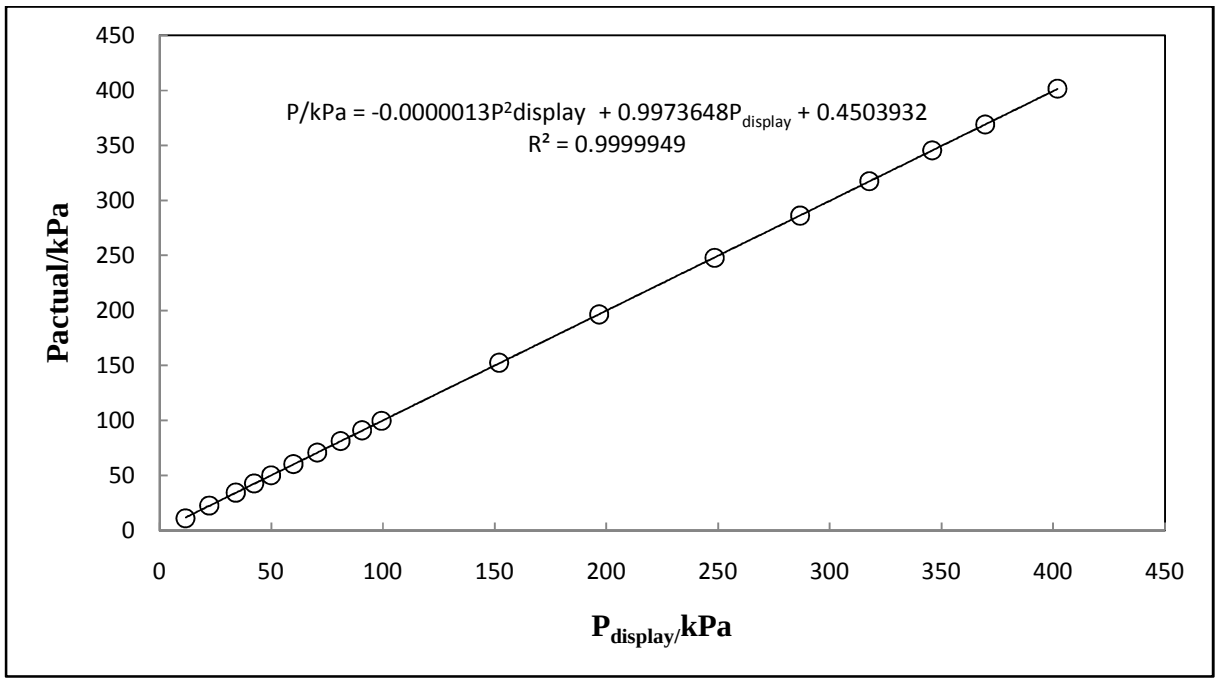

Figure 5-9: Calibration of the pressure transducer for the medium pressure VLE dynamic-analytic apparatus, second-order relation between the actual and display pressure.

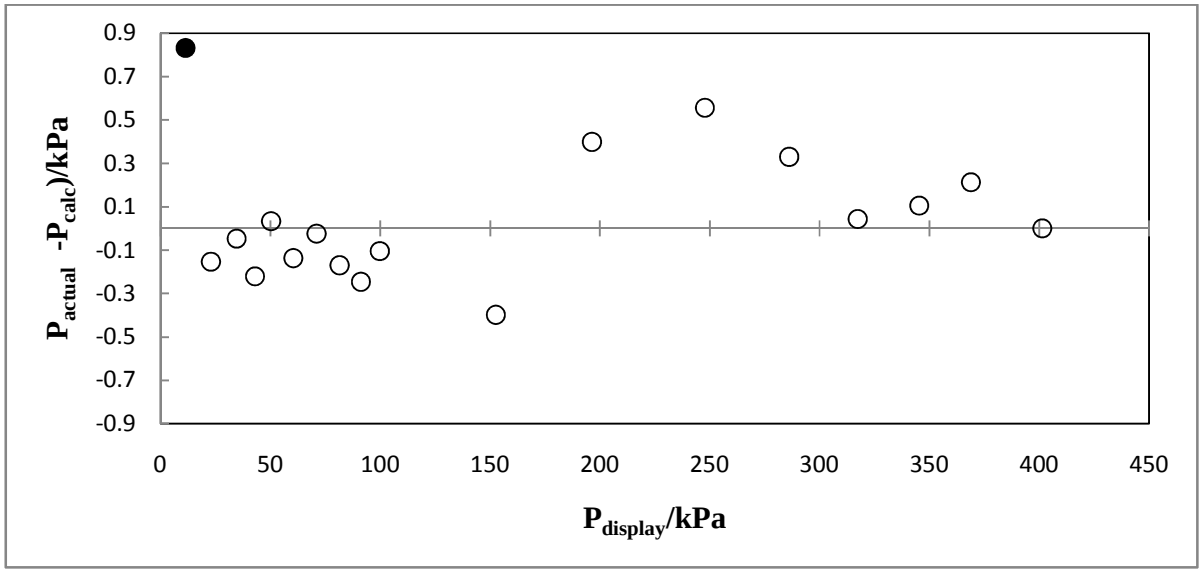

Figure 5-10: Deviations from the actual pressure, resulting from the use of a second-order equation for the low pressure dynamic analytic VLE apparatus, ●maximum deviation.

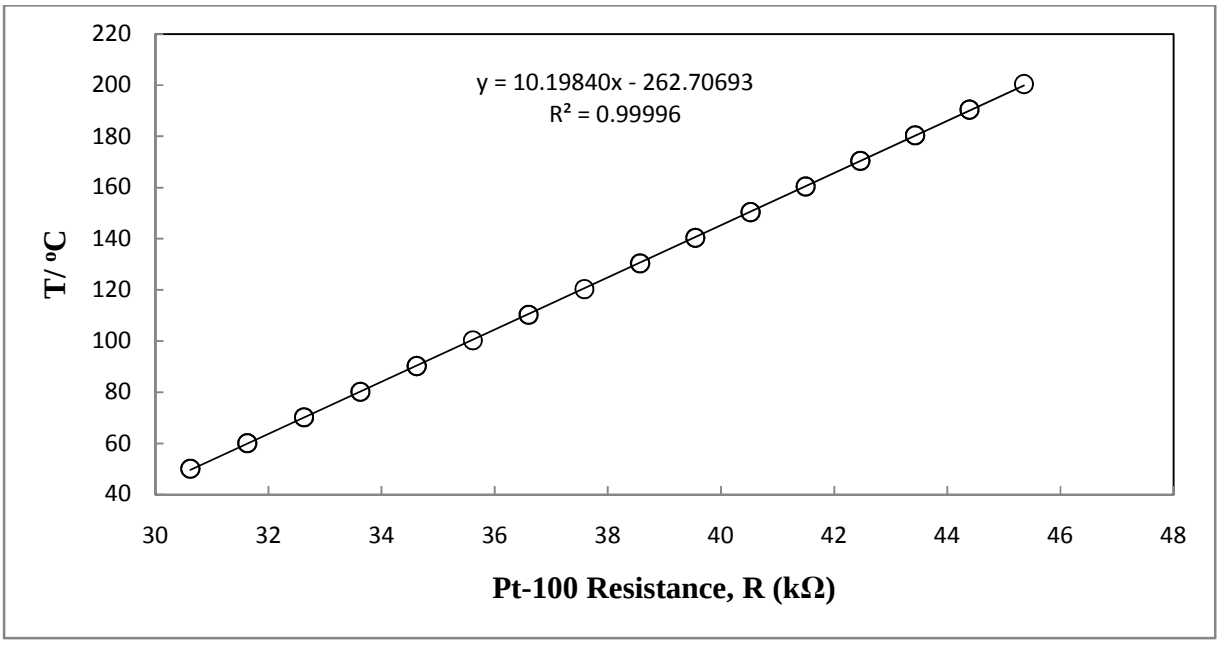

Figure 5-11: Calibration of the Pt-100 surface element for the dynamic atmospheric VLE apparatus, linear relation between the actual and probe temperatures.

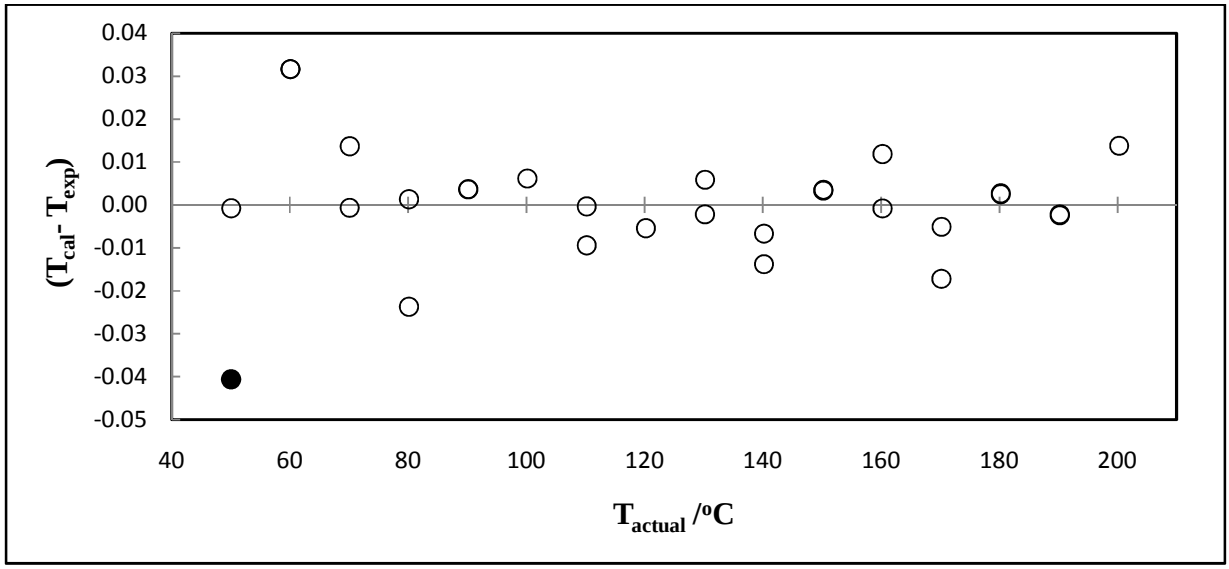

Figure 5-12: Deviations from the true temperature, resulting from the use of a linear relation for the dynamic atmospheric VLE apparatus, ●maximum deviation.

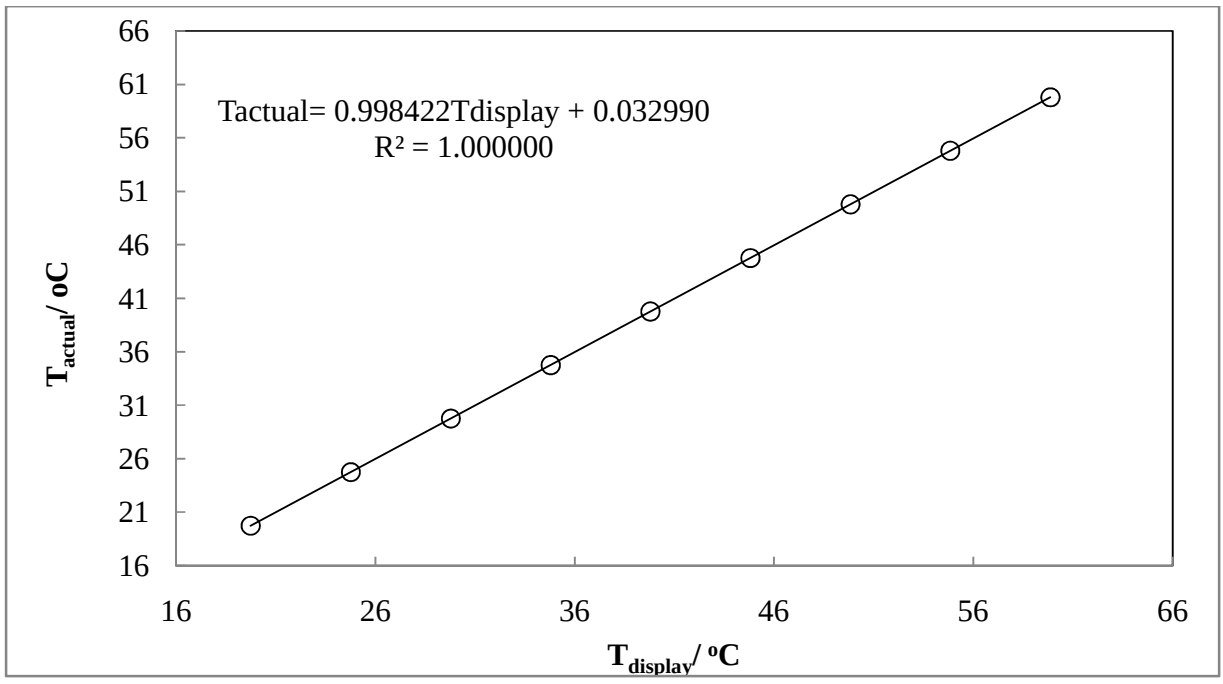

Figure 5-13: Calibration of the Pt-100 surface element for the static analytic LLE apparatus, linear relation between the actual and probe temperatures.

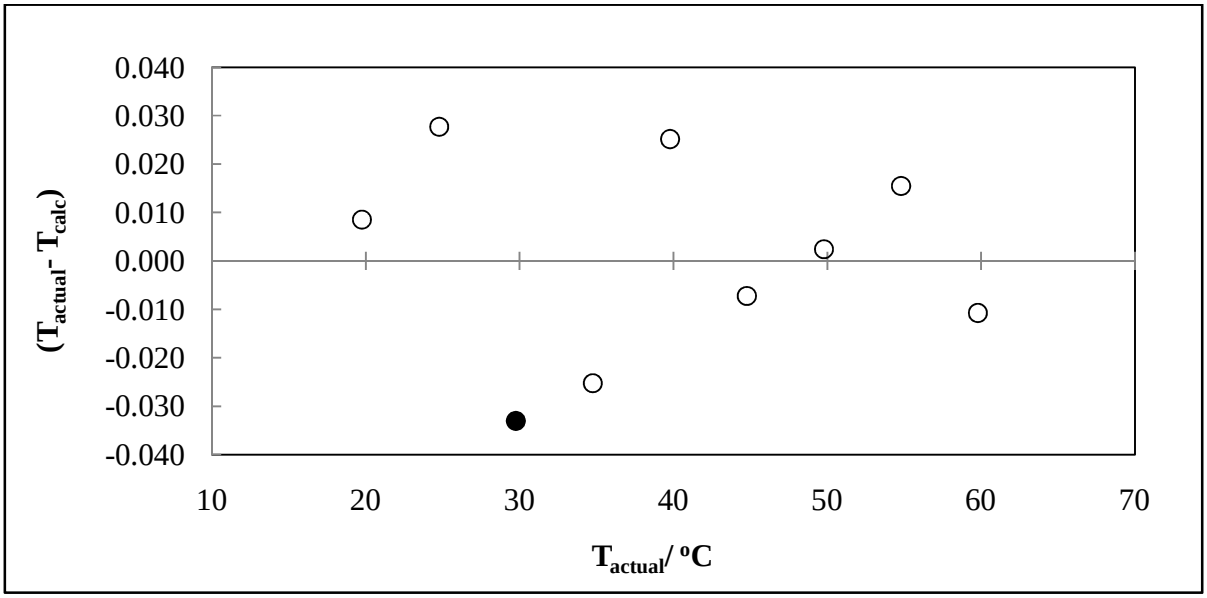

Figure 5-14: Deviations from the true temperature, resulting from the use of a linear relation for the static analytic LLE apparatus, ●maximum deviation.

5.5.2.2. GC Calibrations and Operating Conditions

Tables 5-2 and 5-3 present the operating conditions of the Shimadzu GC 2010 and GC 2014 respectively. The columns used in the GC ovens are presented in Table 5-4. The given GC operational conditions provided proper separation of the chemical species and sharp peaks for each measured system, thus increased confidence in measured molar compositions.

Table 5-2: Shamadzu GC 2010, gas chromatograph operating conditions.

Operating conditions		
System	Cyclohexane + Ethanol test	Dipe + propan-1-ol
Column used	HP-5 capillary	HP-5 capillary
Detector type	TCD	TCD
Carrier gas	Helium	Helium
Carrier gas flow (ml.min-1)	3.36	3.41
Oven Temperature control mode	Isothermal	Isothermal
Injector temperature /^{o} C	240	240
Column temperature /^{o}C	70	70
Detector temperature /^{o}C	240	240
Flow control mode	Linear velocity	Linear velocity
Pressure	20 kPa	16.6 kPa
Total flow	20 ml/min	20ml/min
Experimental run times(min)	6.5	6

Table 5-3: Shimadzu GC 2014 gas, chromatograph operating conditions.

Operating conditions		
System	Dipe + propan-1-ol	Water + propan-1-ol
Column used	Porapak® Q	Porapak® Q
Detector type	TCD	TCD
Carrier gas	Helium	Helium
Carrier gas flow (ml.min-1)	35	35
Oven Temperature control mode	Isothermal	Isothermal
Injector temperature /^{o} C	250	250
Column temperature /^{o}C	230	230
Detector temperature /^{o}C	250	250
Flow control mode	Linear velocity	Linear velocity
Pressure	467.5 kPa	467.5 kPa
Total flow	23.3 mL/min	23.3 mL/min
Experimental run times(min)	8	8

Table 5-4: GC column specifications used for composition analyses.

Column	Porapak®Q	HP-5 capillary
Serial number		19091J-413
Type	Packed	capillary
Tmax	250	250
Column length/m	2.5	30
Film thickness/µm	-	1µm
material of construction	stainless steel	
OD / mm	3.2	-----
ID / mm	2.2	0.32
mesh range	50/80	-----

CHAPTER 6

EXPERIMENTAL RESULTS

This chapter presents the experimental vapour pressure data. The VLE and LLE results for the test systems and new systems that were measured in this work. A detailed analysis of the experimental measurements is given in Chapter 7.

6.1 Uncertainty in Measurements

This section deals with the uncertainty, an important yet often neglected aspect in the measurements of experimental data. It is important to note the difference between the uncertainty and error. Error is quantified as the difference between the measured value and the actual value of the property being measured, while uncertainty refers to the quantification of the doubt about the experimentally measured result (Bell, 1999). To quantify the uncertainty in a given set of measurements, it is important to identify all possible sources contributing uncertainty. For experimental measurements of phase equilibrium, the mostly visible sources are the instruments used for measurements and the stability of the measured variable(θ).Having identified and quantified the individual uncertainties from different sources, a combined standard uncertainty(u_c) is introduced as combination of all the calculated uncertainty:

$$u_c = \pm \sqrt{\sum_i u_i(\theta)^2} \tag{6.1}$$

$u_i(\theta)$ is the uncertainty resulting from any possible sources (for example from the temperature or pressure calibration chart).

6.1.1 Uncertainty in Pressure, Temperature and Composition

The most important variables in the phase equilibrium measurements are temperature and pressure. Uncertainty in these variables arises from imperfections of calibration curves and repeatability deviations of a single transducer reading. The combined standard uncertainty in the temperature measurements is estimated as:

$$u_c(T) = \pm\sqrt{u_{calib}(T)^2 + u_{rep}(T)^2} \tag{6.2}$$

and for pressure:

$$u_c(P) = \pm\sqrt{u_{calib}(P)^2 + u_{rep}(P)^2} \tag{6.3}$$

The subscripts *calib* and *rep* denotes calibration and repeatability, respectively.

Imprecision present in the TCD calibration can be regarded as highest contributor in the molar composition uncertainty. Soo (2011) encouraged neglecting the uncertainty on repeated samples, since the manual sampling aspect of the VLE apparatuses used is not ideal and sample repeatability uncertainty contributes to approximately 1 % of the final uncertainty. This is justified by the low value of the standard deviation from the averaging of the repeated samples (≥ 5 samples injections per data point) thus the uncertainty in the composition of all the measurements is estimated as:

$$u_c(x) = \pm\sqrt{u_{calib,max}(x)^2} \tag{6.4}$$

The reported combined standard uncertainties in the measurements are presented in Table 6-1 below. The temperature and pressure uncertainty are averaged over the entire data set (i.e. average over all different isothermal data sets). The temperature and pressure uncertainties are very satisfactory, indicating a good calibration results, repeatability and control scheme. The uncertainties in composition are relatively low for all systems. This shows the well effectiveness of both TCD calibration procedures (Raal and Muhlbauer, (1998) and mixture density measurement technique) used in this thesis.

Table 6-1: Experimental uncertainties for temperature, pressure, and mole fraction of the VLE binary systems.

System	$u_c(T)$ /K	$u_c(P)$/kPa	$u_c(x)$
Ethanol (1) + cyclohexane (2)	±0.02	±0.23	±0.008
Diisopropyl ether (1) + 1-propan-1-ol (2)	±0.02	±0.23	±0.013
Water(1) + 1-propan-1-ol (2)	±0.02	±0.23	±0.007
Furan(1) + n-hexane (2)	±0.01		±0.005
Furan(1) + Methylbenzene (2)	±0.01		±0.004

6.1.2 Basic Equations Used for Statistical Analysis of Results

The basic equations used for calculation are given below:

$$\Delta = \frac{m_{\text{exp}} - m_{calc}}{m_{\text{exp}}} \tag{6.5}$$

$$AAD\ (\%) = \frac{100}{N}\sum_{i=1}^{N}\left|\Delta\right|_i \tag{6.6}$$

$$Bias\ (\%) = \frac{100}{N}\sum_{i=1}^{N}\left(\Delta\right)_i \tag{6.7}$$

The deviation Δ represents the relative deviation of a calculated thermodynamic property m from a corresponding experimentally measured value. AAD refers to average absolute deviation of data set with N experimental points.

6.2 Pure Component Data

6.2.1 Vapour Pressure

The vapour pressure data were measured for the components used in this project except for furan, n-hexane and toluene for which the abundant literature data were used. The vapour pressure data were correlated with Wagner and Antoine equations. The experimental vapour

pressure data and deviations from the fitted Wagner and Antoine are presented in Tables 6-2 and shown in Figures 6-1. Table 6-11 and 6-12 presents average deviations of the Wagner equation for various literature data for furan, n-hexane and toluene. The vapour pressure trends are graphical shown in Figure 6-2 for these components.

Table 6-2: Measured vapour pressure data

T ±0.02 / K	P ±0.23/ kPa	ΔP_{wagner} / kPa	$\Delta P_{Antoine}$ / kPa	ΔT_{Wagner} / K	$\Delta T_{Antoine}$ / K
			Ethanol		
315.41	20.1	-0.01	0.03	0.00	0.03
323.61	30.0	0.02	-0.03	0.02	-0.02
329.68	39.9	-0.03	0.01	-0.02	0.01
334.69	50.0	0.02	-0.04	0.01	-0.02
338.84	60.0	-0.01	-0.01	0.00	-0.01
342.46	70.0	-0.01	-0.01	0.00	0.00
345.65	80.0	0.00	0.00	0.00	0.00
351.06	99.7	0.01	0.04	0.00	0.01
	AAD	**0.01**	**0.02**	**0.01**	**0.01**
			Cyclohexane.		
308.91	20.4	0.0	-0.3	0.00	-0.30
325.73	40.4	0.5	0.6	-0.34	0.41
337.18	60.4	0.4	0.6	-0.18	0.28
346.07	80.4	0.1	0.0	0.02	0.00
354.11	100.4	2.9	-3.4	0.93	-1.06
	AAD	**0.9**	**1.2**	**0.29**	**0.41**
			Diisopropyl ether		
307.92	30.0	0.0	-0.4	0.00	0.00
315.10	40.0	0.0	-0.3	-0.01	0.00
326.00	60.0	0.0	0.0	0.00	0.00
334.30	80.0	0.0	0.3	-0.01	0.02
341.25	100.1	0.3	0.1	0.09	-0.19
341.29	100.5	0.0	0.4	0.14	0.13
353.17	144.0	0.4	0.1	0.09	-0.28

364.79	200.1	0.2	-0.1	0.04	-0.19
373.21	250.5	-0.4	-0.2	-0.06	0.32
376.18	270.6	-0.9	0.0	-0.14	0.80
	AAD	**0.22**	**0.19**	**0.06**	**0.08**
			Propan-1-ol.		
333.17	20.0	0.2	-0.2	0.24	-0.15
341.41	30.1	0.0	0.0	0.00	-0.01
347.53	40.0	0.3	0.2	-0.15	0.11
356.79	60.0	0.6	0.5	-0.24	0.17
363.81	80.0	0.7	0.5	-0.21	0.15
369.61	100.1	0.3	0.2	-0.08	0.05
369.90	100.2	0.8	-0.9	0.20	-0.23
374.45	120.1	0.0	0.0	-0.00	0.00
378.65	140.0	0.4	-0.2	0.07	-0.04
382.45	160.0	1.2	-0.8	0.21	-0.14
	AAD	**0.5**	**0.3**	**0.14**	**0.11**
			Water		
334.37	20.1	0.00	-0.2	0.00	-0.23
349.17	40.0	-0.01	0.4	-0.01	0.26
359.05	60.0	0.03	0.3	0.01	0.14
366.52	80.0	-0.01	0.0	0.00	0.00
372.89	101.2	-0.01	-0.5	0.00	-0.14
	AAD	**0.01**	**0.3**	**0.01**	**0.15**

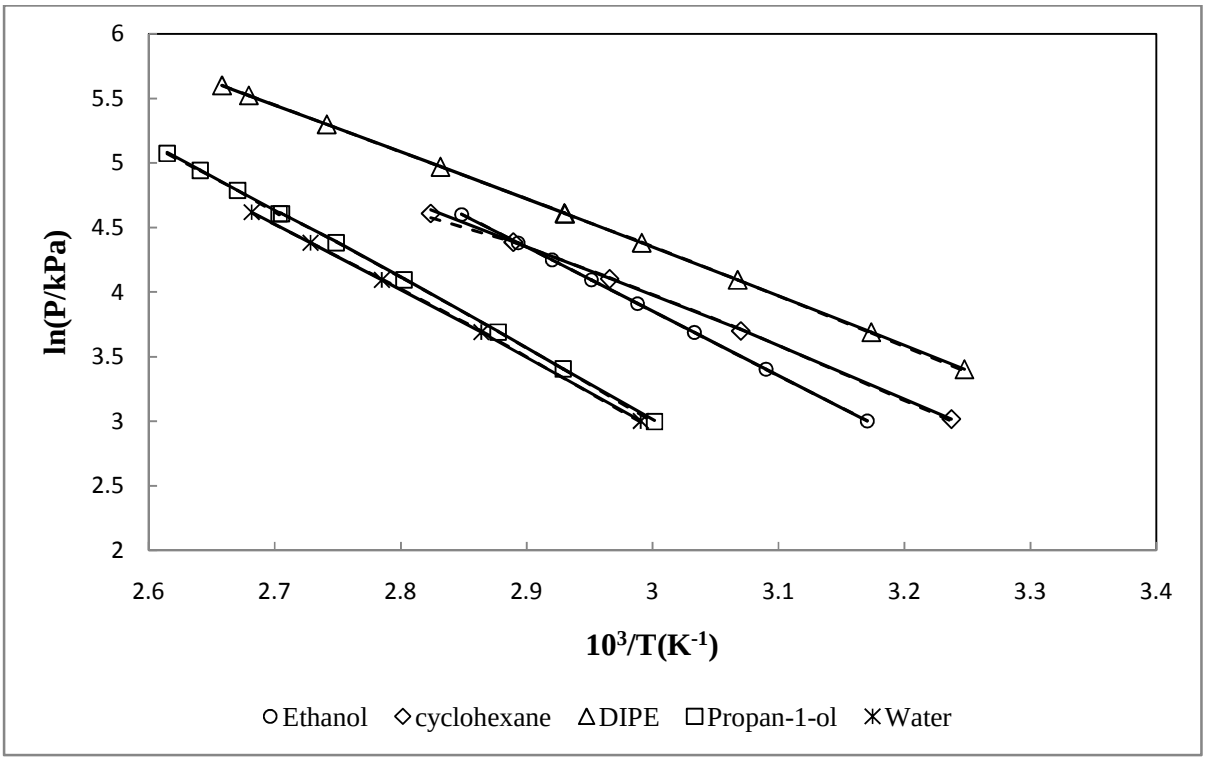

Figure 6-1: Measured vapour pressure data for components used in this work, coreelating models: — Wagner, - - - Antoine.

Table 6-3: Comparison of average deviation between literature vapour pressure data and the Wagner model for furan.

Reference first author	NO of points	Year	T/K	AAD(%)	Bias%	AD(max)%
Guthrie, G. B	13	1952	276-335	0.0187	0.0079	3.55
Kobe, K. A	22	1956	366-483	0.5253	-0.0219	0.27
Overall	35			0.3372	-0.0108	3.55

Table 6-4: Comparison of average deviation between literature vapour pressure data and the Wagner model for toluene and n-hexane.

Data sets	NO of points	NO of Data sets	T/K	AAD(%)	Bias%	AD(max)%
Toluene	1018	>20	199-592	0.7715	-0.277	6.512
n-hexane	1381	>20	178-507	0.6173	0.542	3.552

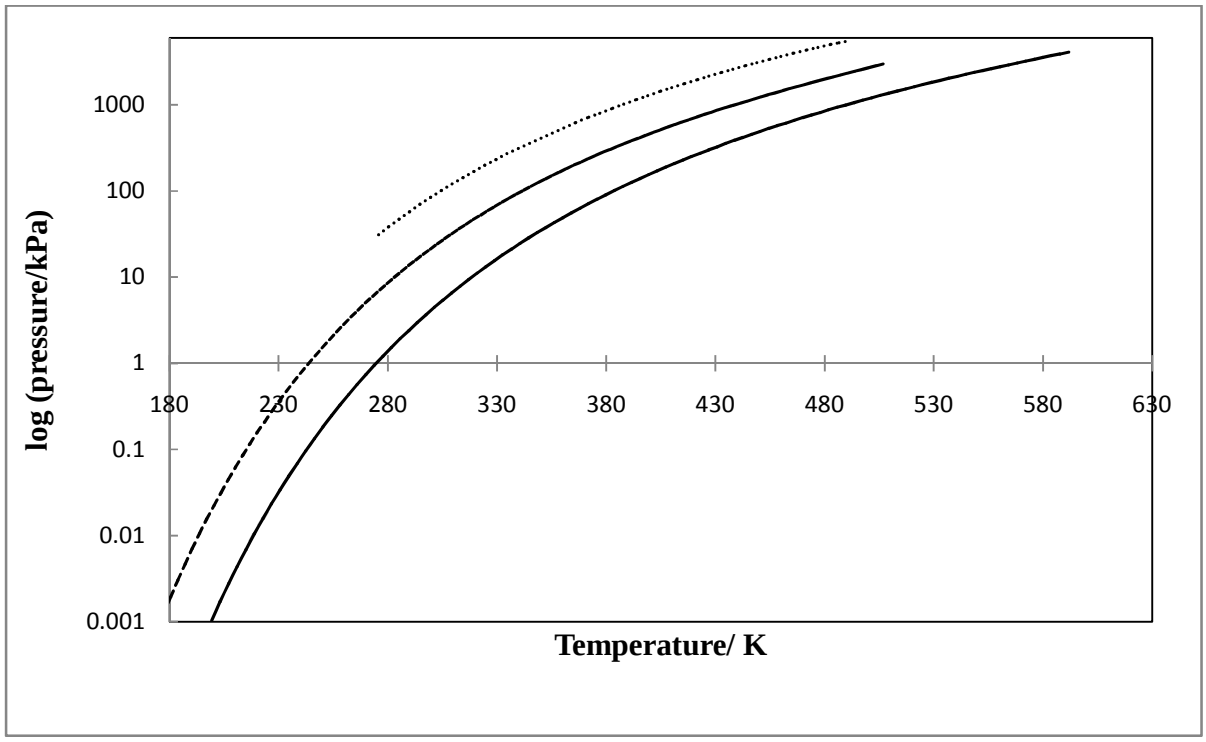

Figure 6-2: Literature vapour pressure correlation by Wagner equation from triple point to critical point, ·····furan - - - n-hexane,— toluene

6.3. Binary Vapour-Liquid Equilibrium Results

6.3.1. Results for the Test System: cyclohexane (1) + ethanol (2) System

Measurements for the cyclohexane (1) + ethanol (2) system at 40 kPa were undertaken on the apparatus of Joseph (2001). The composition analysis of this system was analysed using the Shimadzu GC2014 gas chromatograph operated under conditions presented in Table 5-3 of section 5.5. Figures 6-3 and 6-4 present the GC calibration plots. The experimental VLE data points are listed in Tables 6-5 and *T-x-y* and *x-y* plots are presented in Figures 6-5 and 6-6. From the figures, the data illustrate the good agreement with data by Joseph (2001). Vapour pressure data that was successfully measured as a test system in the Medium pressure VLE still of Lilwanth (2011), in addition five data points previously measured in the still of Joseph (2001) points measured using the still of Lilwanth (2011) for the system of diisopropyl ether (1) + 1-

propanol (2). The measured points were in excellent agreement thus, it was not necessary to undertake further test system measurements on medium pressure still.

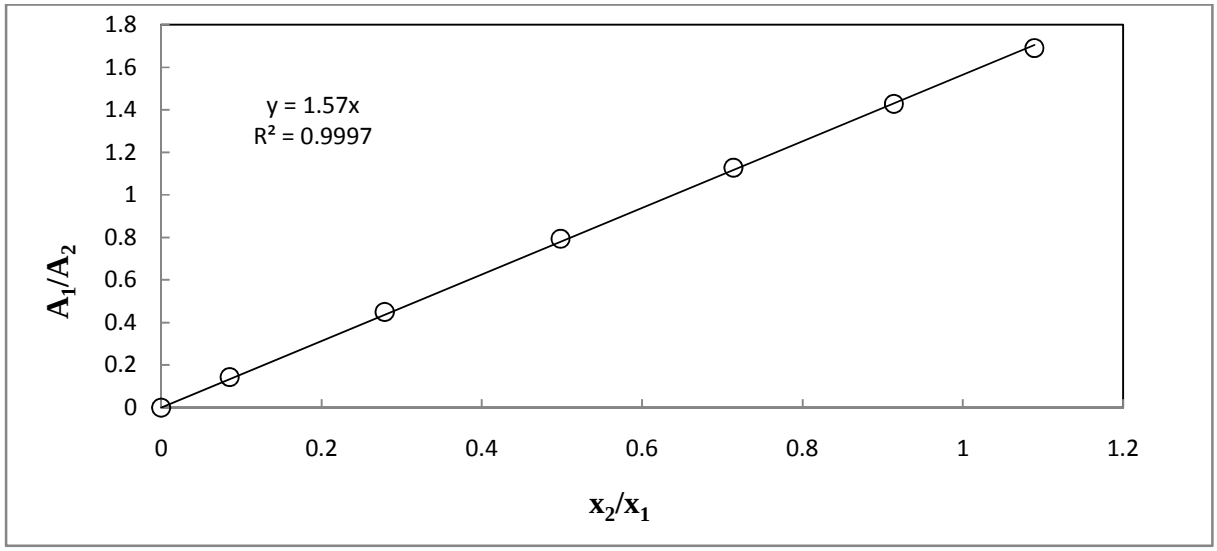

Figure 6-3: TCD Calibration for the ethanol (1) + cyclohexane (2) system using the area ratio method of Raal and Mülhbauer, (1998) (Cyclohexane dilute region).

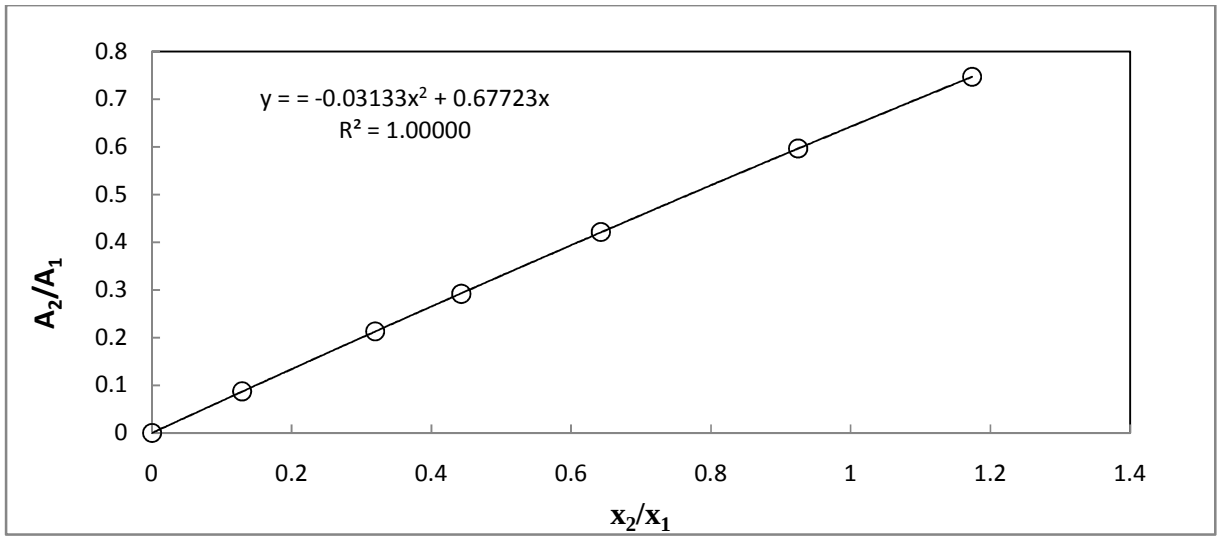

Figure 6-4: TCD Calibration for the ethanol (1) + cyclohexane (2) system using the area ratio method of Raal and Mülhbauer, (1998) (Ethanol dilute region).

Table 6-5: Vapour-liquid equilibrium data for the ethanol (1) + cyclohexane (2) system at 40 ±0.23/kPa.

T ±0.02/K	x_1	y_1	T±0.02/K	x_1	y_1
329.68	0	0	315.25	0.299	0.577
328.51	0.007	0.059	314.99	0.357	0.588
327.54	0.013	0.102	314.86	0.401	0.595
322.10	0.059	0.331	319.44	0.988	0.778
321.09	0.074	0.367	320.65	0.987	0.830
320.51	0.084	0.393	318.03	0.979	0.737
318.97	0.114	0.443	320.24	0.990	0.803
318.00	0.139	0.470	315.32	0.907	0.660
317.41	0.159	0.494	314.85	0.822	0.636
316.77	0.177	0.517	314.73	0.722	0.616
316.18	0.209	0.541	314.69	0.629	0.617
315.53	0.264	0.561	325.73	1.000	1.000

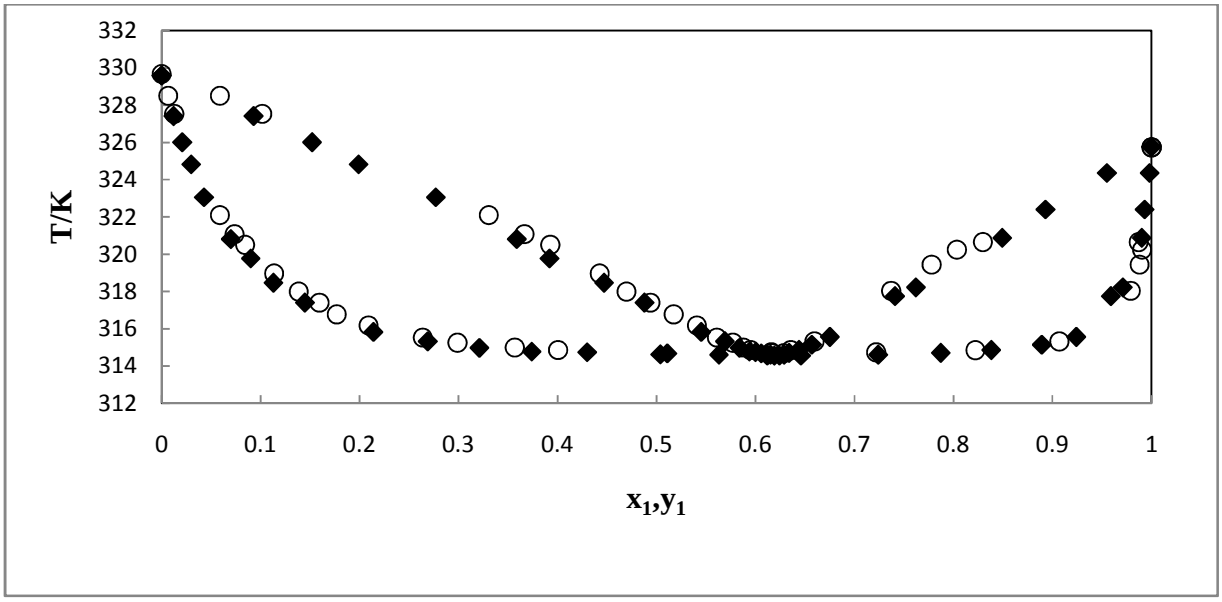

Figure 6-5: Experimental T-x-y data for the ethanol (1) + cyclohexane (2) system at 40 kPa, ○ this work, ♦ Joseph *et al*. (2001).

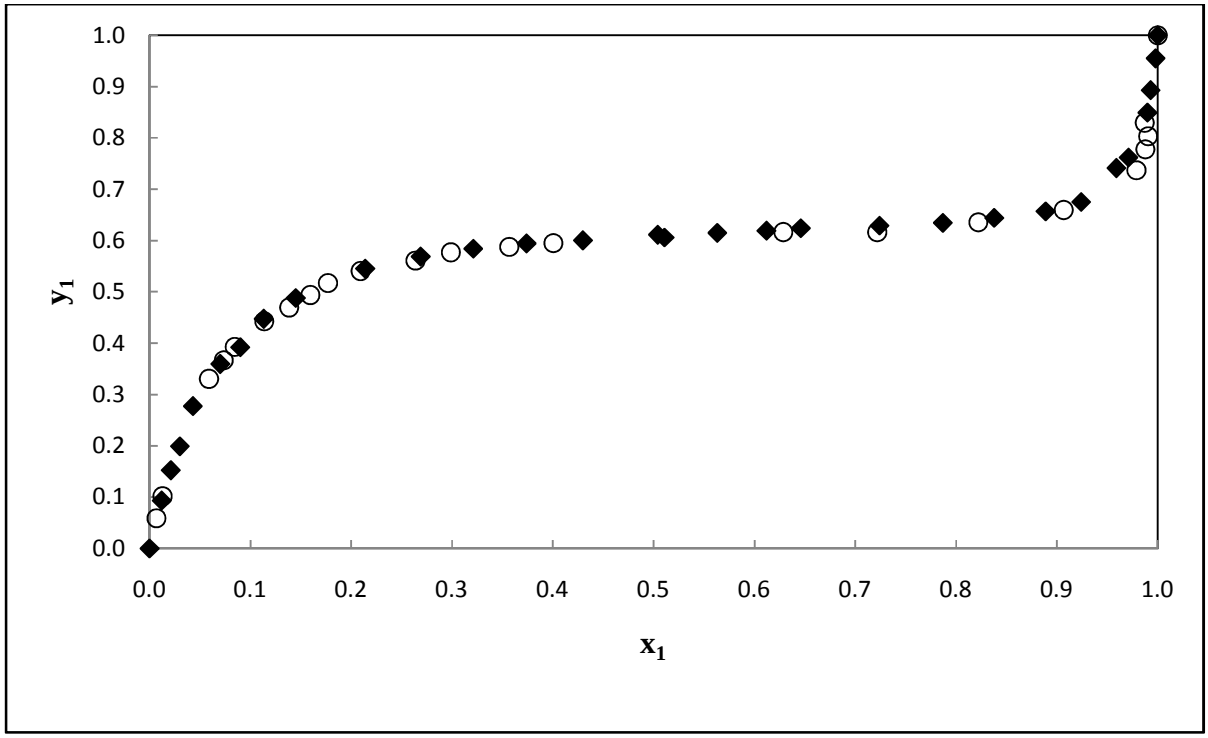

Figure 6-6: Experimental x-y data for the ethanol (1) + cyclohexane (2) system at 40 kPa, ○ this work, ♦ Joseph *et al*. (2001).

6.3.2 Diisopropyl ether (1) + Propan-1-ol (2) System

New VLE data were measured at 333.15 K, 353.15 K and 373.15 K. The composition analysis of this system was carried out using the Shimadzu GC2014 gas chromatograph using the running conditions presented in table 5-3 and 5-4 of section 5.5. Figures 6-7 and 6-8 present the GC calibration plots. The experimental VLE data points are listed in Tables 6-6 to 6-8 and *x-y* and *P-x-y* plots are presented in figures 6-9 to 6-14.

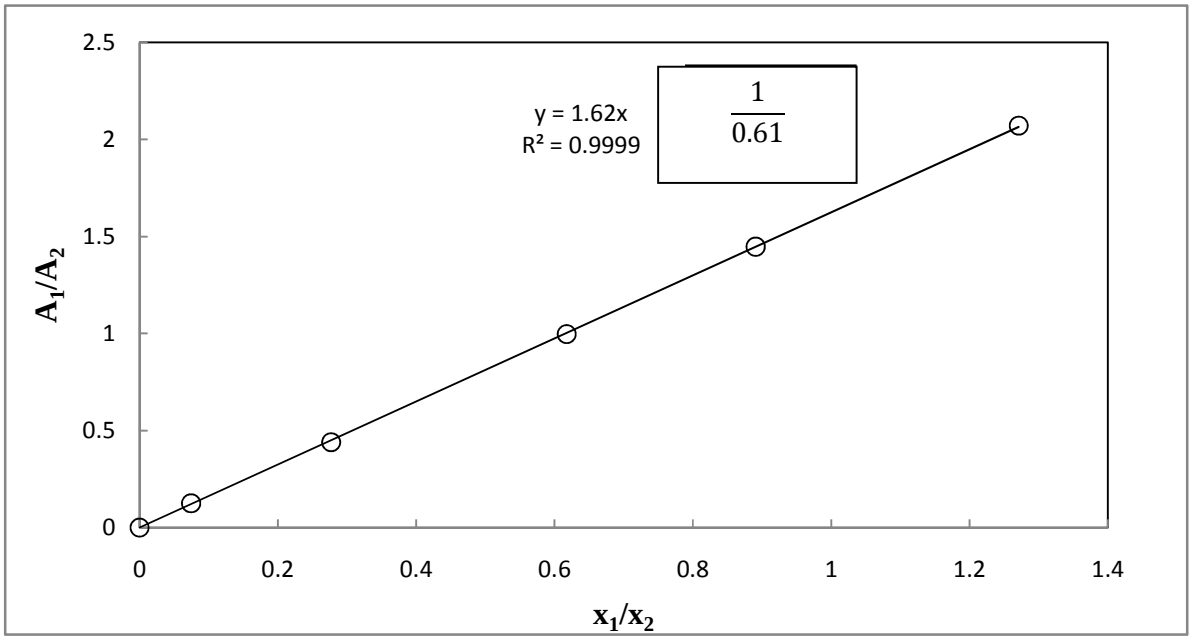

Figure 6-7: TCD calibration for the diisopropyl ether (1) + propan-1-ol (2) system using the area ratio method of Raal and Mülhbauer (1998), (Diisopropyl ether dilute region).

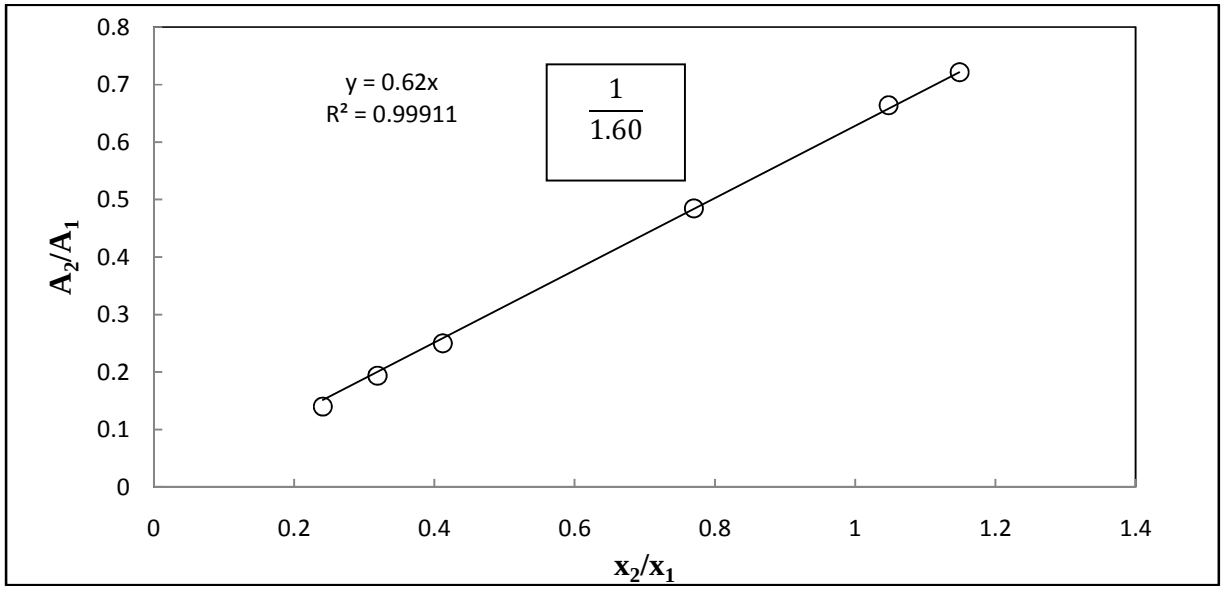

Figure 6-8: TCD calibration for the diisopropyl ether (1) + propan-1-ol (2) system using the area ratio method of Raal and Mülhbauer (1998), (propan-1-ol dilute region).

Table 6-6: P-x-y data for diisopropyl ether (1) + propan-1-ol (2) at 333.15 K.

P/kPa	x_1	y_1	P/kPa	x_1	y_1
20.0	0.000	0.000	43.2*	0.164	0.597
20.3	0.001	0.010	45.5	0.194	0.622
20.6	0.003	0.022	51.8	0.273	0.687
21.1*	0.006	0.050	49.0	0.241	0.662
21.3	0.007	0.056	54.8	0.310	0.715
22.9	0.016	0.123	59.5	0.392	0.752
23.1*	0.019	0.133	64.6	0.506	0.809
25.4	0.032	0.217	67.5	0.583	0.835
28.9	0.057	0.328	70.4	0.688	0.861
29.4*	0.057	0.342	73.1	0.783	0.890
33.8	0.092	0.442	74.9	0.851	0.916
34.9*	0.095	0.462	75.9	0.895	0.933
38.5	0.127	0.530	76.5	0.960	0.970
42.1	0.160	0.580	76.5	1.000	1.000

*Points measured from the medium pressure VLE glass apparatus.

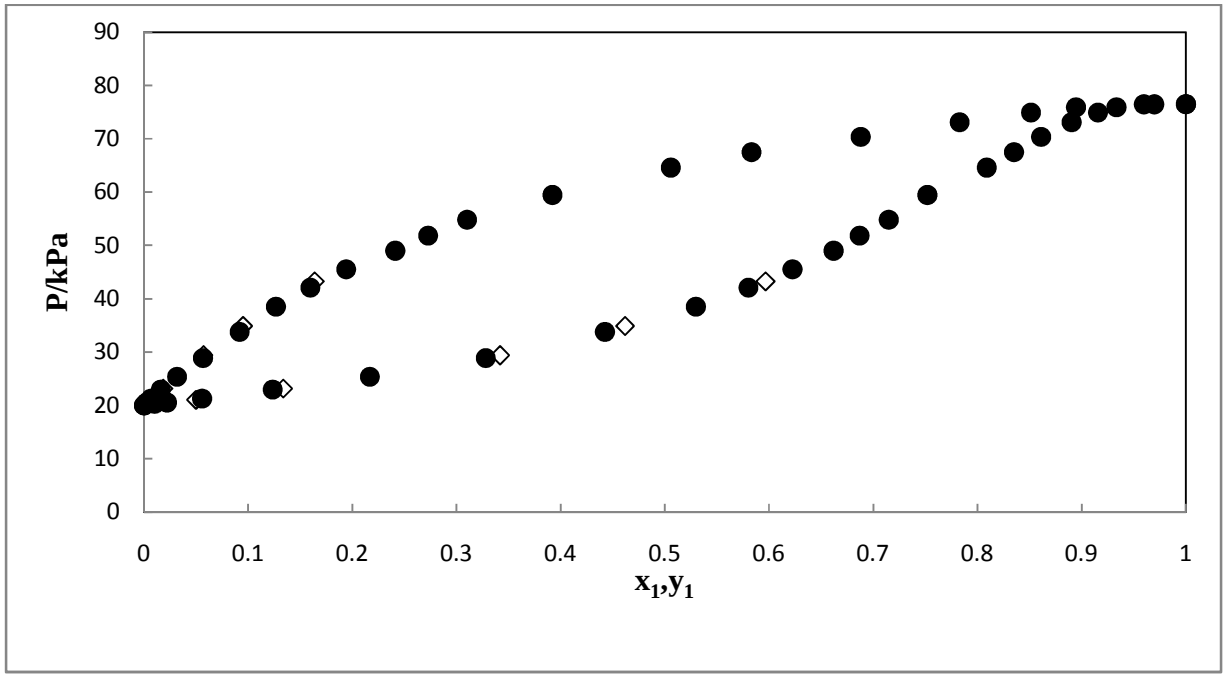

Figure 6-9: Measured P-x-y data for the diisopropyl ether (1) + propan-1-ol (2) system at 333.15 K, ● low pressure VLE still, ◊ Medium pressure VLE still.

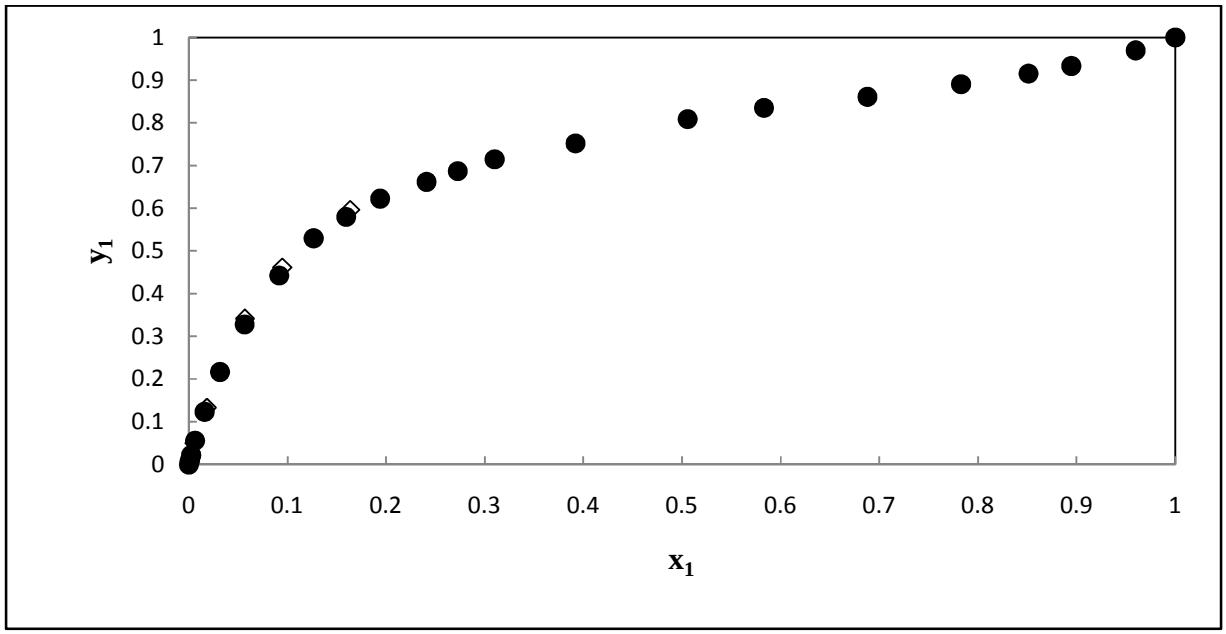

Figure 6-10: Measured x-y data for the diisopropyl ether (1) + propan-1-ol (2) system at 333.15 K, ● Low pressure VLE still, ◊ Medium pressure VLE still.

Table 6-7: P-x-y data for diisopropyl ether (1) + propan-1-ol (2) at 353.15 K.

Pressure/kPa	x_1	y_1
50.8	0.000	0.000
56.9	0.011	0.061
61.6	0.027	0.140
70.4	0.061	0.259
77.4	0.097	0.361
82.4	0.124	0.415
89.9	0.172	0.485
97.3	0.205	0.529
106.0	0.268	0.602
116.9	0.339	0.657
128.9	0.461	0.735
139.5	0.611	0.791
144.1	0.764	0.845
145.6	0.839	0.880
144.7	0.920	0.930
144.7	0.991	0.991
144.0	1.000	1.000

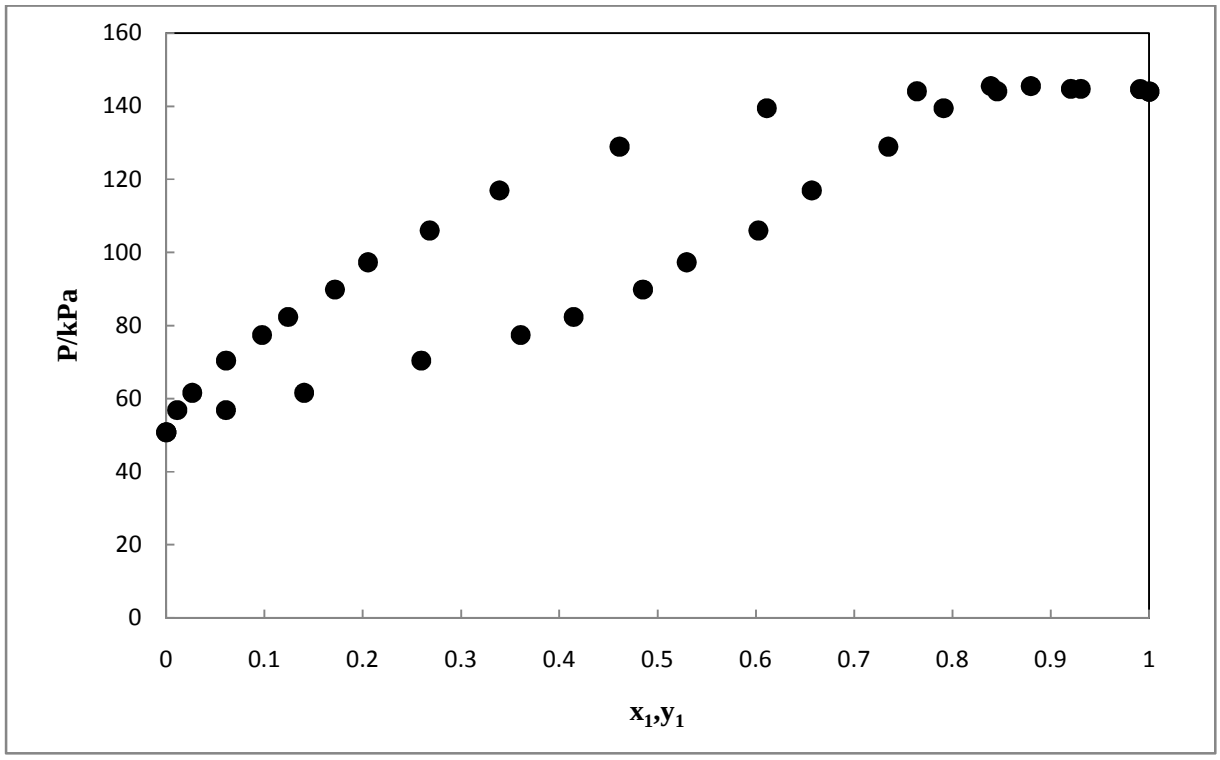

Figure 6-11: Measured P-x-y data for the diisopropyl ether (1) + propan-1-ol (2) system at 353.15 K.

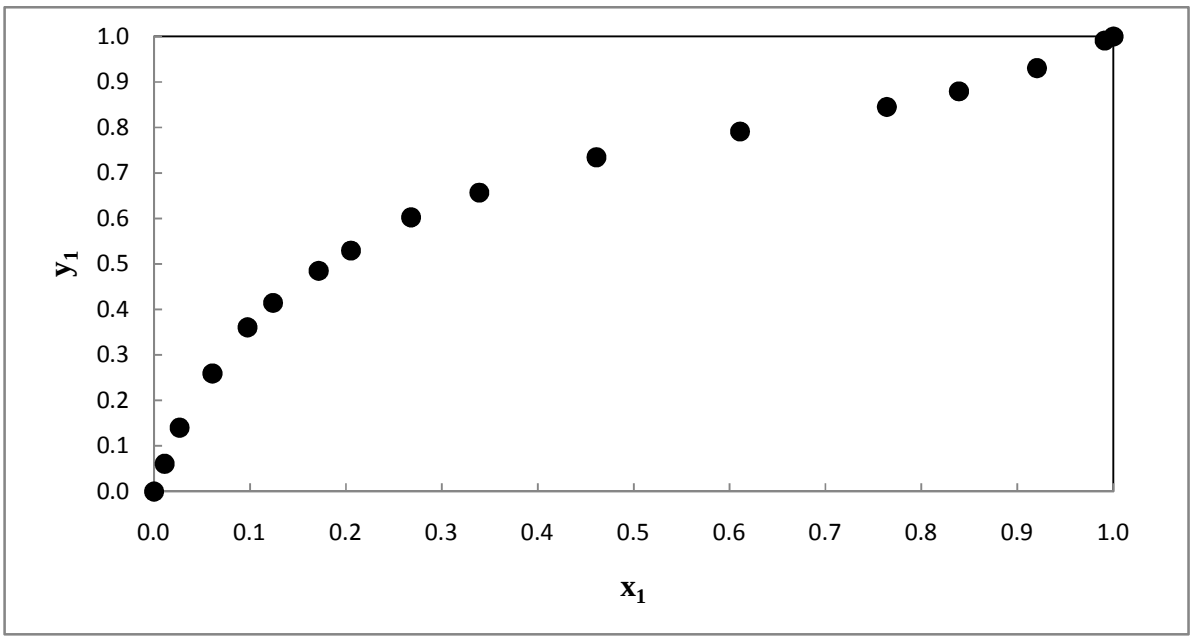

Figure 6-12: Measured x-y data for the diisopropyl ether (1) + propan-1ol (2) system at 353.15 K.

Table 6-8: P-x-y data for diisopropyl ether (1) + propan-1-ol (2) at 373.15 K.

Pressure/kPa	x_1	y_1
112.4	0.000	0.000
128.4	0.026	0.101
144.9	0.059	0.217
160.5	0.102	0.329
176.1	0.149	0.399
191.6	0.205	0.469
208.5	0.278	0.538
220.1	0.346	0.592
235.1	0.438	0.656
247.2	0.576	0.719
254.9	0.764	0.809
255.4	0.775	0.819
255.1	0.941	0.936
253.0	0.952	0.946
250.8	1.000	1.000

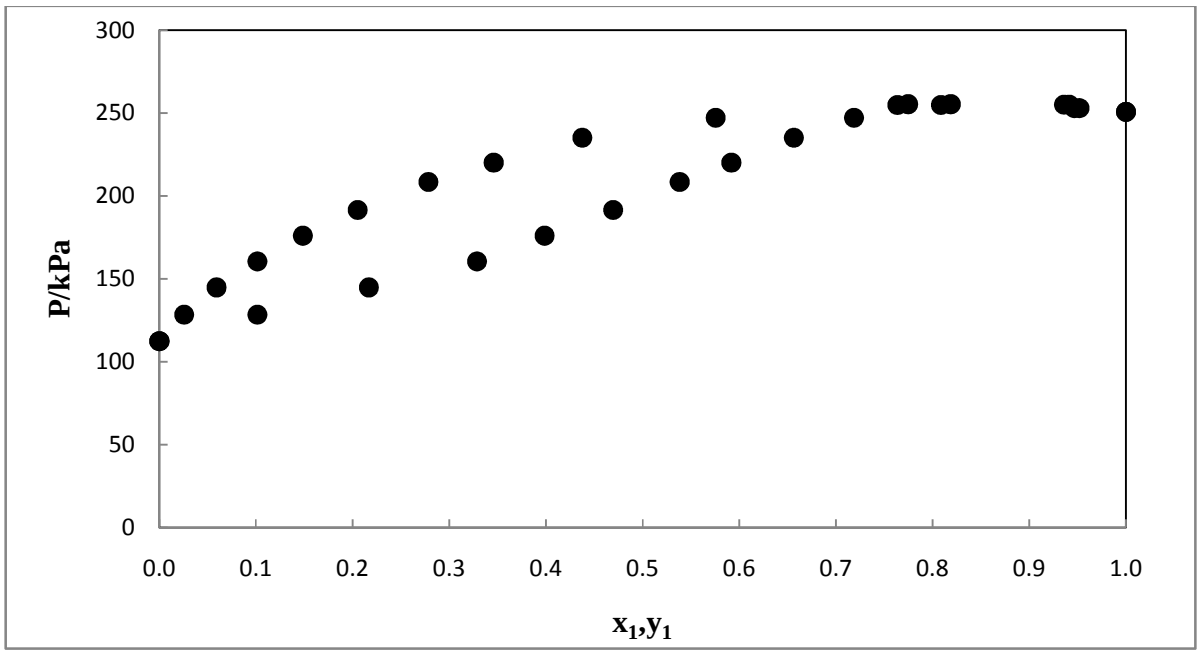

Figure 6-13: Measured P-x-y data for the diisopropyl ether (1) + propan-1-ol (2) system at 373.15 K.

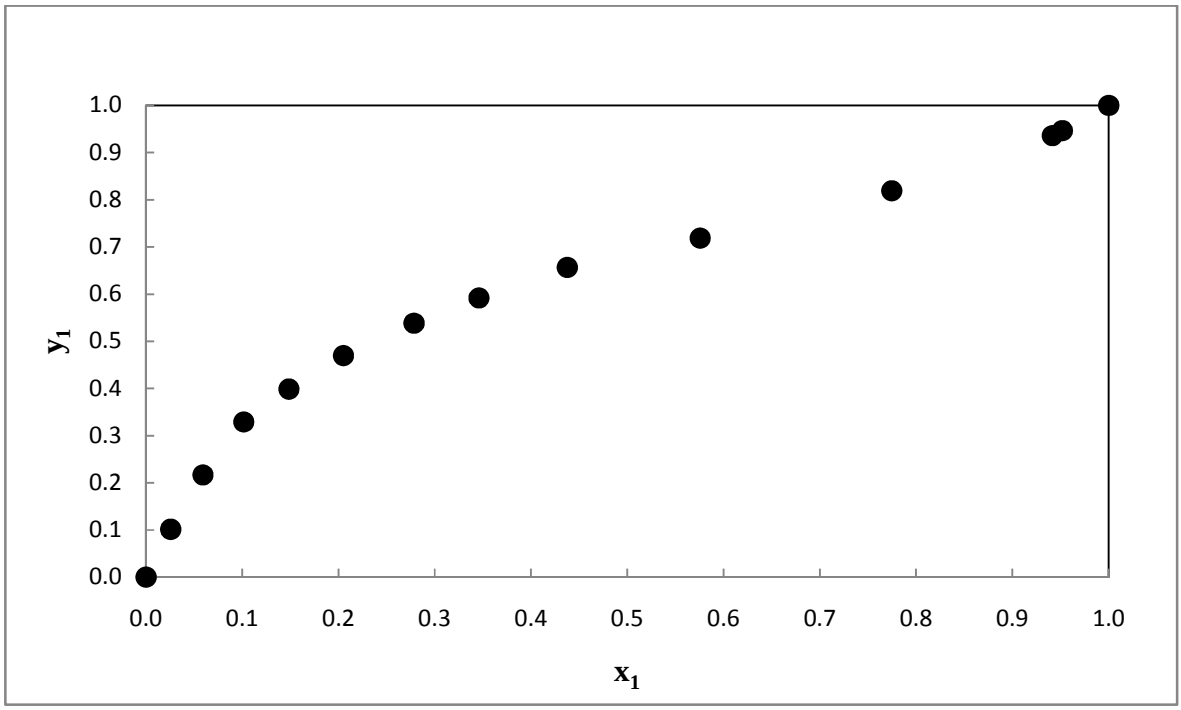

Figure 6-14: Measured x-y data for the diisopropyl ether (1) + propan-1-ol (2) system at 373.15 K.

6.3.3 Water (1) + propan-1-ol (2) System

The water + propan-1-ol system have been measured at 101.3 kPa and 333.15 K and can be found in literature such as DDB, DECHEMA series. To extend the data to other temperatures, the VLE data were measured at 358.15 K and 368.15 K. The composition analysis of this system was carried out using the Shimadzu GC2014 gas chromatograph using the operating conditions presented in Tables 5-3 and 5-4. Figures 6-15 and 6-16 present the GC calibration plots. The experimental VLE data points are listed in Tables 6-9 and 6-10 and *x-y* and *P-x-y* plots are shown in Figures 6-17 to 6-20.

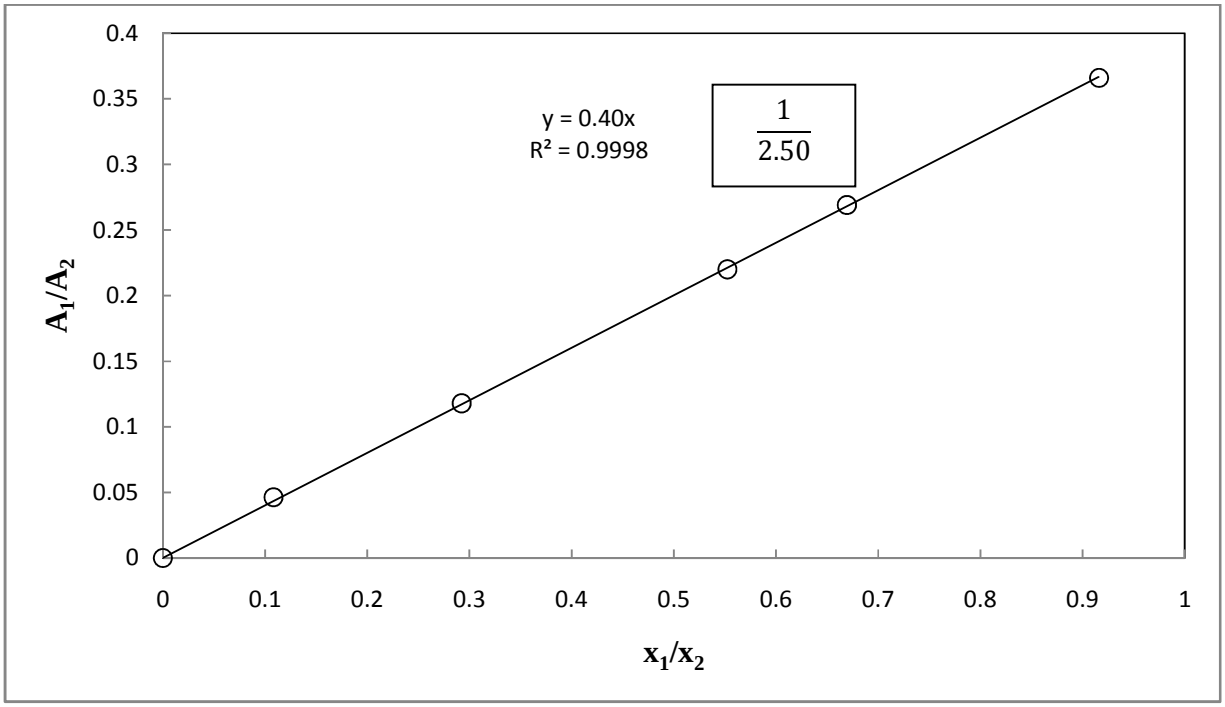

Figure 6-15: TCD calibration for the water (1) + propan-1-ol (2) system using the area ratio method of Raal and Mülhbauer (1998), (Water dilute region).

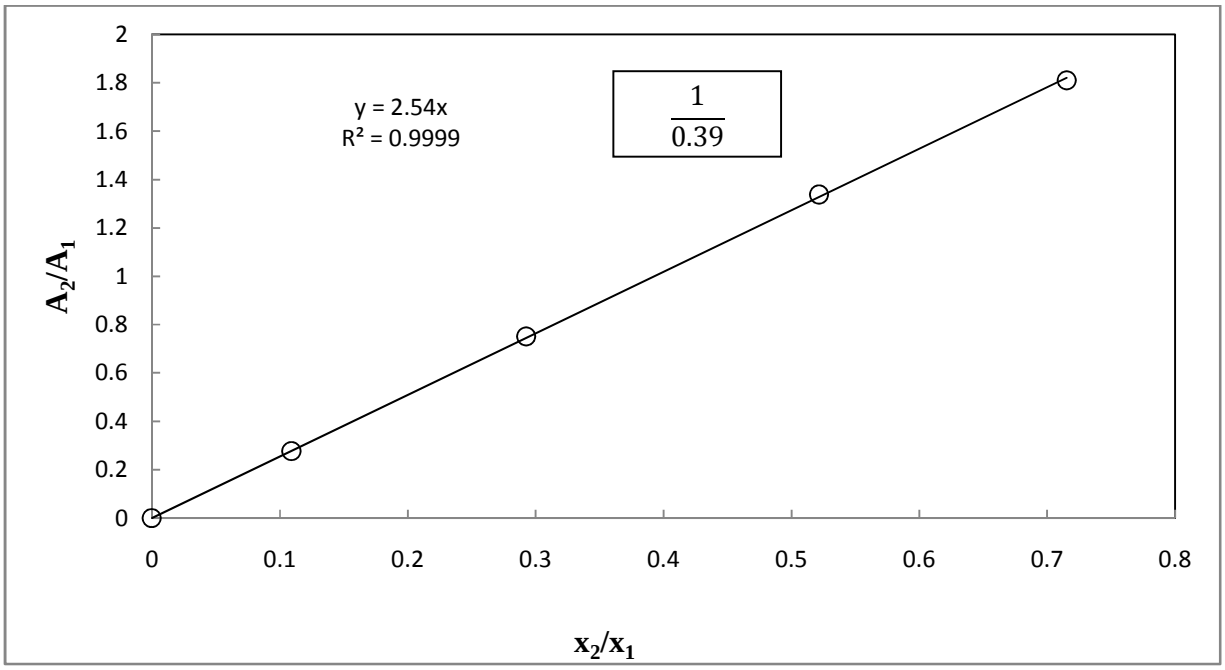

Figure 6-16: TCD calibration for the water (1) + propan-1-ol (2) system using the area ratio method of Raal and Mülhbauer (1998), (propan-1-ol dilute region).

Table 6-9: P-x-y data for water (1) + propan-1-ol (2) system at 358.15 ±0.01 K.

P/kPa	x_1	y_1
63.5	0.000	0.000
69.3	0.051	0.130
73.1	0.080	0.188
77.3	0.125	0.267
83.2	0.207	0.373
86.5	0.274	0.432
89.3	0.354	0.479
90.9	0.433	0.510
91.8	0.527	0.557
91.8	0.580	0.566
91.7	0.645	0.579
90.0	0.881	0.613
85.6	0.948	0.647
80.4	0.969	0.694
72.6	0.984	0.780
57.9	1.000	1.000

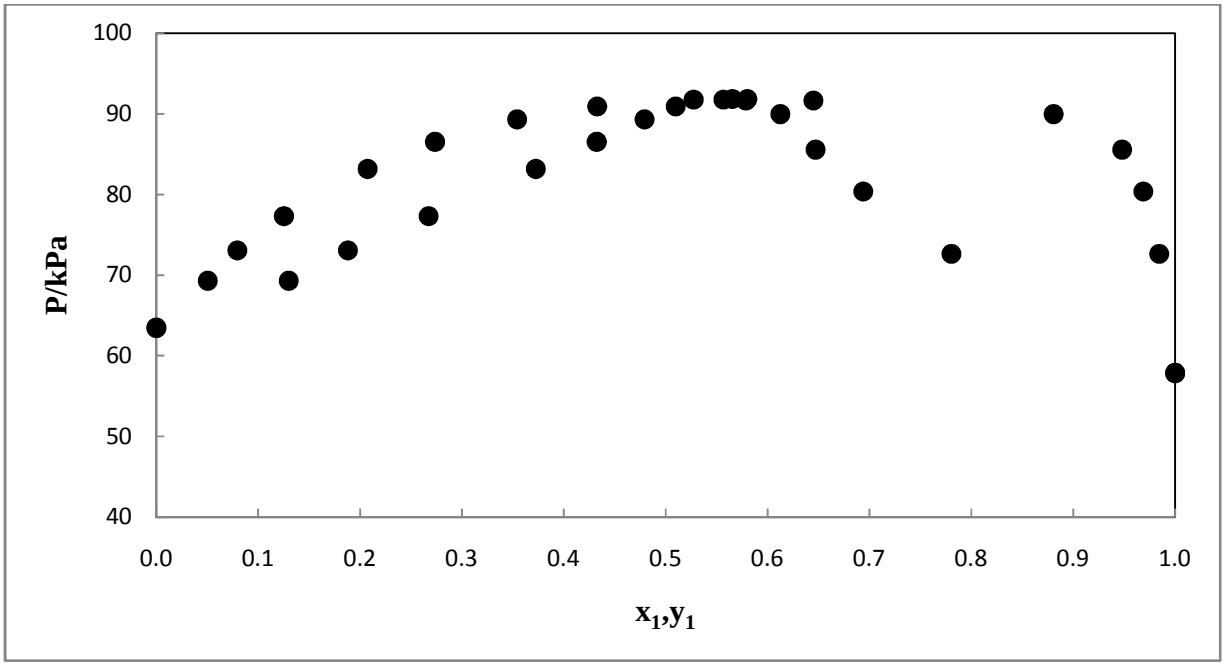

Figure 6-17: Measured P-x-y data for the water (1) + propan-1-ol (2) system at 358.15 K.

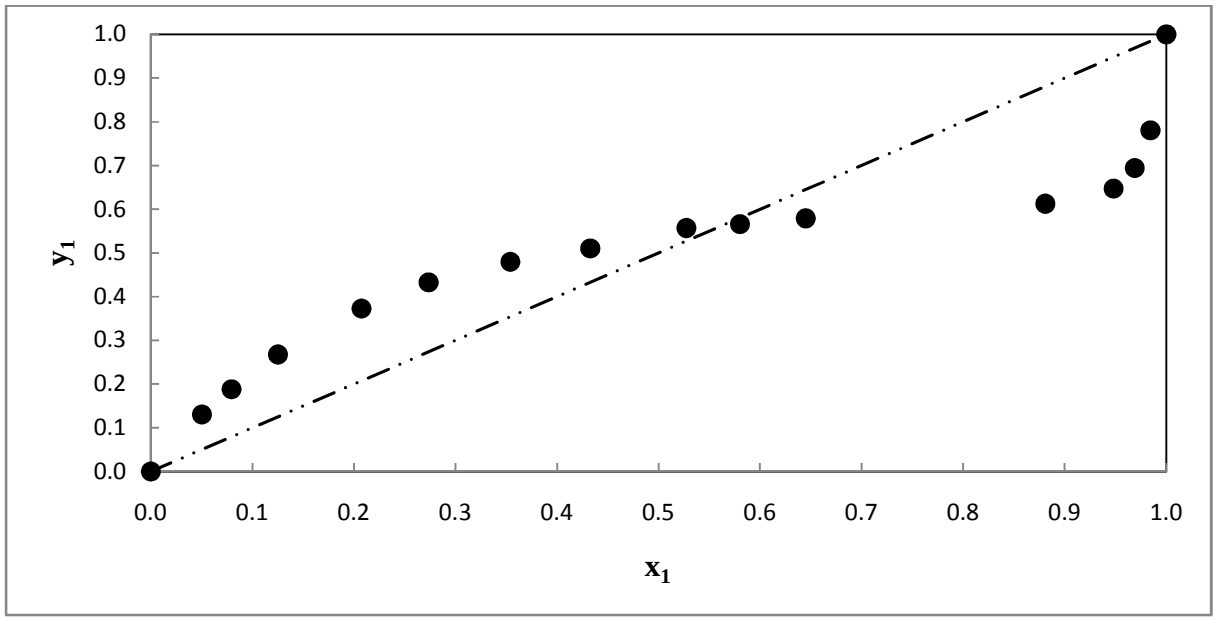

Figure 6-18: Measured x-y data for the water (1) + propan-1-ol (2) system at 358.15 K.

Table 6-10: P-x-y data for water (1) + propan-1-ol (2) system at 368.15 ±0.01 K.

P/kPa	x_1	y_1
103.1	0.054	0.134
108.9	0.092	0.210
115.7	0.141	0.288
121.0	0.191	0.348
126.5	0.266	0.418
129.3	0.304	0.461
132.2	0.409	0.502
133.6	0.504	0.541
133.6	0.589	0.566
133.4	0.635	0.574
132.9	0.691	0.587
128.7	0.908	0.622
122.3	0.956	0.661
110.8	0.978	0.741
85.15	1.000	1.000

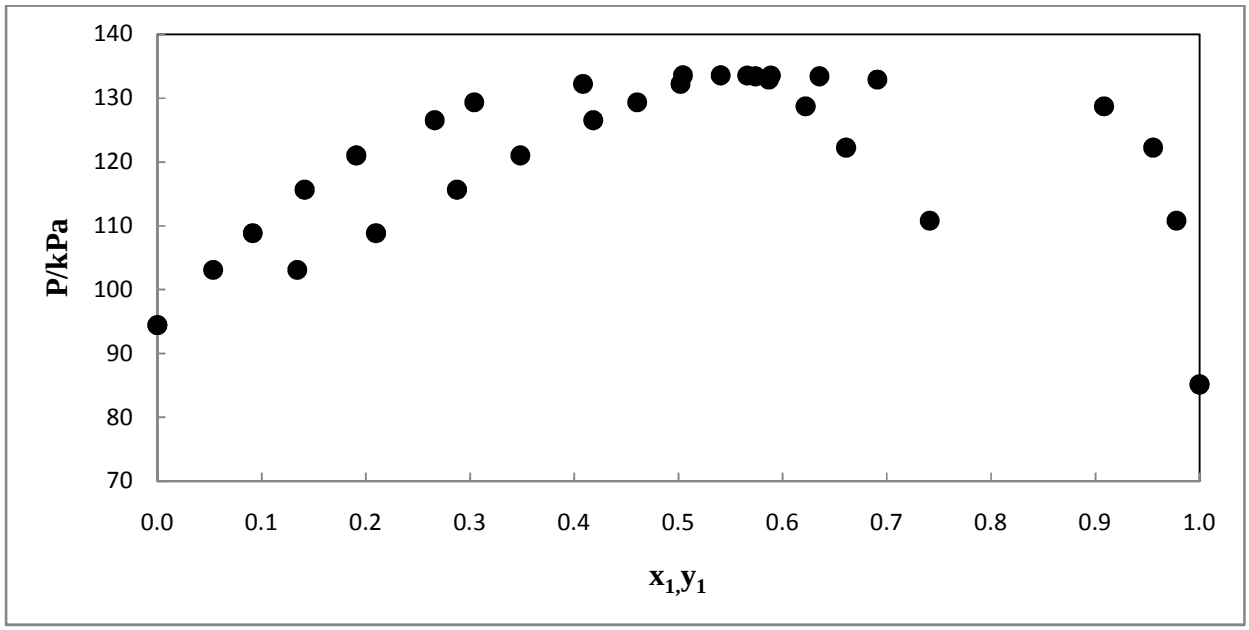

Figure 6-19: Measured P-x-y data for the water (1) + propan-1-ol (2) system at 368.15 K.

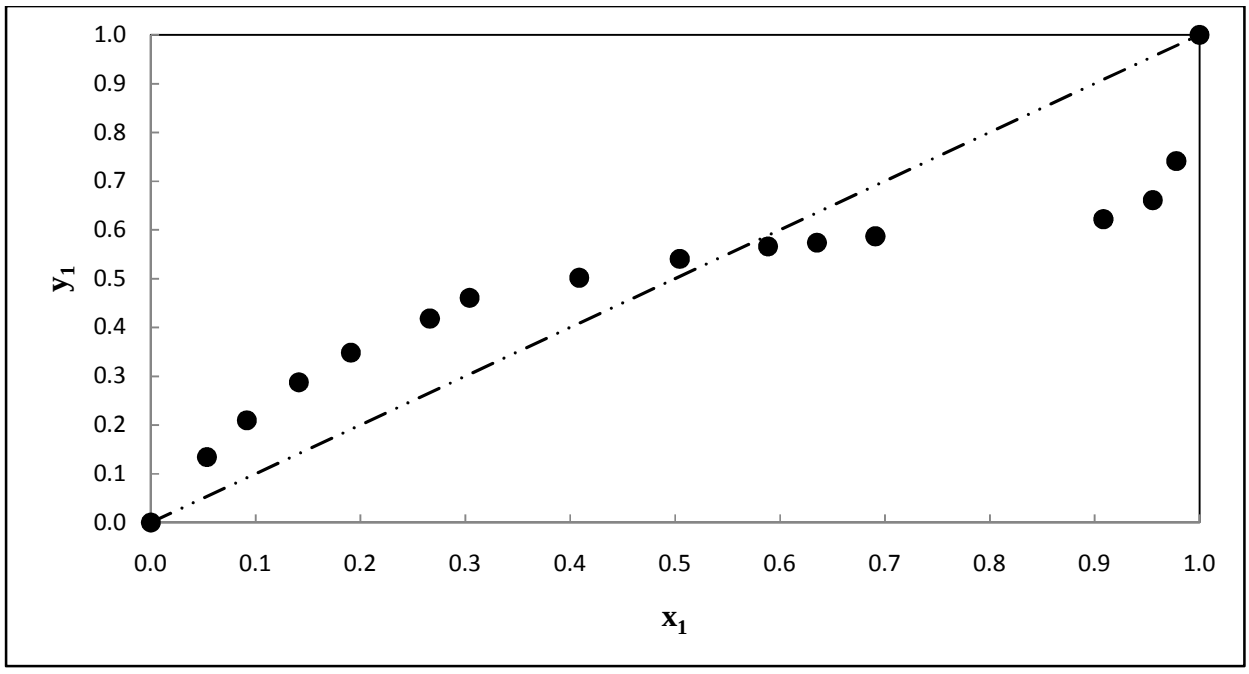

Figure 6-20: Measured x-y data for the water (1) + propan-1-ol (2) system at 368.15 K.

6.3.4 Furan (1) + n-hexane (2) System

The VLE data for furan (1) + n-hexane (2) were only measured at 101.3 kPa. This is due to limitation of the available atmospheric VLE still. The composition analysis of this system was carried out using an Anton Paar DM5000 density meter with reported uncertainty of ±0.00001g/cm^3 and ±0.01 K. The density data for various synthetic mixtures is presented in the section below together with excess volume data.

6.3.4.1 Density of Mixtures: Furan (1) + n-hexane (2) System

The density data at selected temperatures are given in Table 6-11. Density-composition plot and molar composition deviations are given in Figures 6-21 and 6-22 respectively. The mixture density data obtained were correlated using a simple polynomial to obtain density-composition relation. In addition, density measurements were used to obtain excess molar volume data and were correlated using the Redlich-Kister equation (Redlich and Kister, 1948). The data correlated well with the Redlich-Kister expansion and are shown in Figure 6-23.

Table 6-11: Density data for furan (1) + n-hexane (2) at selected temperatures.

	293.15 ±0.01 K	**298.15 ±0.01 K**	**303.15 ±0.01 K**
x_1(mol)	**Density(g/cm^3)**	**Density(g/cm^3)**	**Density(g/cm^3)**
0.000	0.6608	0.6570	0.6533
0.120	0.6778	0.6739	0.6700
0.199	0.6902	0.6861	0.6822
0.365	0.7214	0.7170	0.7128
0.511	0.7552	0.7505	0.7460
0.623	0.7862	0.7814	0.7766
0.786	0.8412	0.8359	0.8308
0.908	0.8919	0.8864	0.8810
1.000	0.9398	0.9340	0.9283

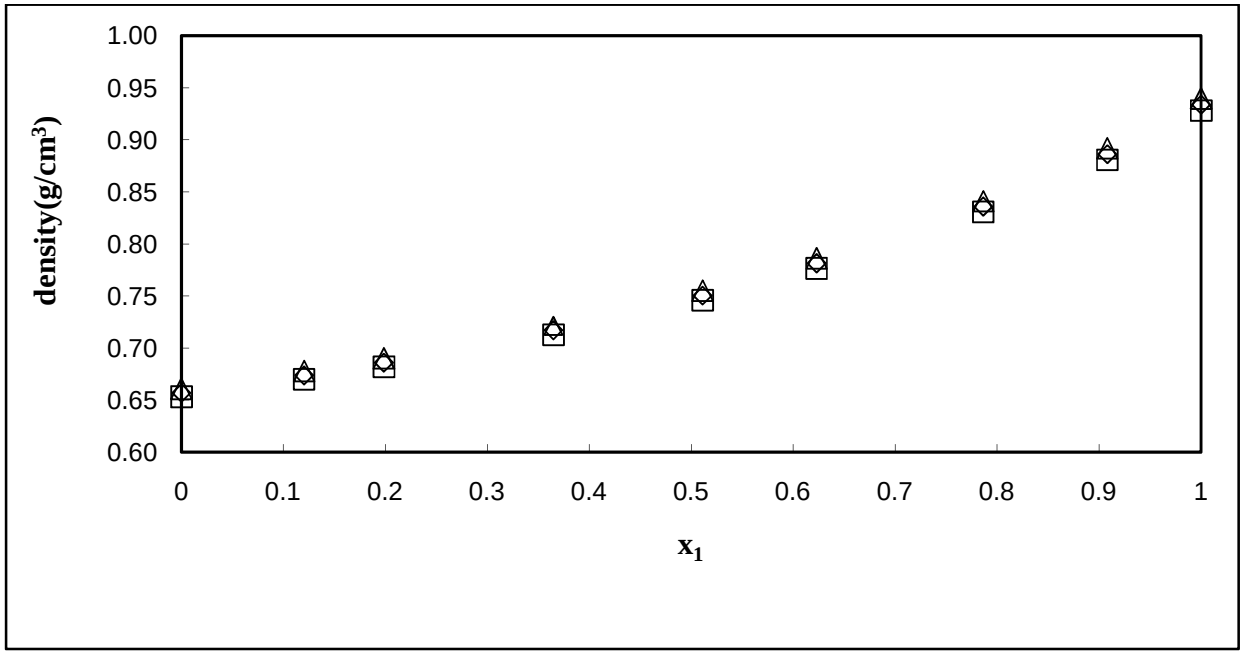

Figure 6-21: Liquid density data against molar composition for system furan (1) + n-hexane (2) at three different temperatures, Δ 293.15 K, ◊ 298.15 K, □ 303.15 K.

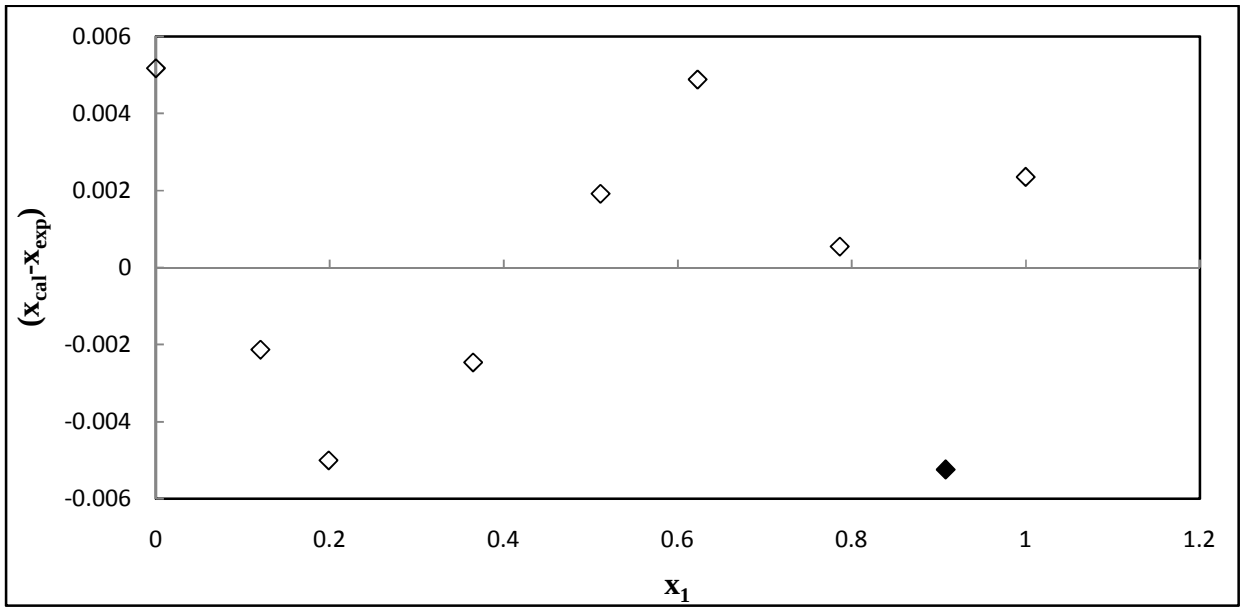

Figure 6-22: Deviation of composition-density model equation, from the measured values for the system furan (1) + n-hexane (2) at 298.15 K, ♦ maximum deviation.

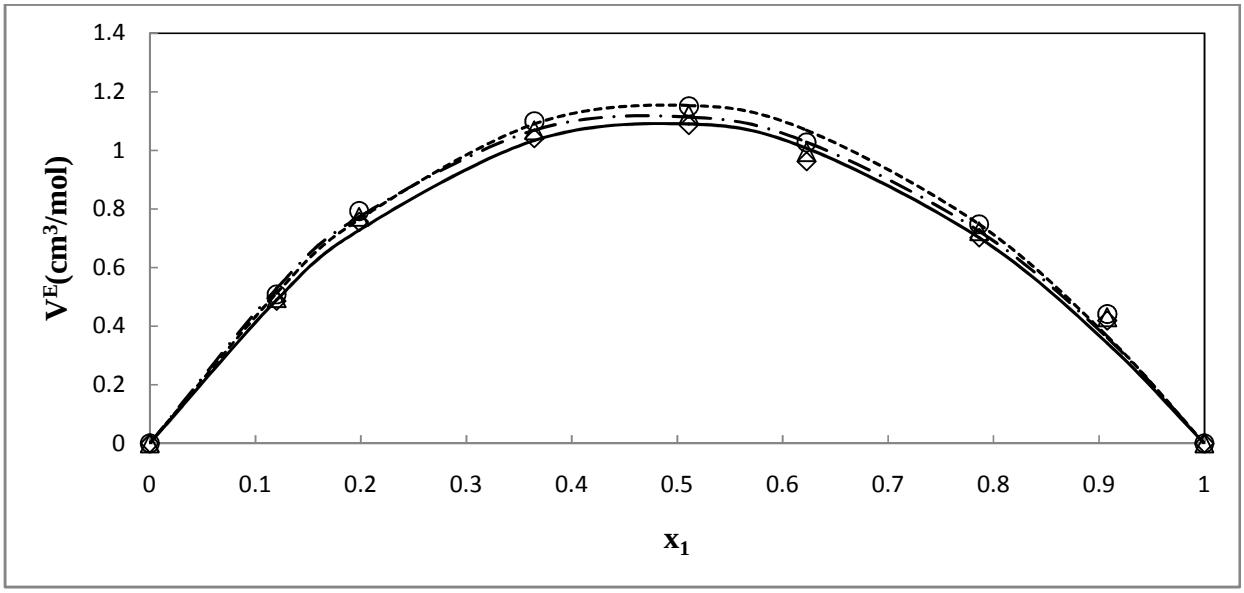

Figure 6-23: Excess Volume against molar composition for the furan (1) + n-hexane (2) system at different isothermal temperatures in comparison with Redlich-Kister correlation, this work: ◊ 293.15 K, Δ 298.15 K, ○ 303.15 K; Redlich-Kister:— RK 293.15 K,— - — - RK 293.15 K, - - - -RK 303.15 K.

6.3.4.2 Vapour-Liquid Equilibrium Data for furan (1) + hexane (2) System

The experimental VLE data points for the system are listed in Table 6-12. T-*x*-*y* and *x*-*y* plots are presented in figures 6-24 and 6-25 respectively.

Table 6-12: T-x-y data for furan (1) + n-hexane (2) at 101.3 kPa.

T±0.01/K	x_1	y_1	T ±0.01/K	x_1	y_1
341.56	0.000	0.000	309.06	0.639	0.847
338.43	0.028	0.121	307.66	0.715	0.874
335.98	0.049	0.206	306.26	0.813	0.908
332.85	0.078	0.304	305.69	0.856	0.924
329.37	0.117	0.408	305.36	0.905	0.939
325.05	0.172	0.520	304.94	0.968	0.978
319.59	0.267	0.646	304.72	0.991	0.992
316.37	0.349	0.719	304.60	1.000	1.000
313.94	0.424	0.759			
311.81	0.493	0.798			
310.26	0.567	0.828			

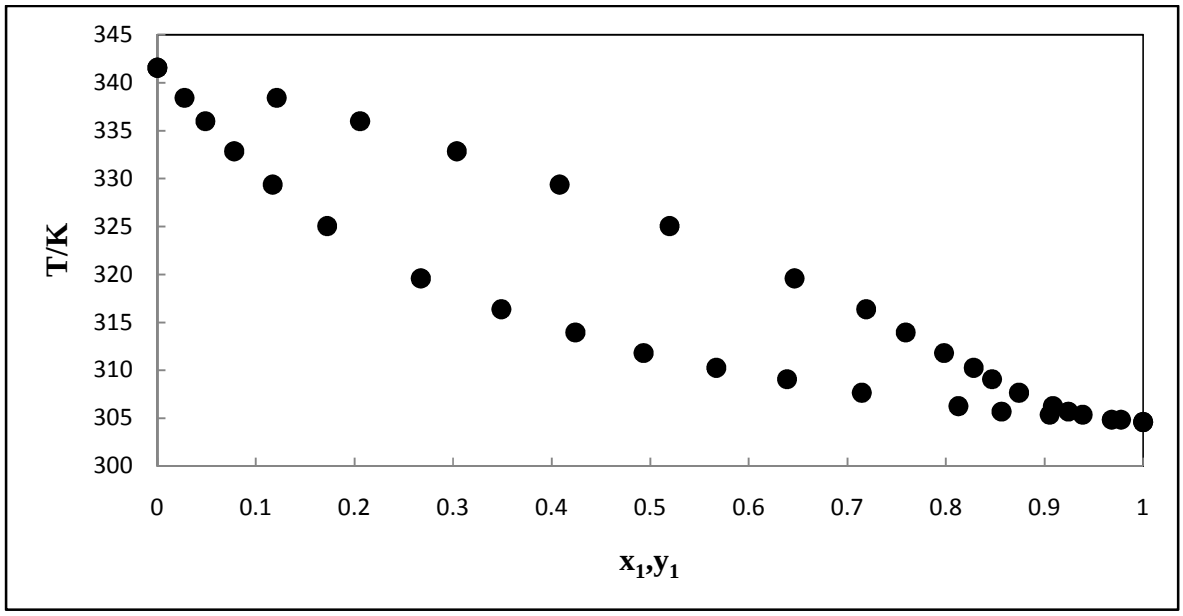

Figure 6-24: Measured T-x-y data for the system of furan (1) + n-hexane (2) at 101.3kPa.

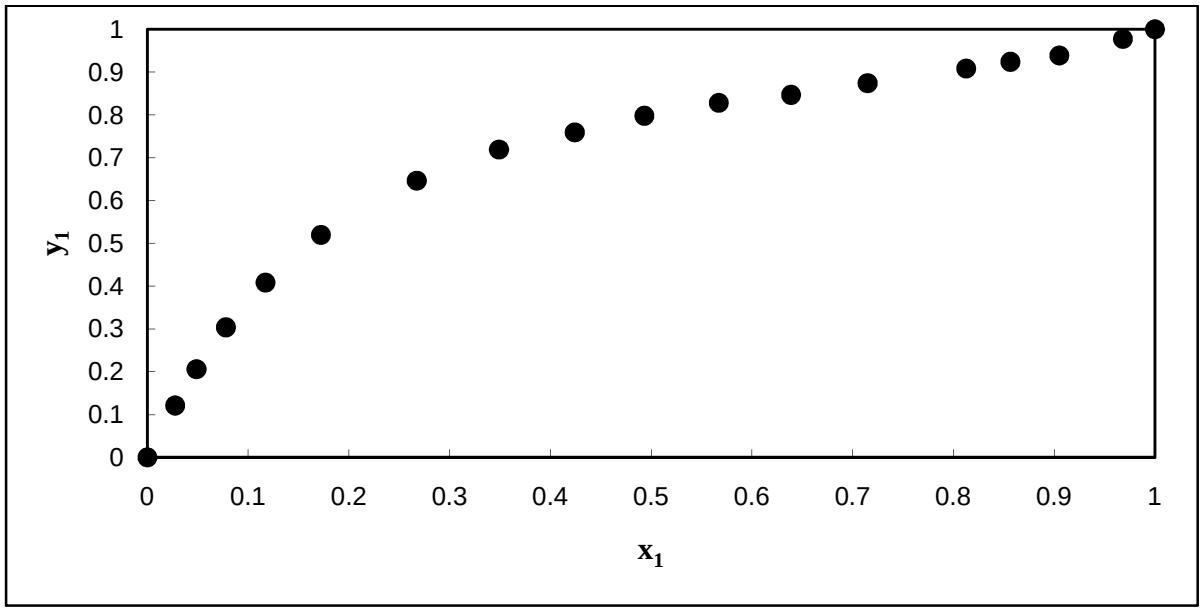

Figure 6-25: Measured x-y data for the system of furan (1) + n-hexane (2) at 101.3 kPa.

6.3.5 Furan (1) + methylbenzene (2) System

The VLE data measurements were carried out at 101.3kPa. The composition analysis of this system was carried out using an Anton Paar DM5000 density meter with reported uncertainty of ±0.00001g/cm^3 and ±0.01 K. The density data for various synthetic mixtures is presented in the section below together with excess volume data.

6.3.5.1 Density of Mixtures: furan (1) + methylbenzene (2) System

The density data at selected temperatures are given in table 6-13. Density-composition plot and molar composition deviations are given in Figures 6-26 and 6-27 respectively. The mixture density data obtained were correlated by a simple polynomial to obtain density-composition relation. In addition, density measurements were used to obtain excess molar volume data. Figure 6-28 shows a plot of excess volume for this system with values low as the uncertainty given by density meter and thus failed to correlate with the Redlich-Kister equation (Redilich and Kister, 1948).

Table 6-13: Density data for furan (1) + methylbenzene (2) at selected temperatures.

	293.15 ±0.01 K	**298.15 ±0.01 K**	**303.15 ±0.01 K**
x_1(mol)	**Density(g/cm^3)**	**Density(g/cm^3)**	**Density(g/cm^3)**
0.000	0.8682	0.8645	0.8610
0.100	0.8733	0.8695	0.8659
0.199	0.8789	0.8750	0.8712
0.387	0.8898	0.8856	0.8815
0.507	0.8977	0.8932	0.8889
0.591	0.9038	0.8991	0.8946
0.761	0.9175	0.9124	0.9075
0.890	0.9292	0.9237	0.9184
1.000	0.9398	0.9340	0.9283

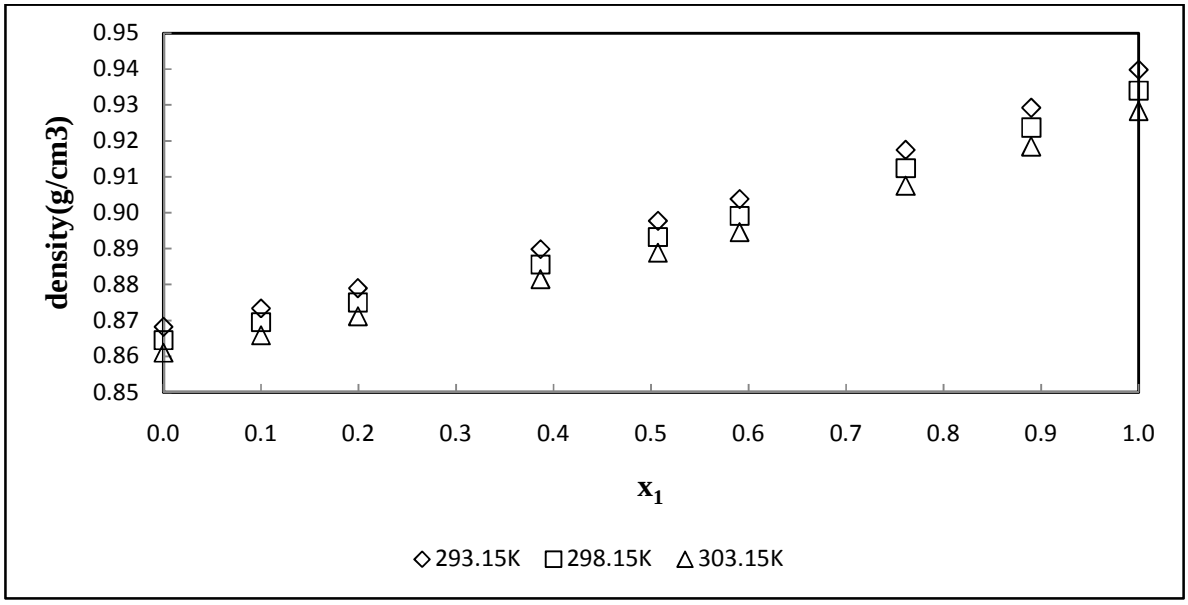

Figure 6-26: Liquid density against molar composition for system furan (1) + methylbenzene (2) at different temperatures, ◊ 293.15 K, □ 298.15 K and Δ 303.15 K.

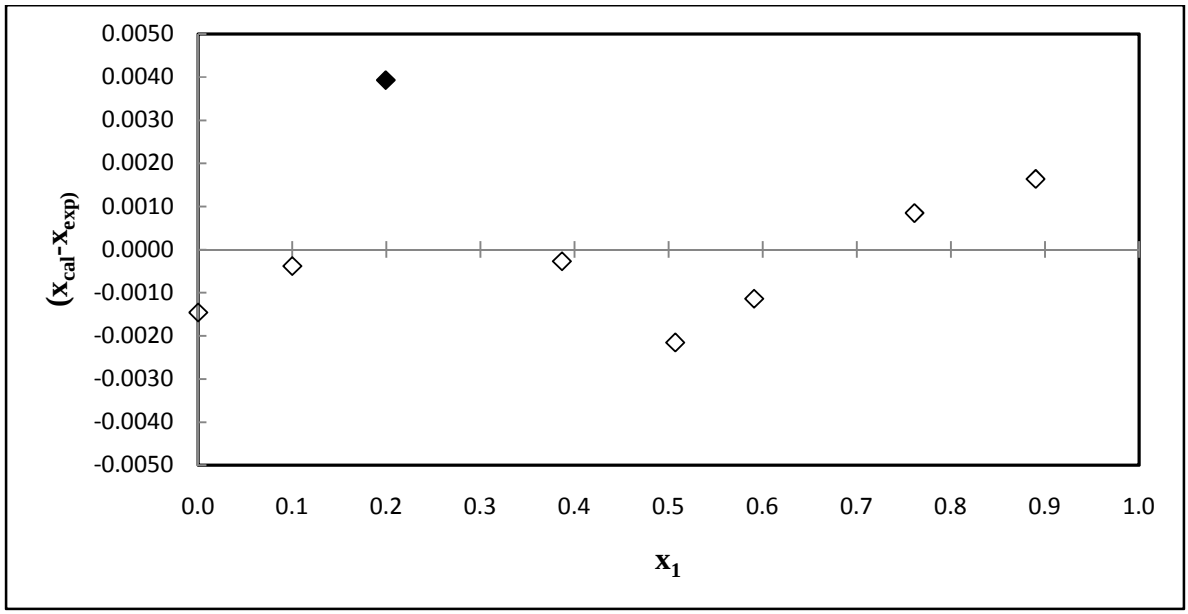

Figure 6-27: Deviation of composition-density model equation, from the measured values for the system furan (1) + n-hexane (2) at 298.15 K, ♦ maximum deviation.

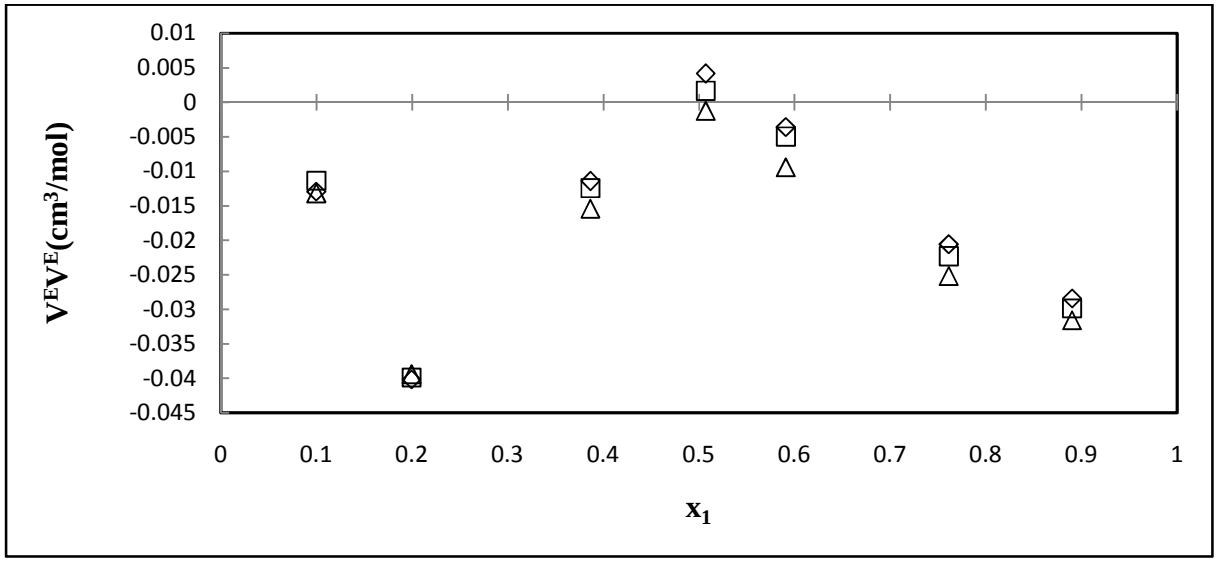

Figure 6-28: Excess Volume against molar composition for the furan (1) + toluene (2) system at different temperatures, ◊ 293.15 K, □ 298.15 K, Δ 303.15 K.

6.3.5.2 Vapour-Liquid Equilibrium Data for furan (1) + methylbenzene (2) System

The experimental isobaric VLE data points for the system are listed in Table 6-14 and T-*x*-*y* and *x*-*y* plots are presented in figures 6-29 and 6-30 respectively.

Table 6-14: T-x-y data for furan (1) + methylbenzene (2) at 101.3 kPa.

T/K	x_1	y_1	T/K	x_1	y_1
304.55	1.000	1.000	360.26	0.125	0.637
305.00	0.995	0.996	363.12	0.106	0.577
305.98	0.958	0.995	364.81	0.098	0.560
308.67	0.869	0.989	369.97	0.068	0.441
312.33	0.758	0.981	372.75	0.045	0.361
318.02	0.610	0.966	375.47	0.037	0.289
320.78	0.552	0.958	376.20	0.036	0.283
324.67	0.481	0.945	377.88	0.029	0.214
330.13	0.414	0.927	379.11	0.017	0.154
334.07	0.353	0.901	380.20	0.013	0.111
336.59	0.326	0.888	381.66	0.007	0.068
340.60	0.289	0.867	381.96	0.010	0.076
348.26	0.207	0.792	383.40	0.000	0.000
352.97	0.168	0.733			
357.97	0.136	0.665			

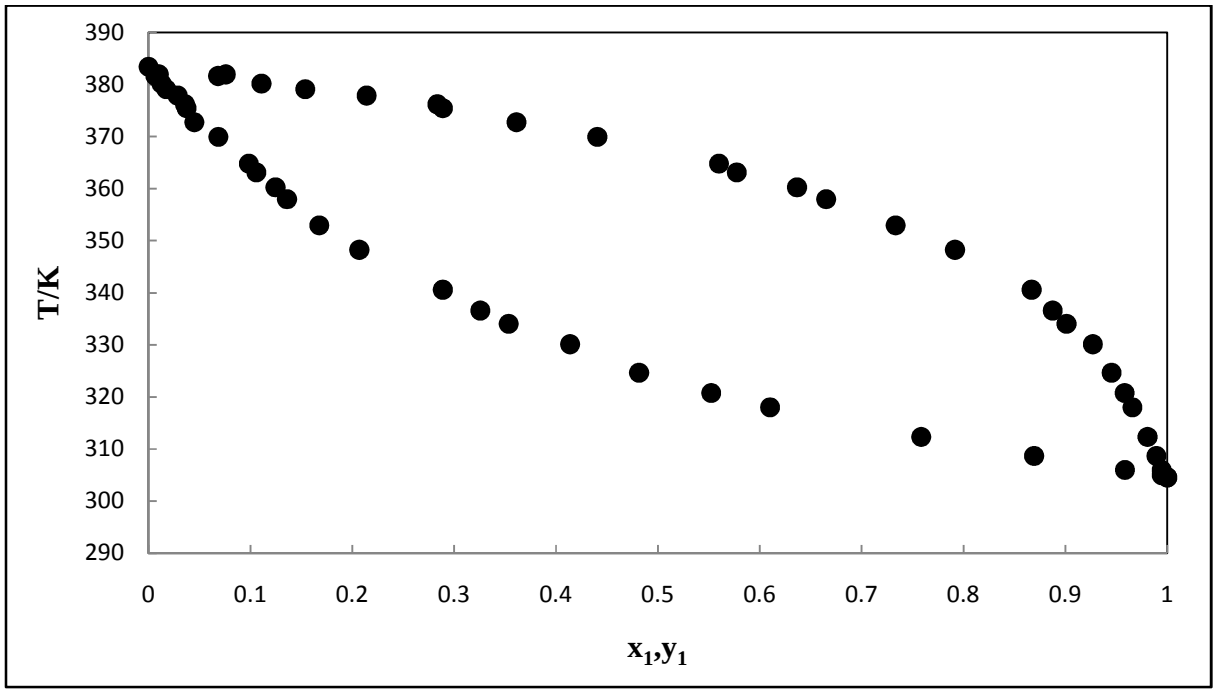

Figure 6-29: Measured T-x-y data for the system of furan (1) + methylbenzene (2) at 101.3kPa.

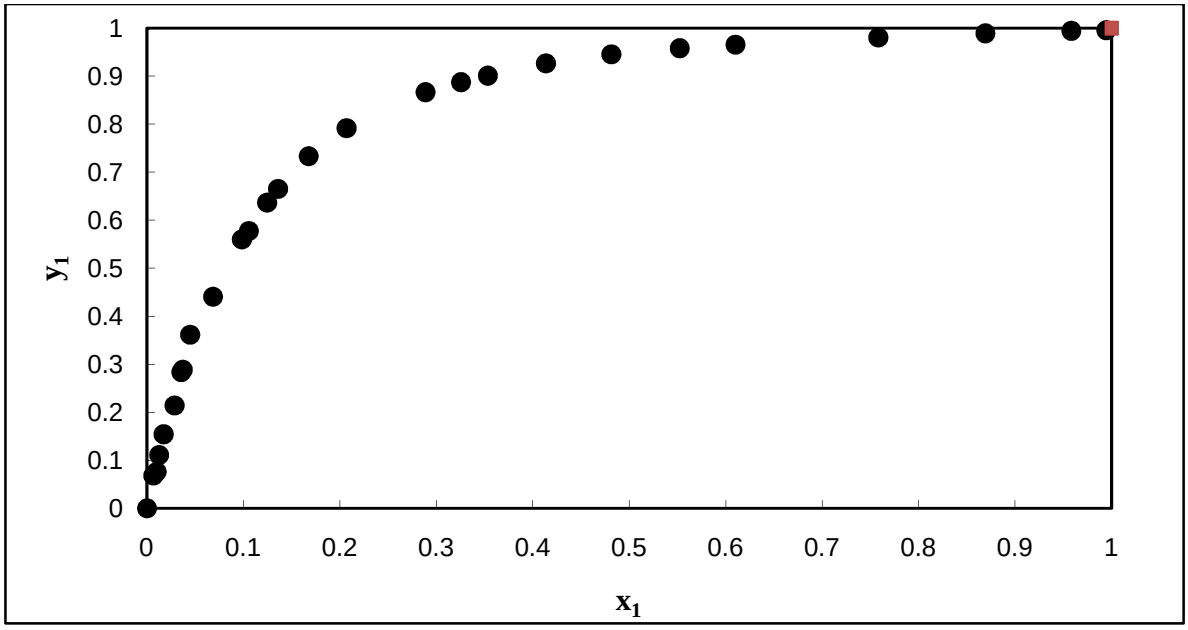

Figure 6-30: Measured x-y data for the system of furan (1) + methylbenzene (2) at 101.3kPa.

6.4 Binary LLE Measured Data

Liquid-liquid equilibrium measurements for the systems; furfural + n-hexane and furan + water were undertaken using the modified LLE apparatus. The liquid-liquid equilibrium compositions were obtained using a Perichrom gas chromatograph. The calibration procedure for the binary systems utilized an accurate number of moles (calculated from volume) to TCD area peaks correlation. Figures 6-31 to 6-34 show the absolute deviations in mole of furfural, n-hexane water and furan for the TCD calibration. The experimental LLE data points are listed in Tables 6-15 and 6-16 for the furfural (1) + n-hexane (2) and water (1) + furan (2) systems respectively. T-*x* plots are presented in Figures 6-35 and 6-36.

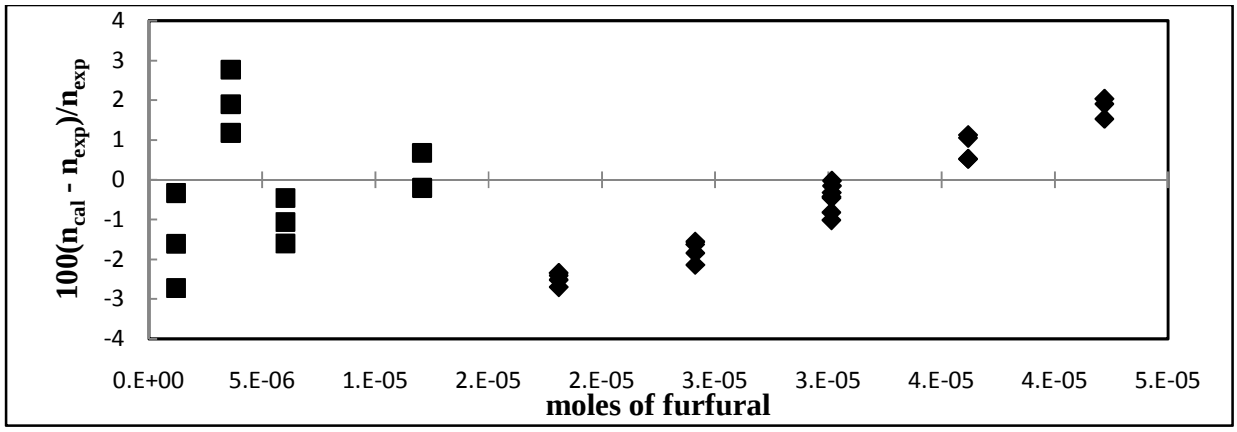

Figure 6-31: Deviation % of correlated furfural mole fraction from measured,■ 1µl syringe, ♦ 5 µl syringe.

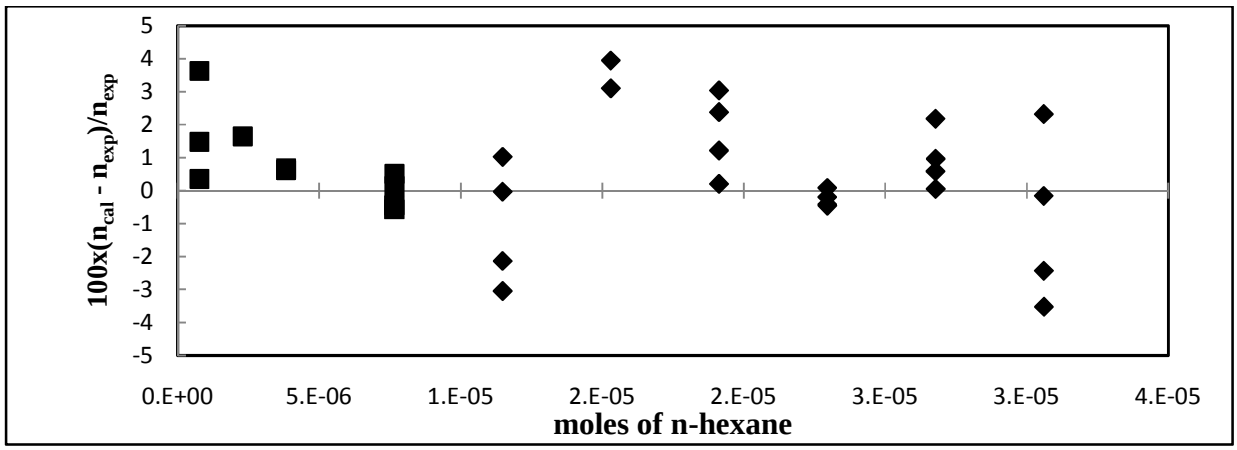

Figure 6-32: Deviation % of correlated hexane mole fraction from measured values,■ 1 µl syringe, ♦ 5 µl syringe.

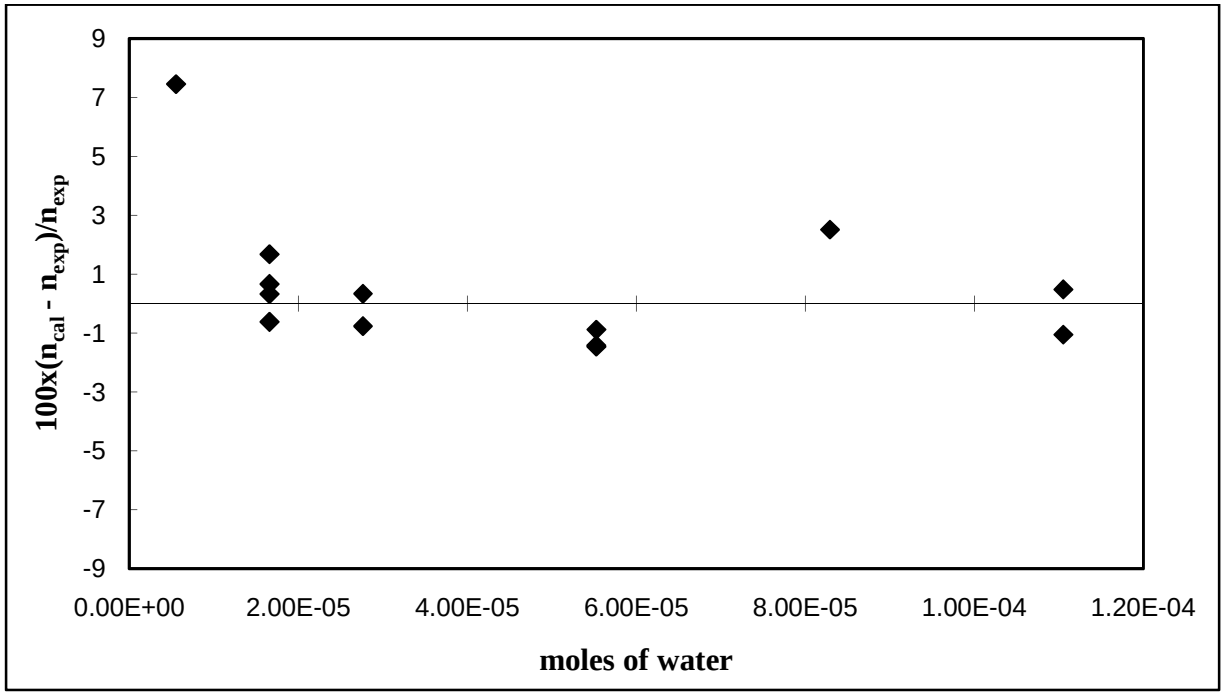

Figure 6-33: Deviation % of correlated water mole fraction from measured values.

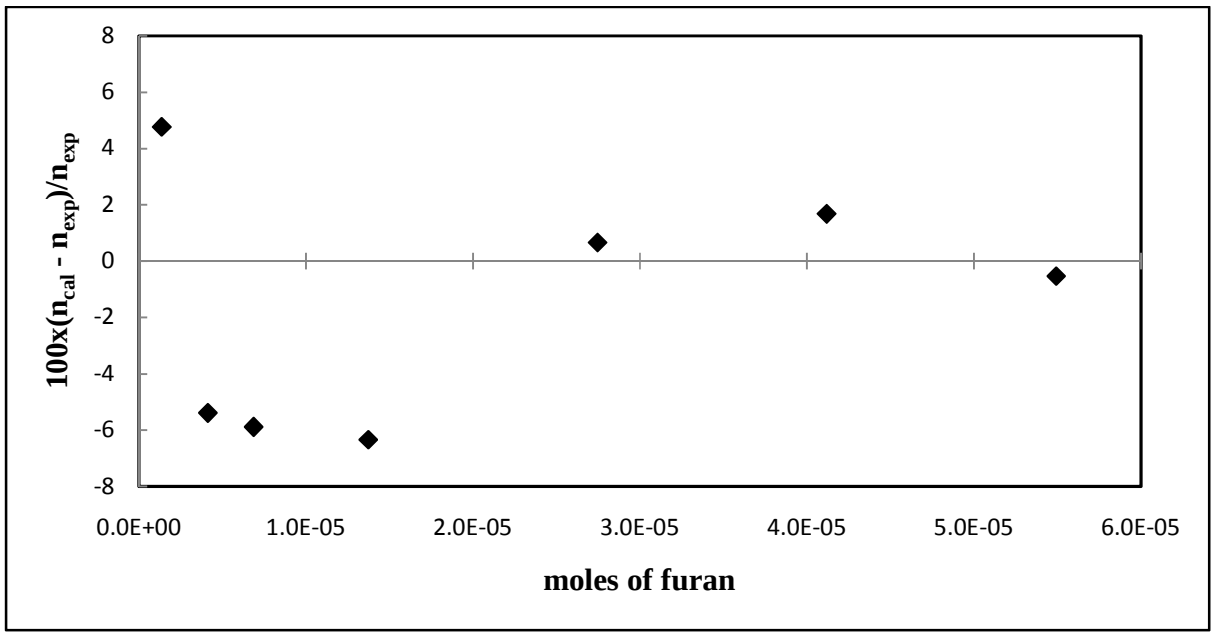

Figure 6-34: Deviation % of correlated furan mole fraction from measured values.

Table 6-15: Binary LLE data for furfural (1) + n-hexane 2) system.L_1 (furfural rich) and L_2 (n-hexane rich) phases.

T±0.01/K	L_1		L_2	
	x_1	x_2	x_1	x_2
295.10	0.0435	0.9565	0.9312	0.0688
298.50	0.0545	0.9455	0.9305	0.0695
303.16	0.0637	0.9363	0.9196	0.0804
308.65	0.0726	0.9274		
308.53			0.9130	0.0870
313.44	0.0852	0.9148	0.9052	0.0948
318.20	0.0926	0.9074	0.8987	0.1013
328.20	0.1169	0.8831	0.8717	0.1283
338.20	0.1500	0.8500	0.8409	0.1591

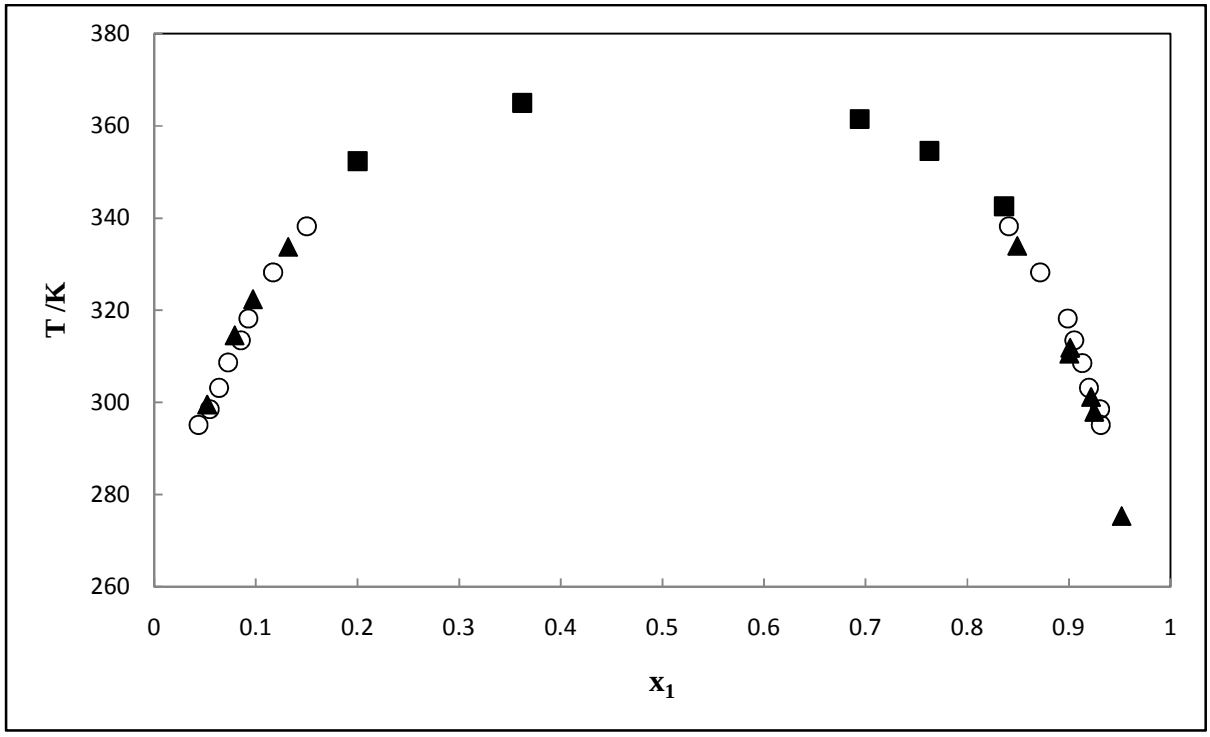

Figure 6-35:Measured and literature T-x data for furfural (1) + n-hexane (2) system at 101.3 kPa, ○ this work, ■ Kolyuchkina *et al*. (1975) and ▲ Kolyuchkina *et al*. (1975) (set 2).

Table 6-16: Measured binary LLE data for water (1) + furan (2) system. L_1 (furan rich) and L_2 (water rich) phases.

T±0.01/K	L_1		L_2	
	x_1	x_2	x_1	x_2
283.88	0.003325	0.996675	0.996763	0.003237
286.58	0.004346	0.995654	0.997607	0.002393
288.40	0.004597	0.995403	0.997588	0.002412
290.22	0.005492	0.994508	0.997548	0.002452
292.93	0.006299	0.993701	0.997518	0.002482
296.59	0.006476	0.993524	0.997407	0.002593
300.27	0.007251	0.992750	0.996976	0.003024

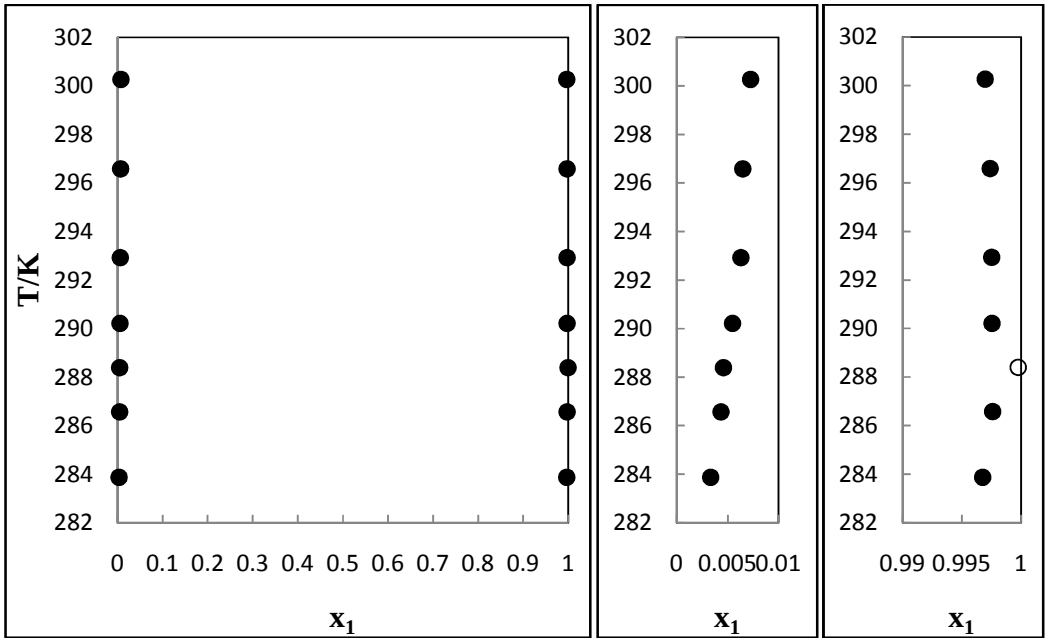

Figure 6-36: Measured T-x diagram for water (1) + furan (2) system at 101.3 kPa, ○ bad point.

CHAPTER 7

DATA REDUCTION AND DISCUSSION

Experimental measurements of phase equilibrium can be considered one piece of the puzzle in thermodynamic systems. To completely understand the phase equilibrium behavior of a particular system, it is important to analyse the experimental data using appropriate thermodynamic models; thus building a basis for the application of the measured data in industrial situations. This chapter deals with reduction of all the measured experimental data using the theoretical aspects discussed in chapter 2. Furthermore a typical industrial application of thermodynamic data is presented to illustrate its application in the design of separation processes. The measured vapour pressure data were correlated by the Wagner (used by Span and Wagner, 2002) and Antoine equations to obtain fitting parameters. The VLE data sets were regressed using the combined $\gamma - \varphi$ technique with appropriate models available in Aspen Plus®. Thermodynamic consistency testing was applied to the measured data to illustrate the quality of the data and extent to which the models fit the measured data.

7.1 Vapour Pressure Data Regression

The Wagner equation (used by Span and Wagner, 2002) and Antoine equation were used for correlating the data. The general form of the Wagner and Antoine equations used for the regression of vapour pressure data are shown below respectively:

$$ln\left(\frac{P}{P_C}\right) = \frac{T_C}{T}\sum_{i=1}^{n} A_i\,\theta^{\alpha_i} \tag{7.1}$$

Where:

$$\theta = 1 - \frac{T}{T_C} \tag{7.2}$$

$$ln\left(\frac{P/kPa}{100}\right) = A + \frac{B}{T/^oC+C} \quad (7.3)$$

A_i and α_i are the regression parameters for the Wagner equation. The number n refers to the number of terms used in the model equation. Tables 7-1 and 7-2 presents the regressed parameters and the average error for the Wagner and Antoine equations respectively. From Table 7-1 it is observed that the Wagner equation correlated the data exceptionally well, with the average error ranging between 0.03 to 0.95 %. The Antoine equation gave similar trend of results with cyclohexane being the only component with average error above 1%. The higher error in cyclohexane is attributed to the "strange behavour"(possible contamination when the end point was measured) of boiling temperature at 100 kPa (shown in Table 6.6). a 3 kPa deviation was observed for both models.

Table 7-1: Parameter values regressed from the vapour data with the Wagner equation.

Component	**A_1**	**A_2**	**A_3**	**α_1**	**α_2**	**α_3**	**$P_{(kpa/kpa)}$,AE%**
Ethanol	-5.1	-8.9	3.3	1.5	0.9	0.9	0.03
Cyclohexane	-6.8	-6.8	2.5	3.3	1.0	1.8	0.95
Diisopropyl ether	-6.2	-8.7	2.7	3.4	1.0	1.3	0.10
Propan-1ol	-5.6	-8.6	3.0	1.5	1.0	0.8	0.58
n-hexane	-56.8	-6.4	-3.8	71.1	1.0	3.4	0.77
Methylbenzene	-56.8	-6.5	-3.6	71.1	1.0	3.9	0.62
Furan	-477.5	546.7	-6.6	8.2	8.5	1.0	0.34
Water	-9.2	-4838.3	166.7	1.2	13.6	8.4	0.02

Table 7-2: Parameter values regressed from the vapour data with Antoine equation.

Component	A	B	C	$P_{(kPa/kPa)}$,AE%
Ethanol	5.3	1642.8	230.5	0.05
Cyclohexane	4.5	1508.3	254.2	1.41
Propan-1-ol	5.0	1513.1	204.0	0.43
Diisopropyl ether	4.2	1278.3	236.3	0.31
Water	5.3	1730.6	228.8	0.65

7.2 Binary VLE Data Regression

The measured VLE have been correlated using the γ-φ approach. Three activity coefficient models were chosen to account for the departure of the liquid phase from ideality, the Wilson (1964), NRTL (Renon and Prausnitz, 1968) and the UNIQUAC (Abrams and Prausnitz, 1975). The vapour phase non-idealities were calculated from the methods of Hayden and O'Connell (1974), Nothnagel *et al*. (1973) and Peng Robinson (1976) equation of state with the Wong-Sandler (1992) mixing rule, which were chosen after a thorough review of model capabilities and successful past applications. The Peng Robinson EoS is capable of representing systems that display significant deviations from ideality. The Wong and Sandler (1992) mixing rule was chosen due to its applicability in a wide range of mixtures containing hydrocarbons and inorganic gases, also mixtures containing aromatic, polar and associating systems. Aspen Plus® process simulator was used as platform for data regression as it is equipped with various models including those capable of describing association and solvation in chemical systems. To avoid confusion in the names of models used; the PR-NRTL, PR-UNIQUAC and PR-Wilson refers to the Peng Robinson (1976) equation (which is used throughout this thesis with the Wong and Sandler (1992) mixing rule) with the three activity coefficient models. Similarly, HOC-NRTL, HOC-UNIQUAC and HOC-Wilson refer to the Hayden and O'Connell (1974) correlation with the three activity coefficient models. The Nothnagel *et al*. (1973) correlation is abbreviated by NTH and is used with the three activity coefficient models.

The measured experimental data ranged from low to moderate pressures, thus the bubble-point pressure and bubble temperature type objective functions for isothermal and isobaric measurements were adopted for minimization. The regression algorithms employed were the *ordinary least squares* and a rigorous *maximum-likelihood* (guarantees global optimum in

parameter estimation) method available in Aspen Plus®. These methods were found to provide better convergence as opposed to the approximate solution method of Deming (1943). Aspen Plus® also provide the method of Barker (1953) which was omitted since it uses liquid composition *x* and bubble point *P* or *T* data, and resulted in poor prediction of vapour phase composition. Below are the two bubble point type objective function used in the correlation of isobaric and isothermal data respectively:

$$OF = \frac{100}{N}\left[\sum_{i}^{N}\left(P_i^{exp} - P_i^{cal}\right)^2 + \sum_{i}^{N}\left(\frac{y_i^{exp} - y_i^{cal}}{y_i^{exp}}\right)^2\right] \tag{7.4}$$

and

$$OF = \frac{100}{N}\left[\sum_{i}^{N}\left(T_i^{exp} - T_i^{cal}\right)^2 + \sum_{i}^{N}\left(\frac{y_i^{exp} - y_i^{cal}}{y_i^{exp}}\right)^2\right] \tag{7.5}$$

Where *N* is the number of experimental data points in the regression and $(y_i^{exp} - y_i^{cal})$ is the deviation between the measured and calculated vapour phase composition for the *i*th data point.

7.2.1 Modeling Results for the diisopropyl ether (1) + propan-1-ol (2) System

Table 7-3 gives the adjustable binary interaction parameters for the different models used in the modeling of diisopropyl ether (1) + propan-1-ol (2) system. The average deviations of pressure (ΔP/kPa) and vapour molar compositions (Δy_1) are given in Table 7-3; also given are the average absolute deviation percent (AAD %) of the vapour mole fraction. No significant difference observed between the models, with PR-NRTL showing the least deviations for the data set at 333.15 K. Generally the combination of the equations of state with the NRTL model gave better fit than both Wilson and UNIQUAC models with the exception of data set at 373.15 K where the NTH-NRTL model gives higher values of (Δy_1). The effect of temperature modeling results is shown significantly by the increase in deviations with temperature. The (AAD %) increases with temperature with the lowest value of 1.07 % (< 5%) observed in the PR-NRTL equation, while highest value at 6.11 % (> 5 %) for the PR-UNIQUAC equation for the 373.15 K data set. To

justify such behavior, it is important to look at possibilities such as stronger short range association and dipole effects of propan-1-ol - propan-1-ol molecules in the vapour phase. The effects will increase with temperature (mobility of molecules at higher temperatures). The shown graphs from Figures 7-1 to 7-12 gives the comparison of the model fits to the VLE data sets. Fig. 7-13 to 7-15 gives the graphical representation of activity coefficients for each data set with experimental activity coefficients given in the appendix D. The calculated activity coefficients are observed to deviate significantly when approaching dilute regions ($x_1 \rightarrow 0$). This can be justified by the fact that models are well known to be inadequate to represent thermodynamic behavior at infinite dilution.

Table 7-3: Modeling Result for the diisopropyl ether (1) + propan-1-ol (2) system.

Model	T±0.02/K	WS k_{ij}	α_{12}	b_{12} J/kmol	b_{21} J/kmol	AAD (ΔP)	AAD (Δy_1)	AAD%(Δy_1)
PR-NRTL	333.15	0.4445	0.29	980.27	-489.56	0.03	0.0041	1.07
	353.15	0.0183	0.30	5241.60	351.99	0.13	0.0131	3.56
	373.15	-0.5711	0.30	8618.80	3857.90	0.30	0.0161	5.68
HOC-NRTL	333.15		0.31	371.62	38.34	0.03	0.0045	1.08
	353.15		0.30	380.65	40.74	0.12	0.0126	3.67
	373.15		0.30	306.52	108.16	0.34	0.0165	5.35
NTH-NRTL	333.15		0.31	371.62	38.34	0.03	0.0041	1.07
	353.15		0.31	387.52	36.44	0.16	0.0134	3.76
	373.15		0.30	320.79	98.35	0.33	0.0182	5.72
PR-WILSON	333.15	0.2553		150.15	-597.19	0.03	0.0048	1.37
	353.15	0.1651		377.66	808.67	0.13	0.0120	4.14
	373.15	0.2840		132.64	-496.98	0.35	0.0163	5.68
PR-UNIQUAC	333.15	0.2561		-421.57	200.18	0.03	0.00479	1.13
	353.15	0.2810		-453.18	221.39	0.13	0.01337	3.65
	373.15	-0.0077		398.23	-101.03	0.33	0.01817	6.11

b_{12} and b_{21}: Binary interaction parameters for the models in Aspen (equivalent to Δg_{12} and $\Delta g_{21,}$for isothermal data set).
kij :Fitting parameter in Wong and Sandler mixing rule.

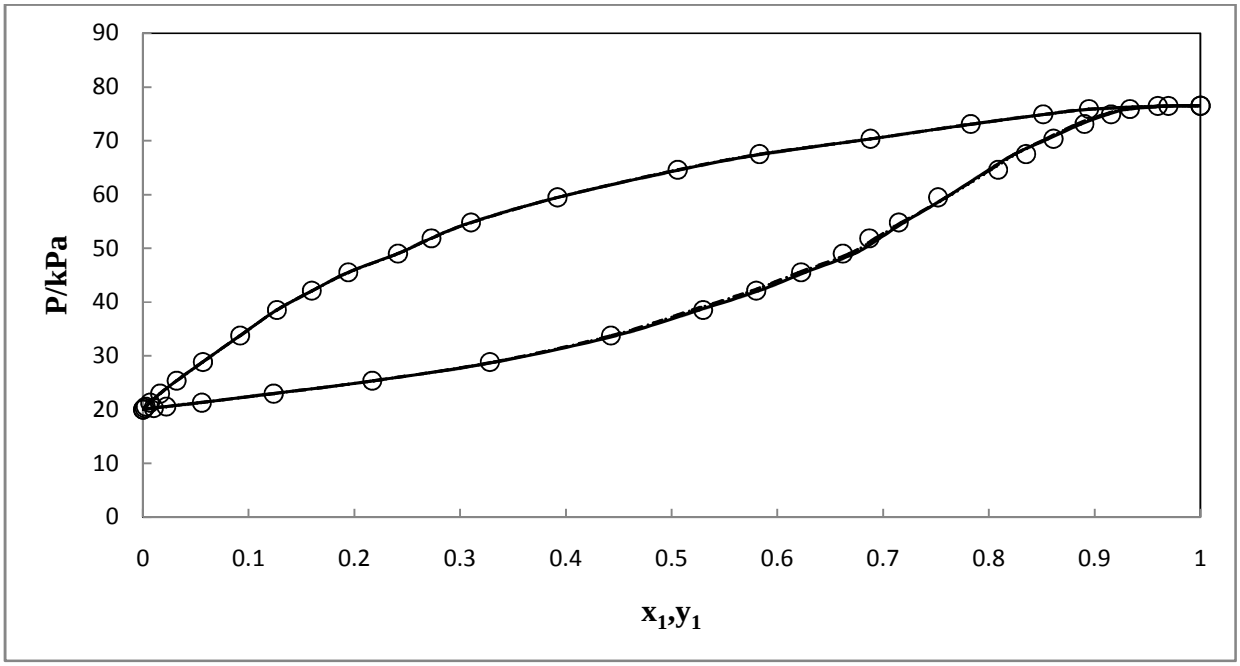

Figure 7-1: Experimental VLE and modeling results, comparison between PR, HOC and NTH model fits to P-x-y data for the diisopropyl ether (1) + propan-1-ol (2) system at 333.15 K:○ this work, — PR-NRTL, - - - HOC-NRTL, ····· NTH-NRTL.

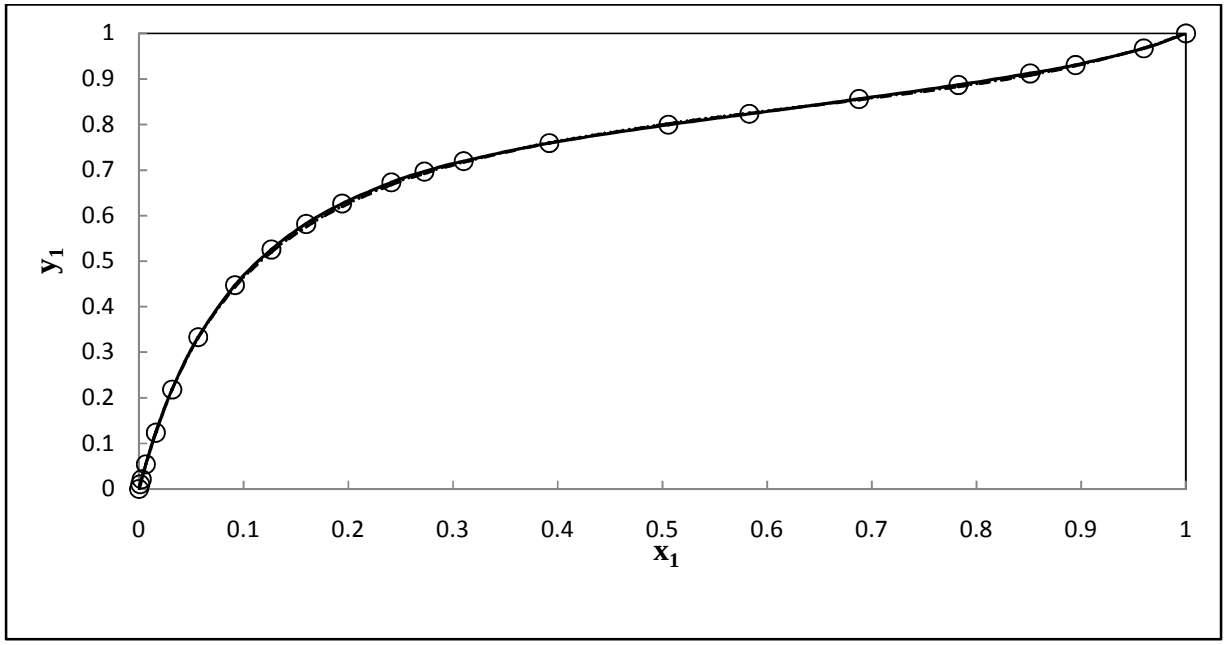

Figure 7-2: Experimental VLE and modeling results, comparison between PR, HOC and NTH model fits to x-y data for the diisopropyl ether (1) + propan-1-ol (2) system at 333.15 K:○ this work, — PR-NRTL, - - - HOC-NRTL, ····· NTH-NRTL.

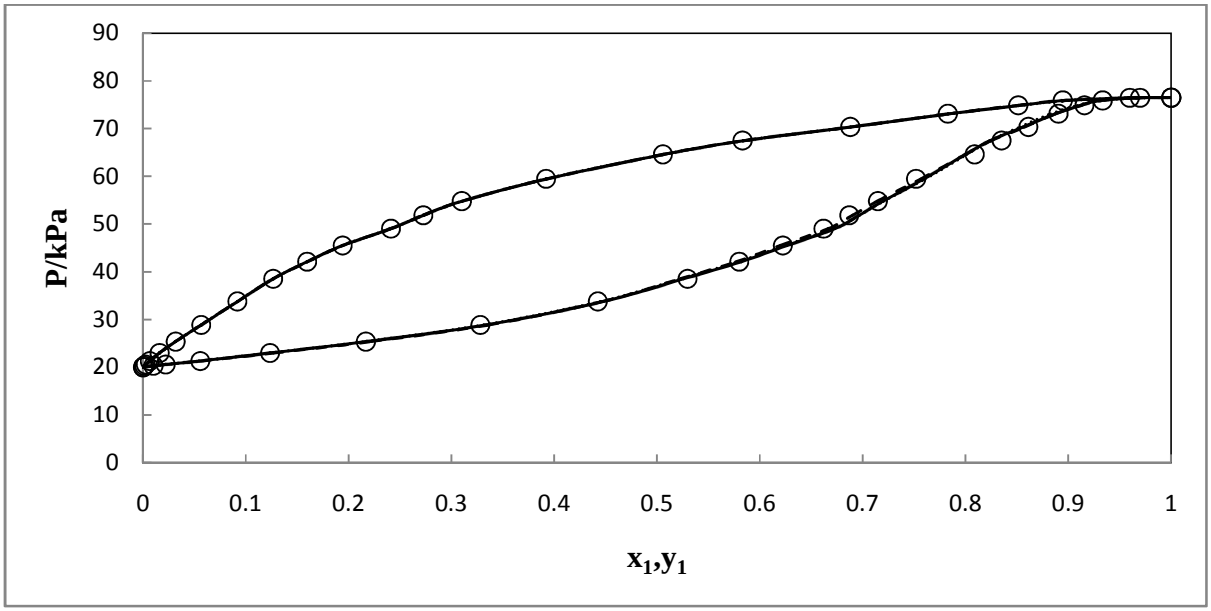

Figure 7-3:Experimental VLE and modeling results, comparison between NRTL, WILSON and UNIQUAC model fits to P-x-y data for the diisopropyl ether (1) + propan-1-ol (2) system at 333.15 K:○ this work, — PR-NRTL, - - - PR-Wilson, ····· PR-UNIQUAC.

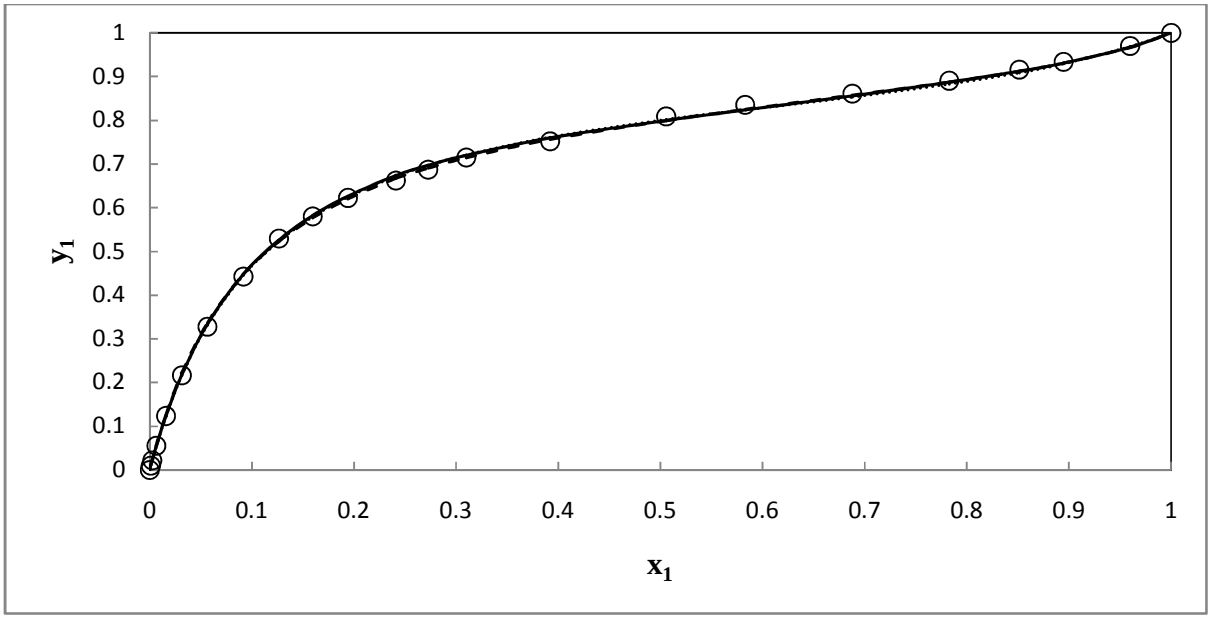

Figure 7-4: Experimental VLE and modeling results, comparison between NRTL, WILSON and UNIQUAC model fits to x-y data for the diisopropyl ether (1) + propan-1-ol (2) system at 333.15 K:○ this work, — PR-NRTL, - - - PR-Wilson, ····· PR-UNIQUAC.

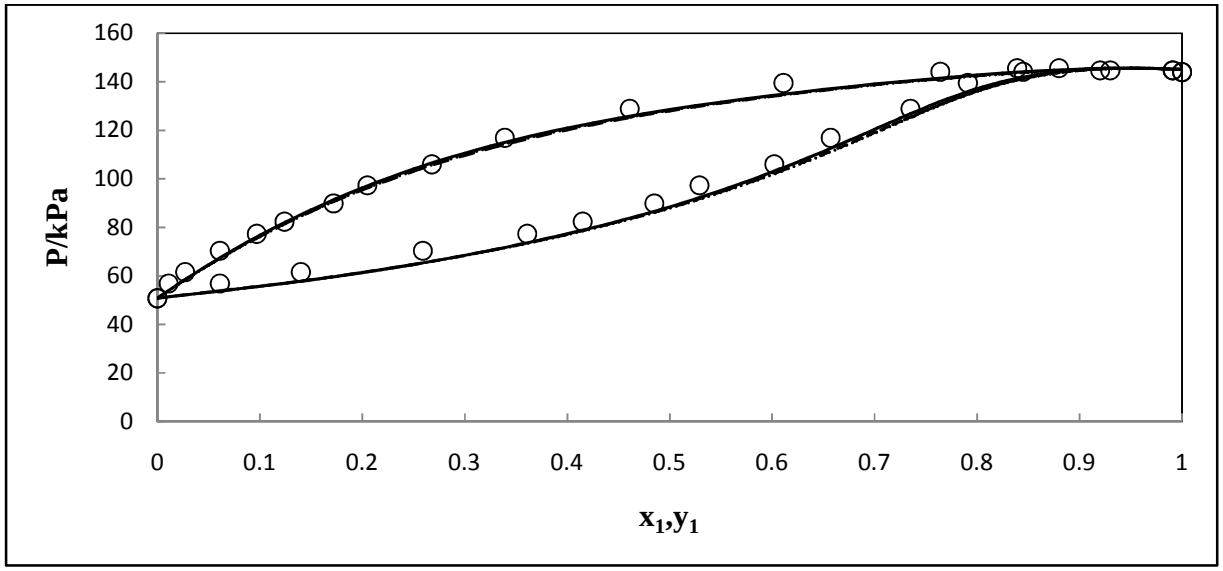

Figure 7-5: Experimental VLE and modeling results, comparison between HOC,NTH and PR model fits to P-x-y data for the diisopropyl ether (1) + propan1-ol (2) system at 353.15 K:○ this work, — PR-NRTL, - - - HOC-NRTL, ····NTH-NRTL.

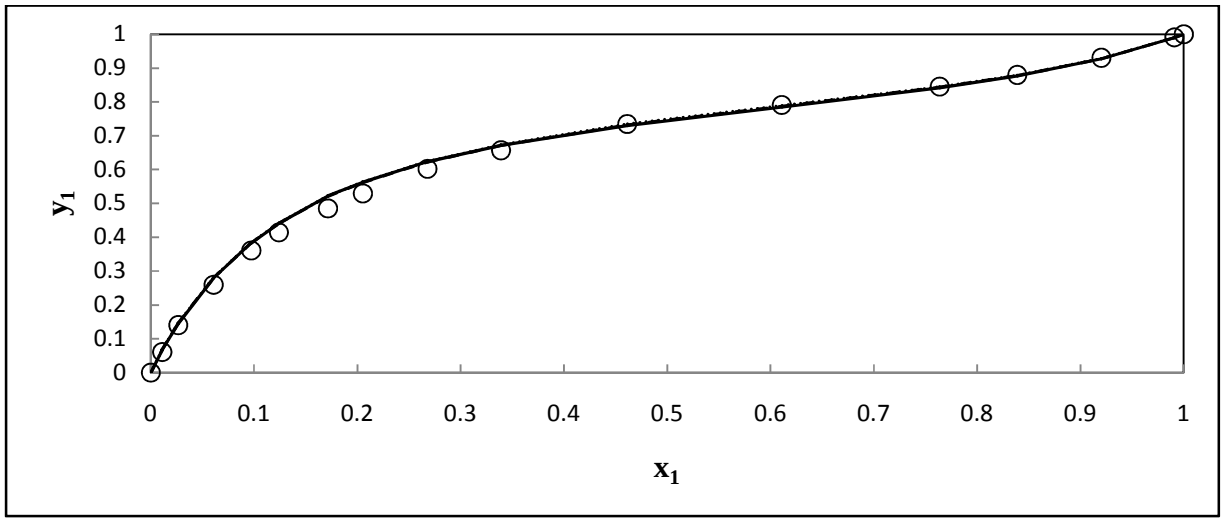

Figure 7-6: Experimental VLE and modeling results, comparison between HOC, NTH and PR model fits to x-y data for the diisopropyl ether (1) + propan-1-ol (2) system at 353.15 K:○ this work, — PR-NRTL, - - - HOC-NRTL, ····NTH-NRTL.

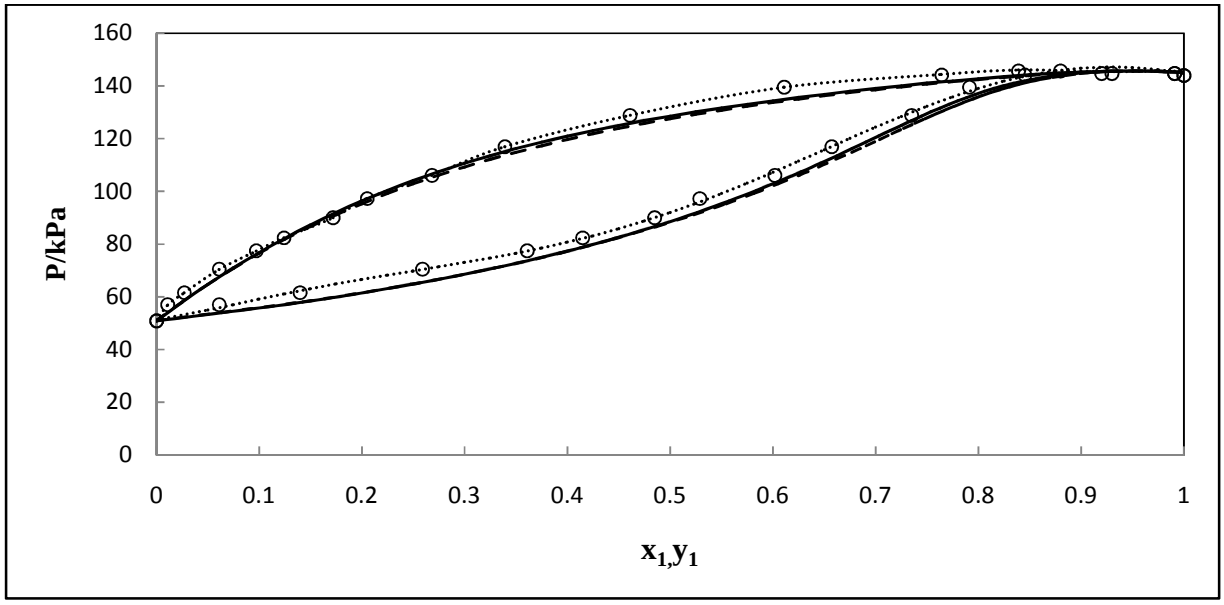

Figure 7-7: Experimental VLE and modeling results, comparison between Wilson, UNIQUAC and NRTL model fits to P-x-y data for the diisopropyl ether (1) + propan-1-ol (2) system at 353.15 K:○ this work, — PR-NRTL, - - - PR-Wilson, ····· PR-UNIQUAC.

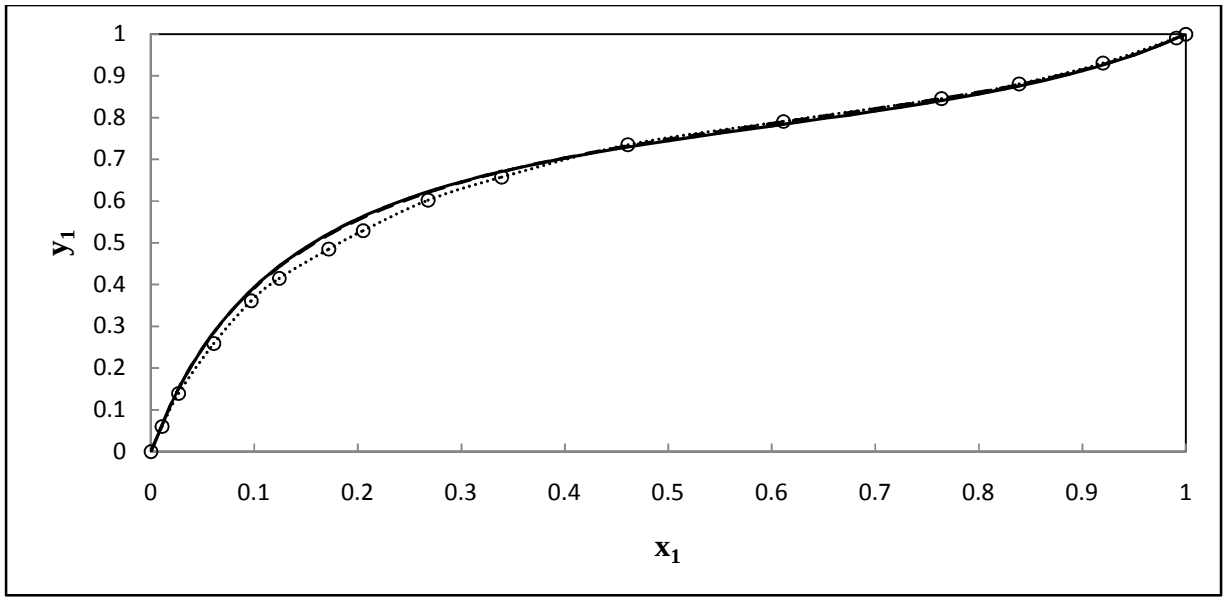

Figure 7-8: Experimental VLE and modeling results, comparison between Wilson, UNIQUAC and NRTL model fits to x-y data for the diisopropyl ether (1) + propan-1-ol (2) system at 353.15 K:○ this work, — PR-NRTL, - - - PR-Wilson, ····· PR-UNIQUAC.

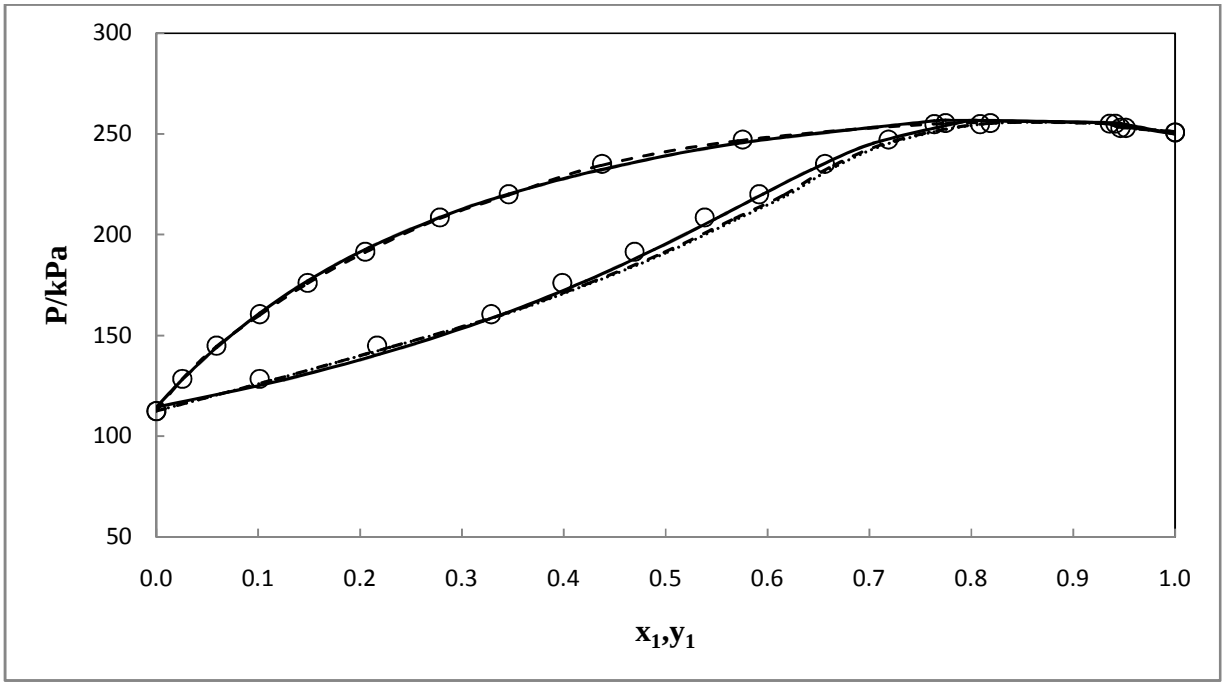

Figure 7-9: Experimental VLE and modeling results, comparison between PR, HOC and NTH model fits to P-x-y data for the diisopropyl ether (1) + propan-1-ol (2) system at 373.15 K:○ this work, — PR-NRTL, - - - HOC-NRTL, ····NTH-NRTL.

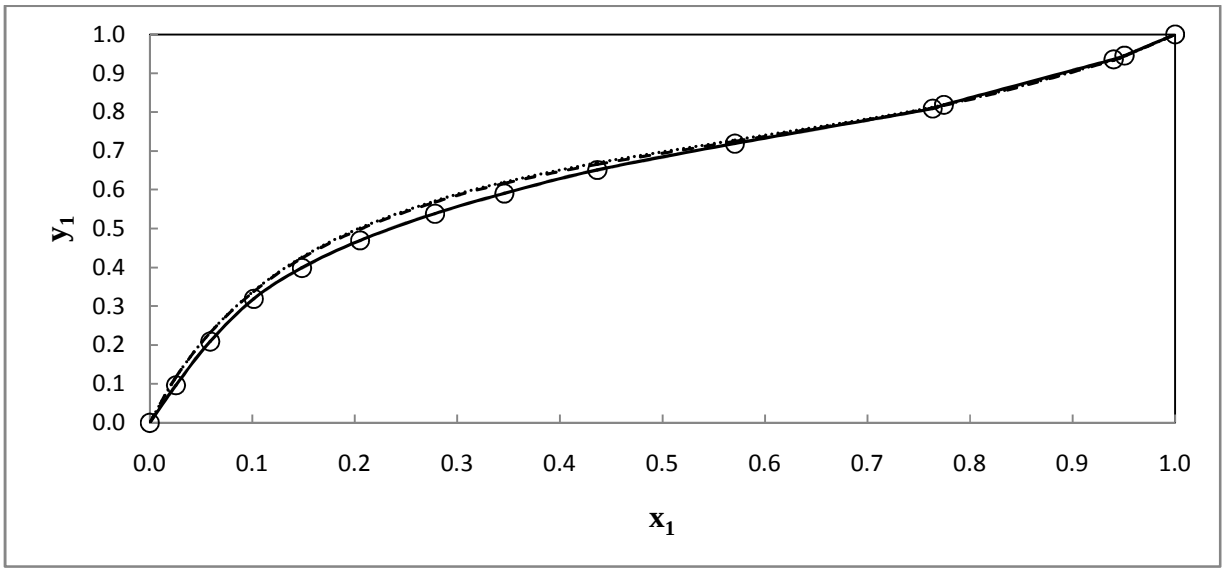

Figure 7-10: Experimental VLE and modeling results, comparison between PR, HOC and NTH model fits to x-y data for the diisopropyl ether (1) + propan-1-ol (2) system at 373.15 K:○ this work, — PR-NRTL, - - - HOC-NRTL, ····NTH-NRTL.

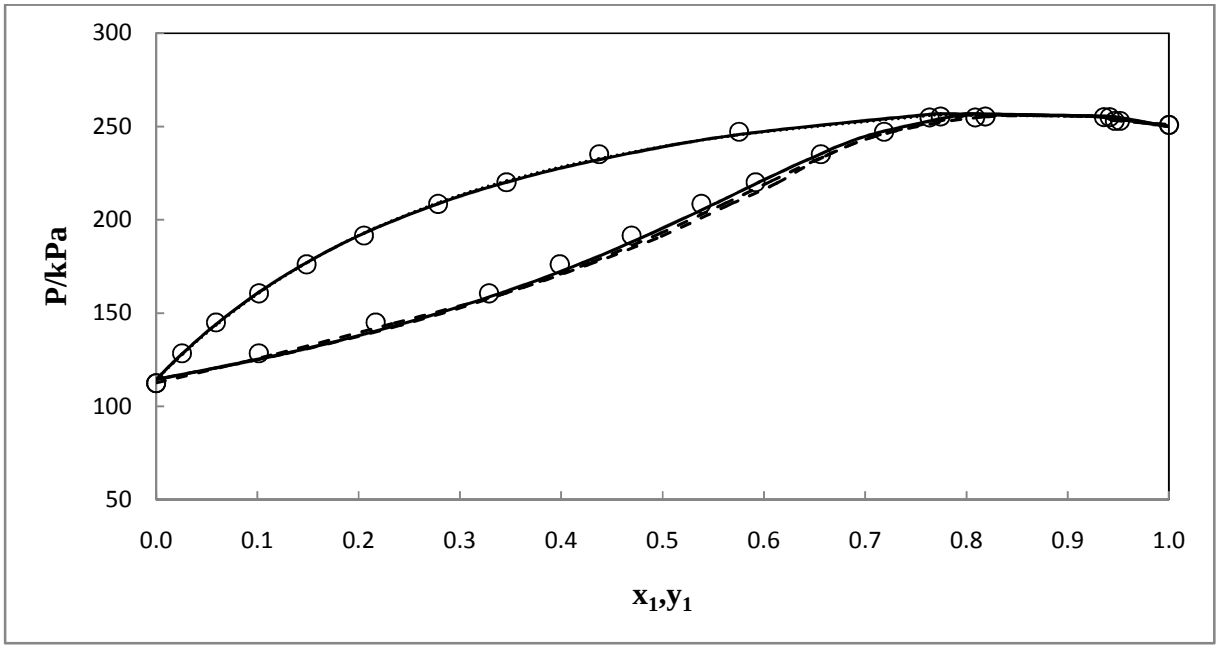

Figure 7-11: Experimental VLE and modeling results, comparison between NRTL, WILSON and UNIQUAC model fits to P-x-y data for the diisopropyl ether (1) + propan-1-ol (2) system at 373.15 K:○ this work, — PR-NRTL, - - - PR-Wilson, ····· PR-UNIQUAC.

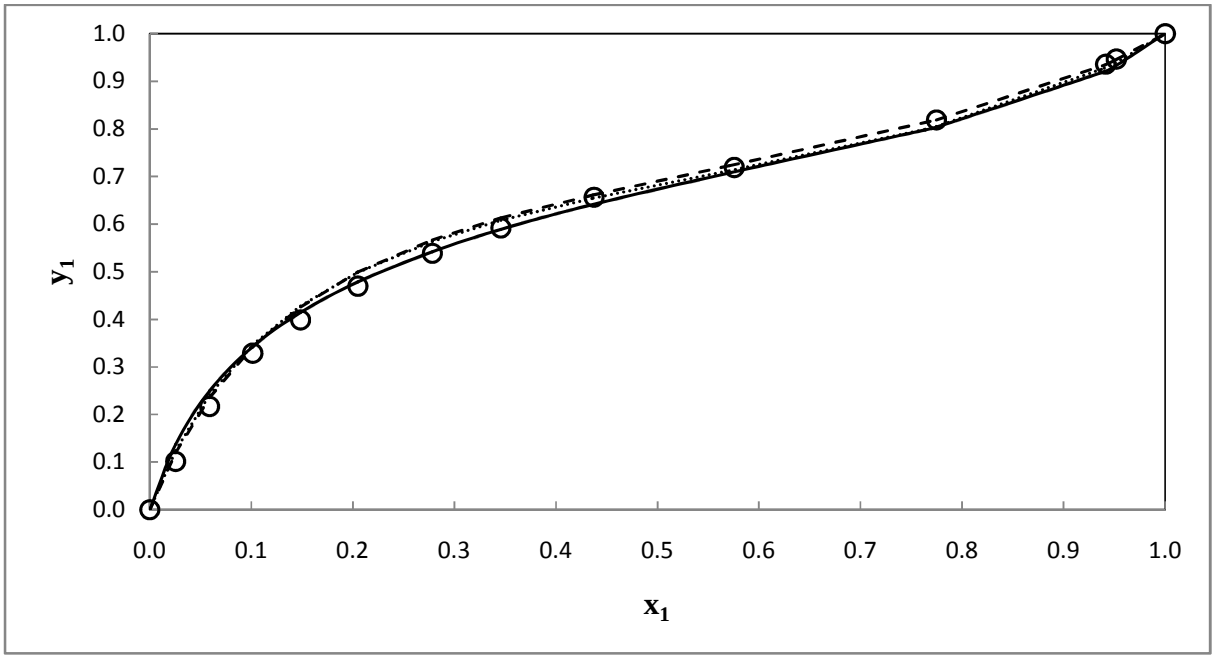

Figure 7-12: Experimental VLE and modeling results, comparison between NRTL, WILSON and UNIQUAC model fits to x-y data for the diisopropyl ether (1) + propan-1-ol (2) system at 373.15 K:○ this work, — PR-NRTL, - - - PR-Wilson, ····· PR-UNIQUAC.

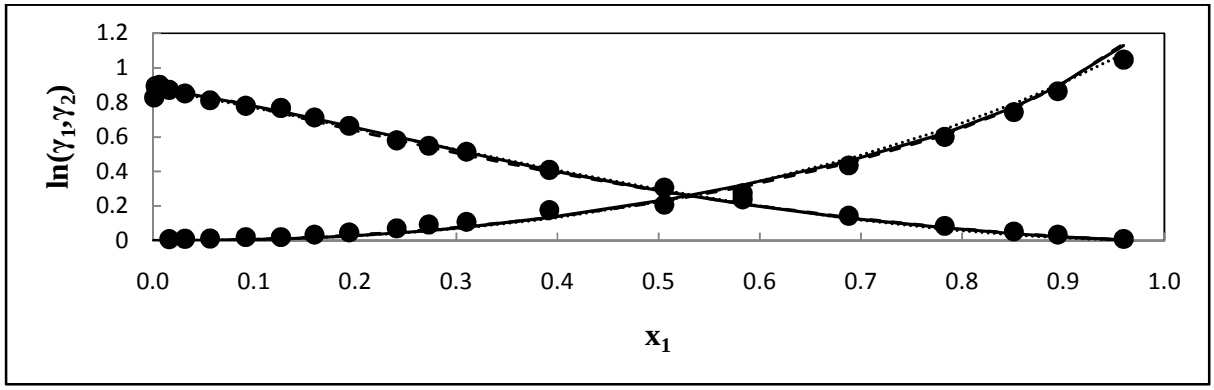

Figure 7-13: Comparison between the experimentally determined liquid-phase activity coefficients and those calculated from the NRTL, Wilson and UNIQUAC model with Peng-Robinson the diisopropyl ether (1) + propan-1-ol (2) system at 333.15 K:● this work, — PR-NRTL, - - - PR-Wilson, ·····PR-UNIQUAC.

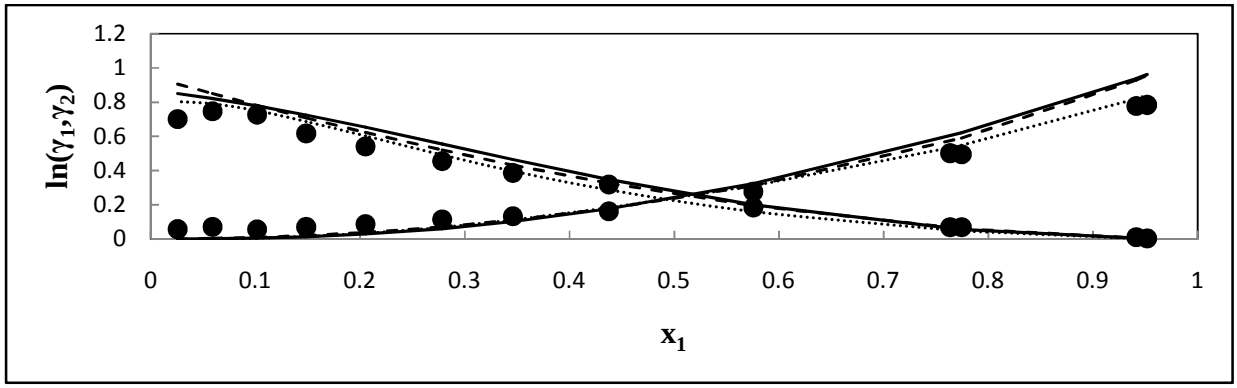

Figure 7-15: Comparison between the experimentally determined liquid-phase activity coefficients and those calculated from the NRTL, Wilson and UNIQUAC model with Peng-Robinson equation, for the diisopropyl ether (1) + propan-1-ol (2) system at 373.15 K:● this work, — PR-NRTL, - - - PR-Wilson, ·····PR-UNIQUAC.

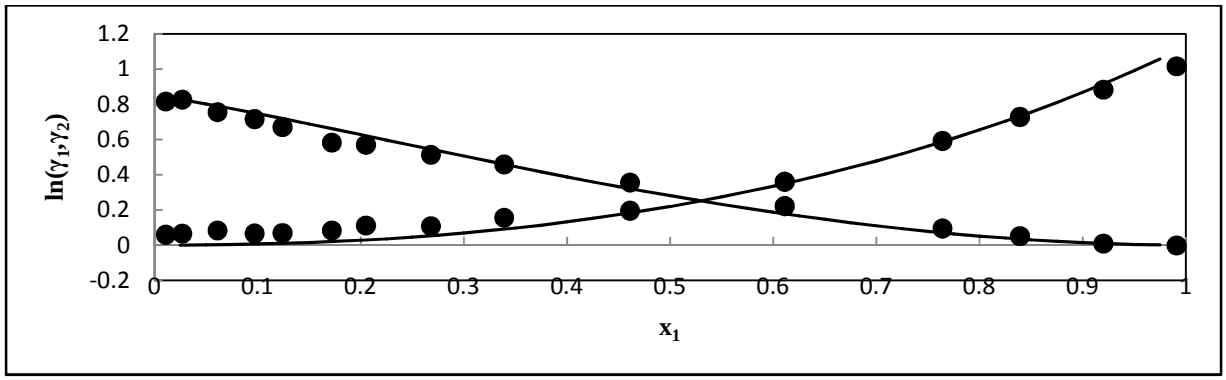

Figure 7-14: Comparison between the experimentally determined liquid-phase activity coefficients and those calculated from the NRTL, Wilson and UNIQUAC model with Peng-Robinson equation, for the diisopropyl ether (1) + propan-1-ol (2) system at 353.15 K:● this work, — PR-NRTL, - - - PR-Wilson, ·····PR-UNIQUAC.

7.2.2 Modeling Results for the water (1) + propan-1-ol (2) System

Table 7-4 provides the adjustable binary interaction parameters for the different models used in the modeling of water (1) + propan-1-ol (2) system. The average deviations of pressure (ΔP/kPa) and vapour molar compositions (Δy_1) are given in Table 7-4 also given are the average absolute deviation percent (AAD %) of the vapour mole fraction. The models fitted the data well, with the minimum and maximum AAD% of 1.51 and 2.58 respectively. The HOC-NRTL model gave the best fit for both data sets; while HOC-UNIQUAC gave the highest deviations of vapour phase mole fraction. The model fit results to the p-x-y data are graphically shown from Figures 7-16 to 7-23. A flat curve near the azeotrope is observed from model calculations suggesting a possibility of liquid-liquid phase split for this system. The possibility of phase split was experimental tested and a single phase was observed with liquid mixture (near azeotrope composition) at temperature as low as 298.15 K. Figures 7-24 and 7-25 show the graphical representation of activity coefficients for each data set with experimental activity coefficients given in the appendix D.

Table 7-4: Modeling result for the water (1) + propan-1-ol (2) system.

Model	T±0.02/K	kij	α_{12}	b_{12} J/kmol	b_{21} J/kmol	AAD (ΔP)	AAD (Δy_1)	AAD% (Δy_1)
PR-NRTL	358.15	-0.073	0.24	1670.47	303.47	0.03	0.008	1.78
	363.15	0.015	0.27	-515.00	1022.34	0.04	0.007	1.71
HOC-NRTL	358.15		0.48	948.70	175.90	0.03	0.007	1.66
	363.15		0.49	-9799.46	-5439.66	0.04	0.007	1.51
NTH-NRTL	358.15		0.47	948.69	173.73	0.03	0.007	1.66
	363.15		0.49	-9799.58	-5442.35	0.03	0.007	1.52
HOC-WILSON	358.15			-590.56	645.83	0.03	0.009	2.21
	363.15			-596.37	661.35	0.04	0.007	1.78
HOC-UNIQUAC	358.15			637.25	-689.83	0.06	0.012	2.65
	363.15			679.65	-721.15	0.10	0.011	2.16

b_{12} and b_{21}: Binary interaction parameters for the models in Aspen (equivalent to Δg_{12} and $\Delta g_{21,}$ for isothermal data set).
kij: Fitting parameter in the Wong and Sandler mixing rule.

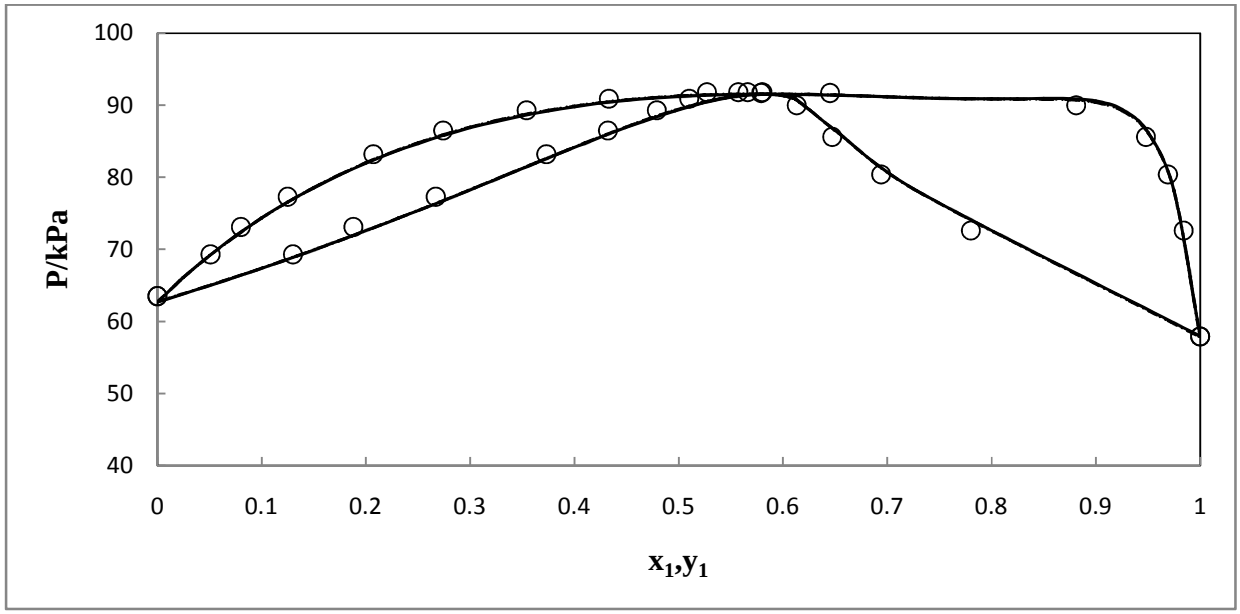

Figure 7-16: Experimental VLE and modeling results, comparison between PR, HOC and NTH model fits to P-x-y data for the water (1) + propan-1-ol (2) system at 358.15 K:○ this work, — PR-NRTL, - - - HOC-NRTL, ····NTH-NRTL.

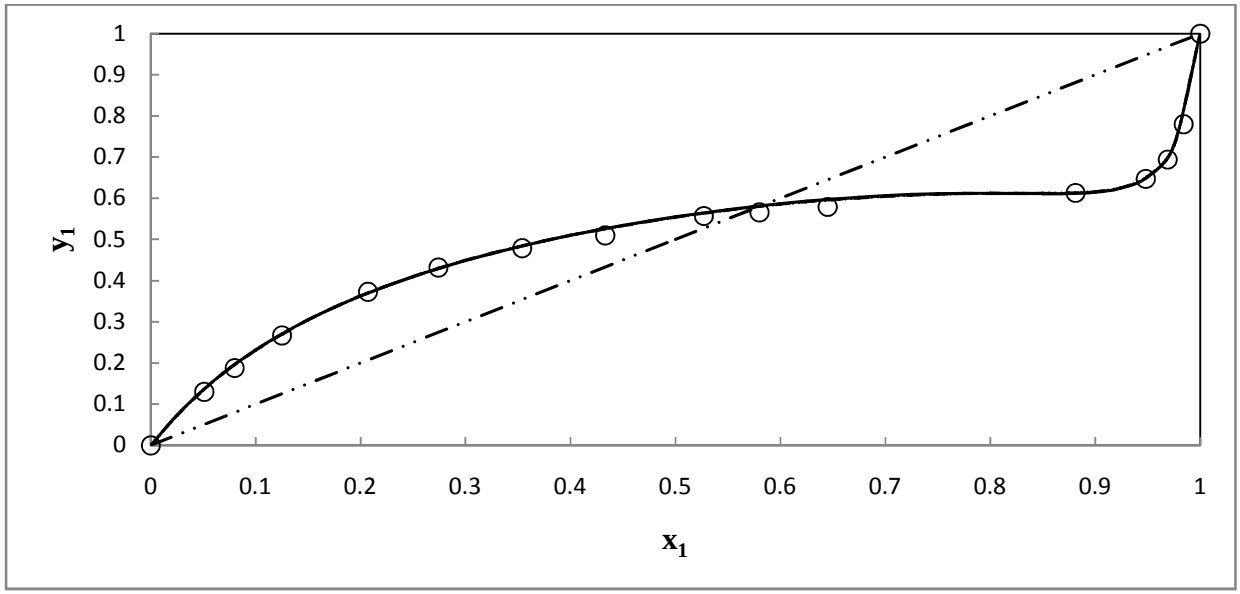

Figure 7-17: Experimental VLE and modeling results, comparison between PR, HOC and NTH model fits to x-y data for the water (1) + propan-1-ol (2) system at 358.15 K:○ this work, — PR-NRTL, - - - HOC-NRTL, ····NTH-NRTL.

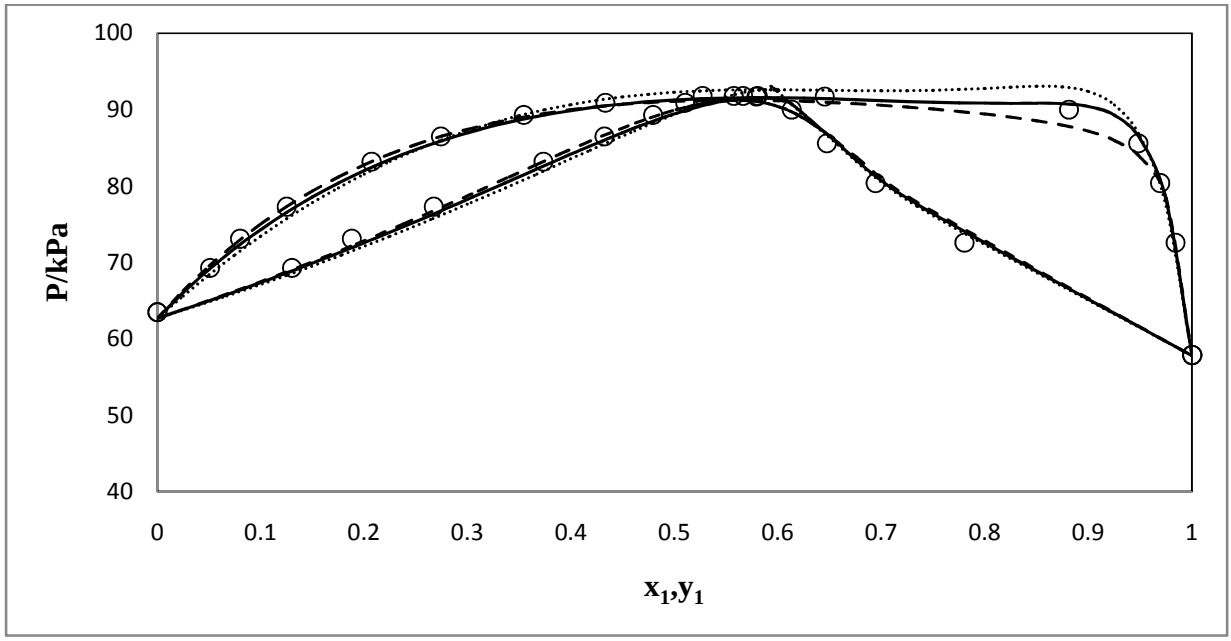

Figure 7-18:Experimental VLE and modeling results, comparison between NRTL, WILSON and UNIQUAC model fits to P-x-y data for the water (1) + propan-1-ol (2) system at 358.15 K:○ this work, — HOC-NRTL, - - - HOC-Wilson, ····· HOC-UNIQUAC.

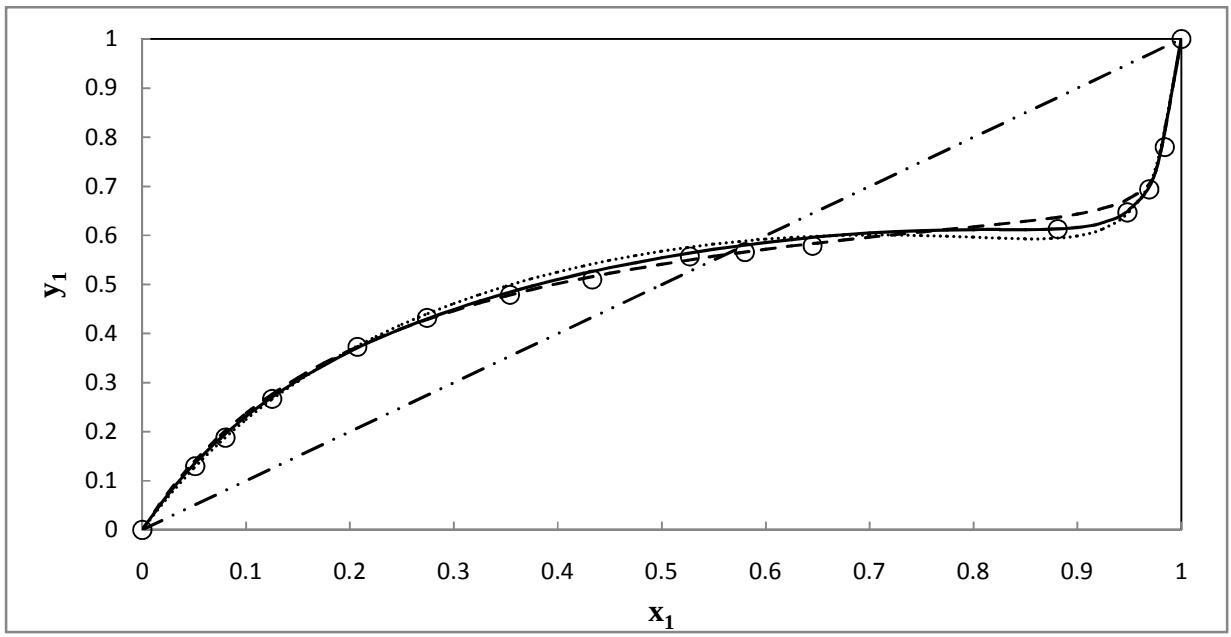

Figure 7-19:Experimental VLE and modeling results, comparison between NRTL, WILSON and UNIQUAC model fits to x-y data for the water (1) + propan-1-ol (2) system at 358.15 K:○ this work, — HOC-NRTL, - - - HOC-Wilson, ····· HOC-UNIQUAC.

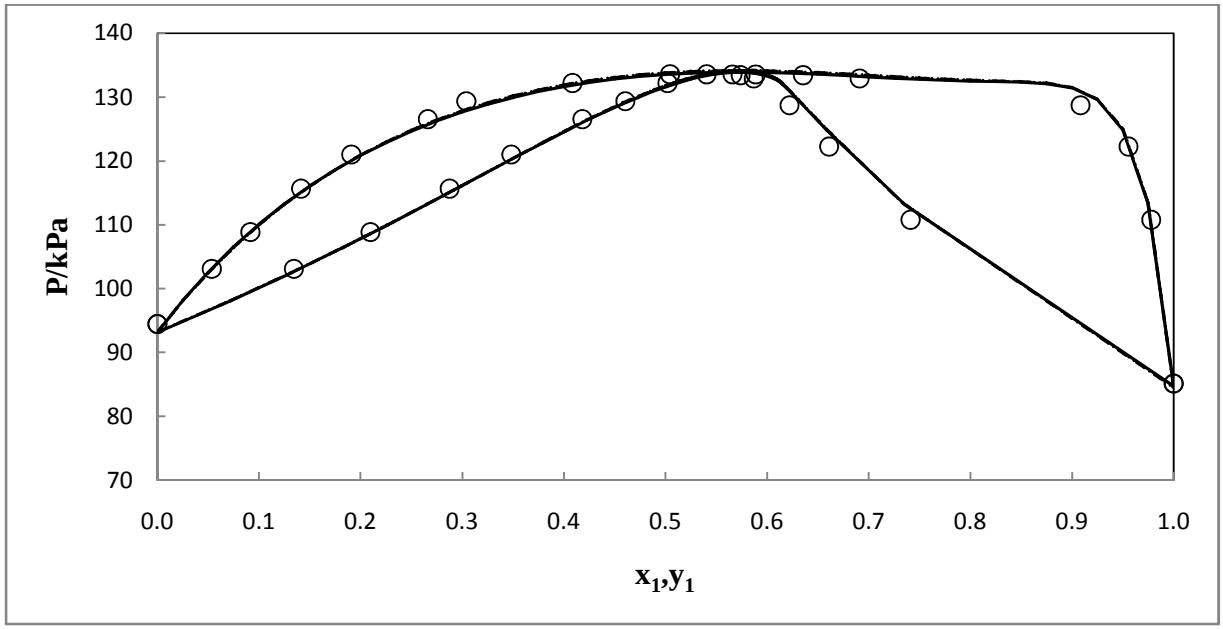

Figure 7-20: Experimental VLE and modeling results, comparison between PR, HOC and NTH model fits to P-x-y data for the water (1) + propan-1-ol (2) system at 368.15 K:○ this work, — PR-NRTL, - - - HOC-NRTL, ····NTH-NRTL.

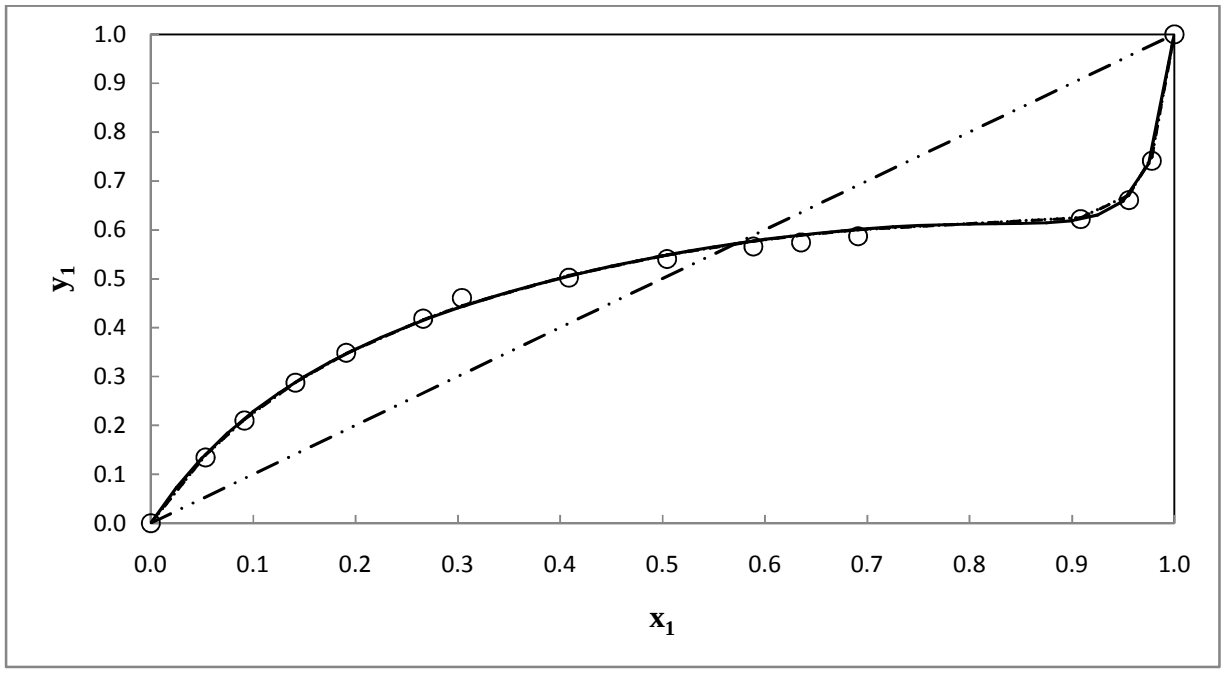

Figure 7-21: Experimental VLE and modeling results, comparison between PR, HOC and NTH model fits to x-y data for the water (1) + propan-1-ol (2) system at 368.15 K:○ this work, — PR-NRTL, - - - HOC-NRTL, ····NTH-NRTL.

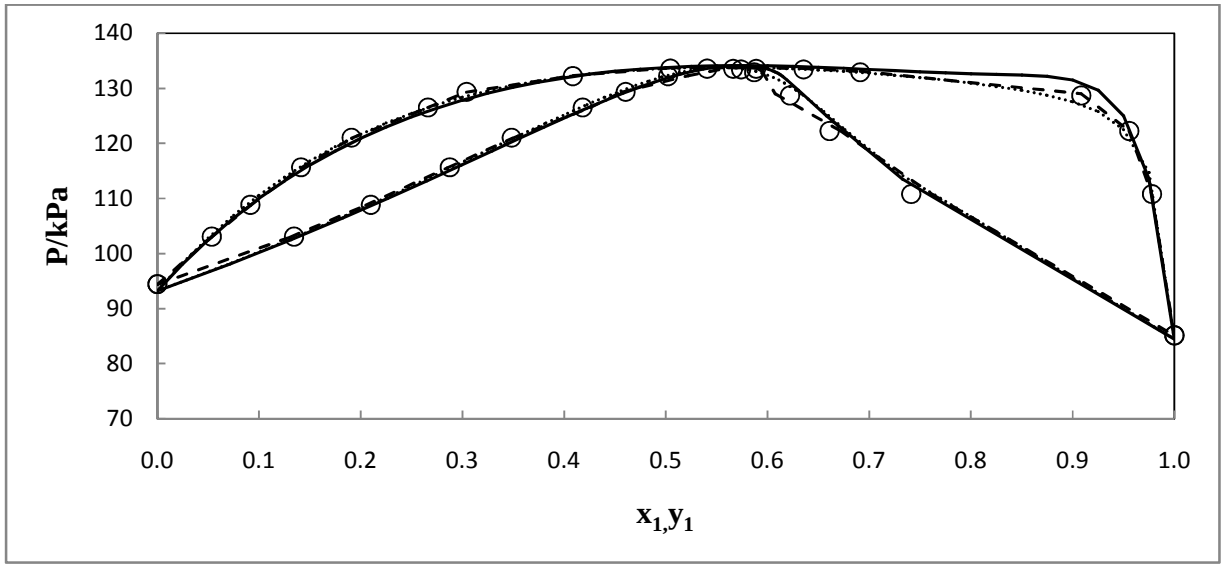

Figure 7-22: Experimental VLE and modeling results, comparison between NRTL, WILSON and UNIQUAC model fits to P-x-y data for the water (1) + propan-1-ol (2) system at 368.15 K:○ this work, — HOC-NRTL, - - - HOC-Wilson, ····· HOC-UNIQUAC.

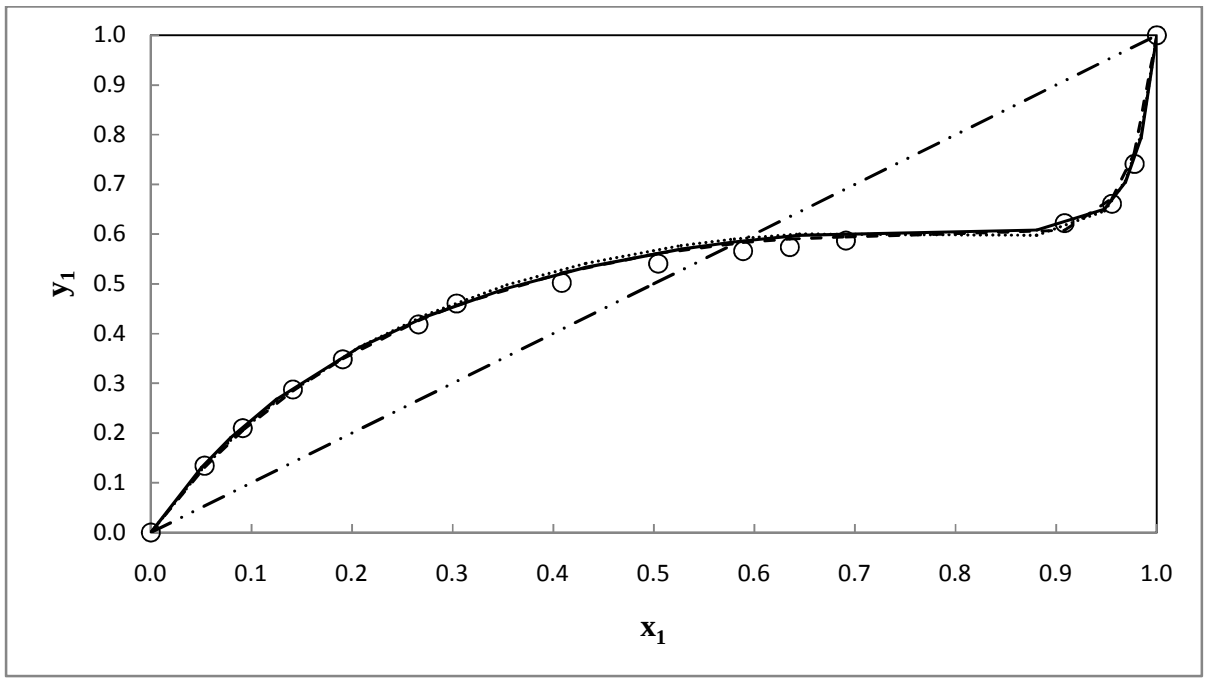

Figure 7-23: Experimental VLE and modeling results, comparison between NRTL, WILSON and UNIQUAC model fits to x-y data for the water (1) + propan-1-ol (2) system at 368.15 K:○ this work, — HOC-NRTL, - - - HOC-Wilson, ·····HOC-UNIQUAC.

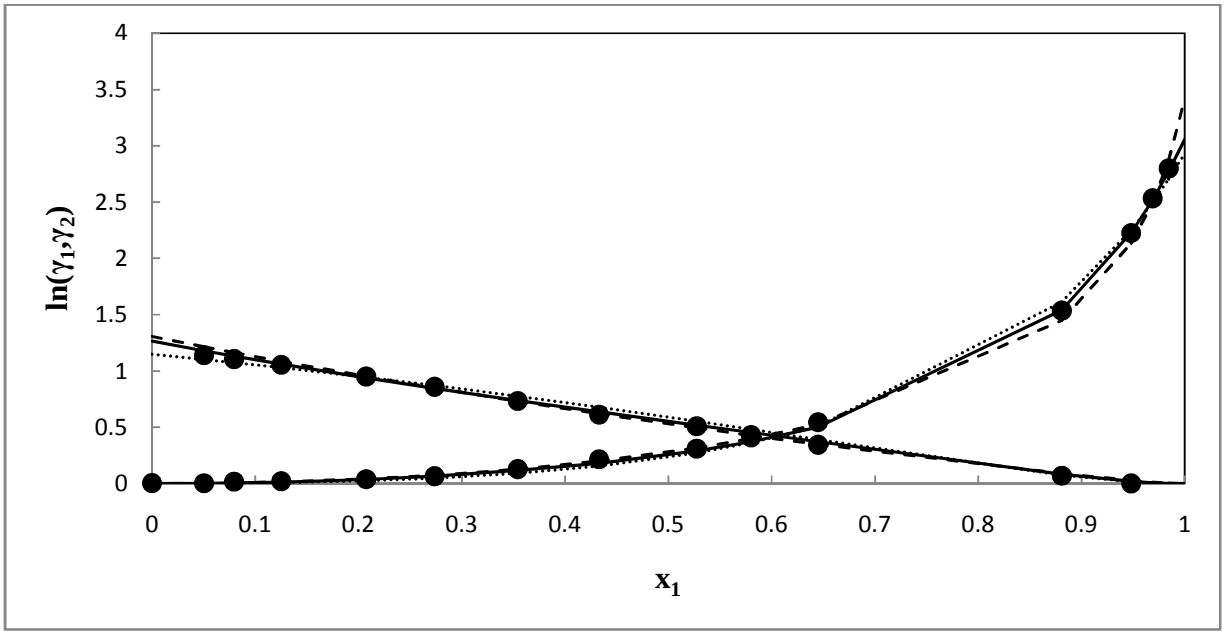

Figure 7-24: Comparison between the experimentally determined liquid-phase activity coefficients and those calculated from the NRTL, Wilson and UNIQUAC model with Hayden and O'Connell correlation, for the water (1) + propan-1-ol (2) system at 358.15 K:● this work, — HOC-NRTL, - - - HOC-Wilson, ·····HOC-UNIQUAC.

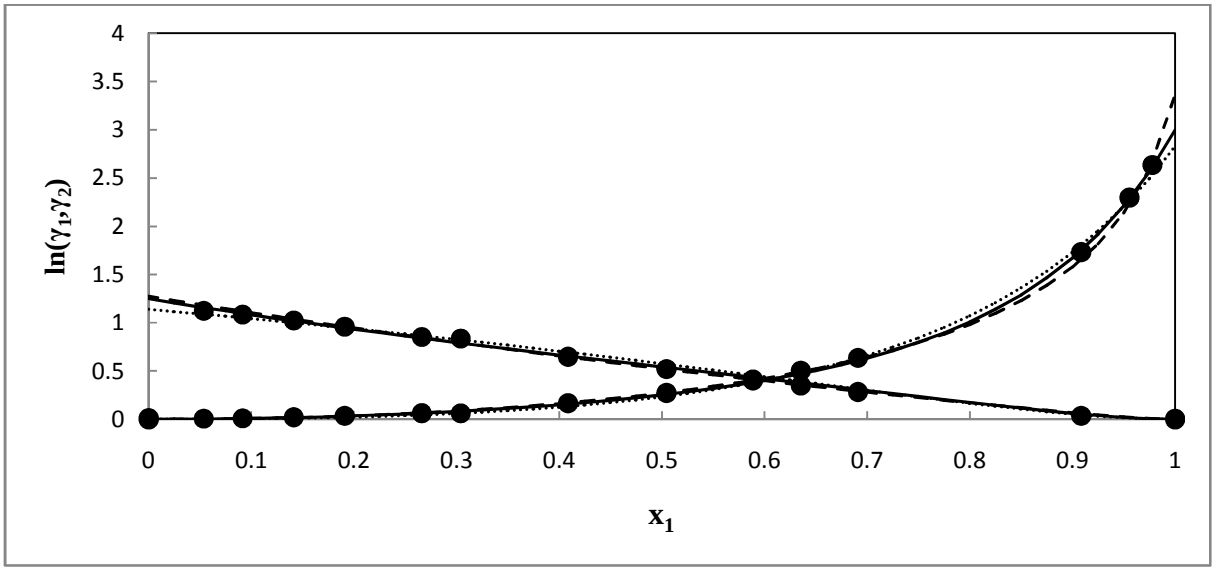

Figure 7-25: Comparison between the experimentally determined liquid-phase activity coefficients and those calculated from the NRTL, Wilson and UNIQUAC model with Hayden and O'Connell correlation, for the water (1) + propan-1-ol (2) system at 368.15 K:● this work, — HOC-NRTL, - - - HOC-Wilson, ·····HOC-UNIQUAC.

7.2.3 Modeling Results for The furan (1) + n-hexane (2) System

Table 7-5 gives the adjustable binary interaction parameters for the different models used in the modeling of furan (1) + n-hexane (2) system. The average deviations of the vapour molar compositions (Δy_1) are given in table 7-5; also given are the average absolute deviation percent (AAD %) of the vapour mole fraction.Figures 7-26 and 7-27 show the graphical representation of model to T-x-y data for this system. The activity coefficients for this data set are graphically shown on Figure 7-28 and the experimental activity coefficient values are given in the appendix D. All the models gave a good represented the data this system. The best fit was given by the PR-NRTL model with AAD of the vapour mole fraction 0.96%; while the UNIQUAC model gave slightly higher value of 1.11 %.

Table 7-5: Modeling results for the furan (1) + n-hexane (2) system at 101.3 kPa.

Model	b_{12}	b_{21}	a_{12}	a_{21}	kij	α12	AAD (Δy)	AAD%(Δy)
PR-NRTL	2848.23	-109.13	-8.22	0.83	0.163	0.49	0.005	0.96
PR-Wilson	1085.68	-3756.67	-3.72	10.76	0.098		0.005	0.99
PR-UNIQUAC	-1500.61	1545.83	4.76	-5.59	-0.015		0.005	1.11

b_{ij} and a_{ij} binary interaction parameters for the activity coefficient models in Aspen,($\Delta g_{ij} = b_{12} + a_{ij}T$).

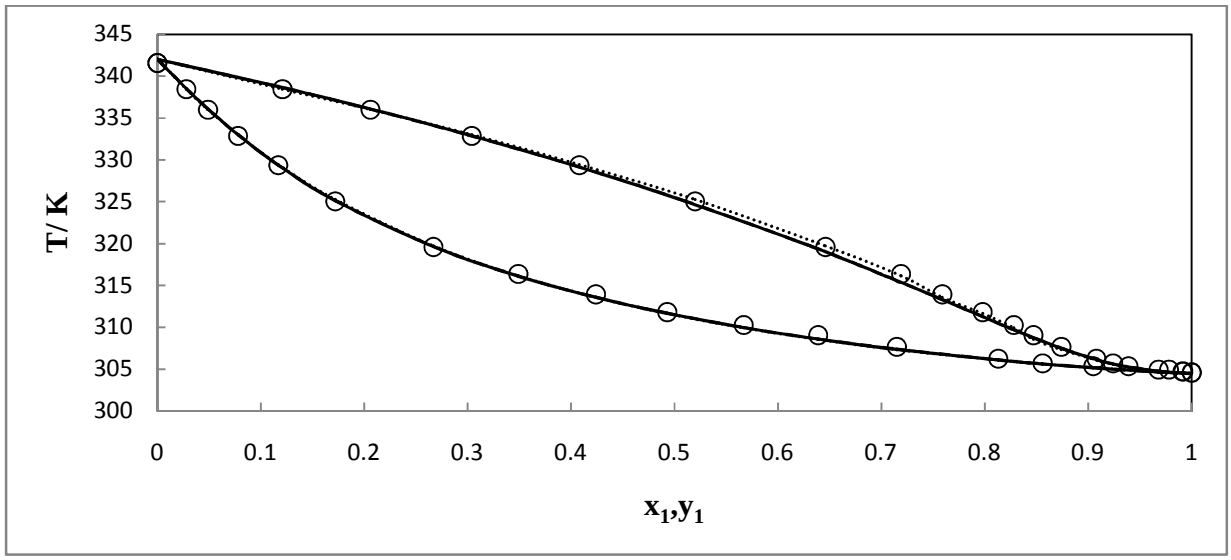

Figure7-26: Experimental VLE and modeling results, comparison between NRTL, WILSON and UNIQUAC model fits to T-x-y data for the furan (1) + n-hexane (2) system at 101.3 kPa: ○ this work, — PR-NRTL, - - - PR-Wilson, ····PR-UNIQUAC.

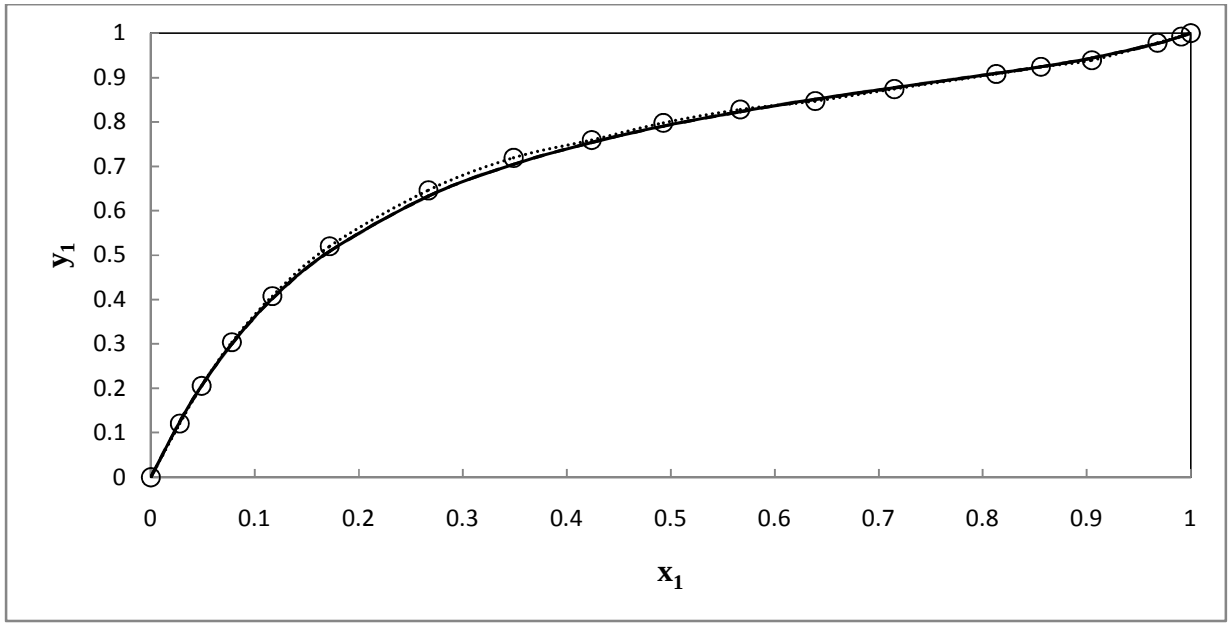

Figure 7-27: Experimental VLE and modeling results, comparison between NRTL, WILSON and UNIQUAC model fits to x-y data for the furan (1) + n-hexane (2) system at 101.3 kPa: ○ this work, — PR-NRTL, - - - PR-Wilson, ·····PR-UNIQUAC.

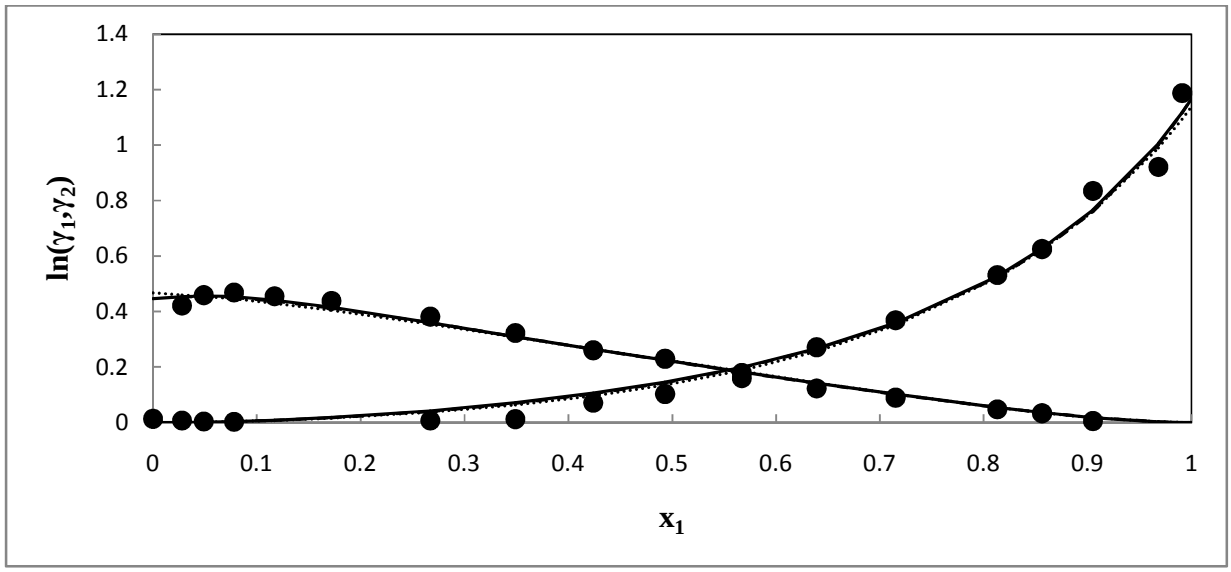

Figure 7-28: Comparison between the experimentally determined liquid-phase activity coefficients and those calculated from the NRTL, Wilson and UNIQUAC model with Peng-Robinson the furan (1) + n-hexane (2) system at 101.3 kPa: ● this work, — PR-NRTL, - - - PR-Wilson, ·····PR-UNIQUAC.

7.2.4 Modeling Results for The furan (1) + methylbenzene (2) System

Table 7-6 gives the adjustable binary interaction parameters for the different models used in the modeling of furan (1) + methylbenzene (2) system. The average deviations of the vapour molar compositions (Δy_1) are given in table 7-6; also given are the average absolute deviation percent (AAD %) of the vapour mole fraction.Figures 7-29 and 7-30 show the graphical representation of model to T-x-y data for this system. The activity coefficients for this data set are graphically shown on figure 7-29 and the experimental activity coefficient values are given in the appendix D. The models gave poor fits for this system, with vapour mole fraction AAD values greater than 5 % for all the models. The largest deviation was observed in furan rich region.

Table 7-6: Modeling results for: the furan (1) + methylbenzene (2) system at 101.3 kPa.

Model	b_{12}	b_{21}	a_{12}	a_{21}	kij	α12	AAD (Δy)	AAD% (Δy)
PR-NRTL	745.28	256.88	5.24	0.66	-1.01	0.488	0.0215	6.99
PR-Wilson	-352.50	-1544.82	1.58	-2.73	0.035		0.0206	5.36
PR-UNIQUAC	-904.65	18.26	-1.56	1.31	0.40		0.0232	5.85

b_{ij} and a_{ij} binary interaction parameters for the activity coefficient models in Aspen,($\Delta g_{ij} = b_{12} + a_{ij}T$).

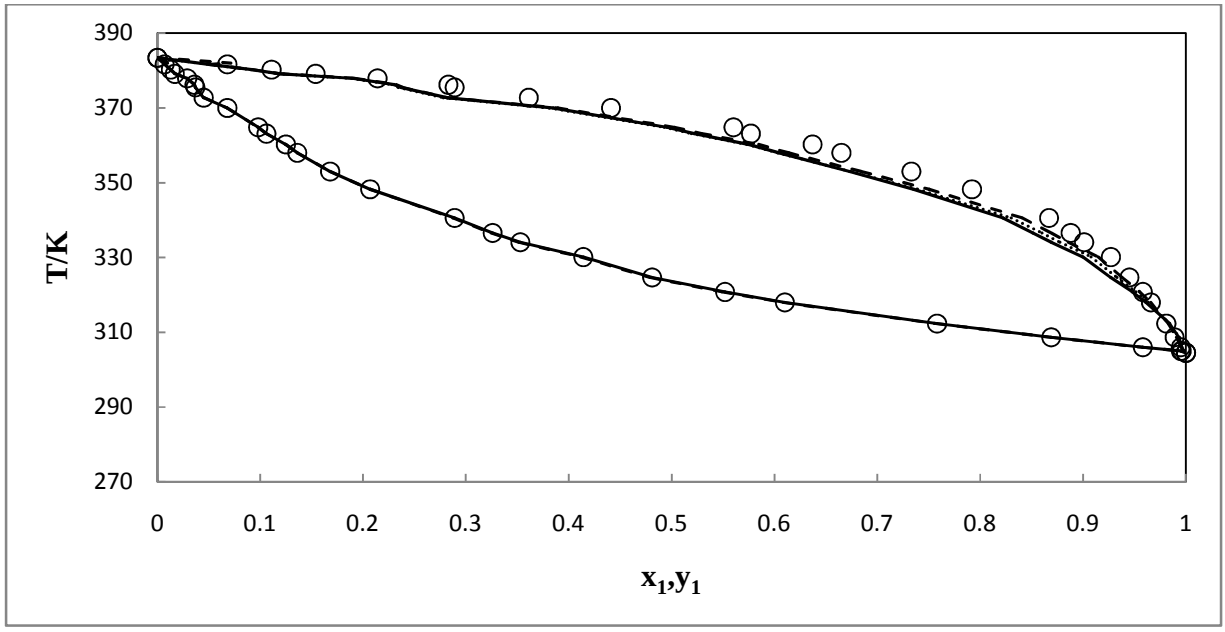

Figure 7-29: Comparison between NRTL and UNIQUAC model fits to T-x-y data for the furan (1) + methylbenzene (2) system at 101.3 kPa. ○ this work, — PR-NRTL, - - - PR-Wilson, ····· PR-UNIQUAC.

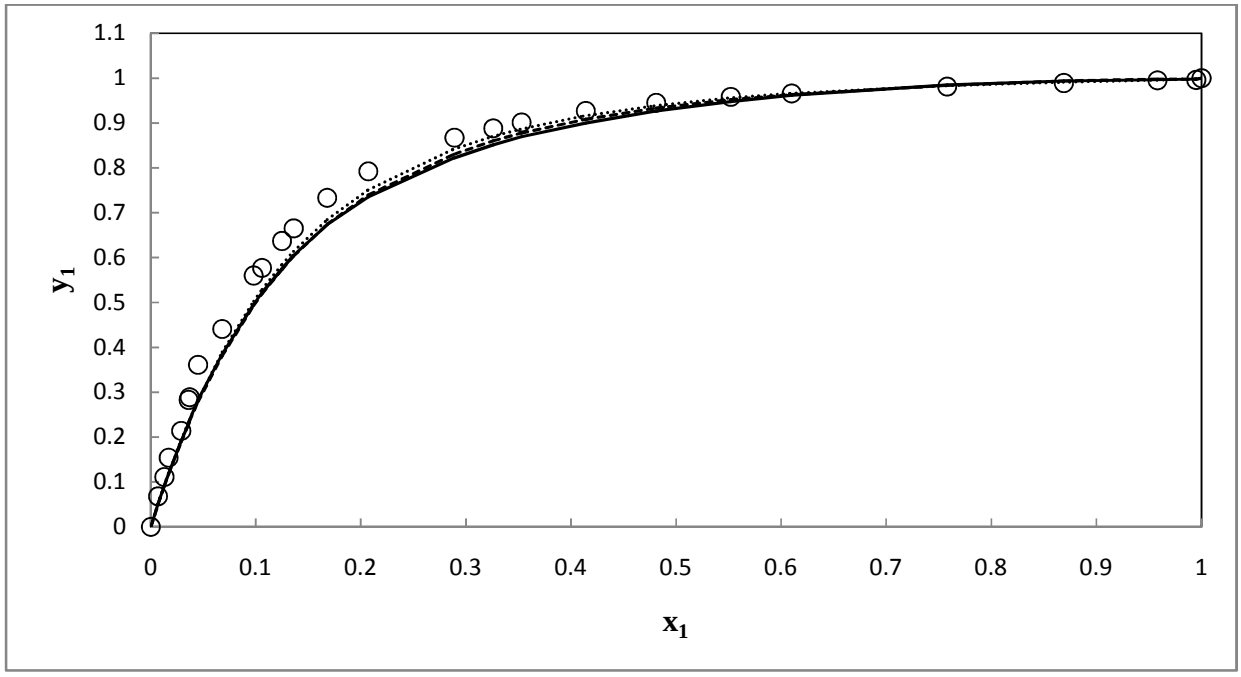

Figure 7-30: Comparison between NRTL and UNIQUAC model fits to x-y data for the furan (1) + methylbenzene (2) system at 101.3 kPa: ○ this work, — PR-NRTL, - - - PR-Wilson, ····· PR-UNIQUAC.

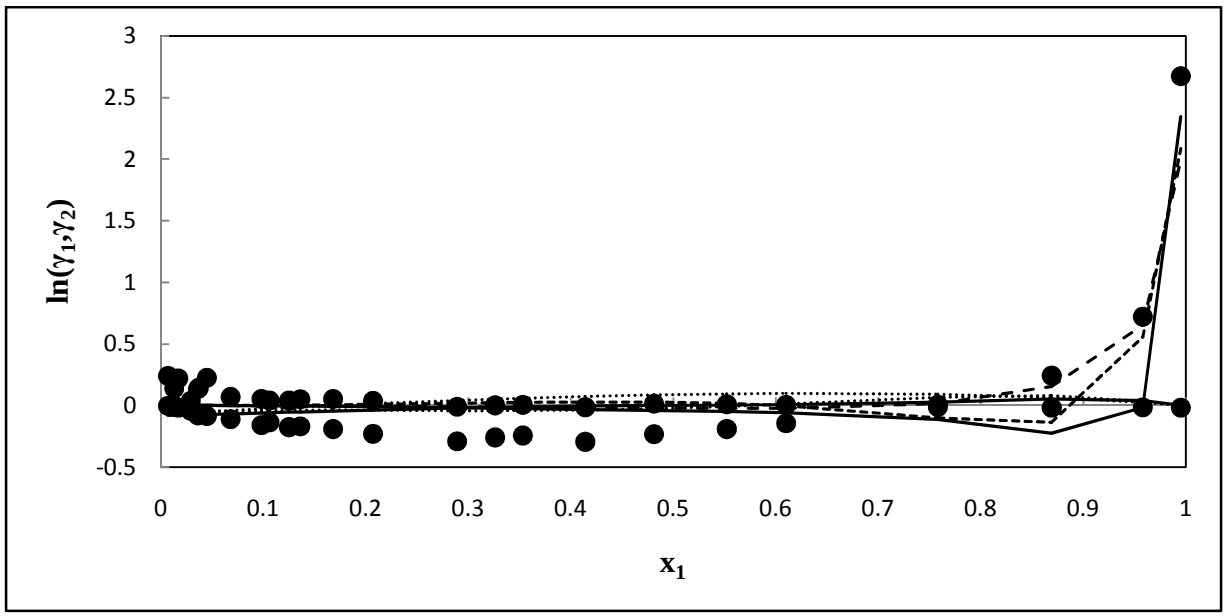

Figure 7-31: Comparison between the experimentally determined liquid-phase activity coefficients and those calculated from the NRTL, Wilson and UNIQUAC model with Peng-Robinson the furan (1) + methylbenzene (2) system at 101.3 kPa: ○ this work, — PR-NRTL, - - - PR-Wilson, ····· PR-UNIQUAC.

7.3 Thermodynamic Consistency Testing

7.3.1 Consistency Test for The diisopropyl ether (1) + propan-1-ol (2) System

The models provided satisfactory data fit for the diisopropyl ether (1) + propan-1-ol (2) system. The ΔP and Δ*y* values for this system are given in appendix D. Table 7-7 presents a summary of the point test analysis for the two data sets. The average vapour phase deviations were found to be less than the point test margin of 0.01 for the 333.15 K data set for all the models used. Both 353.15 K and 373.15 K data sets struggled to pass the point test margin with only half of data points passing the point test. The direct test (Van Ness, 1995) was used for the second data consistency testing. The root mean square deviations using PR-NRTL were found to be 0.0345, 0.0789 and 0.1318 for 333.15 K, 353.15 K and 373.15 K data sets respectively. The 333.15 K, 353.15 K and 373.15 K data sets respectively fall on index 2 (high quality data), 4 and 6 (medium quality data) on Table 2-3. In conclusion the models fitted the water (1) + propan-1ol (2) system well with the data sets passing both consistency tests.

Table 7-7: Results of the thermodynamic consistency testing for the diisopropyl ether (1) + 1-propanol (2) systems at 333.15, 353.15 and 373.15 K.

	PR-NRTL	PR-UNIQUAC	PR-Wilson	HOC-NRTL	NTH-NRTL
			333.15 ±0.02/K		
No points	20	20	20	20	20
No consistence	20	19	18	19	19
ΔPavg((kPa))	0.03	0.03	0.03	0.03	0.03
Δy1avg	0.004	0.005	0.005	0.005	0.004
			353.15±0.02/K		
No points	15	15	15	15	15
No consistence	8	8	7	8	8
ΔPavg((kPa))	0.13	0.13	0.13	0.12	0.16
Δy_1avg	0.013	0.013	0.012	0.013	0.013
			373.15 ±0.02/K		
No points	12	12	12	12	12
No consistence	4	5	5	4	4
ΔPavg((kPa))	0.28	0.33	0.35	0.34	0.33
Δy_1avg	0.016	0.018	0.016	0.017	0.018

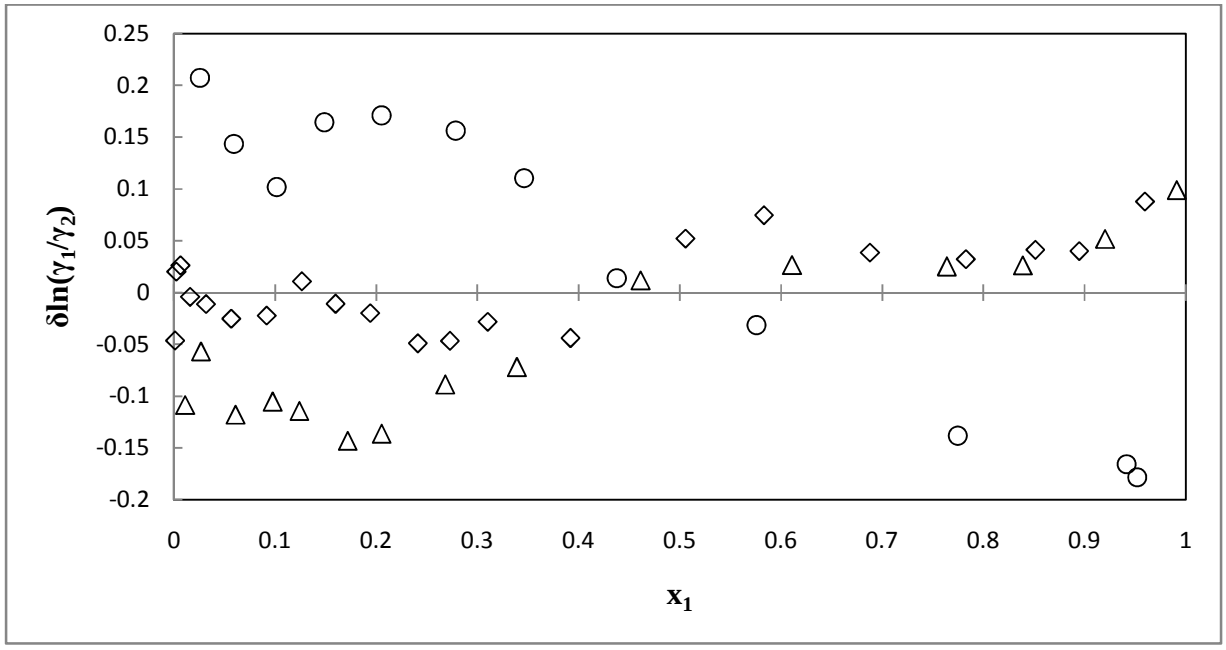

Figure 7-32: Deviation of the PR-NRTL model activity coefficients from the experimental values for the diisopropyl ether (1) + propan-1-ol (2) system. ◊ 333.15, Δ 353.15 , ○ 373.15 K

7.3.2 Consistency Test for The water (1) + propan-1-ol (2) System

The models provided satisfactory data fit for the water (1) + propan-1-ol (2) system. The ΔP and Δ*y* values for this system are given in appendix D. Table 7-8 presents a summary of the point test analysis for the two data sets. The average vapour phase deviations were found to be less than the point test margin of 0.01 for all the models except the HOC-UNIQUAC with a value of 0.012 for the 358.15 K data set. The direct test (Van Ness, 1995) was also used for data consistency testing for this system. The root mean square deviations using HOC-NRTL were found to be 0.0209 and 0.0255 for 358.15 K and 368.15 K data sets respectively. The 358.15 K and 368.15 K data sets respectively fall on index 1 and 2 (high quality data) on Table 2-3. In conclusion the models fitted the water (1) + 1-propanol (2) system well with the data sets passing both consistency tests.

Table 7-8: Results of the thermodynamic consistency point testing for the water (1) + propan-1-ol (2) systems at 358.15, 368.15 K.

	HOC-NRTL	HOC-UNIQUAC	HOC-Wilson	PR-NRTL	NTH-NRTL
			358.15 ±0.02/K		
Number of points	14	14	14	14	14
Number consistence	11	5	11	11	11
ΔTavg(K)	0.03	0.05	0.03	0.03	0.03
Δy_1avg	0.007	0.012	0.009	0.008	0.007
			368.15±0.02/K		
Number of points	14	14	14	14	14
Number consistence	10	6	11	10	10
ΔTavg(K)	0.03	0.11	0.04	0.04	0.03
Δy_1avg	0.007	0.011	0.007	0.007	0.007

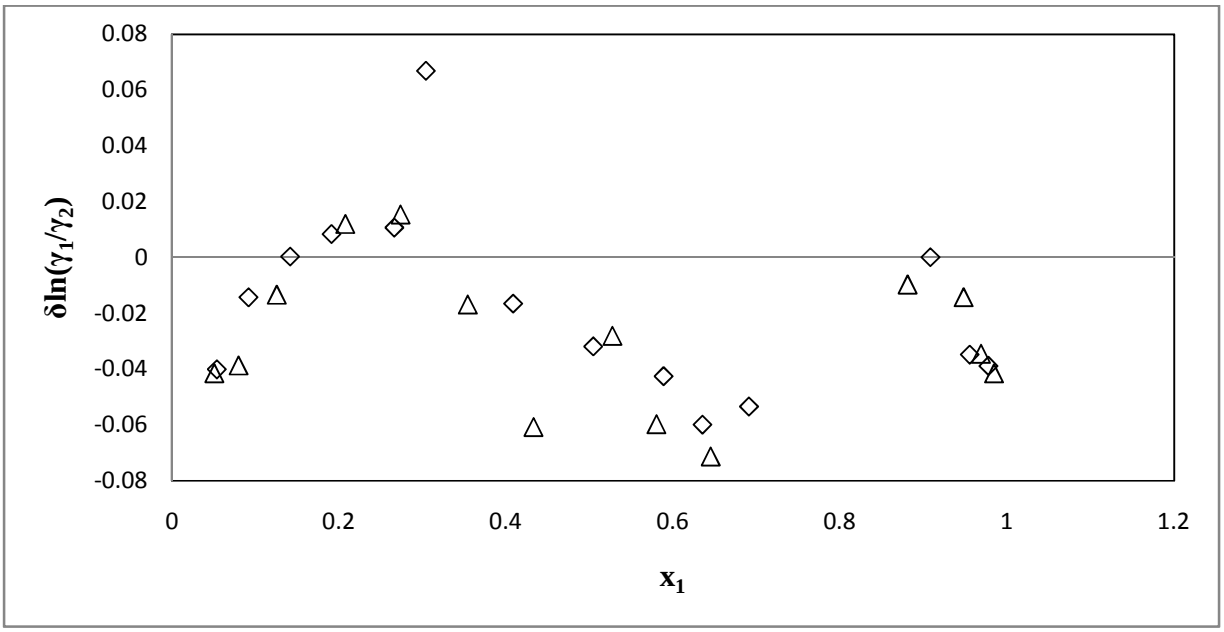

Figure 7-33: Deviation of the HOC-NRTL model activity coefficients from the experimental values for the water (1) + propan-1-ol (2) system. ◊ 358.15, Δ 368.15 K.

7.3.3 Consistency Test for The furan (1) + n-hexane (2) System

The models were observed to give good fit of the furan (1) + n-hexane (2) data set. The ΔT and Δ*y* values for this system are given in appendix D. Table 7-9 present a summary of the point test analysis for this system. The average vapour phase deviations were found to be far less than the point test margin of 0.01 for all the models. The direct test (Van Ness, 1995) was also used for data consistency testing for this system. The root mean square deviation of $\delta \ln (\gamma_1 \gamma_2)$ using PR-NRTL was found to be 0.0391 falling on index 2 (high quality data) on Table 2-3. In conclusion, the furan (1) + n-hexane data set was found to pass both point and direct tests for thermodynamic consistency.

Table 7-9: Furan (1) + n-hexane (2) system at 101.3 kPa.

	PR-NRTL	PR-Wilson	PR-UNIQUAC
Number of points	16	16	16
Number consistence	13	13	13
ΔTavg(K)	0.04	0.04	0.01
Δy_1avg	0.005	0.005	0.005

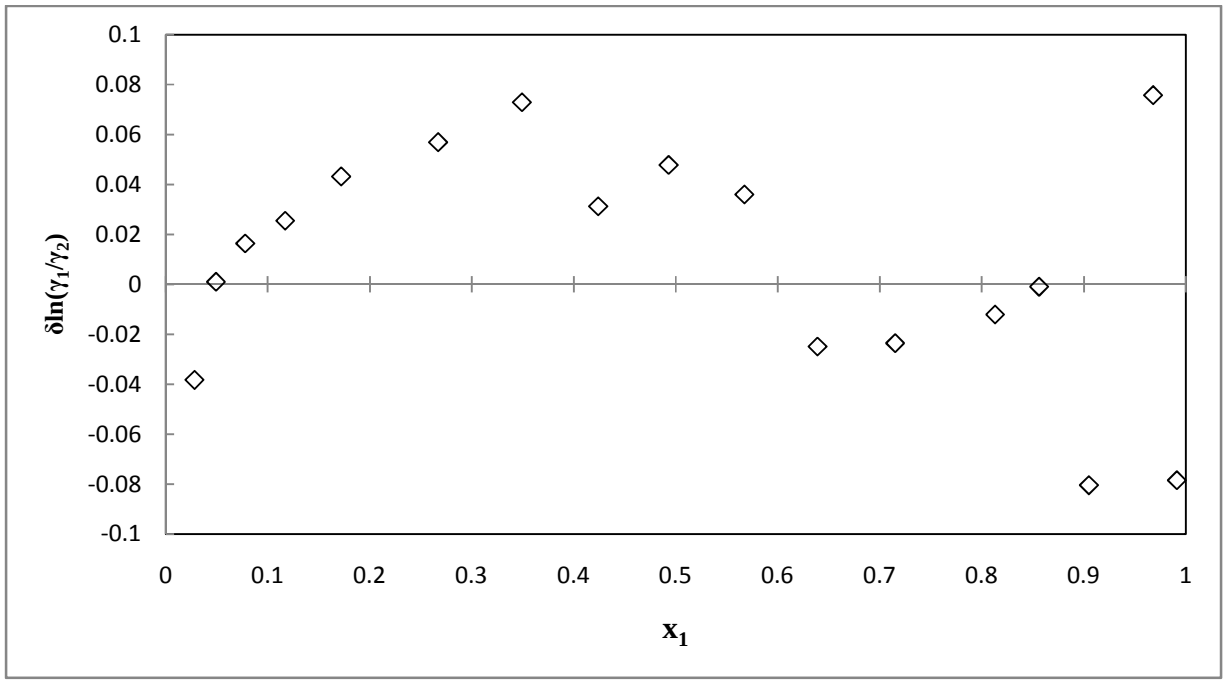

Figure 7-34: Deviation of the PR-NRTL model activity coefficients from the experimental values for the furan (1) + n-hexane (2) system at 101.3 kPa.

7.3.4 Consistency Test for The furan (1) + methylbenzene (2) System

The furan (1) + methylbenzene (2) system was poorly fitted by the models. The ΔT and Δ*y* values for this system are given in appendix D. Table 7-10 presents a summary of the point test analysis for this system. The average vapour phase deviation as high as 0.023 for the PR-UNIQUAC model which is significantly higher than the 0.01 value required for data to be dubbed thermodynamic consistent with the chosen models. The numbers of points consistent with the models are also given in the table. The direct test of Van Ness (1995) for consistency was undertaken to get a different view on the consistency and from table 7-10 it is shown that the root mean square deviation for this system is 0.177 which falls under index 8 of Table 2-3 (index 1: high quality data and index 10: poor quality data. Conclusively the new measured VLE data for furan (1) + methylbenzene (2) system at 101.3 kPa was found to be the least consistence among all the measured data in this work and may in future be measured using different technique and equipment to build more confidence on the data.

Table 7-10: Furan (1) + methylbenzene (2) system at 101.3 kPa.

	PR-NRTL	PR-Wilson	PR-UNIQUAC
Number of points	22	22	22
Number consistence	6	8	7
ΔTavg(K)	0.61	1.29	0.96
Δy_1avg	0.022	0.021	0.023

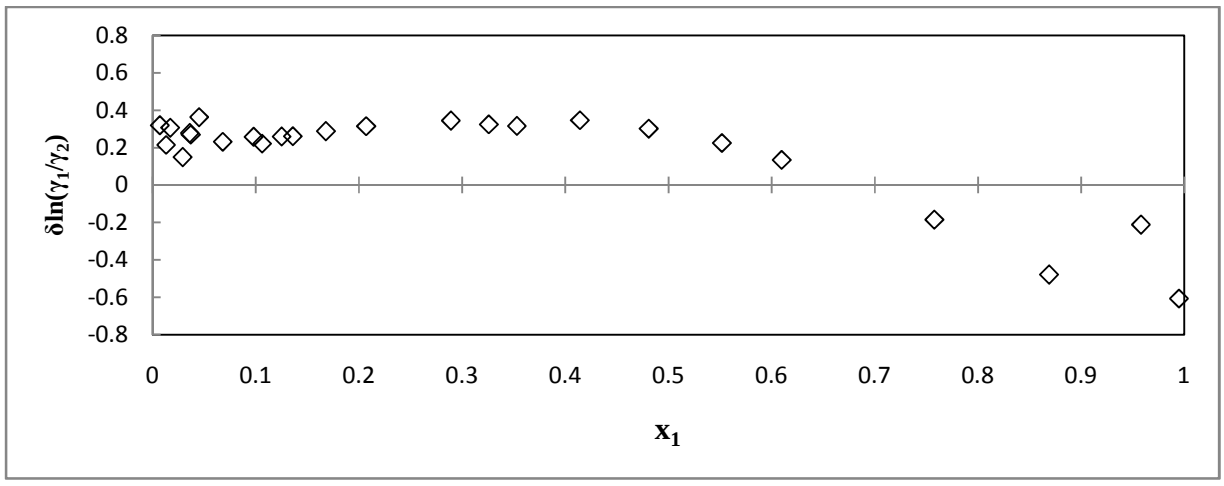

Figure 7-35: Deviation of the PR-NRTL model activity coefficients from the experimental values for the furan (1) + methylbenzene (2) system at 101.3 kPa.

7.3.5 Root Mean Square Deviation (direct test)

Table 7-11: Root Mean Square deviation between model and experimental activity coefficient – Van Ness (1995) direct test.

Binary system	**Model**	**Data set**		
diisopropyl ether (1) + propan-1-ol (2)	**PR-NRTL**	**333.15 K**	**353.15 K**	**373.15 K**
RMS value		0.03481	0.0789	0.1318
water (1) + propan-1ol (2)	**HOC-NRTL**	**358.15 K**	**368.15 K**	
RMS value		0.0209	0.0255	
Furan(1) + n-hexane (2)	**PR-NRTL**	**101.3 kPa**		
RMS value		0.0391		
Furan(1) + methylbenzene (2)	**PR-NRTL**	**101.3 kpa**		
RMS value		0.1770		

7.4 Relative Volatility

Relative volatility is an important factor in separation of chemical mixtures by distillation. It measures the degree to which the pair of chemical species can be separated in a conventional distillation column. A big difference in volatility of chemical species indicates the easier the two compounds can be distilled; while species with similar volatility (i.e. the relative volatility approaches a unity) will require enormous amount of energy and infinite number of equilibrium stages in a conventional distillation system. A mathematical expression for relative volatility in binary VLE system with *i* and *j* species is given as:

$$\alpha_{ij} = \frac{\frac{y_i}{x_i}}{\frac{y_j}{x_j}} = \frac{K_i}{K_j} \tag{7.6}$$

Where, α is the relative volatility, *x* and *y* are the respective liquid and vapour compositions, and the subscript *i* and *j* refers to component *i* and component *j*. K is the vapour-liquid distribution ratio. When α_{ij} equals a unity, the two chemical species cannot be separated by conventional distillation regardless of the energy input to the system and the number of equilibrium stages in the separation column. Under such conditions, the system is referred to be at azeotropic

composition. Various techniques are employed to either break or shift the azeotrope in a given azeotropic system. The water (1) + propan-1-ol (2) and diisopropyl ether (1) + propan-1-ol (2) systems measured in this work exhibits azeotropic behaviour at a given temperatures. The effect of azeotrope on their distillation and methods to separate the species is discussed in detail in section 7.6. The relative volatility and model predictions are given in Figures 7-36 to 7-42 for all the measured VLE systems. A good representation of relative volatility data by the models for all systems is observed except for the furan (1) + methylbenzene (2) system. This is attributed to the poor prediction of the vapour phase mole fraction for this system.

7.4.1 Relative Volatility Data for The diisopropyl ether (1) + propan-1-ol (2) System

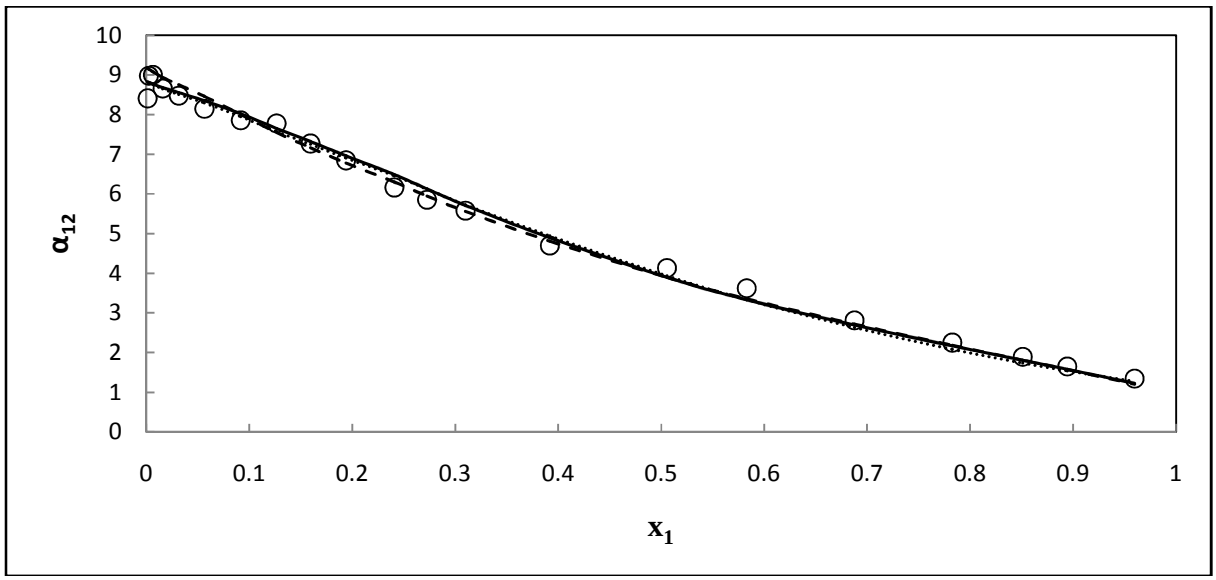

Figure 7-36: Comparison between the experimentally determined relative volatility and values calculated from the NRTL, Wilson and UNIQUAC model with Peng-Robinson the diisopropyl ether (1) + propan-1-ol (2) system at 333.15 K: ○ this work, — PR-NRTL, - - - PR-Wilson, ····· PR-UNIQUAC.

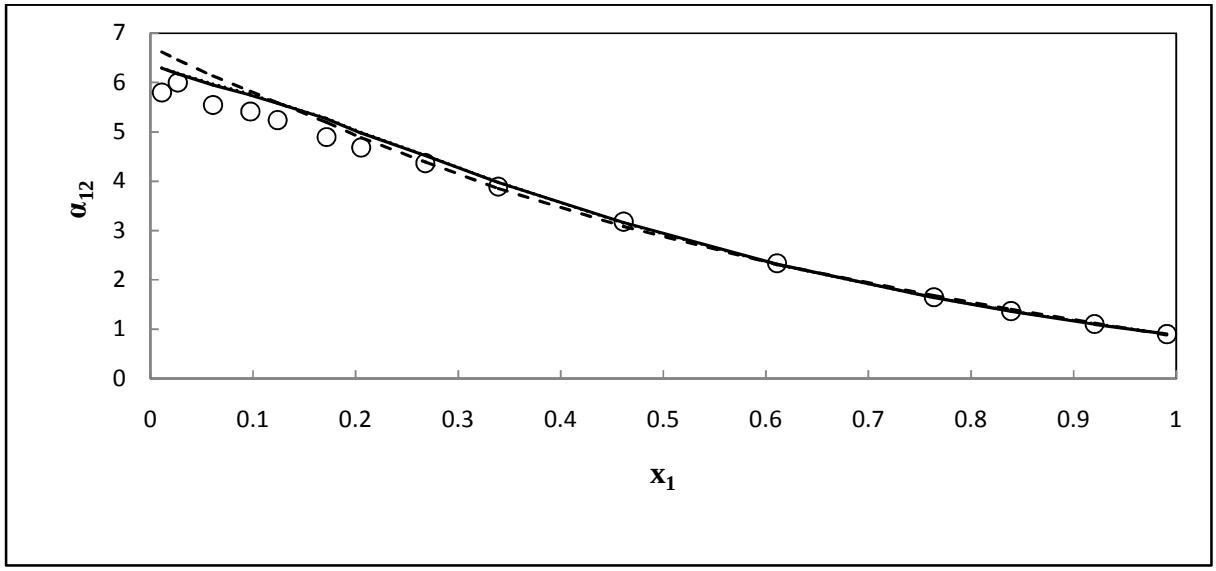

Figure 7-37: Comparison between the experimentally determined relative volatility and values calculated from the NRTL, Wilson and UNIQUAC model with Peng-Robinson the diisopropyl ether (1) + propan-1-ol (2) system at 353.15 K: ○ this work, — PR-NRTL, - - - PR-Wilson, ·····PR-UNIQUAC.

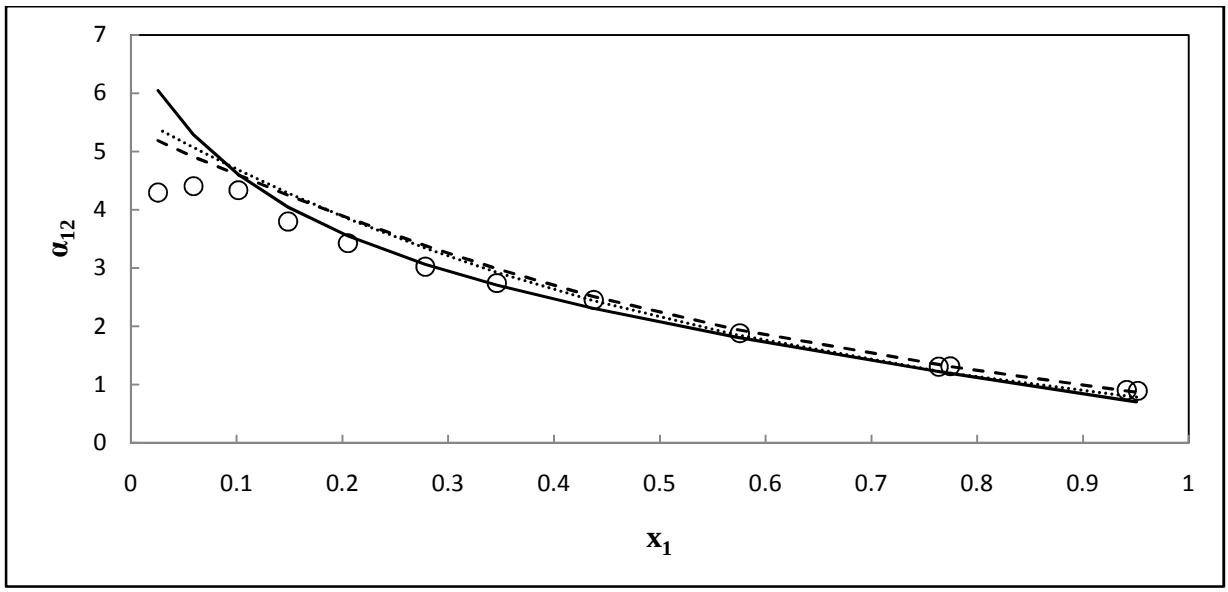

Figure 7-38: Comparison between the experimentally determined relative volatility and values calculated from the NRTL, Wilson and UNIQUAC model with Peng-Robinson the diisopropyl ether (1) + propan-1-ol (2) system at 373.15 K: ○ this work, — PR-NRTL, - - - PR-Wilson, ·····PR-UNIQUAC.

7.4.2 Relative Volatility Data for The water (1) + propan-1-ol (2) System

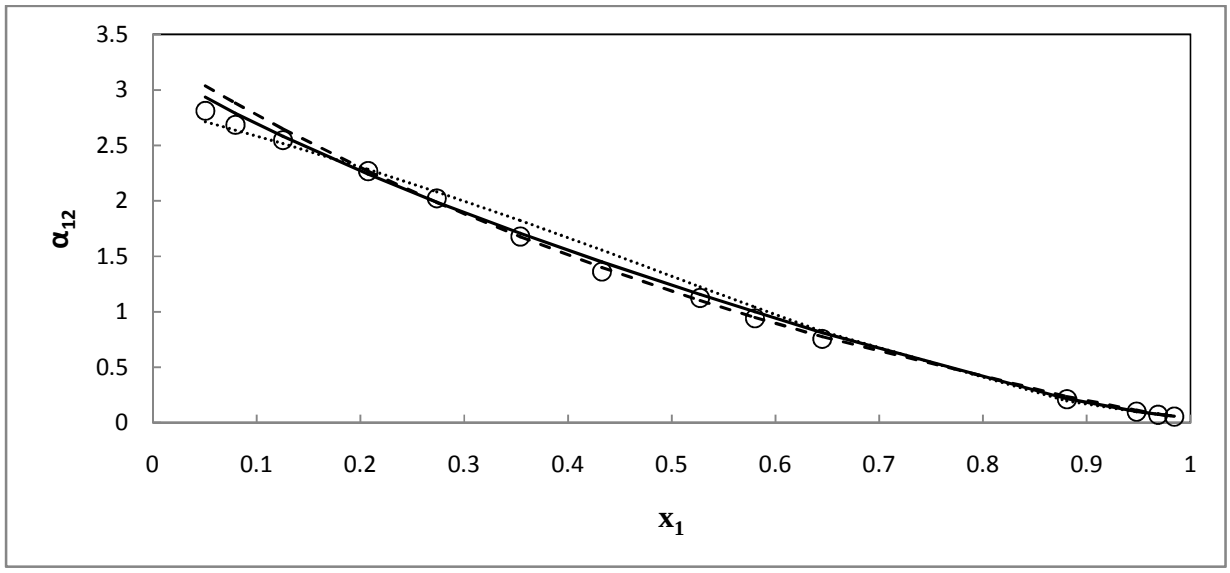

Figure 7-39: Comparison between the experimentally determined relative volatility and values calculated from the NRTL, Wilson and UNIQUAC model with Hayden and O'Connell technique the water (1) + propan-1-ol (2) system at 358.15 K:○ this work, — HOC-NRTL, - - - HOC-Wilson, ⋯⋯HOC-UNIQUAC.

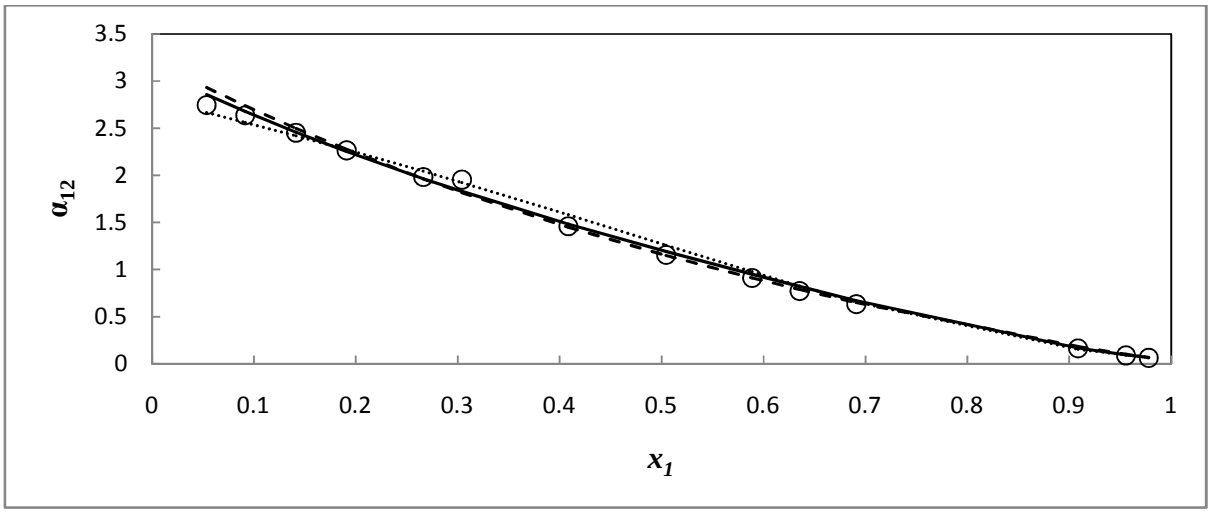

Figure 7-40: Comparison between the experimentally determined relative volatility and values calculated from the NRTL, Wilson and UNIQUAC model with Hayden and O'Connell technique the water (1) + propan-1-ol (2) system at 368.15 K: :○ this work, — HOC-NRTL, - - - HOC-Wilson, ⋯⋯HOC-UNIQUAC.

7.4.3 Relative Volatility Data for The furan (1) + n-hexane (2) System.

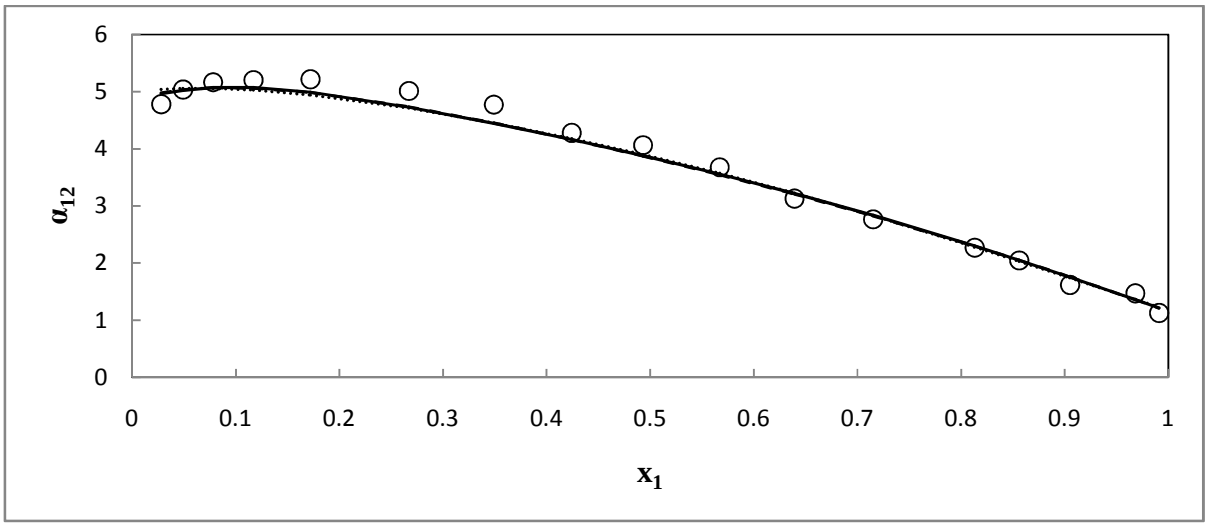

Figure 7-41: Comparison between the experimentally determined relative volatility and values calculated from the NRTL, Wilson and UNIQUAC model with Peng-Robinson for the system of furan (1) + n-hexane (2) at 101.3 kPa:○ this work, — PR-NRTL, - - - PR-Wilson, ⋯⋯PR-UNIQUAC.

7.4.4 Relative Volatility Data for The furan (1) + methylbenzene (2) system.

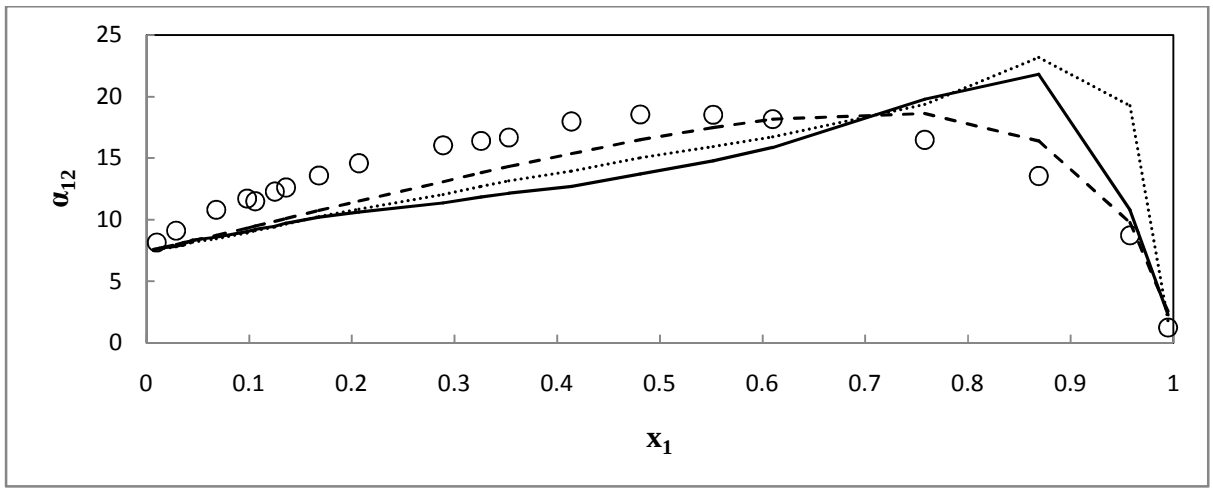

Figure 7-42: Comparison between the experimentally determined relative volatility and values calculated from the NRTL, Wilson and UNIQUAC model with Peng-Robinson for the system of furan (1) + methylbenzene (2) at 101.3 kPa:○ this work, — HOC-NRTL, - - - HOC-Wilson, ⋯⋯HOC-UNIQUAC.

7.5 Reduction of Binary LLE Data

The NRTL activity coefficient model of Renon and Prausnitz, (1968) was used to correlate the experimental data for both LLE systems (furfural + n-hexane and furan + water),, with the non-randomness parameter (α_{ij}) set as 0.3. Equation 7.9 below gives the objective function used to minimise the difference between the experimental and the calculated points:

$$F = \sum_{j}^{N} \sum_{l}^{\pi} \sum_{i}^{c} \left| x_{i,j}^{lexp} - x_{i,j}^{lcal} \right| \tag{7.9}$$

Where N, π and c represent the number of data points, the number phases and the number of components $x_{i,j}^{lexp}$ is the experimental molar fraction and $x_{i,j}^{lcal}$ the calculated molar fraction respectively. The objective function was optimized with least squares optimization technique to find the binary interaction parameters. The interaction parameters of the NRTL model (Renon and Prausnitz, 1968) are given as a linear function of temperature:

$$\Delta g_{12} = c_{12}^{0} + C_{12}T \tag{7.10}$$

$$\Delta g_{21} = c_{21}^{0} + C_{21}T \tag{7.11}$$

Coefficientsc_{12}^{0},c_{21}^{0},C_{12} and C_{21} are presented on table 7-12 and were regressed using an in-house developed regression program (coded in Matlab™) and commercial software Simulis® Thermodynamics for comparison. In a nutshell, the Simulis® Thermodynamics software from ProSim provides high quality thermophysical properties and phase equilibria calculations of pure components and mixtures. The software had been available in the CEP/TEP laboratory, and was thus utilized for the LLE calculations. The result for furfural (Furan-2-carbaldehyde) + n-hexane systems is found to be in agreement with the data sets available in literature by Kolyuchkina (1975), although a slight inconsistency exists between the two literature data sets. The data were also correlated using the Cox Herington model (Cox and Herington, 1956) in order to extrapolate the behavior of the system at critical conditions. Both the Cox Herington and NRTL model

equations were found to be in agreement with the available data points far from critical region, but a significant deviation between the two models is observed close to the critical point. The Cox-Herington extrapolation results in a higher upper critical equilibrium point (~375 K) than the general trend produced by available literature data and NRTL calculation. The possible justification of the high deviation resulting from the Cox-Herington model is the great dependence of the calculated parameters on the value of Tc, which is initially assumed and optimized during curve fitting. Cox and Herington (1956) showed a different representation of coexistence data for a wide temperature range. The average absolute deviations obtained comparing calculated and experimental two-phase compositions for furfural (Furan-2-carbaldehyde) + n-hexane system are <2.5 % for NRTL model and <5.73 % for Cox Herington model. The AAD of < 5.92 % was obtained for furan + water system and was attributed to difficulties to obtain highly precise values of species mole fraction in the dilute region. To further analyze the data, the distribution coefficients and selectivity of furfural to n-hexane was calculated as follows:

$$S_{12} = \frac{x_1^{\alpha} / x_2^{\alpha}}{x_1^{\beta} / x_2^{\beta}} = \frac{D_{12}^{\alpha}}{D_{12}^{\beta}} \tag{7.14}$$

Where α and β represent the two liquid phases. The LLE T-x data are graphically shown on Figures 7-43 and 7-45, and it can be seen from the figures that there is good agreement of the measured data with the NRTL model.

Table 7-12: NRTL binary interaction parameters for LLE system.

System	Software	C_{12}	C_{21}	$C_{12}T$	$C_{21}T$	α_{12}	AAD%
Furfural (1) + n-hexane (2)	Matlab™	1224	1554	2,03	-7,48	0,3	2.56
	Simulis™	1221	1553	-1,89	-7,52	0,3	2.50
water(1) + furan (2)	Matlab™	5537	3164	-104.58	-31.53	0.3	5.92

Table 7-13: Cox Herington regression parameters for LLE system.

system	K^{α}	K^{β}	x_c	σ	AAD%
Furfural (1) + n-hexane (2)	-0,116	-0,098	0,524	0,325	5,73

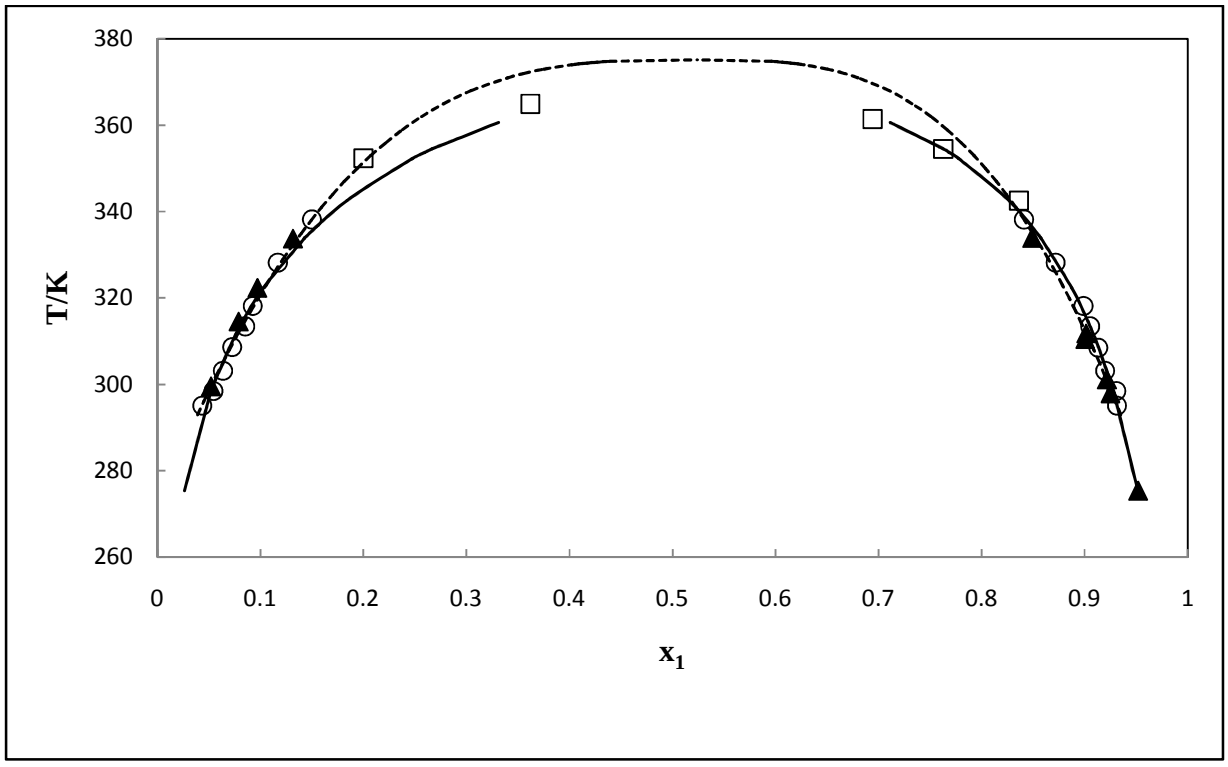

Figure 7-43: Experimental LLE and modeling results, comparison between NRTL and Cox-Herington model fits to T-x data for furfural (1) + n-hexane (2) system at 101.3 kPa: ▲Kolyuchkina, □ Kolyuchkina set 2 ○ this work, —NRTL, - - - Cox-Herington

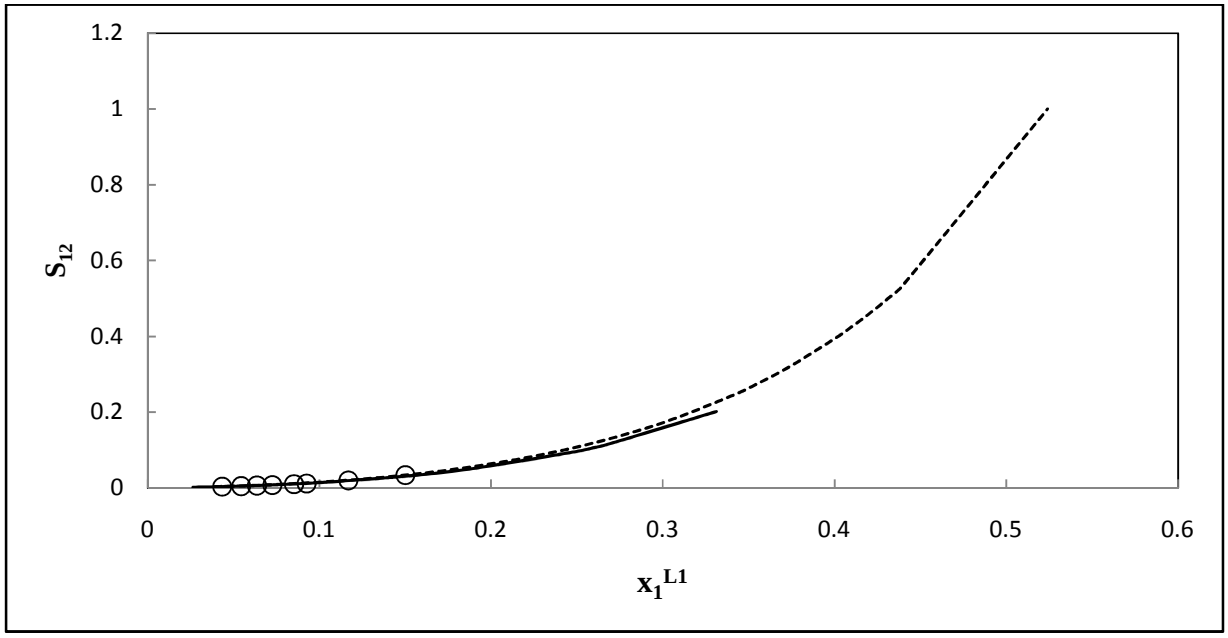

Figure 7-44: Selectivity for furfural (1) + n-hexane (2) system in comparison with NRTL model calculation: ○ this work, — NRTL, - - - Cox-Herington

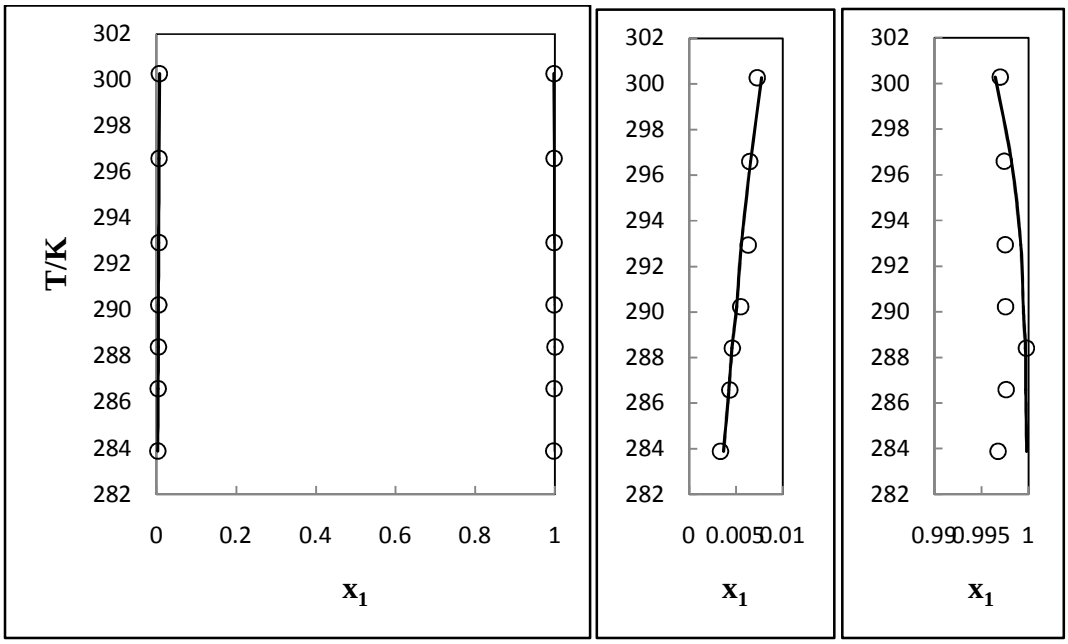

Figure 7-45: Experimental LLE and NRTL modeling fit to T-x data for water (1) + furan (2) system at 101.3 kPa: ○ this work, — NRTL.

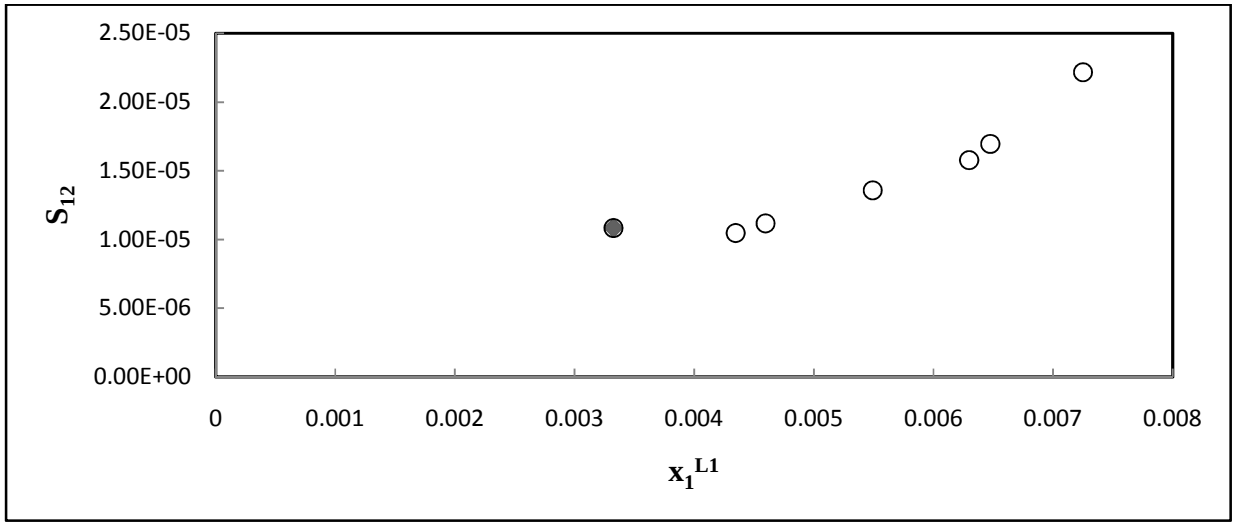

Figure 7-46: Selectivity data for water (1) + furan (2) system at 101.3kPa: ○ this work.

7.6 Simulation of The propan-1-ol Dehydration Process via Azeotropic Distillation System in Aspen Plus

The importance of phase equilibria data can be well illustrated during process design and simulation. According to Luyben (2006), successful process design involves three basic steps: The first is known as *Conceptual design*, where approximate and historical methods are employed to develop a preliminary process flowsheet. The second step is *Preliminary Design*, which involve rigorous simulation methods to evaluate the steady state and dynamic performance of the proposed flowsheet. The last step is the *Detailed Design*, for which the simulated units are specified in great detail, with all the specifics such as column diameter, valve sizes, heat exchanger areas, types of distillation trays and reflux piping.

This section presents the simulation and analysis of an azeotropic distillation process for the separation of propan-1-ol + water minimum boiling azeotropic mixture using Aspen Plus®. The work was undertaken as part of an illustration of the use of experimental data and thermodynamic models used in process simulation with the measured experimental data in order to establish confidence in the simulated results. Notable only the first two steps of process design have been undertaken in this section. The process simulation presented below illustrates a simple application of diisopropyl ether as a light entrainer. According to Laroche *et al.* (1991) the

entrainer for azeotropic distillation can be the lightest, the heaviest, or even the intermediate boiling component in the system; even though there has been no published reports of industrial processes with azeotropic separation column that uses a light entrainer with no azeotrope formation. Nonetheless, there are scholars such as Hunek *et al*. (1989) who experimentally investigated the use of methanol (Light) as entrainer for the separation of the ethanol (L) + water (H) azeotrope. They checked its reliability of the results with pilot-plant experiments.

To date, there have not been industrial processes using diisopropyl ether as an entrainer for recovery of alcohols in alcohol-water mixtures. This section provides a preliminary process simulation which can aid in development of propan-1-ol dehydration process using diisopropyl ether. Only the key separation units have been simulated with no preliminary sizing of equipment (i.e. sizing of column diameters, heat exchanger surface areas, other units was not undertaken). The Aspen design methodology adapted for distillation columns was based on the work of Luyben (2006) using the Redifrac column (provides better thermodynamics). A systematic procedure was used to allow the comparison between possible separation schemes with respect to solvent considerations and efficiency of the separation.

7.6.1 Thermodynamic Model Validation

The NRTL-HOC thermodynamic model was used in the simulation of the propan-1-ol dehydration process in Aspen Plus process simulator version 7.1. Model validation was done using the measured experimental data obtained in this thesis. The choice of using the HOC-NRTL model was based on the correlated results especially the water + propan-1-ol binary system which is known to associate, making it difficult to accurately calculate activity coefficients with non associating models. Aspen Plus has various data banks with model parameters fitted to literature data. The HOC data bank present model parameters for various systems for a given temperature ranges. For accurate design of a separation process, it is safe to verify the model description of the system of interest outside the model parameter temperature range. The measured data also allow for updating the temperature range applicability of the model parameters available in the data bank. Figures 7-47 and 7-48 show a typical example of binary mixtures generated by NRTL-HOC together with experimental data measured in this work. Figure 7-49 shows the ternary diagram with the comparison of experimental data with the

correlated HOC-NRTL and the predictive UNIFAC models for the water (1) + propan-1-ol (2) + diisopropyl ether (3) system. The HOC model is observed to represent the phase behaviour well in both the organic (DIPE rich region) and aqueous (water rich region) phases. In conclusion, the HOC-NRTL model in Aspen Plus (with binary interaction parameters in the HOC-data bank) shows good representation of the water (1) + propan-1-ol (2) + diisopropyl ether (3) system; and may be used to simulate a more reliable propan-1-ol dehydration process plant.

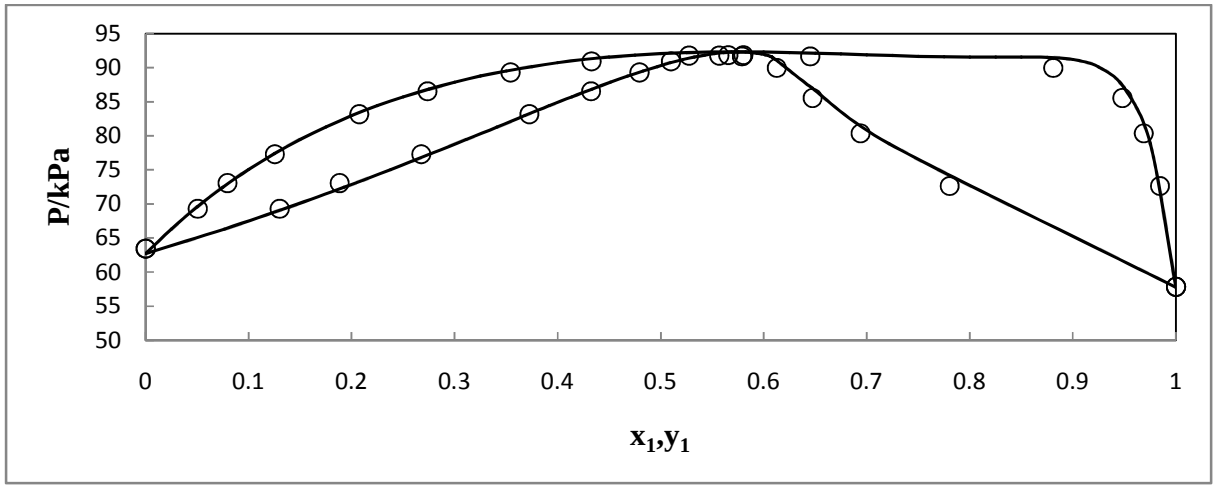

Figure 7-47: Model validation with experimental data for water (1) + propan-1-ol (2) binary system at 358.15 K: ○ this work, — HOC-NRTL.

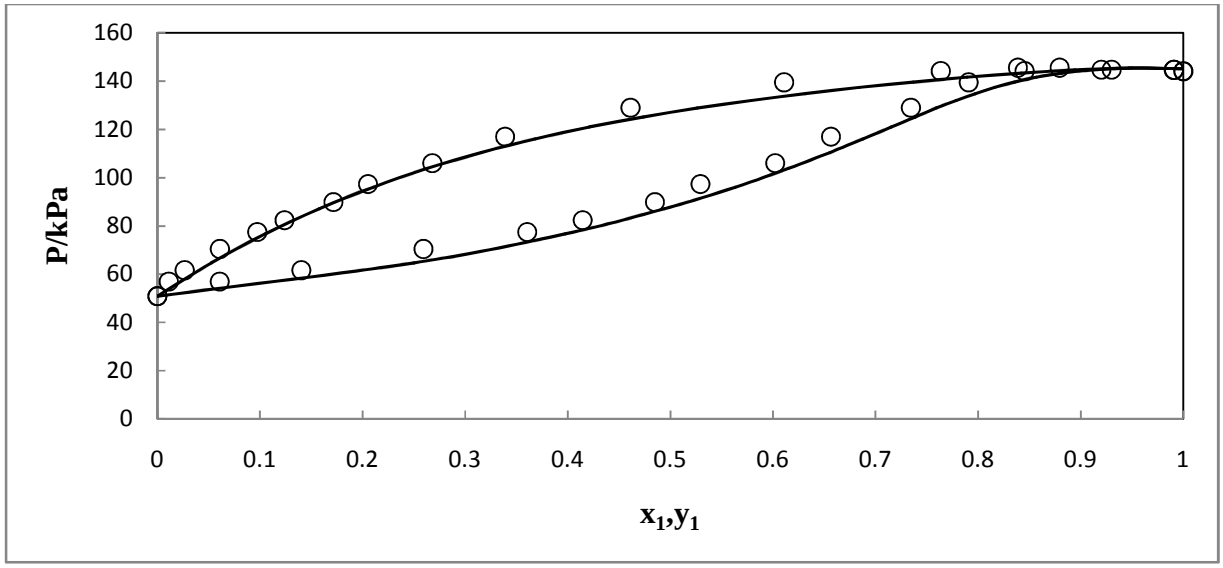

Figure 7-48: Model validation with experimental data for diisopropyl ether (1) + propan-1-ol (2) binary system at 353.15 K: ○this work, — HOC-NRTL.

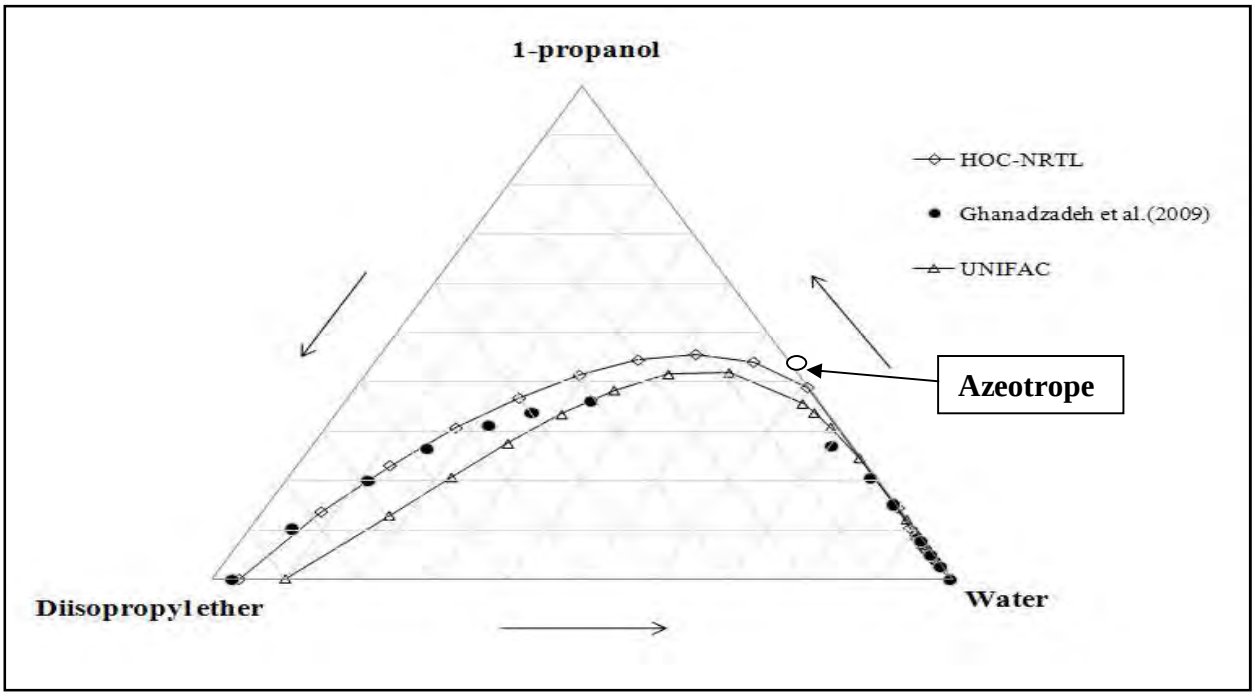

Figure 7-49: Comparison of HOC-NRTL and UNIFAC models with measured data for (water + propan-1-ol + diisopropyl ether) system at 308.2 K.

7.6.2 Aspen Input Data

The best possible design of separation process in Aspen Plus relies on systematic trial and error procedure. Various separation flowsheet arrangement and input parameters were proposed and were carefully evaluated to obtain the best possible process configuration. As an initial start, it was important to look at other process such as ethanol dehydration simulated by Gil *et al*. (2005). Their simulation featured 20 theoretical stages, which is between 18 and 24 recommended by Lee and Pahl (1985) and Meirelles *et al*. (1992). The rest of the simulation relied on sensitivity analysis to obtain the best possible input parameters. Table 7-13 below shows the initial input parameters that were used to simulate the azeotropic column.

Table 7-14: Azeotropic column initial input data used in the simulation.

Simulation parameter	Value
Feed flow (kmol/h)	100
Separating agent to feed ratio	0.8
Feed molar composition: Water	0.6
Propan-1-ol	0.4
Temperature of feed (K)	338.15
Temperature of the entrainer (K)	333.15
Molar reflux ratio in extractive column	0,95
Number of theoretical stages for the Azeotropic column	22
Process feed stage	12
Pressure in the extractive column (kPa)	130

7.6.3 Process Flowsheet and Simulation Sequence

The azeotropic distillation process involves a two stage separation; the separation of the two azeotropic components in the presents of the solvent and the recovery of the solvent. The flowsheet configuration will vary such that the best possible results are obtained. The final process flow diagram and Aspen flowsheet resulting in the highest recovery of 1-propanol are given in Figures 7-50 and 7-51 respectively. With reference to Figure 7-51, the simulations sequence starts by feeding the water rich mixture (60 molar % water) in the dehydration column at stage 12. The separation requires anhydrous propan-1-ol, thus, the separation is to pass the azeotropic composition in order to rich pure propan-1-ol. The DIPE solvent is fed on stage 18 since it is a light boiling entrainer and allows for formation of a heterogeneous azeotropic mixture at the top of the column and a binary mixture of the water + propan-1-ol stream with t small % of solvent at the bottom. The top stream is cooled resulting in the formation of two phase mixture DIST1 which separates into a solvent rich phase (organic phase) and water rich phase in the first decanter (DECANT1). The equimolar stream at the bottom of azeotropic column has a composition passed the azeotrope (59 mole% H_2O) is sent to the first recovery column (RCOL1) and results in highly pure propan-1-ol bottom stream (PROD1, 96.44% (wt/wt)). The propan-1-ol fraction recovery in this stream is 34.2% of the initial feed and is relatively low. The top stream of the recovery column DIST2 consisting of water, propan-1-ol and DIPE is combined in the first decanter with stream DIST1. The first decanter allows for

removal of 79.4 % of feed water in the aqueous phase. The organic phase from the decanter is made of mostly the DIPE solvent and propan-1-ol and the rest being water is separated in the second recovery column (RCOL2), which produces a bottom product of 99.72 % (wt/wt) propan-1-ol with fractional recovery of 57.4%. The top product DIST3 consist mainly of DIPE and the remainder of water, with small traces of propan-1-ol is sent to the second decanter (DECANT2) where the rest of process water is removed. The organic phase in the second decanter consists of 96.22 % (wt/wt) solvent with the rest being propan-1-ol. The solvent recovered is 99.36 % of the initial solvent fed to the process, and is returned to the azeotropic column where it is combined with the makeup stream which is used at the start of the process simulation. It is important to note that the purge stream shown in Figure 7-51 is used to aid the convergence of the process simulation when closing the aspen loop by slowly increasing the split ratio of the recycle stream towards stream 9. This is crucial because sending the whole recycle stream in the azeotropic column in Aspen results in disruption of the simulation and severe errors, thus failure to convergence. This method is mostly adapted by process simulators to quickly converge the simulated Aspen process. The simulated column results are given in Table 7-15 and the process stream results are given in appendix F. Figures 7-52 to 7-54 shows the Molar composition profile inside the distillation column.

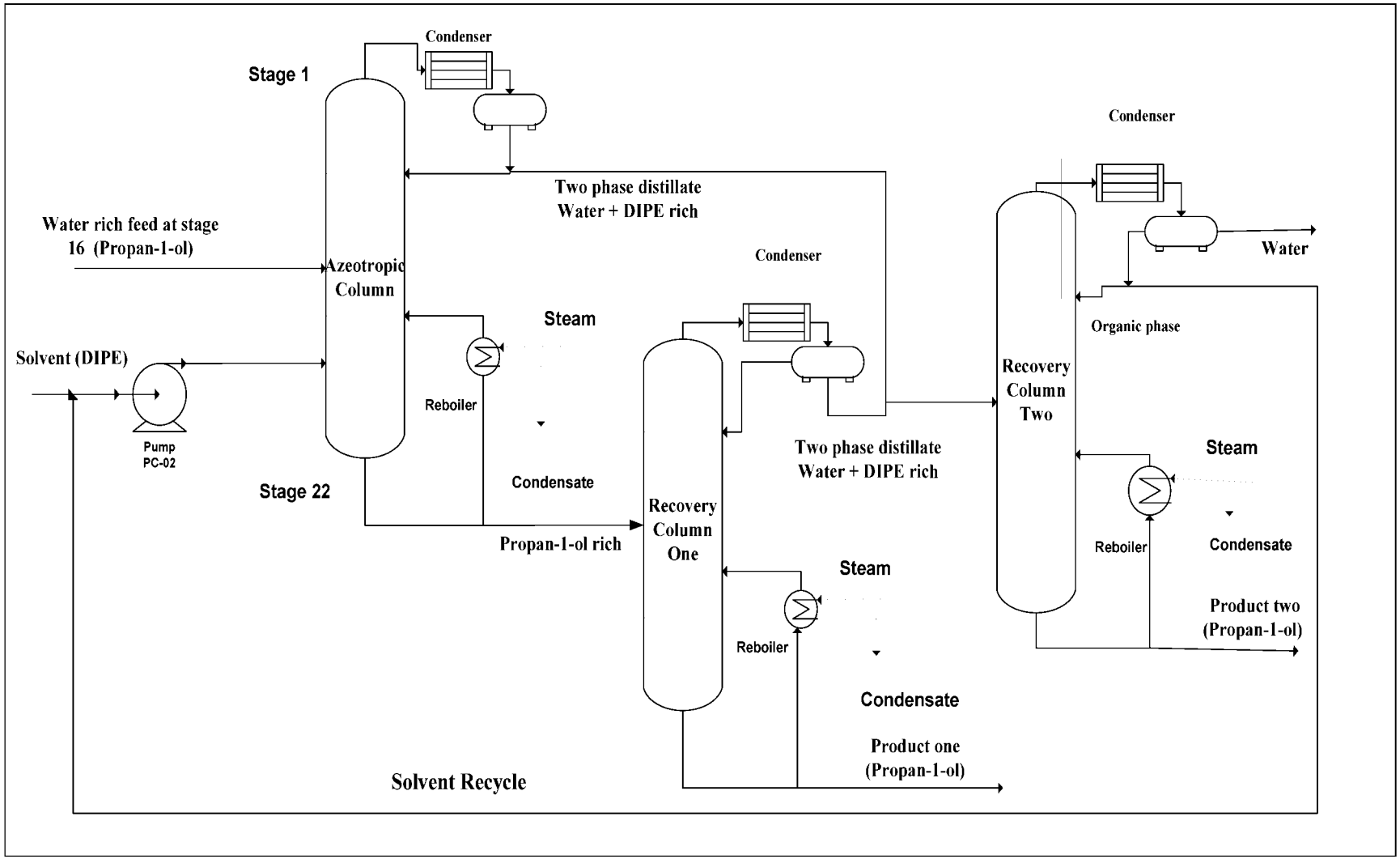

Figure 7-50: The propan-1-ol dehydration process via azeotropic distillation of water + propan-1ol using diisopropyl ether as an entrainer.

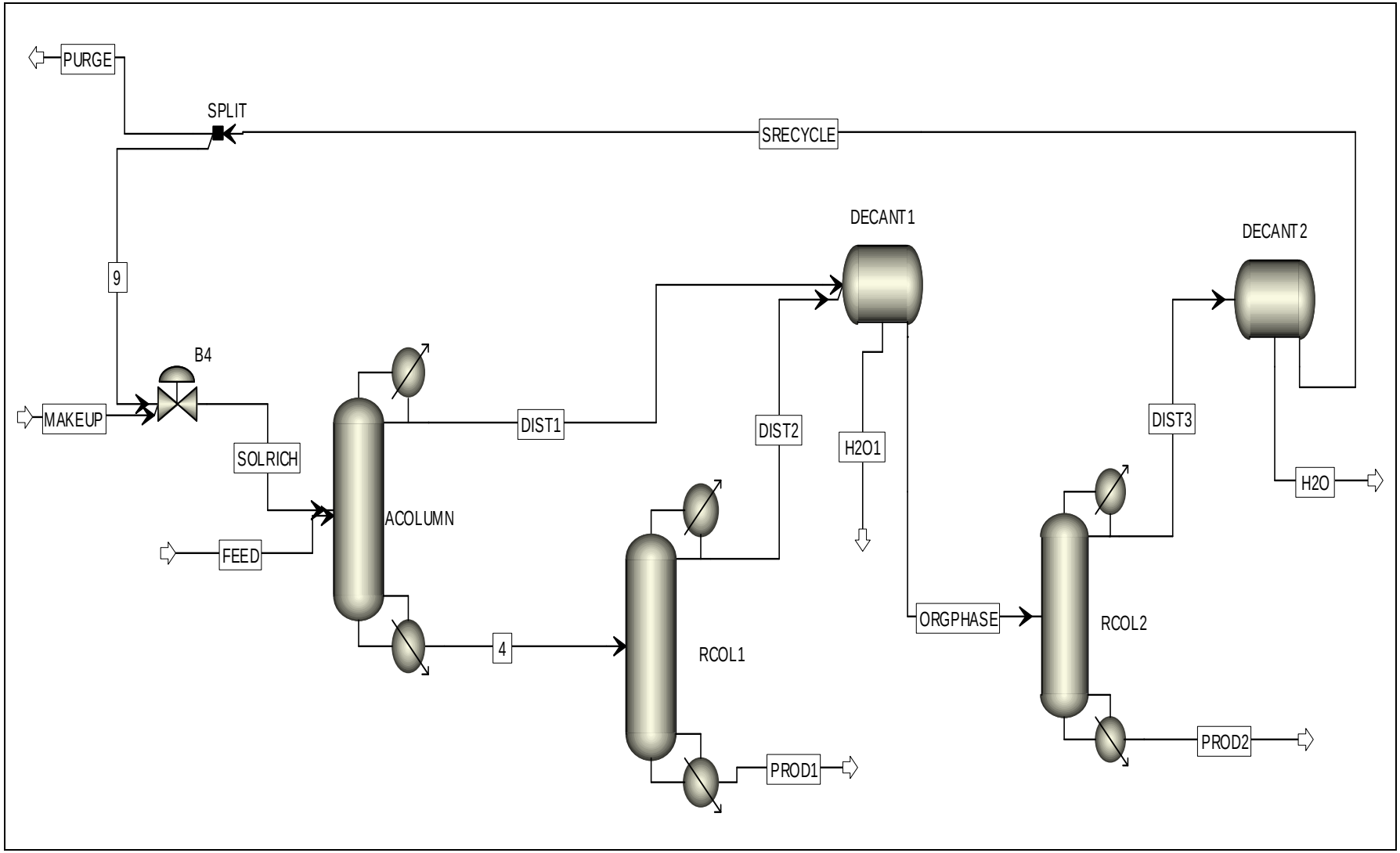

Figure 7-51: Aspen Plus flowsheet of the propan-1-ol dehydration process via the azeotropic distillation of water + propan-1-ol using diisopropyl ether as an entrainer.

Table 7-15: Column specifications for the propan-1-ol dehydration process.

Parameter	Value
Azeotropic column(Redifrac)	
Separating agent molar flow (kmol.hr^{-1})	45.32
Distillate molar flow (kmol.hr^{-1})	60.01
Molar composition of propan-1-ol in the bottoms	0.490
Mass fraction of propan-1-ol in the bottoms	0.761
Temperature of the process feed (K)	338.15
Temperature of the entrainer (K)	333.15
Molar reflux ratio in the column	0.95
Number of theoretical stages in the column	22
Process feed stage	16
Pressure in the column (kPa)	130
Entrainer feed stage	18
Solvent to feed ratio (S/F)	0.45
First recovery column (Redifrac)	
Number of theoretical stages in the column	10
Pressure in the column (kPa)	120
Feed stage of first bottoms	5
Molar reflux ratio in the column	1.5
Distillate molar flow (kmol.hr^{-1})	70
Second recovery column (Redifrac)	
Number of theoretical stages in the column	10
Pressure in the column (kPa)	100
Feed stage of organic phase mxiture	5
Molar reflux ratio in the column	5
Distillate molar flow (kmol.hr^{-1})	56
Net energy consumption (sum of reboiler and condenser duties)	
Energy consumption azeotropic column (kJ/s)	245.3
Energy consumption of the first recovery column (kJ/s)	-7.63
Energy consumption of the second recovery columns (kJ/s)	228.5

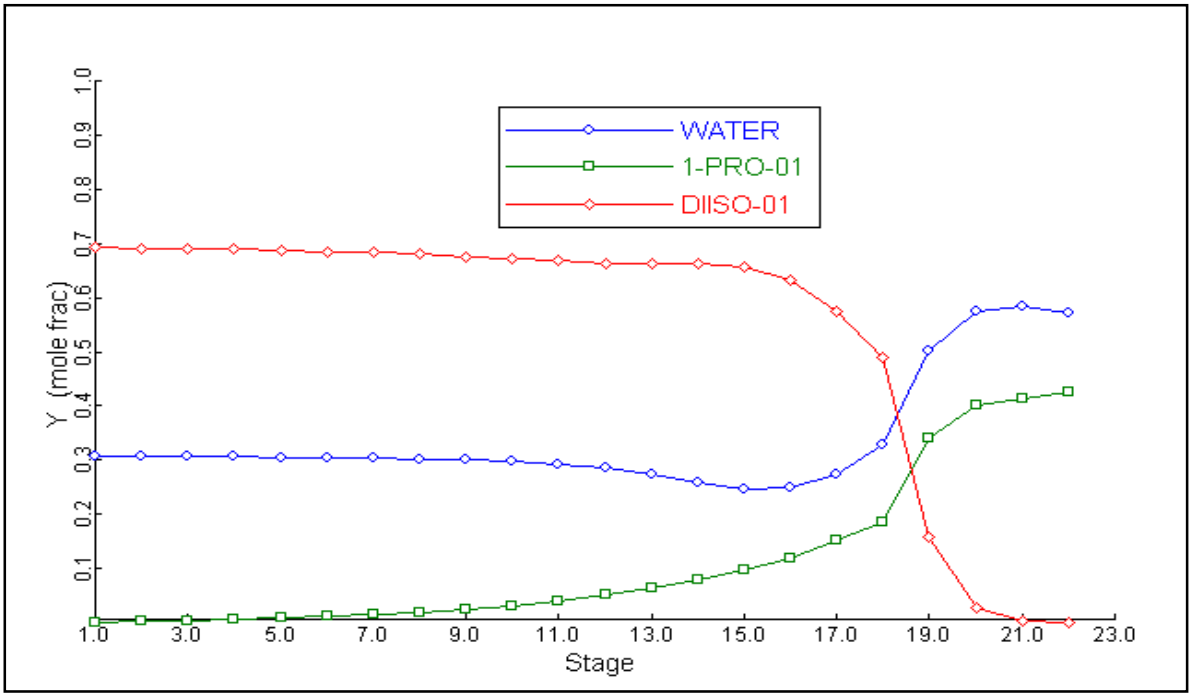

Figure 7-52: Composition profile in the azeotropic column.

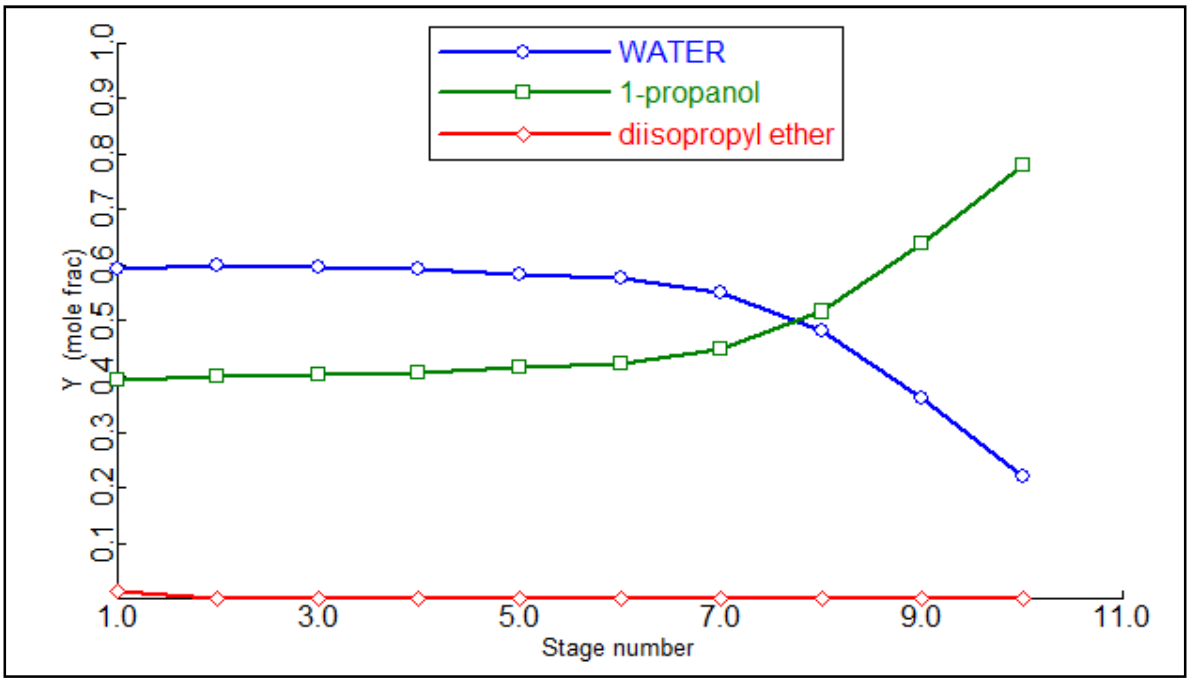

Figure 7-53: Composition profile in the first recovery column.

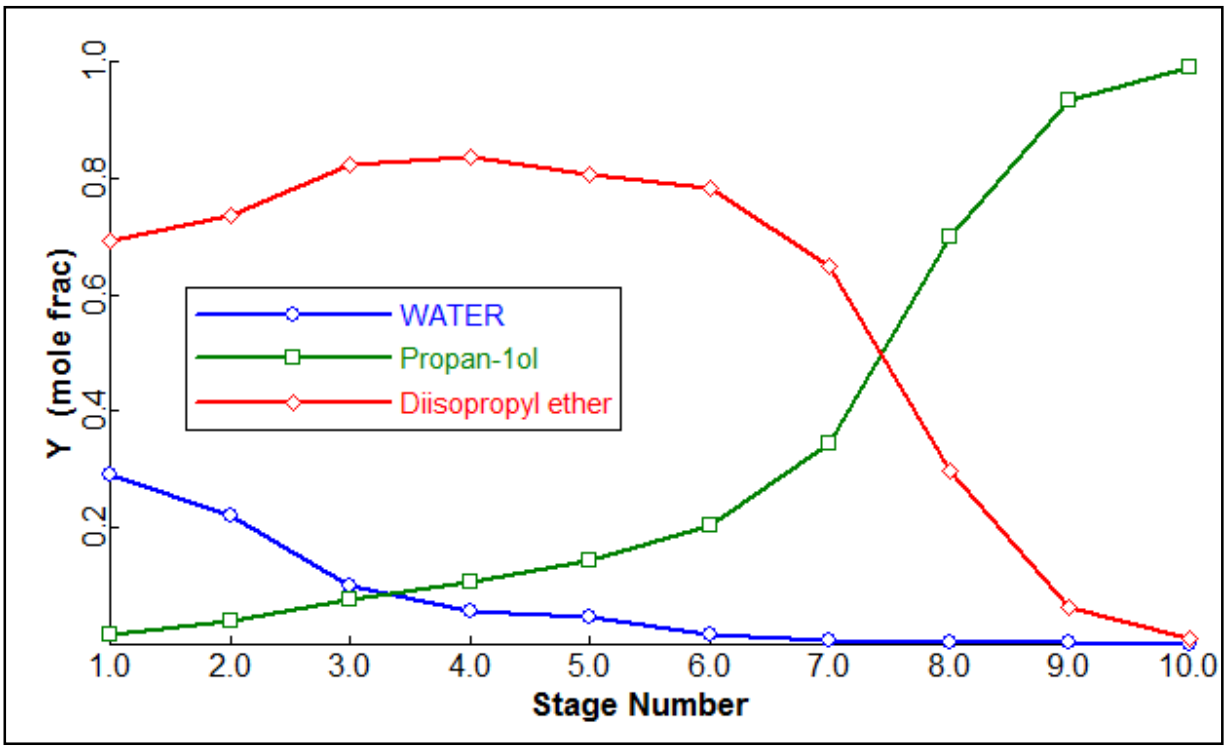

Figure 7-54: Composition profile in the second recovery column.

7.6.4 Sensitivity Analysis

Sensitivity analysis is very useful tool, available in Aspen plus to find optimum operating conditions in process design. Typical examples of sensitivity analysis in process design include: variation of operating column parameters (Number of theoretical stages, reflux ratio, etc) and feed stream parameters such as solvent to feed ratio for enhanced distillation techniques.

Figures 7-55 and 7-56 show sensitivity analysis done for the purity of produced 1-propanol against: molar flow solvent (DIPE) and the number of theoretical stages of the azeotropic column. An optimum solvent flow was found at 40 moles/hr. A further increase in solvent flow induced decrease in the purity of the1-propanol product. The solvent feed stage in the azeotropic column was found to have less effect on purity if propan-1ol.

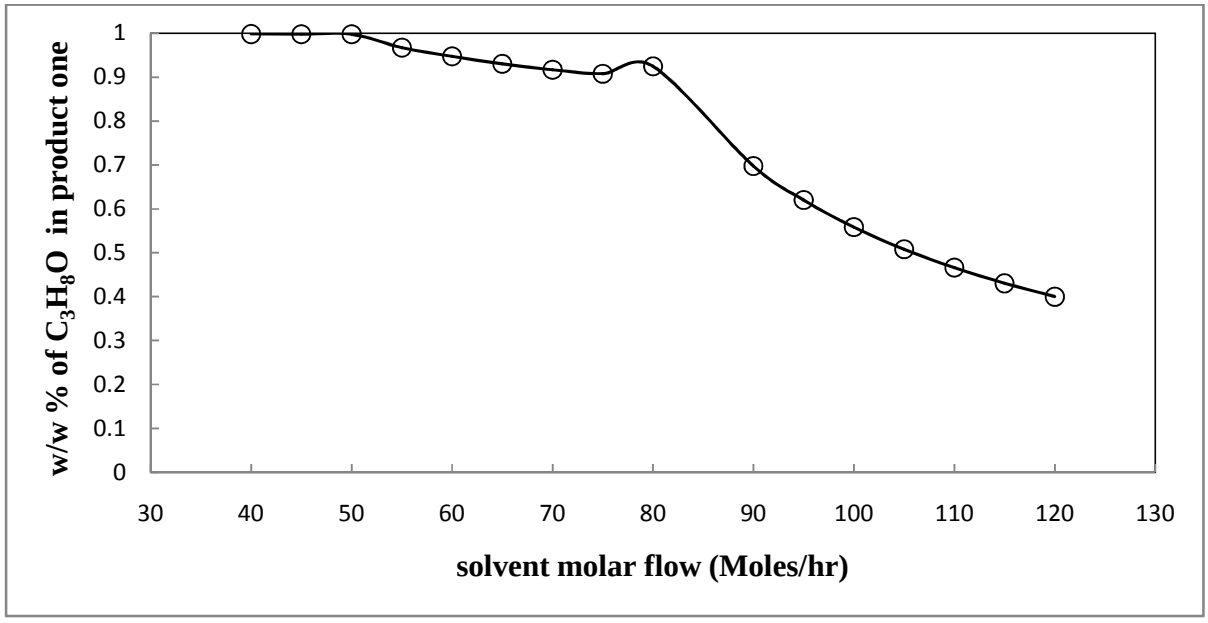

Figure 7-55: Sensitivity analysis of propan-1-ol purity against solvent (DIPE) molar flow.

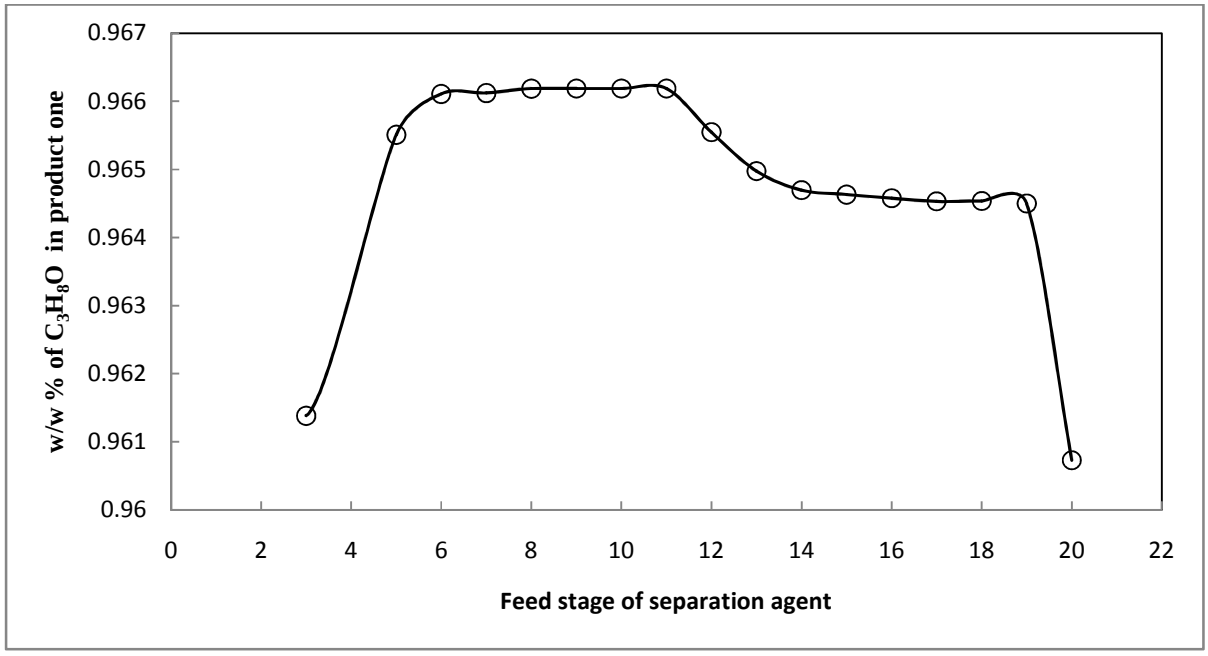

Figure 7-56: Sensitivity analysis of propan-1-ol purity against feed stage of the solvent.

7.6.5 Diisopropyl Ether as an Entrainer Benchmarked Against n-Pentanol

The above work has solely focused on the use and potential application of DIPE. It is important to not overlook the fact that, there are several factors to consider when choosing azeotropic distillation or extraction solvent for a particular design. To provide a feel of such a design scenario, a brief comparison of DIPE and pentanol as potential solvent of water dehydration is given in table 7-16. The relative low cost of DIPE, its low solubility in water and high separation factor for water + propan-1-ol system merits its potential as extraction solvent in the dehydration of light alcohols. Looking from solvent recovery and energy consumption for system using DIPE against n-pentanol, Figure 7-57 provides an argument case for n-pentanol, as the system is certainly more ideal and will allow for low energy consumption (vacuum operation) in comparison with DIPE system in Figure 7- 48.

Table 7-16: Comparison between DIPE and n-pentanol as potential extraction solvent.

solvent	**DIPE**	**n-Pentanol**
Purity	(≥ 99 %)	(≥ 99 %)
Boiling point	138	68
Solubility in water at 20 ^{o}C	1%w/w	2.2 % w/w
separation factors	258[1]	~ 38[2]
price	US $ 2200-2600 / Metric Ton)[3]	(US $3300-3500 / Metric Ton)[4]

[1] Ghanadzadeh *et al.* (2009), [2] Cristina Stoicescu *et al.* 2010, [3] http://www.alibaba.com/product-gs/371087946/Diisopropyl_ether_99_0_.html

[4] http://www.alibaba.com/product-gs/538492451/99_liquid_pharmaceutical_amyl_alcohol.htm

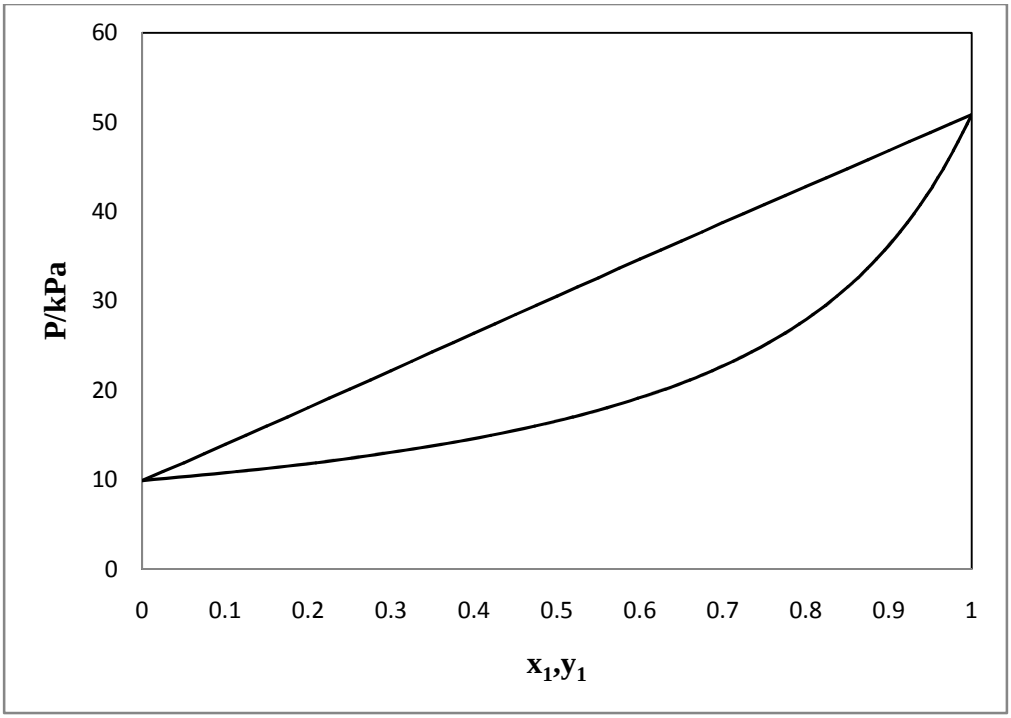

Figure 7-57: Model prediction for propan-1-ol (1) + n-pentanol (2) binary system at 353.15 K:— HOC-NRTL.

CHAPTER 8

CONCLUSIONS

8.1 Experimental Measurements

The key to successful design and simulation of several industrial separation processes is experimental measurements and thermodynamic modeling of phase equilibrium data. This work presented different types of phase equilibrium measurements (VLE and LLE) which are essential in; separation of propan-1-ol from water using diisopropyl ether and the ongoing research of biofuels. A survey of available literature data for systems comprised of these compounds was undertaken and the systems chosen for VLE measurements were: (i) diisopropyl ether + propan-1-ol at 333.15 K, 353.15 K and 373.15 K and (ii) water + propan-1-ol at 358.15 K and 368.15 K for the azeotropic separation of water + 1-propanol system, (iii) furan + n-hexane at 101.3 kPa and (iv) furan + methylbenzene at 101.3 kPa for the biofuels initiative. In addition, LLE measurements of some intermediate compounds in the biofuels systems were made possible by the development and commissioning of an improved LLE apparatus. The LLE apparatus was used to measure data for the systems of furfural + n-hexane at 101.3 kPa and water + furan and 101.3 kPa.

The VLE measurements were undertaken using three different apparati: the still of Joseph (2001) and the still of Lilwanth (2011) for diisopropyl ether + propan-1-ol and water + propan-1-ol system undertaken at the UKZN thermodynamic Laboratories (South Africa), the third apparatus used was the atmospheric VLE glass still available at CEP/TEP Laboratory (France). Uncertainties in the measurements were estimated as follows: The uncertainty in pressure measurements with the glass apparatus of Joseph (2001) was estimated to be ±0.23 kPa and it was well controlled within 0.1 kPa during operation. The accuracy of the measured temperature was estimated as ±0.02 K. The apparatus of Lilwanth (2011) was controlled within 0.1 kPa during operation and the pressure and temperature uncertainties in all the systems were estimated to be ±0.23 kPa and ±0.02 K respectively. The Temperature uncertainty in the atmospheric VLE

glass still was estimated to be ±0.01 K. The uncertainties in molar compositions were estimated as ±0.013 and ±0.007 for the isothermal VLE systems of diisopropyl ether (1) + propan-1-ol (2) and water (1) + propan-1-ol (2) respectively. For the isobaric VLE systems of cyclohexane (1) + ethanol (2), furan + n-hexane and furan + methylbenzene, the estimated uncertainties were calculated as ±0.008, ±0.005 and ±0.004 respectively.

8.2 Theoretical Analysis

The measured vapour pressure data were correlated using the Wagner and Antoine equation to obtain the model parameters. All vapour pressure data correlated well with average % error less than 1 % except for Cyclohexane with 1.41 % error for the Antoine model equation.The modelling of measured phase equilibrium data for the systems of diisopropyl ether (1) + propan-1-ol (2) and water (1) + propan-1-ol (2) was undertaken using suitable thermodynamic models. The isothermal VLE data sets were modelled using the Hayden and O'Connell (1974), Nothnagel *et al*. (1973) and the Peng-Robinson (1976) equation of state paired with Wilson (Wilson, 1964), NRTL (Renon and Prausnitz, 1968) and UNIQUAC (Abrams and Prausnitz, 1975) activity coefficient models. All the models used are available in Aspen Plus process simulator and the $\gamma - \varphi$ approach was utilised in the regression of model parameters. The adapted solution algorithms were the *ordinary least square* and *maximum-likelihood* optimization techniques, used to minimise the pressure-molar composition objective function. The models were found to provide satisfactory fits for all the data sets, although poor results were observed for diisopropyl ether (1) + propan-1-ol (2) at higher temperatures (highest vapour phase mole deviations of 6.11 %). The Isobaric VLE data for the systems furan + n-hexane and furan + methylbenzene were also regressed using the $\gamma - \varphi$ technique. The NRTL, Wilson and UNIQUAC activity coefficient models in Aspen Plus were used to account for the liquid phase non-idealities. The vapour phase non idealities were accounted for by the Peng-Robinson equation of state. The VLE data are well correlated by both activity coefficient models with an exception of vapour behavior for the system of furan + methylbenzene (highest vapour phase mole deviations of 6.99 %). The LLE data for furfural + n-hexane system were correlated using NRTL model in an in-house developed Matlab regression program. In addition, the Cox-Herington equation was utilized to calculate the entire coexistence curve and determine the upper critical equilibrium point (~375 K) for this system. Similarly, the NRTL model was used to correlate

experimental LLE data for water + furan system. The highest deviations in phase compositions were found to be about 2.56 and 5.92 % for the systems of furfural + n-hexane and water + furan respectively.

The water (1) + propan-1-ol (2) VLE phase diagram showed a minimum boiling azeotrope, which was highly common in alcohol + water mixtures. The azeotropic composition often lies almost halfway through the phase equilibrium curve, thus pressure swing distillation will have almost no effect in achieving high recovery of pure propan-1-ol. All the other systems were found to exhibit common VLE behaviour (i.e. intermediate-boiling) except for diisopropyl ether (1) + propan-1-ol (2) at higher temperatures (353.15 and 373.15 K). The azeotrope is observed at high DIPE concentrations (> 95 mole %), which is hardly the case during solvent aided separation. The newly measured LLE system of water + furan showed a very wide gab of miscibility (very low solubility of furan in water), thus furan can be used in recovery of highly furan soluble compounds from mixtures with water.

8.3 Aspen Plus Simulation of the Propan-1-ol Dehydration Process

The simulated propan-1-ol dehydration process is a typical example of an industrial separation process using diisopropyl ether as an entrainer. Aspen simulated designs can obviously impose some doubts when used without any experimental data for verification. The separated systems were experimentally measured in this project to increase the availability of experimental data. This section presented a preliminary separation process design. The HOC-NRTL model was used to account for non-idealities in the phase equilibrium calculations. The simulated results obtained are very promising and illustrate a classical separation process with overall recovery of propan-1-ol of 92% of the two cut product streams with one stream at high grade of 99.72% (wt/wt) and lower grade at 96.44% (wt/wt) for the designed process scheme. The simulated separation process is based on recovery of 50 ton per day of the total propan-1-ol fed to the system. A brief comparison of DIPE and n-pentanol as separating agent in propan-1-ol dehydration process was undertaken. This was to illustrate some of the factors worth considering prior choosing a separating solvent for a particular solvent-aided separation process.

CHAPTER 9

RECOMMENDATIONS

Although it is arguable that phase equilibrium data prediction is the most effective way to obtain phase data, the measurement of accurate and reliable experimental data is still the key to phase equilibrium data. This work sums up different phase equilibrium measurements and a continuation of an ongoing project in the investigation of heavy chemical intermediates in biofuels. The dehydration of propan-1-ol by azeotropic distillation using an entrainer such as diisopropyl ether is an example of dehydration of alcohols which often exhibits azeotropes with water. A pilot scale azeotropic distillation plant can be commissioned using the Aspen simulated results. A further investigation of further alcohol-ether systems is not only important to the dehydration of alcohols; it is of great importance to renewable fuels for automobiles. According to the European Fuel Oxygenates Association (EFOA), fuel ethers are also good blending components for gasoline. Their combination of high octane and oxygen content facilitates the preparation of high-performance, and cleaner burning fuels. Similarly the alcohols are known for high octane and their combination with ethers broadens the research possibilities for high-performance; thus understanding of phase equilibrium for such compounds is justified.

The other part of this work involved laying ground to experimental investigation of heavy chemical intermediates in biofuels.These intermediates often form systems that exhibit LLE and SLE and the measurements of various combinations of these compounds will result in well rich database of phase equilibrium for biofuels. The LLE apparatus has been developed and presented in chapter 4 of this thesis for such measurements, thus only continuation of the measurements is required. The LLE apparatus is capable to undertake vapour-liquid-liquid equilibrium (VLLE) measurements and it would be interesting to explore this capability; not to mention help in further improve the apparatus should there be any shortcomings. It also is recommended to extend the LLE measurements to ternary systems. In addition, biomass consist of broad spectrum of chemicals, a well representative solvent can be selected and investigated in other to obtain good model predictions.

REFERENCES

Abbott, M.M. and Van Ness, H.C., (1977). *An Extension of Barker's method for Reduction of VLE data*, Fluid Phase Equilibria, 1, 3-11.

Abrams, D.S., and Prausnitz, J.M., (1975). *Statistical Thermodynamics of Liquid Mixtures: A New Expression for the excess Gibbs Energy of Partly or Completely Miscible Systems.* American Institute of Chemical Engineers Journal, 21(1), 116-127.

Agarwal, A.K., (2007). *Biofuels (alcohols and biodiesel) applications as fuels for internal combustion engines,* Progress in Energy and Combustion Science, 33, 233-238.

Alonso-Trist´an, C., Segovia, J.J., Chamorro, C.R., Montero, E.A., Villama˜n´an, M.A., (2006).*Vapour–liquid equilibrium of octane enhancing additives in gasolines 7,* Fluid Phase Equilibria, 245, 52–56.

Ana, C., Go´mez, M., Mo´nica, B., de Doz, G., So´limo, N.H., (1998). *Influence of temperature on the liquid–liquid equilibria containing two pairs of partially miscible liquids Water+furfural+1-butanol ternary system*, Fluid Phase Equilibria, 153, 279–292.

Arce, A., Ageitos, J.M. and Soto, A., (1996). *VLE for water + ethanol + 1-octanol mixtures. Experimental measurements and correlations,* Fluid Phase Equilibria 122, 117-129.

Arce, A, Marchiaro, A., Rodrı´guez, O., and Soto, A., (2002). *Liquid-Liquid Equilibrium of Diisopropyl Ether + Ethanol + Water System at Different Temperatures,* Journal of Chemical Engineering Data, 47, 529-532.

Arun Kumar, U.K. and Mohan, R., (2011). *Liquid-Liquid Equilibria Measurement of Systems Involving Alkanes (Heptane and Dodecane), Aromatics (Benzene or Toluene), and Furfural,* J. Chem. Eng. Data, *56* (3), pp 485–490

Ashour, I. and Aly, G., (1996). *Effect of computational technique for EOS binary interaction parameters on the prediction of binary VLE data*, Computer Chemical Engineering, 20, 79-91.

Baba-Ahmed, A., Guilbot, P. and Richon D. (1999). *New equipment using a static analytic method for the study of vapour–liquid equilibria at temperatures down to 77 K*, Fluid Phase Equilibria (166) 225–236.

Barker, J.A., (1953). *Determination of Activity Coefficients from Total Pressure Measurements.* Australian Journal of Chemistry, *6*, 207-210.

Baudilio, C., van Grieken, R., José, L., Peña, L., Juan, J., Espada L., (2006). *A generalized model to predict the liquid–liquid equilibrium in the systems of furfural + lubricating oils,* Chemical Engineering Science, 61, 8028–8039.

Bell, S., 1999 A *Beginner's Guide to Uncertainty of Measurement*, National Physical Laboratory, Teddington, Middlesex, United Kingdom, issue 2.

Biddiscombe, D.P. and Martin, J.F., (1958). *Vapour pressures of phenol and the cresols*, Trans. Faraday Soc., 54, 1316-1322.

Black, C. and Distler, D., (1972). *Dehydration of Aqueous Ethanol Mixtures by Extractive Distillation. Extractive and azeotropic distillation*. Advances in chemistry series, 115, 1-15.

Black, C., (1980). *Distillation modeling of ethanol recovery and dehydration processes for ethanol and gasohol*. Chemical Engineering Progress, 76, 78-85.

Breil, M.P., Tsivintzelis, I.M., and Kontogeorgis, G., (2010). *Modeling of phase equilibria with CPA using the homomorph approach*, Fluid Phase Equilibria.

Cabezas, J.L. and Coca, S.B.J., (1991). *Isobaric vapor—liquid equilibrium data for furfural with chlorinated hydrocarbons*, Fluid Phase Equilibria, 62, 163-166.

Chan Hwang, I., Kwak, M. J. Y., Parkand, S., Han, K., (2007). *Isothermal VLE and VE at 303.15 K for the Binary and Ternary Mixtures of Di-isopropyl Ether (DIPE) + 1-Propanol + 2,2,4-Trimethylpentane* J. Chem. Eng. Data, 52, 2503-2508.

Chien-Bin SOO, (2011). *Experimental Thermodynamic Measurements of Biofuel-related Associating Compounds and Modeling using the PC-SAFT Equation of State*, École Nationale Supérieure des Mines de Paris.

Clifford, S.L., (2003). *Low-Pressure Vapour-Liquid Equilibrium and Molecular Simulation of Carboxylic acids*, Thesis (MSc), University of Natal, Durban, South Africa.

Cox, J.D., and Herington, E. F. G., Trans. (1956). Faraday Soc., 52, 926.

Daubert, T. E., Jalowka, J. W. and Goren, V., (1987). *Vapor pressure of 22 pure industrial chemicals*, AIChE Symp. Ser., 83(256), 128-156.

De Haan, A.B., (1995). *Vapor-Liquid Equilibria and Excess Enthalpies for Octane +N-Methylacetamide, Cyclooctane + N-Methylacetamide, and Octane + Acetic Anhydride at 125 ^{o}C,* J. Chem. Eng. Data, 40**,** 1228-1232.

Dohrn R., Christov M., *High-Pressure Fluid-Phase Equilibria: Experimental Methods and Systems Investigated (1994-1999),* Fluid phase equilibria, 202, 153-218

Dohrn R., Fonseca J. M. S., Peper S., (2011), *High-Pressure Fluid-Phase Equilibria: Experimental Methods and Systems Investigated (2005-2008),* Fluid phase equilibria, 300, 1-69

Dortmund Data Bank, Purchased, (2009). *DDBST Software and Separation Technology GmbH*, Oldenburg.

Doherty M. F., (2008). *Azeotropic distillation*, in AccessScience, ©McGraw-Hill Companies, http://www.accessscience.com

Economou, I. G., and Donohue, M. D., (1875). *Chemical, Quaichemical and Perturbation Theories for Associating Fluids*, AIChE J, 37.

Emel'yanenko, V. N., Dabrowska, A., Verevkin, S. P., Hertel, M. O., Scheuren, H., Sommer, K., (2007). *Vapor Pressures, Enthalpies of Vaporization, and Limiting Activity Coefficients in Water at 100 deg C of 2-Furanaldehyde, Benzaldehyde, Phenylethanal, and 2-Phenylethanol*,J. Chem. Eng. Data, 52, 468-471.

Fakhr Hoseini, S.M., Tavakkoli, T., and Hatamipour, M.S., (2009). *Extraction of aromatic hydrocarbons from lube oil using n-hexane as a co-solvent*, Separation and Purification Technology, 66, 167–170.

Fele, L. and Grilc, V., (2003). *Separation of Furfural from Ternary Mixtures*, J. Chem. Eng. Data, 48, 564-570.

Fischer, K., and Gmehling, J., (1994). *P-x- y and γ^{∞} Data for the Different Binary Butanol-Water Systems at 50 ^{o}C.* J. Chem. Eng. Data, 39,309-315.

Gess, M.A., Danner, R.P., and Nagvekar, M., (1991). *Thermodynamic Analysis of Vapor-Liquid Equilibria: Recommended Models and a Standard Data Base*, Design Institute for Physical Property Data, American Institute of Chemical Engineers.

Ghanadzadeh, H., Ghanadzadeha, A., Bahrpaimaa, K.H., (2009). *Measurement and prediction of tie-line data for mixtures of (water + 1-propanol + diisopropyl ether): LLE diagrams as a function of temperature*, Fluid Phase Equilibria, 277, 126–130.

Gill I.D., Uyazán A.M., Aguilar. J.L., Rodríguez G. and. Caicedo L.A., (2005). S*imulation of ethanol extractive distillation with a glycols mixture as entrainer*, National University of Colombia.

Gillespie, D T C, (1946), *Vapour-Liquid Equilibrium Still for Miscible Liquids*, Industrial and Engineering Chemistry, Analytical, Vol. 18, pp. 575-577.

Gomis, V., Rulz, F., Asensi, J.C. and Saquete, M.D., *(*1997). *Procedure for checking and fitting experimental liquid-liquid equilibrium data*, Fluid Phase Equilibria, 129, 15-19.

Gross, J. and Sadowski, G., (2001). *Perturbed-Chain SAFT: As Equation of State Based on a Perturbation Theory for Chain Molecules*. Industrial and Engineering Chemistry Research, 40, 1244-1260.

Gui, H., Ming, L., Ho, L., (2002). *Liquid–liquid equilibria of ternary mixtures of water + 2-propanol with ethyl acetate, isopropyl acetate, or ethyl caproate*, Fluid Phase Equilibria, 202, 239–252.

Guthrie, G.B., Scott, D.W., Hubbard, W.N., Katz, C., McCullough, J.P., Gross, M.E., Williamson, K.D. and Waddington, G., (1952). *Thermodynamic properties of Furan*, J. Am. Chem. Soc., 74, 4662-9.

Hála, E., Pick, J., Fried, V., and Villim, O., (1967). *Vapour-Liquid Equilibrium, 2nd edition*, Pergamon Press, Oxford.

Harris, R.A., (2004). *Robust Equipment for the Measurement of Vapour-Liquid Equilibrium at High Temperatures and High Pressures.* Thesis (PhD), University of Kwazulu-Natal, Durban, South Africa,

Hauschild, T., Wu, H.S., Sandler, S.I., (1987). *Vapor-Liquid Equilibrium of the Mixtures 2-Furaldehyde/1-Butanol and 2-Furaldehyde/4-methyl-2-pentanone*,J. Chem. Eng. Data, 32, 226.

Hayden, J.G., and O'Connell, J.P., (1975). *A Generalised Method for Predicting Second Viral Coefficients*, Industrial and Engineering Chemistry. Process Design and Development, 14, 209-216.

Hefter, G.T., Barton, A.F.M., and Chand, A., (1991). J. Chem. Eng.Soc. Faraday Trans. 87,591-596.

Hill, A.E., (1923). J. Chem. Soc. 45, 1143-1155, as cited by Weir and De Loos, 2005.
Holderbaum, T., and Gmehling, J., (1991). Fluid phase equilibria, 70, 251-265.

Huanga, H., Ramaswamy, S., Tschirner, U.W. and Ramaraob, B.V., (2008). *A review of separation technologies in current and future biorefineries*, Separation and Purification Technology, University of Minnesota, 62,1–21.

Hung, Y. C., Ming, L., and Ho-mu Lin, L., (2008).*Vapor-Liquid Phase Boundaries of Binary Mixtures of Carbon Dioxide with Ethanol and Acetone*, J. Chem. Eng. Data, National Taiwan University of Science and Technology, 53, 2393–2402.

Iwarere, S.A., (2010). *Measurement of Phase Equilibria for Oxygenated Hydrocarbon Systems*. Thesis (MSc), University of KwaZulu-Natal, Durban, South Africa.

Joseph, M.A., Raal, J.D., and Ramjugernath, D., (2001). *Phase equilibrium properties of binary systems with diacetyl from a computer controlled vapour–liquid equilibrium still*, Fluid Phase Equilibria, 182, 157–176.

Kahlbaum, G. W. A., (1898). *Studies on Vapor Pressure Measurements: II, Z.* Phys. Chem., Stoechiom. Verwandtschaftsl., 26, 577-658.

Kneisl, P., Zondlo, J.W., and Whiting, W.B., (1989). *The Effect of Fluid Properties on Ebulliometer Operation.* Fluid Phase Equilibria, 46, 85-94.

Kolbe, B., and Gmehling, J., (1985). *Thermodynamic Properties of Ethanol + Water I. Vapour-Liquid Equilibria Measurement from 90 to 150 "C by the Static Method,* Fluid Phase Equilibria, 23, 213-226.

Kolyuchkina, G. Y., Ponomarev, V. N., Timofeev, V. S., (1975). *Phase equilibria in saturated hydrocarbons + furfural systems.* Izv. Vyssh. Uchebn. Zaved., Khim. Khim. Tekhnol., 18, 1582-1585.

Kovack III, J .W. and Seider, W. S., (1987). *Heterogeneous Azeotropic Distillation: Experimental and Simulation Results ,* AIChE Journal. 33(8), 1300- 1314.

Laroche, L (1991). *Homogeneous azeotropic distillation : entrainer selection.* Dissertation (Ph.D.), California Institute of Technology.

Laugier S., and Richon D.,(1986) *New apparatus to perform fast determinations of mixture vapor-liquid equilibria up to 10 MPa and 423 K*. Rev. Sci. Instrum., 57, 469-472.

Lee, L-s., and Shen H-c., (2003). *Azeotropic Behavior of a Water + n-Propanol + Cyclohexane Mixture Using Cyclohexane as an Entrainer for Separating the Water + n-Proponal Mixture at 760 mmHg*. Ind. Eng. Chem. Res. 42, 5905-5914

Lewis, G.N., and Randall, M., (1923).Thermodynamics and the Free Energy of Chemical Substances, McGraw-Hill, New York.

Lee, F., Pahl, R. (1985). *Solvent Screening Study and conceptual extractive distillation process to produce anhydrous ethanol from fermentation broth*. Industrial Engineering Chemical Process Des. Dev, 24, 168-172.

Li, Q., Xing, F., Lei, Z. ,Wang, B., and Chang, Q., (2008). *Isobaric Vapor–Liquid Equilibrium for Isopropanol + Water +1-Ethyl-3-methylimidazolium Tetrafluoroborate,* J. Chem. Eng. Data**,** 53, 275–279.

Lilwanth, H., (2011). *Vapour-Liquid Equilibrium Measurements at Low-to-Moderate Pressures using a Glass Recirculating Still,* MSc. Engineering (in progress), University of Kwa-Zulu Natal, Durban, South Africa.

Lladosa, E., Nelson, F. . Martínez, B,Juan. Montón., J, de la Torre, (2011).,*Measurements and correlation of vapour–liquid equilibria of 2-butanone and hydrocarbons binary systems at two different pressures,* Fluid Phase Equilibria 307,24–29.

Lohmann, J., Roepke, T., and Gmehling, J., 1998.J. Chem. Eng. Data, 43, 856-860.

Luyben, W. L. (2006). *Distillation Design and Control using ASPEN simulation*, John Wiley & Sons, Inc., Hoboken, New Jersey.

Malanowski, S. and Anderko, A., (1992). *Modelling Phase Equilibria: Thermodynamic Background and Practical Tools*. John Wiley, New York.

Meirelles, A., Weiss, S., Herfurth, H. (1992). *Ethanol dehydration by extractive distillation*. Journal Chemistry and Tech Biotechnology, 53, 181-188.

Michelsen, M.L., (1990). Fluid phase equilibria, 60, 213-219.

Narasigadu, C., (2006). *Phase Equilibrium Investigation of the Water and Acetonitrile Solvent with Heavy Hydrocarbons.* Dissertation (MSc). University of KwaZulu-Natal, Durban, South Africa.

Nothnagel, K.H., Abrams, D.S. and Prausnitz, J.M., (1973). *Generalized Correlation for Fugacity Coefficients in Mixtures at Moderate Pressures. Application of Chemical Theory of Vapor Imperfections.* Industrial and Engineering Chemistry Process Design and Development, 12(1), 25-35.

Novák, J.P., Matouš, J., and Pick, J., (1987). *liquid-liquid equilibria*, Elsevier, Amsterdam.

Passarello J.-P., NguyenHuynh D., de Hemptinne J.-C., Tobaly P., (2011), *Extention of polar GC-SAFT to systems containing some oxygenated compounds: application to ethers, aldehydes and ketones*, Fluid Phase Equilibria, 307, 142-159.

Perry, R.H. and Green, D.W., (1998). *Perry's Chemical Engineers' Handbook.7th Edition*. McGraw-Hill, New York.

Philip, L., Jackson, L., Richard, A., (1995). *Wilsak, Thermodynamic consistency tests based on the Gibbs-Duhem equation applied to isothermal, binary vapor-liquid equilibrium data*, Fluid Phase Equilibria, 103, 155-197.

Pillay, J.C., (2010). *Measurement of Binary Vapour-Liquid Equilibria For Oxygen Containing Compounds.* Thesis (MSc), University of KwaZulu-Natal, Durban, South Africa.

Poling, B.E., Prausnitz, J.M. and O'Connell, J.P., (2001). *The Properties of Gases and Liquids*. 5th Edition. New York: McGraw-Hill.

Prikhodko, I.V., Letcher, T. M., and de Loos, T.W., (1997). *Liquid-Liquid Equilibrium Modeling of Ternary Hydrocarbon +Water + Alkanol Systems*, Industrial and Engineering Chemistry Research, 36, 4391-4396.

Petrucci, R.H., Harwood, W.S., Herring, G.E., and Madura, J., (2006). *General Chemistry*, 9th edition, Prentice Hall.

Raal, J.D., and Mühlbauer, A.L., (1994).*The Measurement of High Pressure Vapour-Liquid-Equilibria Part I Dynamic Methods*, Asia Pacific journal of chemical engineering, 2(2-3), 69-87.

Raal, J.D., and Mühlbauer, A.L., (1998). *Phase Equilibria: Measurement and Computation*. Taylor and Francis, Bristol, P. A.

Rackett, H.G., (1970). *Equation of State for Saturated Liquids.* J. Chem. Eng. Data, 15(4), 514-517.

Rattan, V.K., Baljinder, K., Gill, and Seema Kapoor, (2008)..*Isobaric Vapor-Liquid Equilibrium Data for Binary Mixture of 2-Methyltetrahydrofuran and Cumene,* World Academy of Science, Engineering and Technology 47.

Redlich, O. and Kister, A.T., (1948). *On the Thermodynamics of Solutions. IV. The Determination of Liquid-Vapor Equilibria by Measuring the Total Pressure.* Journal of the American Chemical Society, 71, 505-507.

Řehák, K., (1999). *Chem. Listy*, 93, 583-585.

Řehák, K., Voňka, P., and Dreiseitlová, J., (2005). Fluid Phase Equilibrium, 230,109-120.

Renon, H., and Prausnitz, J.M., (1968). *Local Compositions in Thermodynamic Excess Functions for Liquid Mixtures,* American Institute of Chemical Engineers Journal,14, 135-144.

Reddy, P., (2006). *Development of a Novel Apparatus for the Measurement of Vapour-Liquid Equilibria at Elevated Temperatures and Moderate Pressures*, Thesis(PhD), University of KwaZulu-Natal, Durban, South Africa.

Reid, C R, Prausnitz, J M, and Polling, B E, (1988). *The Properties of Gases and Liquids*, 4th Edition, McGraw Hill Book Company, Singapore.

Renewable Energy Policy Network for the 21st Century (REN21)., (2009), *Renewables global status report 2010*. France.

Rifai, I., and Durandet, J., (1962). *Rev. Inst. France di Petrol*, 17, 1232, as given by Novak *et al*. 1987.

Rogalski and Malanowski, 5 (1980), Fluid Phase Equilib. 97-112

Sandler, S.I., (1999). *Chemical and Engineering Thermodynamics*, 3rd Edition John Wiley and Sons, New York.

Schneider, G.M., (1976). Pure applied Chemistry, 47,277-291.

Schmidt1, K.A.G., Maham, Y.,and Mather, A.E., (2007). *Use of the NRTL equation for simultaneous correlation of vapour-liquid equilibria and excess enthalpy applications to aqueous alkanolamine systems*, Journal of Thermal Analysis and Calorimetry, 89, 1, 61–72.

Sebastiani, E., and Lacquaniti, L., (1967). *Acetic Acid-Water System Thermodynamical Correlation of Vapor-Liquid Equilibrium Data*. Chemical Engineering Science, 22, 1155-1162.

Singh Nigam, P., Singh, A., (2011). *Production of liquid biofuels from renewable resources, Progress in Energy and Combustion Science*, University College Cork, Ireland, 37, 52-68.

Smith, J.M., Van Ness, H.C., and Abbott, M.M., (2001). *Introduction to chemical engineering thermodynamics*, 6th edition, McGraw-Hill.

Smyth, C P (1955), "Dipole Moment and Molecular Structure", CCP5 Quarterly, 4, 13 -25.

Soave, G., (1972). *Equilibrium Constants from a Modified Redlich-Kwong EOS.* Chemical Engineering Science, 39, 357.

Šobr, J., and Hynek, V., (1976). *Sci. Papers Prague inst. Chem. Technology*, 125-132.

Stoicescu C., Iulian O. and Isopescu R., (2010). *Liquid-Liquid Phase Equilibria Of (1-Propanol + Water + N-Alcohol) Ternary Systems At 294.15 K. 1-Propanol + Water + 1-Butanol Or 1-Pentanol Or 1-Hexanol.*, Revue Roumaine de Chimie

Su¨heyla, C., Dilek O¨ zmen Umur Dramur, E., (2006). *(Liquid + liquid) equilibria of (water + 1-propanol + solvent)*, Fluid Phase Equilibria, Istanbul University, 239, 150 – 160.

Tsonopoulos, C., (1974). "*An Empirical Correlation of the Second Viral Coefficients*," American Institute of Chemical Engineers Journals, 20, 263-272.

Tan R.R and Culaba A.B., (2004) *Life-Cycle Assessment of Conventional and Alternative Fuels for Road Vehicles*. Manila.

Udeye V., Mopoung S., Vorasingha A. and Amornsakchai P., (2009). *Ethanol heterogeneous azeotropic distillation design and construction*, International Journal of Physical Sciences Vol. 4 (3), pp. 101-106.

Van Ness, H.C., (1995). Thermodynamics *in the Treatment of Vapor/Liquid Equilbria (VLE) Data*. Pure and Applied Chemistry, 67(6), 859-872.

Van Ness, H.C., and Abbott, M.M., (1982). *Classical Thermodynamics of Non-electrolyte Solutions: With Applications to Phase Equilibria*. McGraw-Hill, New York.

Van Ness, H.C., Byer, S.M., and Gibbs, R.E., (1973).*Vapour-Liquid Equilibrium: Part I. An Appraisal of Data Reduction Methods*. American Institute of Chemical Engineers Journal, 19, 238-244.

Vorenberg, D. G., Raal, J. D., and Ramjugernath, D., (2005). *Vapor-Liquid Equilibrium Measurements of MTBE and TAME with Toluene*,J. Chem. Eng. Data,50, 56-59.

Walas, S M., (1985). "Phase Equilibrium in Chemical Engineering", Butterworth, Boston.

Wilson, G.M., (1964). *Vapor-Liquid Equilibrium. XI. A New Expression for the Excess Free Energy of Mixing*. Journal of the American Chemical Society, 86, 127-130.

Wolbach, J.P., and Sandler, S.I., (1997). *Using Molecular Orbital Calculations to Describe the Phase Behavior of Hydrogen-Bonding Fluids*. Industrial and Engineering Chemistry Research, 36, 4041-4051.

Yang, C., Xu, W., Peisheng, M., (2004). *Excess Molar Volumes and Viscosities of Binary Mixtures of Dimethyl Carbonate with Chlorobenzene, Hexane, and Heptane*. J. Chem. Eng. Data 49,1802-1808.

APPENDIX A

EXPERIMENTAL ACTIVITY COEFFICIENTS AND RELATIVE VOLATILITY

Table A-1: Experimental activity coefficient and relative volatility data for diisopropyl ether (1) + propan-1-ol (2) system at 333.15 K, 353.15 K and 373.15 K.

P±0.23/kPa	x_1	y_1	γ_1	γ_2	α_{12}
20.3	0.0012	0.0100	2.2990	0.9887	8.4074
20.6	0.0025	0.0220	2.4582	0.9904	8.9755
21.3	0.0065	0.0556	2.4738	0.9944	8.9986
23.0	0.016	0.1234	2.4030	1.0046	8.6574
25.4	0.0316	0.2166	2.3527	1.0062	8.4731
28.9	0.0565	0.3279	2.2602	1.0070	8.1471
33.8	0.0917	0.4423	2.1898	1.0142	7.8555
38.5	0.1265	0.5296	2.1611	1.0139	7.7742
42.1	0.1596	0.5799	2.0444	1.0276	7.2686
45.5	0.194	0.6223	1.9470	1.0409	6.8452
49.0	0.241	0.6618	1.7904	1.0652	6.1628
51.8	0.2726	0.6868	1.7344	1.0882	5.8513
54.8	0.31	0.7147	1.6748	1.1046	5.5758
59.5	0.3919	0.7518	1.5076	1.1825	4.7000
64.6	0.5056	0.8087	1.3610	1.2185	4.1337
67.5	0.583	0.835	1.2712	1.3024	3.6197
70.4	0.6878	0.861	1.1557	1.5277	2.8116
73.1	0.7827	0.8903	1.0894	1.8014	2.2532
74.9	0.8512	0.9155	1.0541	2.0778	1.8940
75.9	0.8945	0.9333	1.0356	2.3459	1.6503
76.5	0.9597	0.9697	1.0099	2.8158	1.3439
353.15 ±0.02/K					
56.9	0.011	0.061	2.284	0.999	5.841
61.6	0.027	0.140	2.129	1.061	5.866
70.4	0.061	0.259	2.046	1.067	5.380
77.4	0.097	0.361	1.954	1.086	5.259
82.4	0.124	0.415	1.791	1.068	5.012
89.9	0.172	0.485	1.768	1.072	4.534
97.3	0.205	0.529	1.670	1.086	4.356

106.0	0.268	0.602	1.582	1.117	4.131
116.9	0.339	0.657	1.427	1.114	3.735
128.9	0.461	0.735	1.248	1.168	3.243
139.5	0.611	0.791	1.099	1.216	2.410
144.1	0.764	0.845	1.053	1.433	1.684
145.6	0.839	0.880	1.009	1.806	1.407
144.7	0.920	0.930	0.998	2.070	1.155
373.15 ±0.02/K					
128.4	0.0256	0.1014	0.1014	2.2327	4.2951
144.9	0.0591	0.2167	0.2167	2.2029	4.4044
160.5	0.1015	0.3287	0.3287	2.1145	4.3345
176.1	0.1485	0.3985	0.3985	1.9862	3.7988
191.6	0.2051	0.4694	0.4694	1.8244	3.4286
208.5	0.2783	0.5383	0.5383	1.6336	3.0235
220.1	0.3459	0.5918	0.5918	1.4866	2.7415
235.1	0.4375	0.6563	0.6563	1.3319	2.4551
247.2	0.5756	0.7187	0.7187	1.1743	1.8838
254.9	0.7636	0.8086	0.8086	1.0536	1.3079
255.4	0.7746	0.8187	0.8187	1.0489	1.3140
255.1	0.9414	0.9358	0.9358	1.0035	0.9073
253.0	0.9518	0.9464	0.9464	1.0024	0.8942

Table A-2: Experimental activity coefficient and relative volatility data for water (1) + propan-1-ol (2) system at 358.15 K, 368.15 K.

P/kPa	x_1	y_1	γ_1	γ_2	α_{12}
358.15 ±0.02/K					
69.3	0.051	0.130	3.066	1.004	2.812
73.1	0.080	0.188	2.969	1.018	2.684
77.3	0.125	0.267	2.829	1.021	2.548
83.2	0.207	0.373	2.559	1.037	2.269
86.5	0.274	0.432	2.340	1.063	2.022
89.3	0.354	0.479	2.068	1.131	1.679
90.9	0.433	0.510	1.832	1.233	1.364
91.8	0.527	0.557	1.656	1.351	1.125
91.8	0.580	0.566	1.531	1.491	0.942
91.7	0.645	0.579	1.406	1.707	0.756
90.0	0.881	0.613	1.070	4.597	0.214
85.6	0.948	0.647	1.000	9.131	0.101
80.4	0.969	0.694	0.986	12.426	0.073

72.6	0.984	0.780	0.988	16.160	0.056
368.15 ±0.02/K					
103.1	0.054	0.134	3.062	1.010	2.745
108.9	0.092	0.210	2.950	1.012	2.636
115.7	0.141	0.288	2.778	1.024	2.452
121.0	0.191	0.348	2.604	1.039	2.265
126.5	0.266	0.418	2.343	1.068	1.983
129.3	0.304	0.461	2.308	1.067	1.954
132.2	0.409	0.502	1.913	1.184	1.460
133.6	0.504	0.541	1.684	1.317	1.156
133.6	0.589	0.566	1.511	1.499	0.911
133.4	0.635	0.574	1.418	1.658	0.773
132.9	0.691	0.587	1.328	1.891	0.635
128.7	0.908	0.622	1.037	5.658	0.166
122.3	0.956	0.661	0.995	9.944	0.091
110.8	0.978	0.741	0.989	13.905	0.065

Table A-3: Experimental activity coefficient and relative volatility data for furan (1) + n-hexane (2) system at 101.3 kPa.

T±0.01/K	x_1	y_1	γ_1	γ_2	α_{12}
338.43	0.028	0.121	1.524554	1.00767	4.7786
335.98	0.049	0.206	1.58298	1.003874	5.0354
332.85	0.078	0.304	1.598428	1.002604	5.1630
329.37	0.117	0.408	1.577159	0.997721	5.2013
325.05	0.172	0.52	1.550635	0.998073	5.2151
319.59	0.267	0.646	1.464903	1.00724	5.0098
316.37	0.349	0.719	1.38064	1.012262	4.7729
313.94	0.424	0.759	1.297705	1.074004	4.2784
311.81	0.493	0.798	1.258736	1.108796	4.0627
310.26	0.567	0.828	1.196054	1.173557	3.6763
309.06	0.639	0.847	1.130674	1.312012	3.1275
307.66	0.715	0.874	1.09389	1.446312	2.7649
306.26	0.813	0.908	1.049109	1.702273	2.2701
305.69	0.856	0.924	1.034354	1.868772	2.0453
305.36	0.905	0.939	1.005794	2.304628	1.6159
304.94	0.968	0.978	0.993945	2.512003	1.4696
304.72	0.991	0.992	0.992452	3.277937	1.1261

Table A-4: Experimental activity coefficient and relative volatility data for furan (1) + methylbenzene (2) system at 101.3 kPa.

T±0.01/K	x_1	y_1	γ_1	γ_2	α_{12}
305.00	0.9950	0.9960	0.9827	13.4360	1.2513
305.98	0.9580	0.9950	0.9851	1.9086	8.7244
308.67	0.8690	0.9890	0.9835	1.1875	13.5536
312.33	0.7580	0.9810	0.9886	0.9400	16.4840
318.02	0.6100	0.9660	1.0058	0.8131	18.1649
320.78	0.5520	0.9580	1.0109	0.7776	18.5121
324.67	0.4810	0.9450	1.0163	0.7483	18.5392
330.13	0.4140	0.9270	0.9866	0.7070	17.9744
334.07	0.3530	0.9010	1.0058	0.7465	16.6809
336.59	0.3260	0.8880	1.0012	0.7374	16.3922
340.60	0.2890	0.8670	0.9899	0.7163	16.0376
348.26	0.2070	0.7920	1.0361	0.7685	14.5870
352.97	0.1680	0.7330	1.0519	0.8036	13.5959
357.97	0.1360	0.6650	1.0463	0.8263	12.6111
360.26	0.1250	0.6370	1.0340	0.8224	12.2837
363.12	0.1060	0.5770	1.0340	0.8592	11.5045
364.81	0.0980	0.5600	1.0453	0.8409	11.7143
369.97	0.0680	0.4410	1.0573	0.8875	10.8127
372.75	0.0450	0.3610	1.2300	0.9138	11.9894
375.47	0.0370	0.2890	1.1292	0.9330	10.5792
376.20	0.0360	0.2830	1.1197	0.9204	10.5692
377.88	0.0290	0.2140	1.0127	0.9558	9.1162

APPENDIX B

THERMODYNAMIC CONSISTENCY TEST

Point test results

Diisopropyl ether (1) + propan-1-ol (2) system

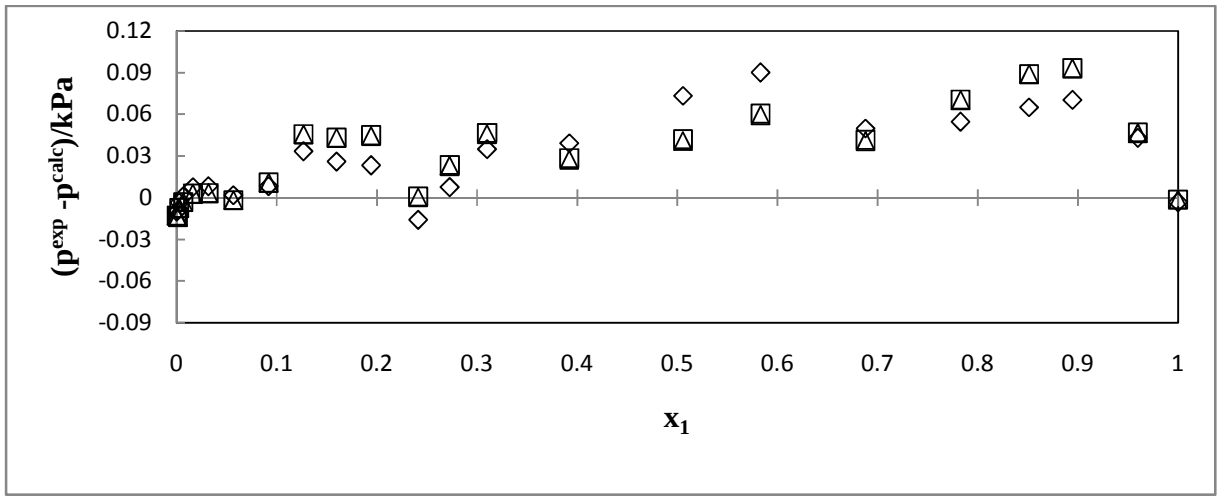

Figure B-1: Point test (varying EoS) pressure-residual for the diisopropyl ether (1) + propan-1-ol (2) system at 333.15K: ◊ PR-NRTL, □ HOC-NRTL, Δ NTH-NRTL.

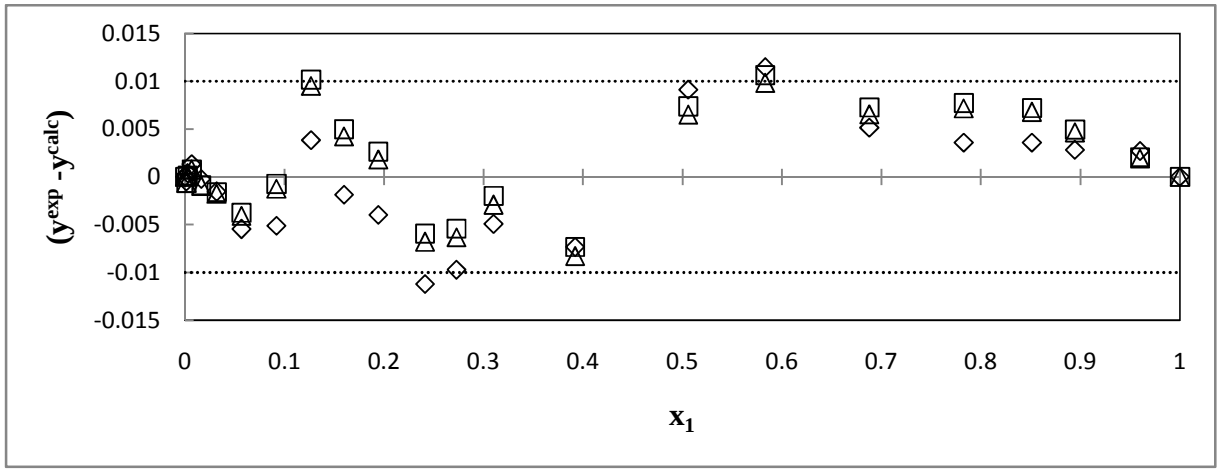

Figure B-2: Point test (varying EoS) Δy_1 for the diisopropyl ether (1) + propan-1-ol (2) system at 333.15K: ◊ PR-NRTL, □ HOC-NRTL, Δ NTH-NRTL.

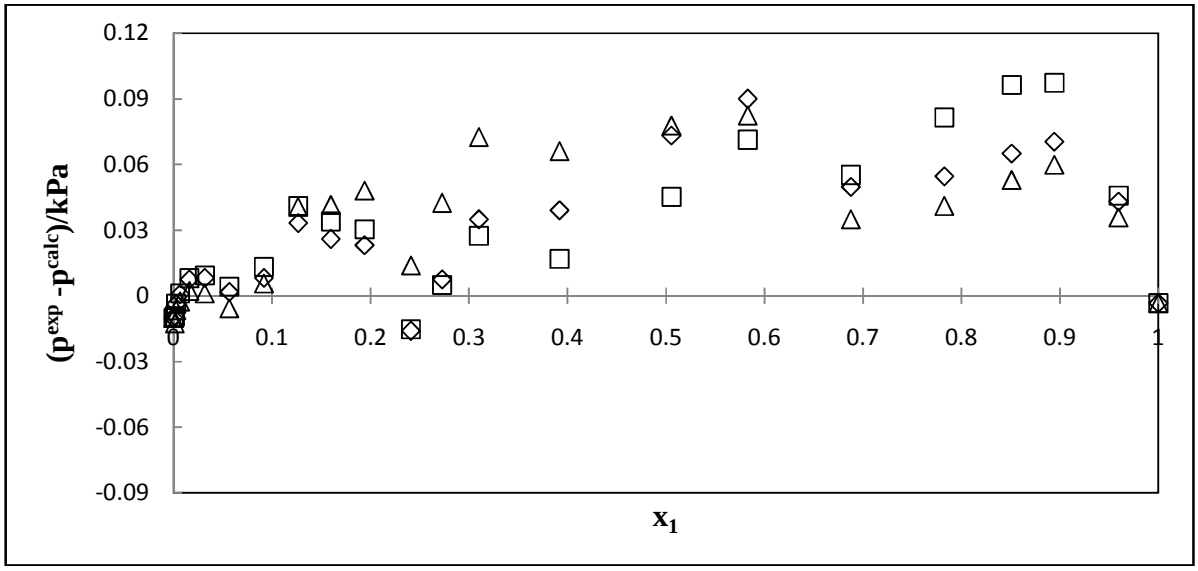

Figure B-3: Point test (varying activity coefficient model): pressure-residual for the diisopropyl ether (1) + propan-1-ol (2) system at 333.15K: ◊ PR-NRTL, □ PR-UNIQUAC, Δ PR-Wilson.

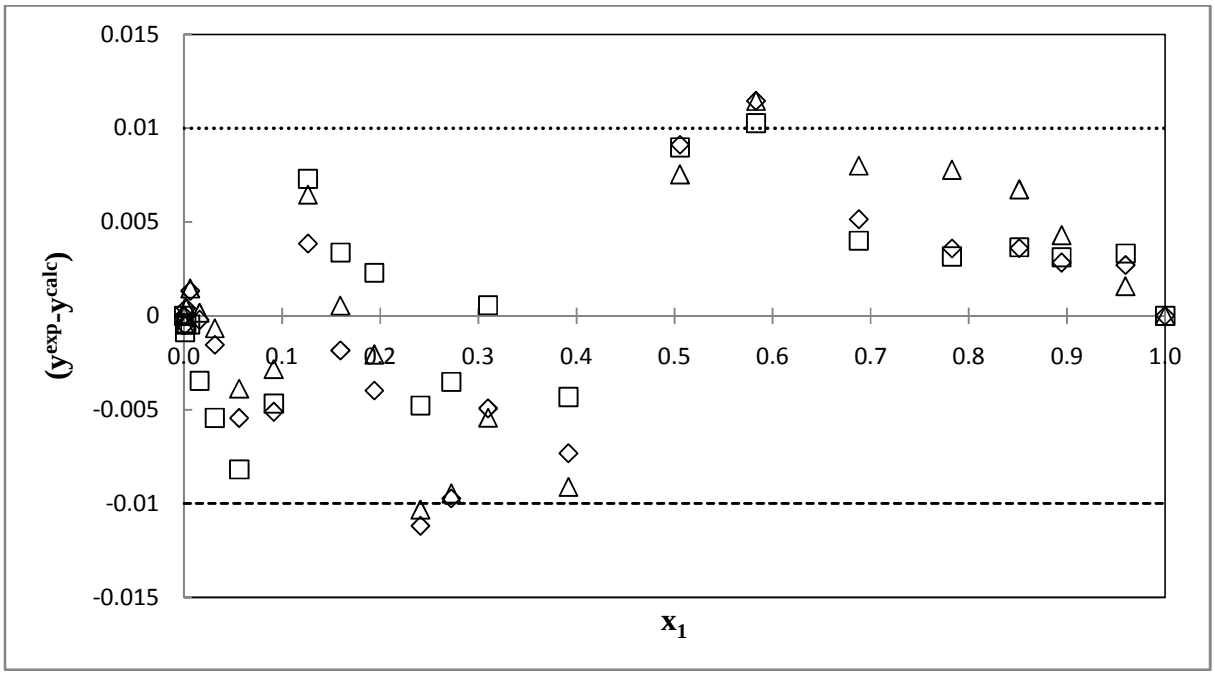

Figure B-4: Point test (varying activity coefficient model): Δy_1 for the diisopropyl ether (1) + propan-1-ol (2) system at 333.15 K: ◊ PR-NRTL, □ PR-UNIQUAC, Δ PR-Wilson.

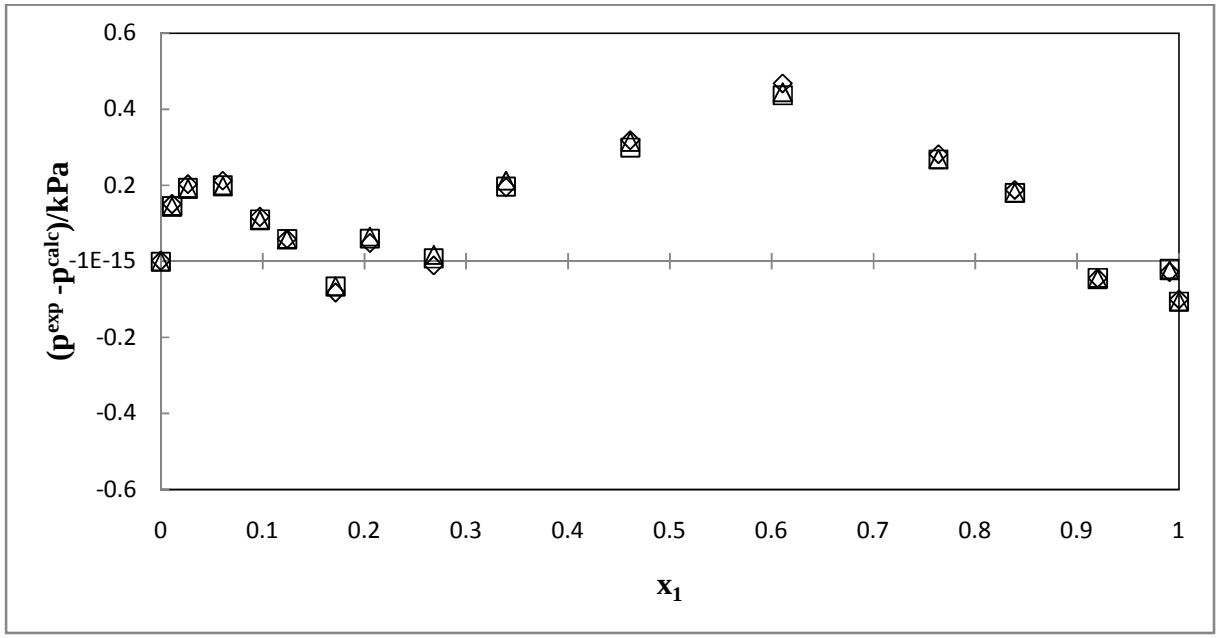

Figure B-5: Point test (varying EoS) pressure-residual for the diisopropyl ether (1) + propan-1-ol (2) system at 353.15 K: ◊ PR-NRTL, □ HOC-NRTL, Δ NTH-NRTL.

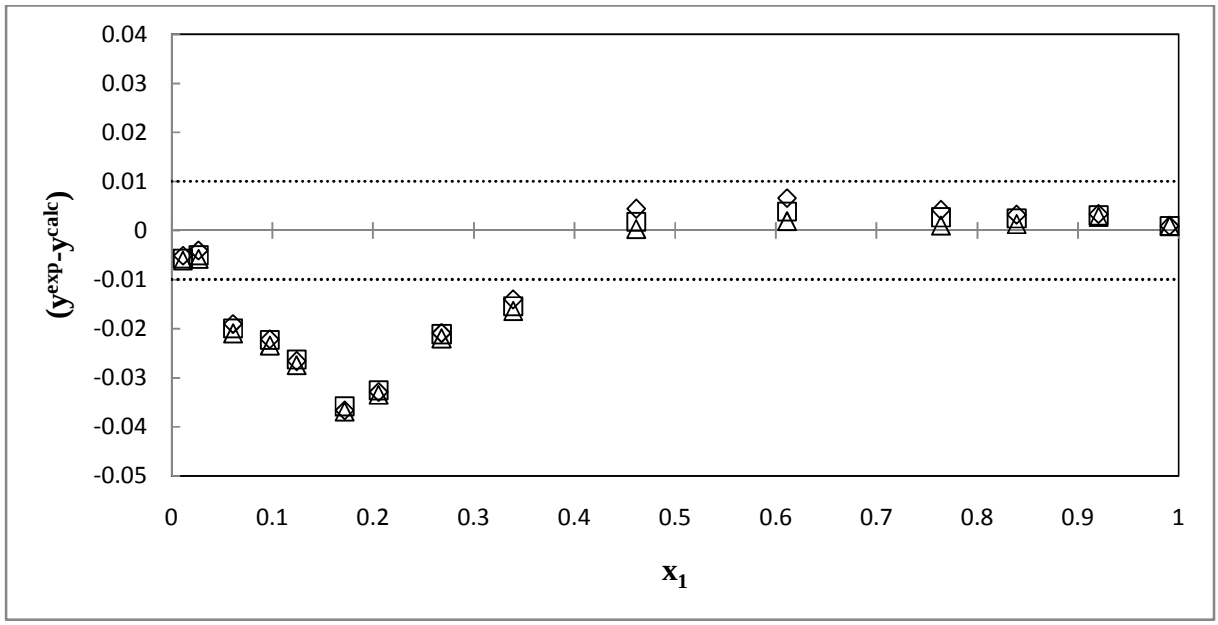

Figure B-6: Point test (varying EoS) Δy_1 for the diisopropyl ether (1) + propan-1-ol (2) system at 353.15 K: ◊ PR-NRTL, □ HOC-NRTL, Δ NTH-NRTL: ◊ PR-NRTL, □ PR-UNIQUAC, Δ PR-Wilson.

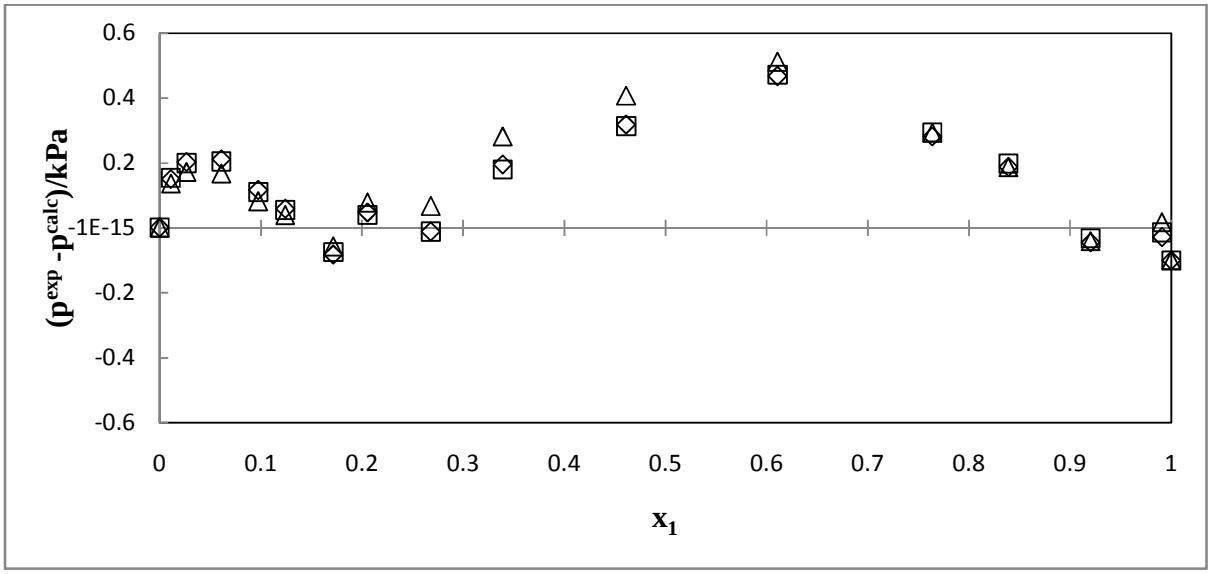

Figure B-7: Point test (varying activity coefficient model) pressure-residual for the diisopropyl ether (1) + propan-1-ol (2) system at 353.15 K: ◊ PR-NRTL, □ PR-UNIQUAC, Δ PR-Wilson.

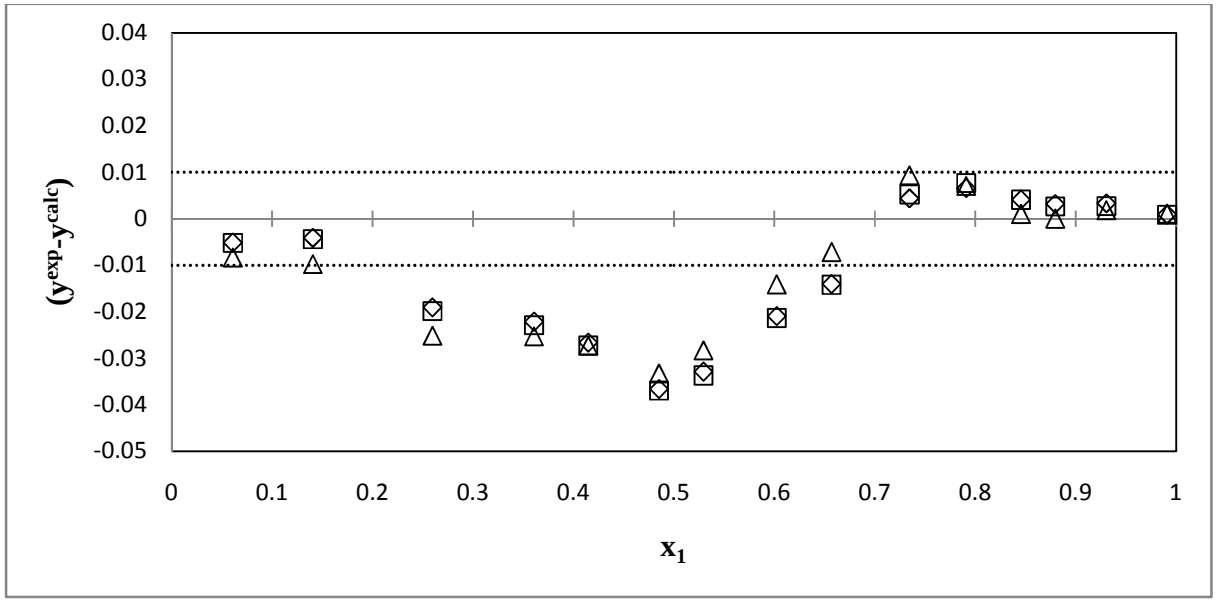

Figure B-8: Point test (varying activity coefficient model) Δy_1 for the diisopropyl ether (1) + propan-1-ol (2) system at 353.15 K: ◊ PR-NRTL, □ PR-UNIQUAC, Δ PR-Wilson.

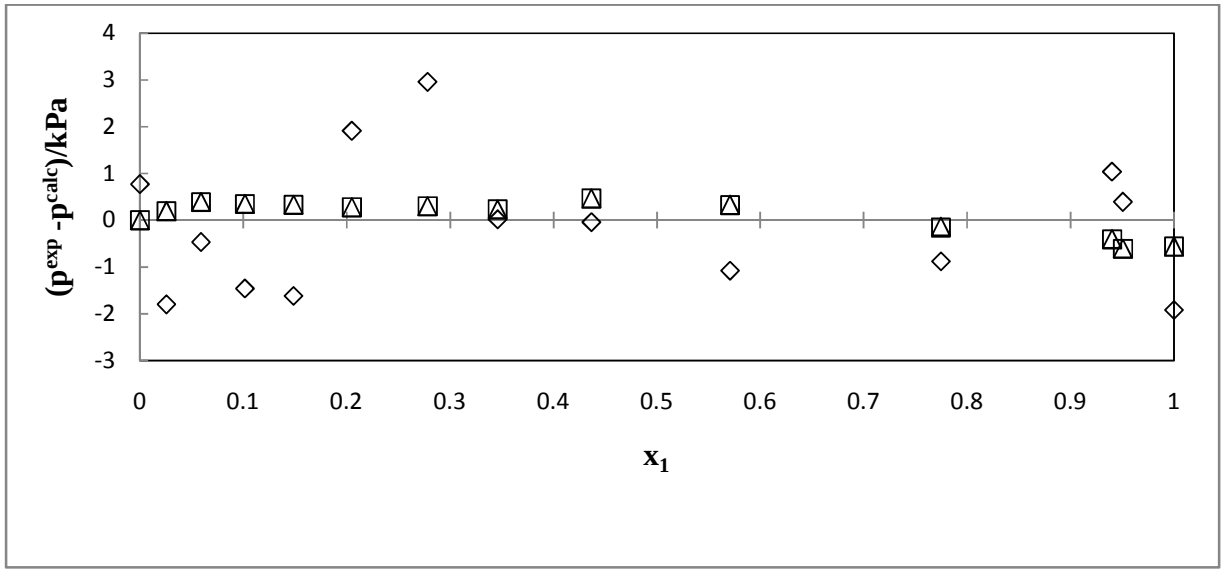

Figure B-9: Point test (varying EoS) pressure-residual for the diisopropyl ether (1) + propan-1-ol (2) system at 373.15 K: ◊ PR-NRTL, □ HOC-NRTL, Δ NTH-NRTL.

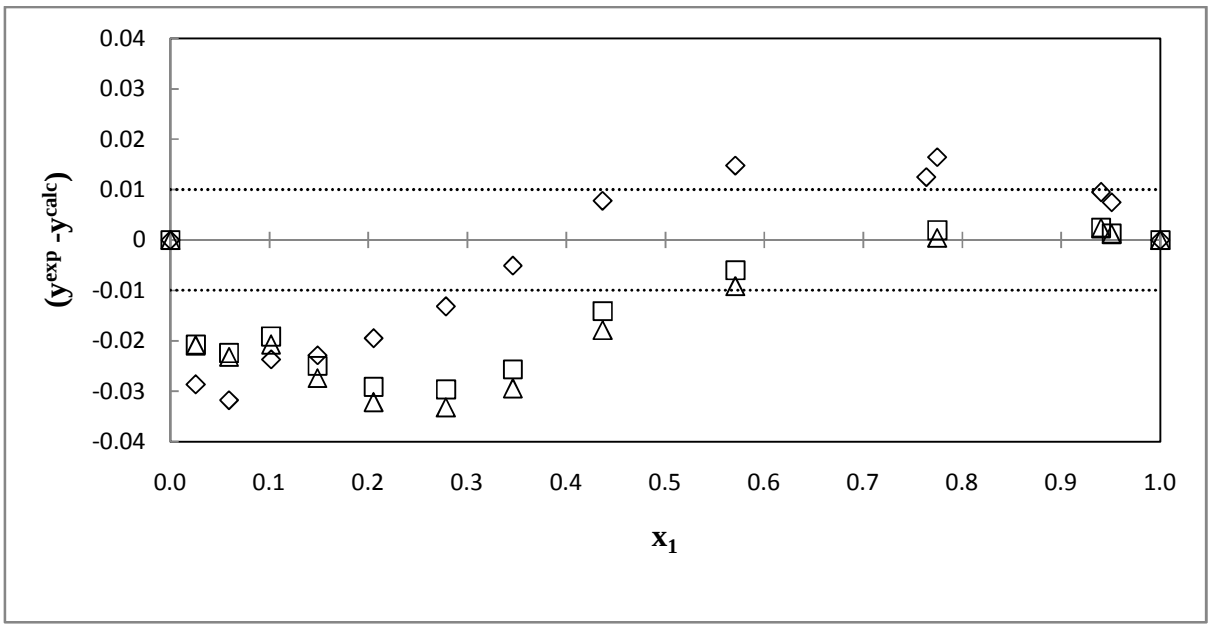

Figure B-10: Point test (varying EoS) Δy_1 for the diisopropyl ether (1) + propan-1-ol (2) system at 373.15 K: ◊ PR-NRTL, □ HOC-NRTL, Δ NTH-NRTL.

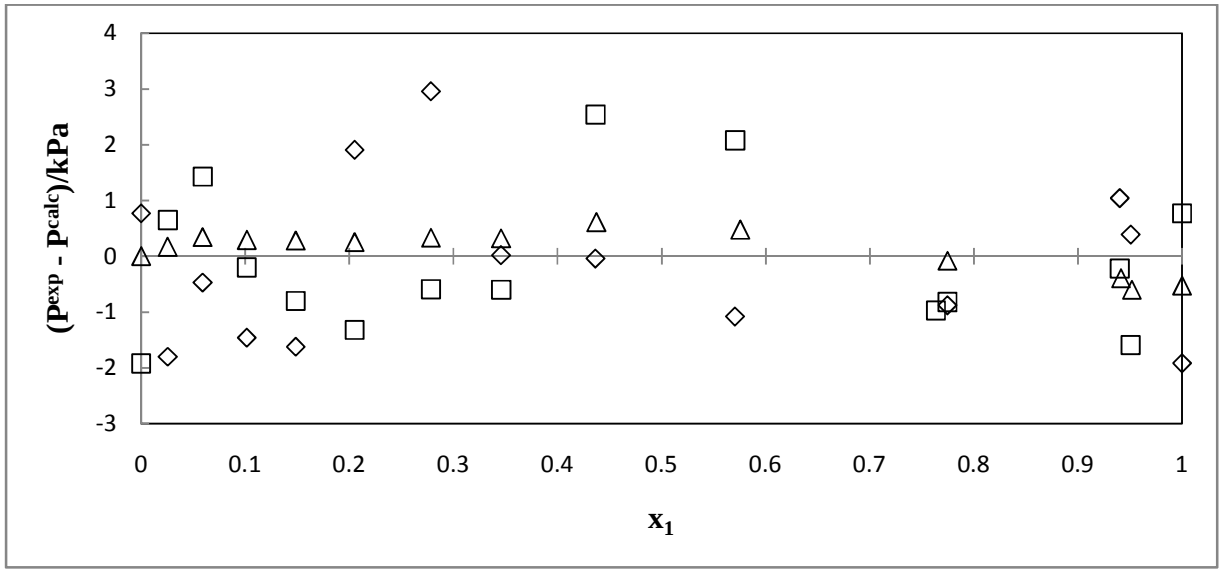

Figure B-11: Point test (varying activity coefficient model) pressure-residual for the diisopropyl ether (1) + propan-1-ol (2) system at 373.15 K: ◊ PR-NRTL, □ PR-UNIQUAC, Δ PR-Wilson.

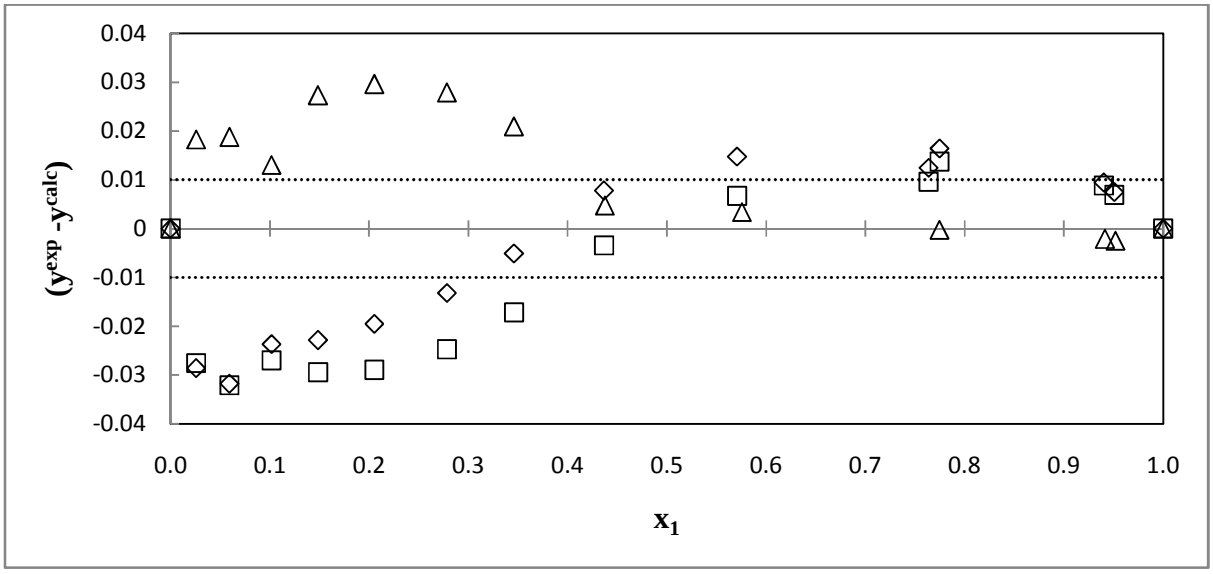

Figure B-12: Point test (varying activity coefficient model) Δy_1 for the diisopropyl ether (1) + propan-1-ol (2) system at 373.15 K: ◊ PR-NRTL, □ PR-UNIQUAC, Δ PR-Wilson.

Water (1) + propan-1-ol (2) System

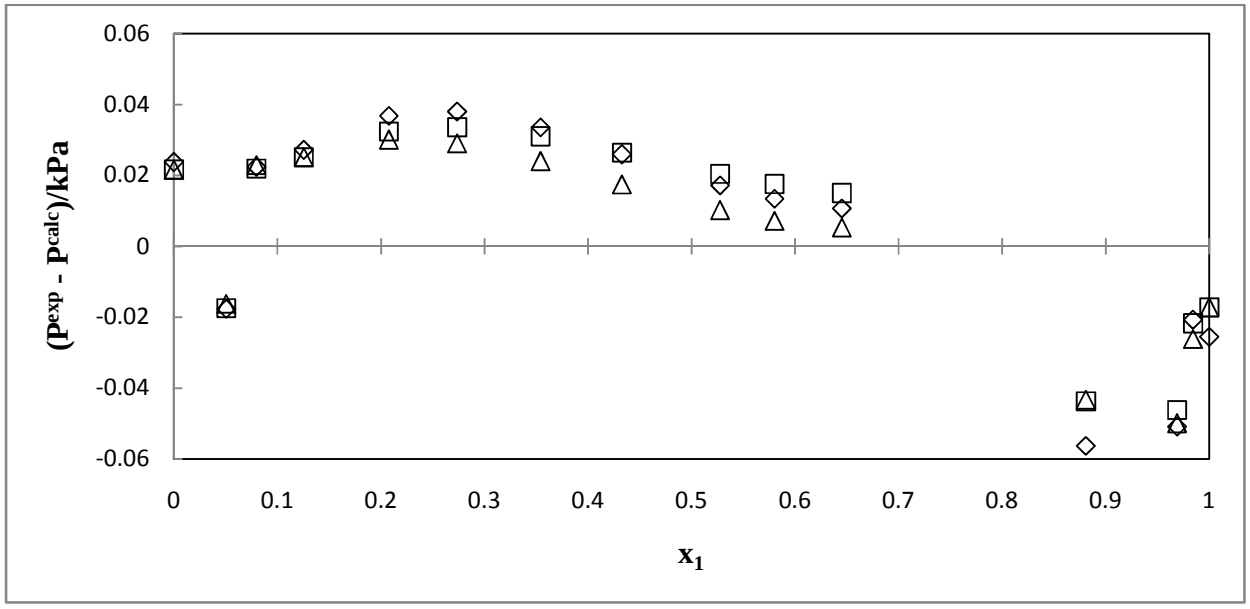

Figure B-13: Point test (varying EoS) pressure-residual for the water (1) + propan-1-ol (2) system at 358.15 K: ◊ PR-NRTL, □ HOC-NRTL, Δ NTH-NRTL.

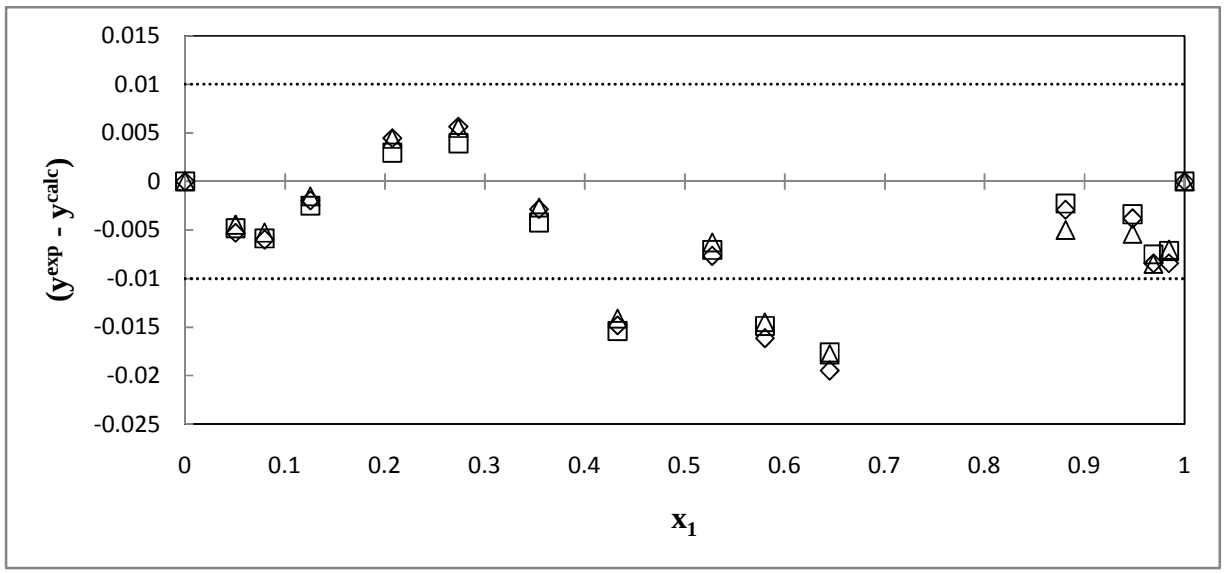

Figure B-14: Point test (varying EoS) Δy_1 for the water (1) + propan-1-ol (2) system at 358.15 K: ◊ PR-NRTL, □ HOC-NRTL, Δ NTH-NRTL.

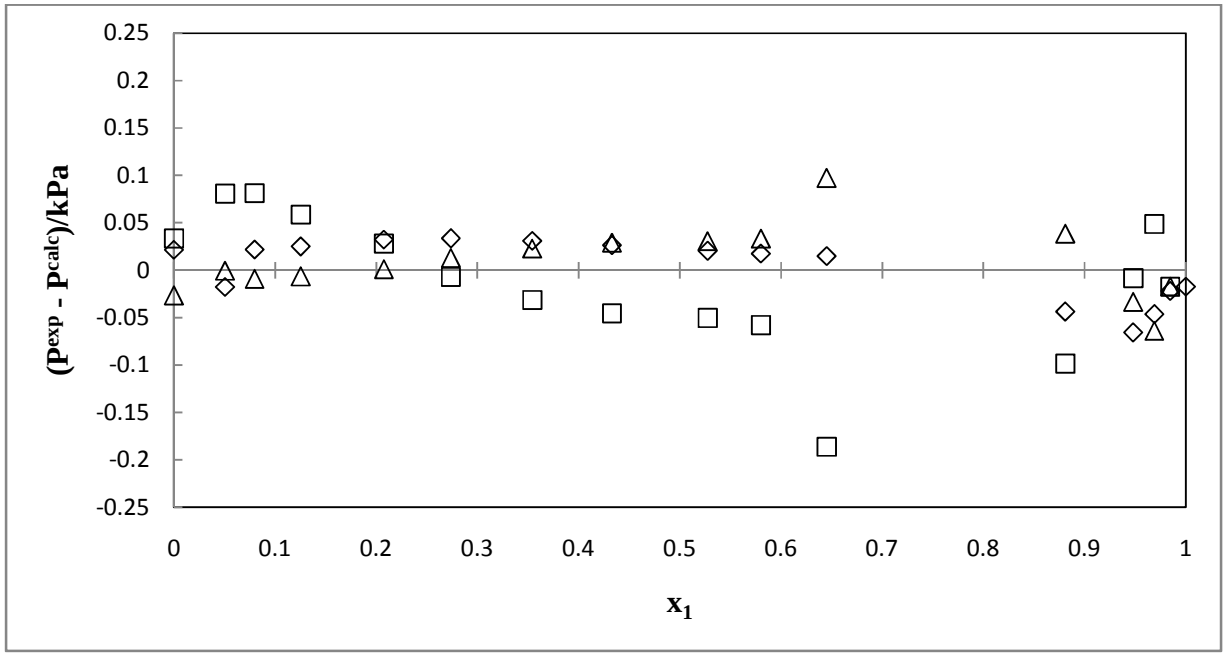

Figure B-15: Point test (varying activity coefficient model) pressure-residual for the water (1) + propan-1-ol (2) system at 358.15 K: ◊ HOC-NRTL, □ HOC-UNIQUAC, Δ HOC-Wilson.

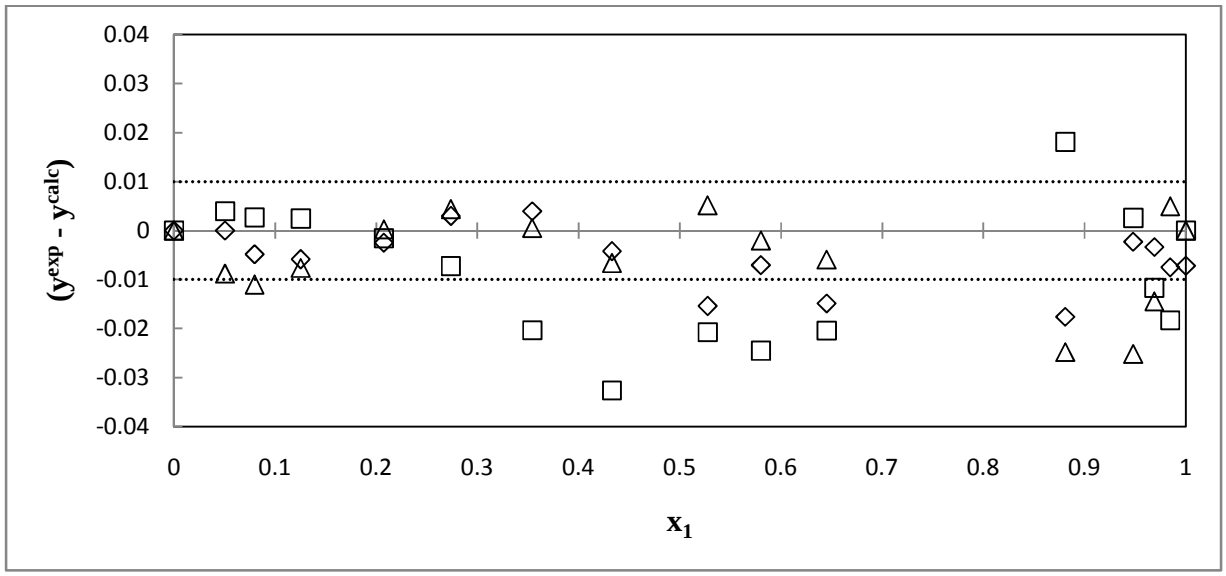

Figure B-16: Point test (varying activity coefficient model) Δy_1 for the water (1) + propan-1-ol (2) system at 358.15 K: ◊ HOC-NRTL, □ HOC-UNIQUAC, Δ HOC-Wilson.

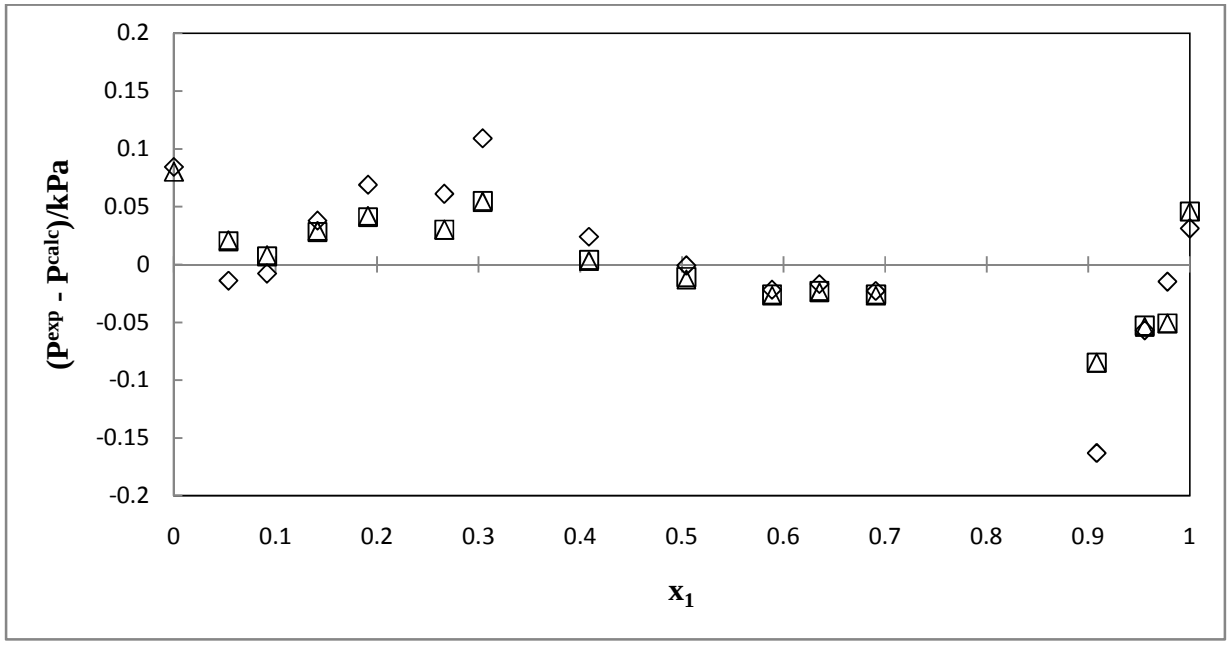

Figure B-17: Point test (varying EoS) pressure-residual for the water (1) + propan-1-ol (2) system at 368.15 K: ◊ PR-NRTL, □ HOC-NRTL, Δ NTH-NRTL.

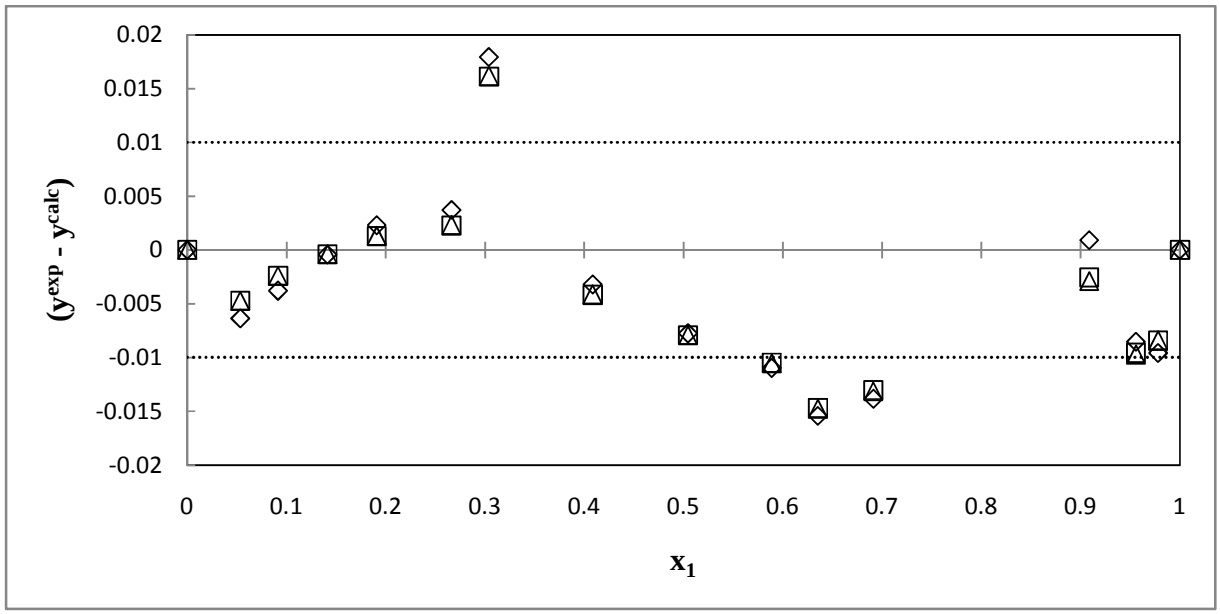

Figure B-18: Point test (varying EoS) Δy_1 for the water (1) + propan-1-ol (2) system at 368.15 K: ◊ PR-NRTL, □ HOC-NRTL, Δ NTH-NRTL.

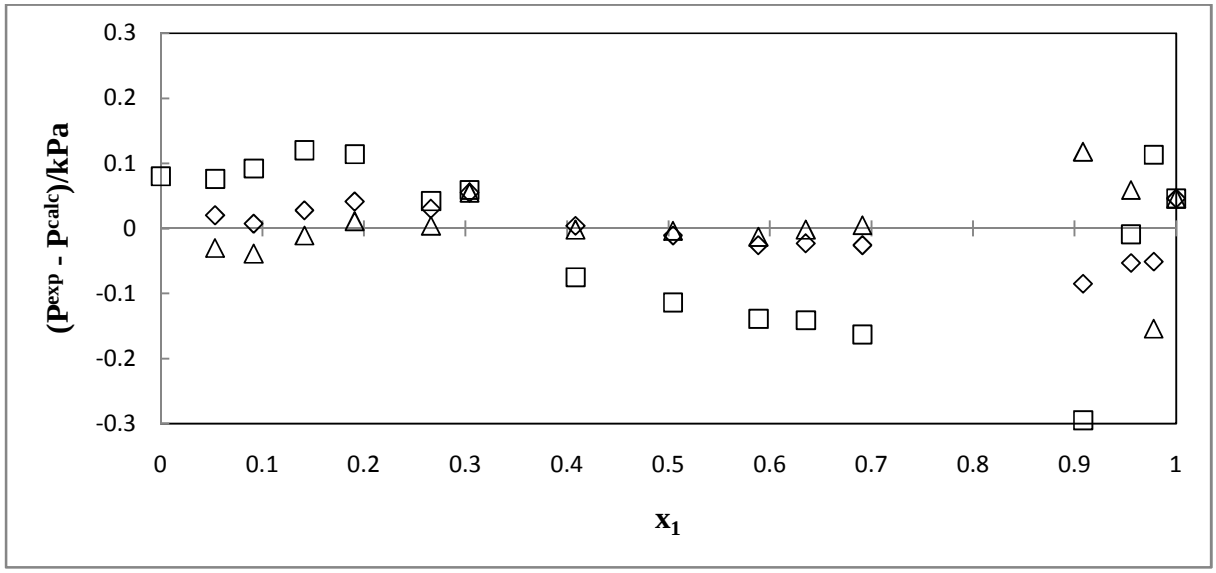

Figure B-19: Point test (varying activity coefficient model): pressure-residual for the water (1) + propan-1-ol (2) system at 368.15 K: ◊ HOC-NRTL, □ HOC-UNIQUAC, Δ HOC-Wilson.

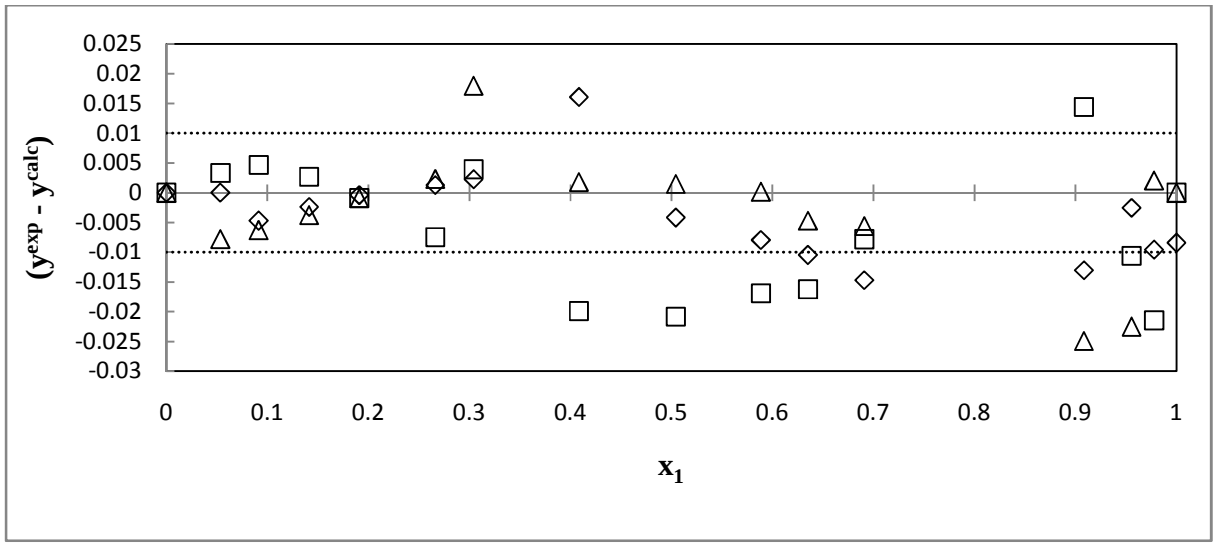

Figure B-20: Point test (varying activity coefficient model): Δy_1 for the water (1) + propan-1-ol (2) system at 368.15 K: ◊ HOC-NRTL, □ HOC-UNIQUAC, Δ HOC-Wilson.

Furan (1) + n-hexane (2) system

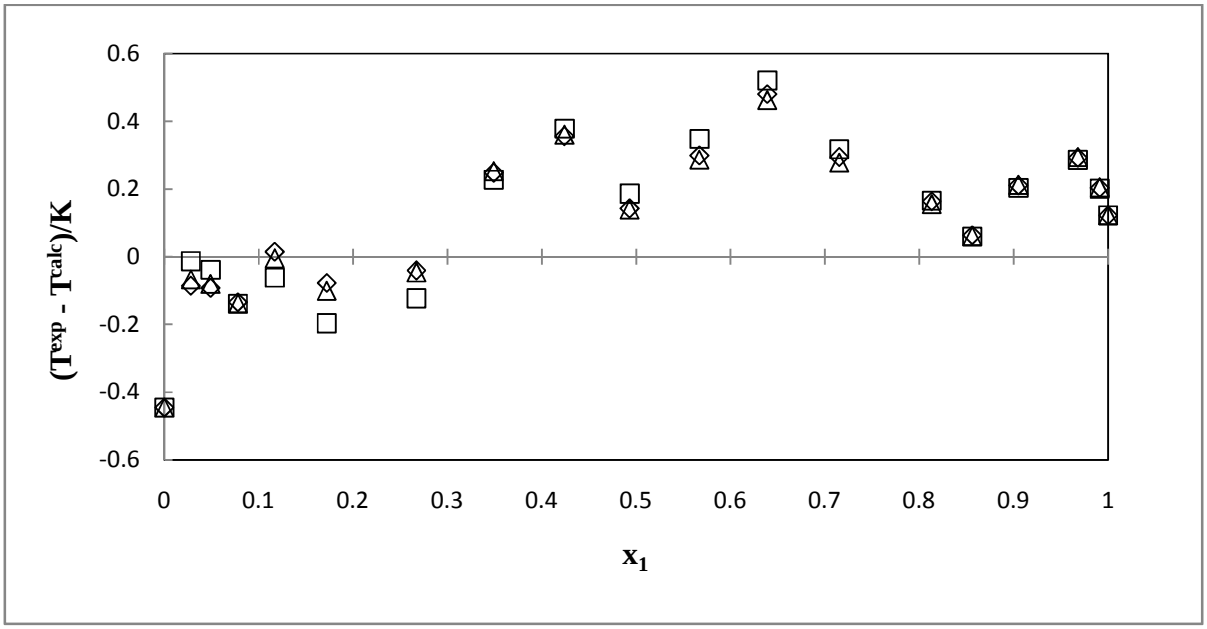

Figure B-21: Point test (varying activity coefficient model): temperature-residual for the furan (1) + n-hexane (2) system at 101.3 kPa: ◊ PR-NRTL, □ PR-UNIQUAC, Δ PR-Wilson.

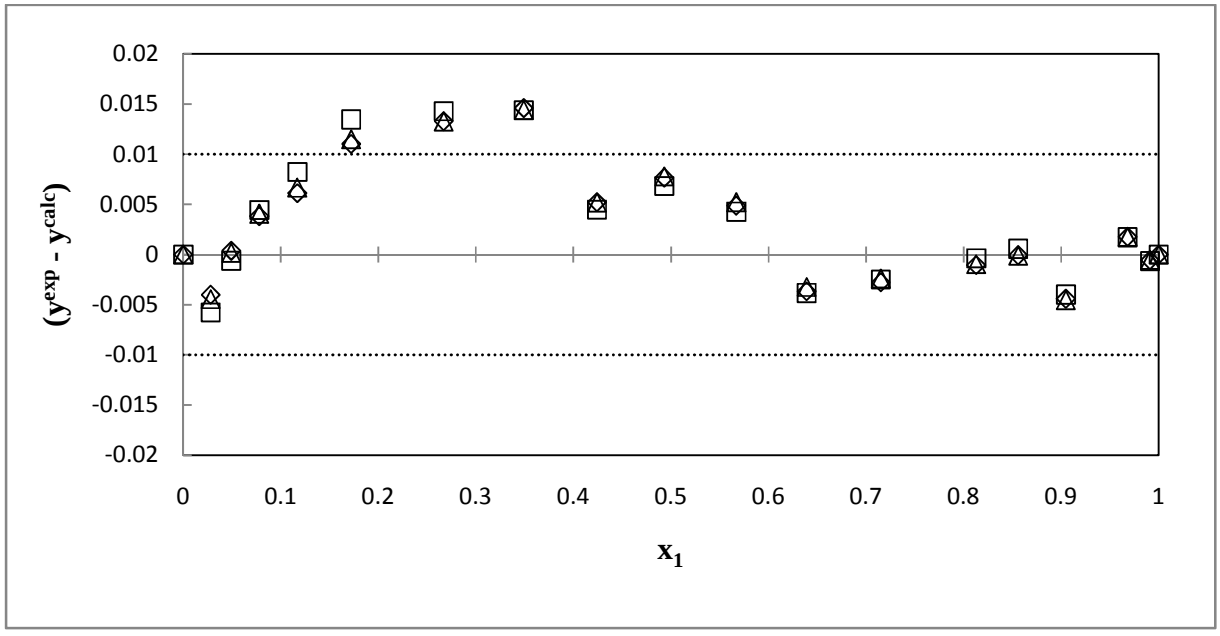

Figure B-22: Point test (varying activity coefficient model): Δy_1 for the furan (1) + n-hexane (2) system at 101.3 kPa: ◊ PR-NRTL, □ PR-UNIQUAC, Δ PR-Wilson.

Furan (1) + methylbenzene (2) system

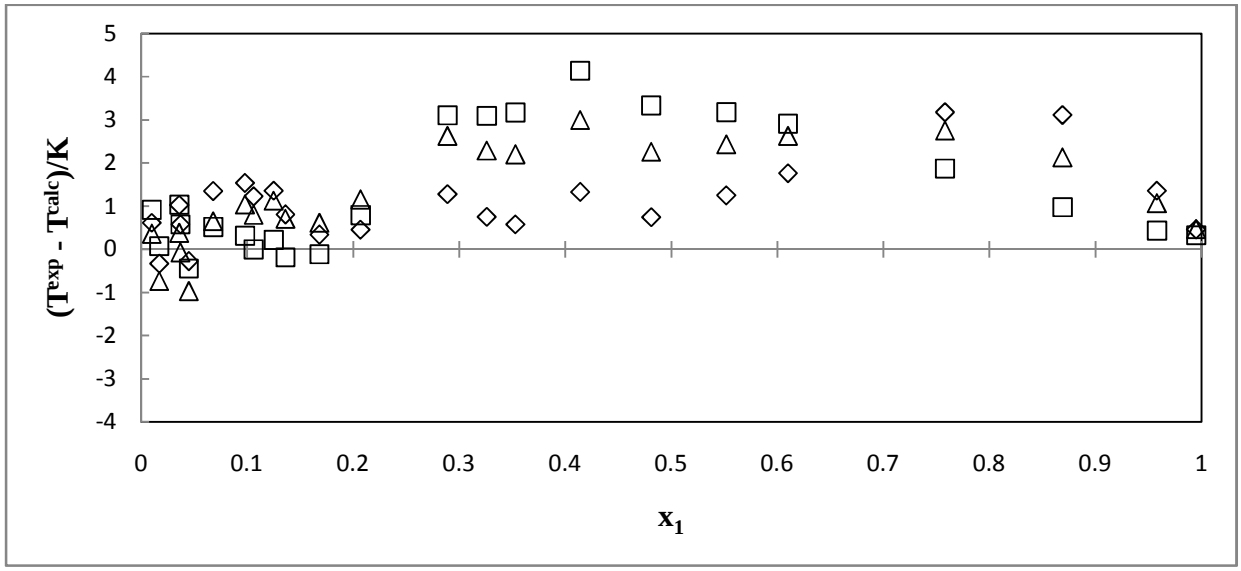

Figure B-23: Point test (varying activity coefficient model), temperature-residual for the furan (1) + methylbenzene (2) system at 101.3 kPa: ◊ PR-NRTL, □ PR-UNIQUAC, Δ PR-Wilson

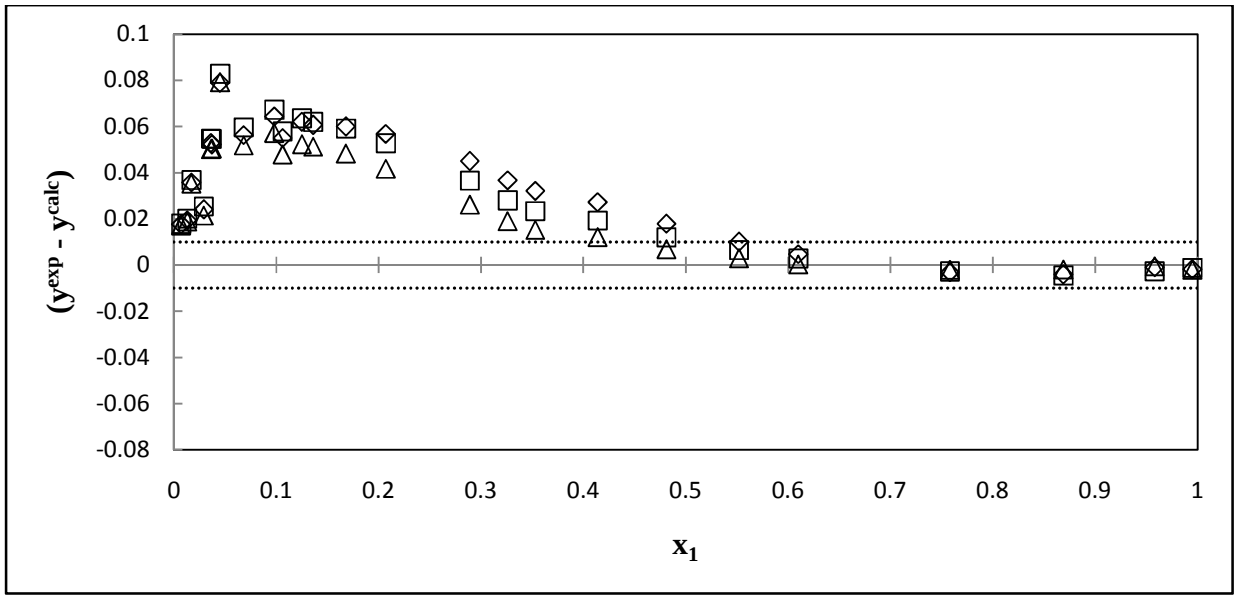

Figure B-24: Point test (varying activity coefficient model), Δy_1 for the furan (1) + methylbenzene (2) system at 101.3 kPa: ◊ PR-NRTL, □ PR-UNIQUAC, Δ PR-Wilson

APPENDIX C

EXPERIMENTAL AND PREDICTED DATA

Diisopropyl ether (1) + 1-propanol (2) system

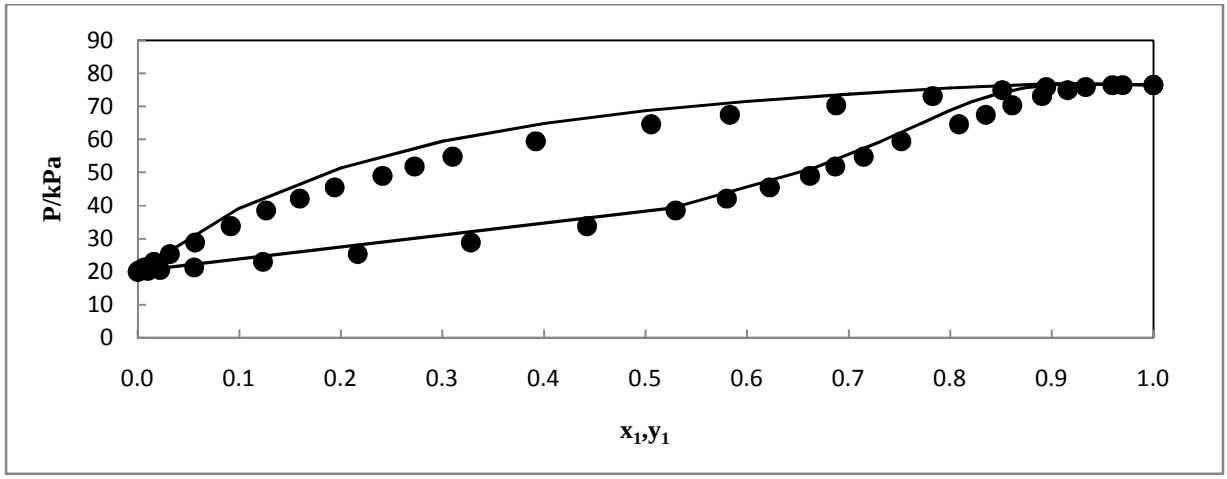

Figure C-1: Comparison of the experimental and predicted data for diisopropyl ether (1) + propan-1-ol (2) at 333.15 K: ● this work, — PSRK.

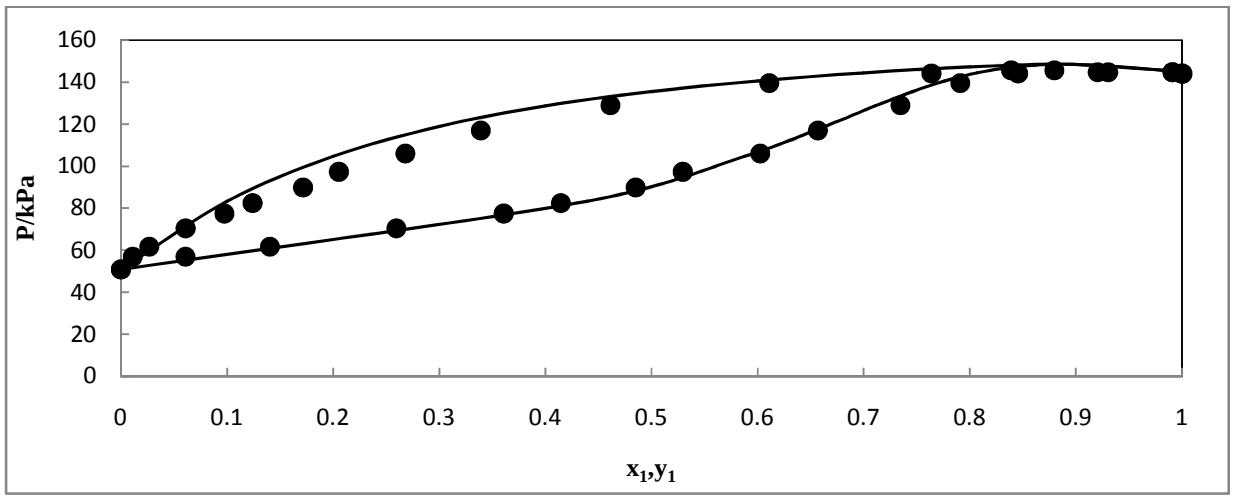

Figure C-2: Comparison of the experimental and predicted data for diisopropyl ether (1) + propan-1-ol (2) at 353.15 K: ● this work, — PSRK.

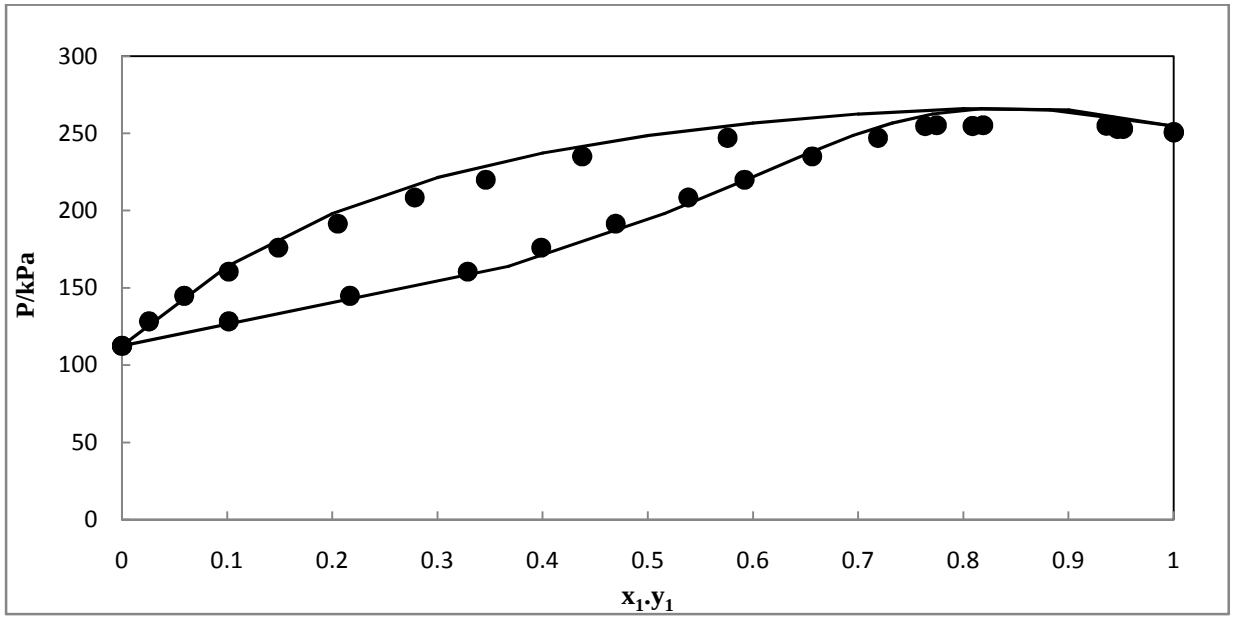

Figure C-3: Comparison of the experimental and predicted data for diisopropyl ether (1) + propan-1-ol (2) at 373.15 K: ● this work, — PSRK.

Water (1) + propan-1-ol (2) system

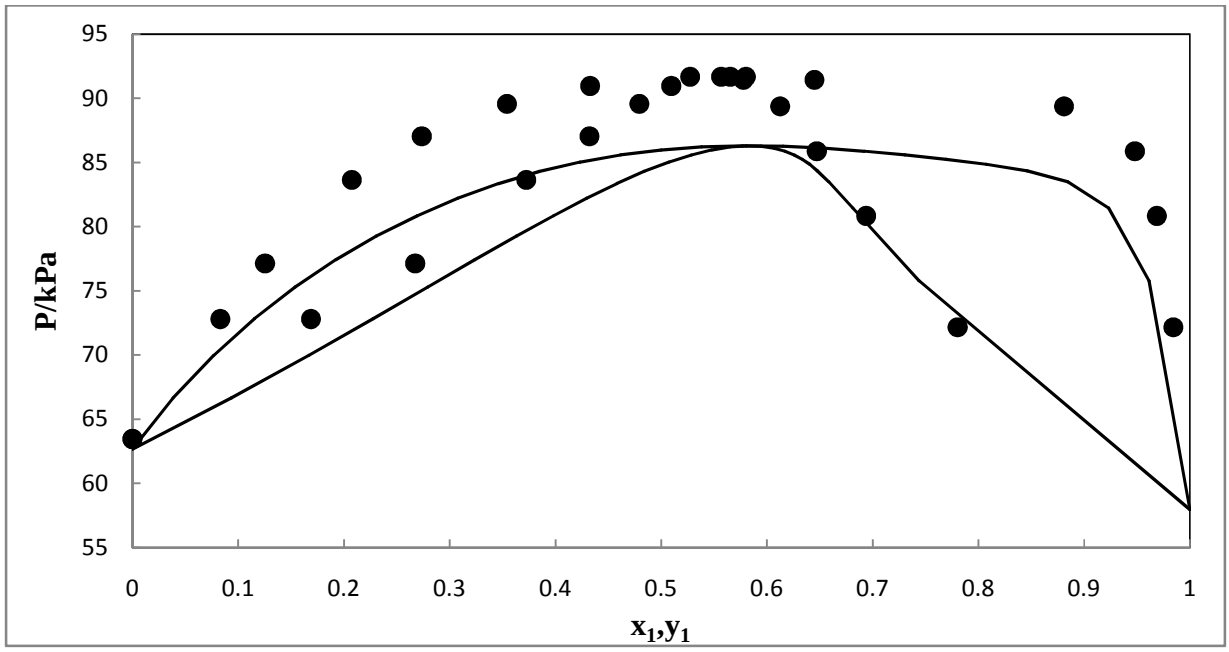

Figure C-4: Comparison of the experimental and predicted data for water (1) + propan-1-ol (2) at 358.15 K: ● this work, — PSRK.

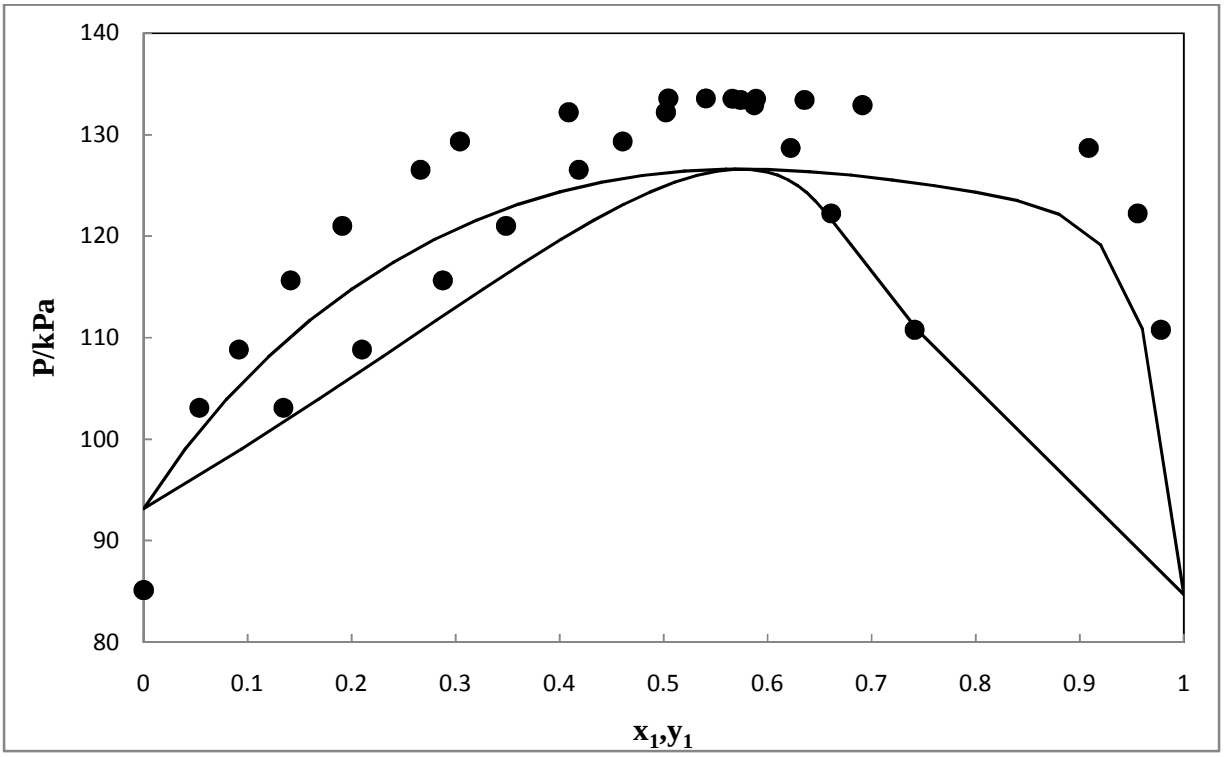

Figure C-5: Comparison of the experimental and predicted data for water (1) + propan-1-ol (2) at 358.15 K: ● this work, — PSRK.

APPENDIX D

PROPAN-1-OL DEHYDRATION: ASPEN STREAM RESULTS

Table D-1a: Stream results for the propan-1-ol dehydration process.

process Variable	process streams						
	4	9	DIST1	DIST2	DIST3	FEED	H2O
Mole Flow (kmol/hr)							
WATER	43.49	1.84	18.35	41.81	12.53	60.00	10.64
propan-1-ol	41.81	2.11	0.31	28.13	2.30	40.00	0.13
diisopropyl ether	0.06	39.91	41.34	0.06	41.16	0.00	0.02
Mole Frac							
WATER	0.5095	0.0419	0.3058	0.5972	0.2238	0.6000	0.9862
propan-1-ol	0.4898	0.0482	0.0051	0.4019	0.0412	0.4000	0.0117
diisopropyl ether	0.0007	0.9099	0.6891	0.0009	0.7351	0.0000	0.0021
Mass Flow (kg/hr)							
WATER	783.43	33.10	330.58	753.17	225.77	1080.92	191.65
Propan-1-ol	2512.42	126.95	18.37	1690.51	138.49	2403.84	7.61
diisopropyl ether	6.41	4077.54	4224.40	6.41	4205.93	0.00	2.28
Mass Frac							
WATER	0.2372	0.0078	0.0723	0.3074	0.0494	0.3102	0.9509
Propan-1-ol	0.7608	0.0300	0.0040	0.6900	0.0303	0.6898	0.0378
diisopropyl ether	0.0019	0.9622	0.9237	0.0026	0.9203	0.0000	0.0113
Total Flow (kg/hr)	3302.26	4237.59	4573.35	2450.08	4570.19	3484.754	201.5408
Temperature K	367.23	283.15	339.69	364.85	333.17	338.15	283.15
Pressure kPa	130.00	100.00	130.00	120.00	100.00	150.00	100.00

Table D-1b: Stream results for the propan-1-ol dehydration process.

process Variable	process streams						
	H2O1	MAKEUP	ORGPHASE	PROD1	PROD2	SOLRICH	SRECYCLE
Mole Flow kmol/hr							
WATER	47.62	0.79	12.54	1.68	0.01	1.84	1.89
Propan-1-ol	3.16	0.00	25.28	13.68	22.97	2.11	2.18
diisopropyl ether	0.21	1.50	41.20	0.00	0.04	41.41	41.14
Mole Frac							
WATER	0.9340	0.0000	0.1587	0.1094	0.0004	0.0405	0.0419
propan-1-ol	0.0619	0.0000	0.3199	0.8906	0.9981	0.0466	0.0482
diisopropyl ether	0.0041	1.0000	0.5214	0.0000	0.0016	0.9129	0.9099
Mass Flow kg/hr							
WATER	857.84	0.00	225.92	30.26	0.15	33.10	34.12
propan-1-ol	189.71	0.00	1519.02	821.91	1380.54	126.95	130.88
diisopropyl ether	21.30	153.26	4209.66	0.00	3.72	4230.81	4203.65
Mass Frac							
WATER	0.8026	0.0000	0.0379	0.0355	0.0001	0.0075	0.0078
Propan-1-ol	0.1775	0.0000	0.2551	0.9645	0.9972	0.0289	0.0300
diisopropyl ether	0.0199	1.0000	0.7070	0.0000	0.0027	0.9635	0.9622
Total Flow kg/hr	1069	153	5955	852	1384	4391	4369
Temperature K	283.15	333.15	283.15	371.08	369.73	284.92	283.15
Pressure kPa	100.00	150.00	100.00	120.00	100.00	200.00	100.00